THE UNIVERSITY *of* EDINBURGH

Biochemical and Biophysical studies of MDM2-Ligand Interactions

A Thesis Submitted for the Degree of Doctor of Philosophy by

SHAO-FANG, WANG B.Sc. M.Sc.

Institute of Structural and Molecular Biology

The University of Edinburgh

2011

ABSTRACT

MDM2, murine double minute 2, is a RING type-E3 ligase protein and also an oncogene. MDM2 plays a critical role in determining the steady levels and activity of p53 in cells using two mechanisms. The N-terminal domain of MDM2 binds to the transactivation domain of p53 and inhibits its transcriptional activity. The RING domain of MDM2 plays a role in the ubiquitination (and degradation) of p53. Several proteins are responsible for the ubiquitination mechanism including the ubiquitin-activating enzyme (E1), ubiquitin-conjugating enzyme (E2) and ubiquitin ligase (E3). Since the E2-E3 interaction is essential for ubiquitination, the protein-protein recognition site is a potential drug target.

Two different MDM2 RING constructs were expressed and purified: MDM2RING (residues 386-491) and MDM2RING△C (residues 386-478). Both constructs were characterised using dynamic light scattering, size exclusion chromatography, mass spectrometry, NMR and electron microscopy. E3 ligase activity *in vitro* was also studied. Taken together these results showed that the MDM2RING construct formed a concentration-dependent oligomeric structure. In contrast, the MDM2RING△C construct formed a dimer at all concentrations. Both MDM2RING and MDM2RING △ C retain E3 ligase activity. However, the MDM2RING△C construct is less active. Full length E2 enzyme UbcH5a was also purified. Various biophysical techniques were used to study its interaction with MDM2 as well as with potential small molecule inhibitors as in principle, small molecules which disrupt the interaction between MDM2 and UbcH5a, could prevent/promote ubiquitination of p53.

The dimerisation of MDM2 is important for its E3 activity and the C8-binding site potentially provides a second druggable site. In this work, peptide 9, which has the same sequence as the C-terminus of MDMX (an MDM2 homologue) was found to inhibit MDM2 E3 activity. Various biological techniques including NMR, fluorescence anisotropy, and electrospray mass spectrometry were used to investigate the interaction between two inhibitory peptides and MDM2. A major part of project involved virtual screening (VS) to search for small molecules which can affect MDM2-dependent ubiquitination. Three potential targets were considered: (1) the C8-binding site of MDM2; (2) the UbcH5a-binding site of MDM2; and (3) the MDM2-binding site of UbcH5a. Several small molecules were identified using our virtual screening database-mining and docking programs that were shown to affect MDM2-dependent ubiquitination of p53.

In terms of understanding the complex biochemical mechanism of MDM2 this work provides two interesting and functionally relevant observations: (i) the MDM2 RING△C construct is a dimer as this would not be expected form the existing studies, and has less E3 ligase activity than MDM2RING; (ii) small molecules that bind MDM2 on the E2 binding site enhanced E3 ligase activity. One model to explain these observations is that binding of small molecule activators family to the RING induces a change in the conformation of the C-terminal tail residues which may enhance E2 binding.

ACKNOWLEDGEMENTS

I would like to gratefully thank my enthusiastic supervisor, Professor Malcolm D. Walkinshaw. His comments help me to establish the direction to the research with his ongoing encouragement throughout this period of study. I am also grateful to Dr. Kathryn Ball, for allowing me to visit her lab and her group members, Vivien Landré and Dr. Susanne Patterson, for teaching me the techniques of *in vitro* ubiquitination.

I must make special acknowledgments to thank members of the Institute of the Structural and Molecular Biology Group for their help and assistance in a variety of tasks during the course of my studies. Thanks for their assistance on the experimental setups and great advice: Dr. Jacqueline Dornan, Sandra Bruce, Dr. Martin Weir, Dr. Elizabeth Blackburn, Dr. Janice Bramham, Dr. Mattew Nowiki, Dr. Julia Richardson, Dr. Hugh Morgan, Dr. Koko-lian Hao and Dr. Iain McNae. Thanks for their assistance on the bioinformatics analysis: Dr. Paul Taylor, Dr. Steven Shave, Dr. Kun-Yi Hsin and Dr. Douglas Houston. I also like to thank Dr. M. C. Sanchez and Dr. Juraj Bella assist on NMR experiments.

I am grateful to thank all my friends in Edinburgh and Taiwan, in particular Can, Silvia Lin and Tzu-Yuan Lin for their care and support during these years.

Lastly I would like to thank my lovely family for their understanding, constant support and encouragement with endless love over all the years.

DECLARATION

The work presented in this thesis is the original work of the author. This thesis has been composed by the author and has not been submitted in whole or in part for any other degree.

SHAO-FANG, WANG

ABBREVIATIONS

a.a.	amino acids
Ac	an acidic domain of MDM2
ADP	adenosine diphosphate
Amp	Ampicillin
APS	Ammonium Phosphate Sulphate
ATP	adenosine triphosphate
BOX-I	Transactivation domain of p53
BOX-V	DNA-binding domain of p53
BSA	Buried Surface Area
CD	Circular Dichroism
CK	Creatine Kinase
CP	Creatine Phosphate
Cyp A/ CsA	Cyclophilin A / cyclosporin A
ddH_2O	Distilled water
DLS	Dynamic Light Scattering
DMSO	Dimethyl sulfoxide
DTT	DL-dithiothreitol
DUB(s)	De-ubiquitin enzyme(s)
E1	Ubiquitin-Activating Protein
E2	Ubiquitin Conjugating Protein
E3	Ubiquitin Ligase Protein
EDTA	Ethylenediaminetetraacetate
EDULISS	EDinburgh University Ligand Selection System
ESI-MS	Electrospray ionization mass spectrometry
FKBP	the immunophilin protein (FK506 binding protein)
GST · Tag	glutathione S-transferase Tag
HAUSP	the herpesvirus-associated ubiquitin-specific protease
HEPES	4-(2-hydroxyethyl)-1-piperazineethanesulfonic acid
HECT	Homologous to E6-AP carboxyl terminus
His-Tag	a 6xHis-Tag
Hotspot	the potential small-molecule binding site
HSQC NMR	Heteronuclear single quantum coherence NMR
HTS	High-Throughput screening
Hy	a hydrophobic pocket of MDM2
IMAC	Immobilised Metal Affinity Chromatorgraphy

IPP	Interatomic Pharmocophore Profiles IPP
IPTG	Isopropyl-1-thio-β-D-galactopyranoside
ITC	Isothermal Titration Calorimetry
Kd	Dissociation constant
LB	Luria-Bertani medium
LogP	Octanol-water partition coefficient
LIDAEUS	Ligand Discovery At Edinburgh University
MALDI-TOD MS	Matrix-Assisted Laser Desorption/ionisation Time-of Flight Mass Spectrometry
MDM2	murine double minute 2
MDM2RING	Residues 386-491 of MDM2
MDM2RING△C	Residues 386-478 of MDM2
M.W.	Molecular Weight
NaCl	Sodium Chloride
NES	the nuclear export signal
NLS	the nuclear localization signal
NMR	Nuclear Magnetic Resonance
NoLS	the nucleolar localisation signal
OD_{600}	Optical density at 600nm
p300/CBP	CREB-binding protein
PEG	Polyethylene glycol
PI	Isoelectric point
PPI	Protein-Protein interactions
RING	Really Interesting New Gene
SCF	Skp1-Cullin-F-box protein
SDS-PAGE	Sodium dodecyl sulfate polyacrylamide gel electrophoresis
SEC	Size Exclusion Chromatography
SPR	Surface plasmon resonance
TDA	Thermal Denaturation Assay
TEMED	Tetramethylethylenediamine
Tm	the melting temperature
TEM	Transmission Electron Microscopy
TFA	Thermal Fluorescence Assay
Tris	Tris (hydroxymethyl)aminomethane
TSA	Thermal Shift Assay
VS	Virtual screening
Ub	Ubiquitin

Ub(A)	an adenylate-linked ubiquitin
Ub(T)	a thioester-linked ubiquitin ()
Ub(T) ~ E1	the activated ubiquitin~E1 complex
UBLs	Ubiquitin-Like Proteins
UFSRAT	Ultra Fast Shape Recognition with Atom Types
UPS	Ubiquitin Protease System
ρABA	ρ-aminobenzamidine
V_{rent}	retention volume
kDa	kilo-Dalton
QELS	Quasi-Elastic Light scattering
ZF	a zinc-finger domain of MDM2
Θ	Ellipticity
11βHSD1	11β –hydroxysteroid dehydrogenase

CONTENTS

LIST OF FIGURES

LIST OF TABLES

1 Introduction

The Ubiquitin Protease System (UPS) is vital in the determination of the fates of a wealth of proteins in cells. There are three proteins involved: E1 (ubiquitin activating enzyme), E2 (ubiquitin conjugating enzyme) and E3 (ubiquitin protein ligase). A number of tumours have been found to be related to the UPS. One example is the observation that tumours which have wild type p53 are correlated with an upregulation of an E3 ligase protein, MDM2 (murine double minute 2). In tumour therapies, several drugs are designed to inhibit the interaction of MDM2 to p53, such as Nutlin (Vassilev et al., 2004), and RITA (Issaeva et al., 2004).

This chapter is divided into two parts: (1) The biology of the UPS, and (2) Virtual screening (VS) strategy to design new ligands. In the first part, an overview of the UPS is provided including roles of many components of the UPS such as ubiquitin, E1s, E2s, and E3s. Ubiquitination plays an important role in regulation of the level of tumour suppressor p53 through MDM2-mediated transcriptional inhibition and MDM2-mediated p53 proteolysis. Therefore, MDM2 is an appealing anticancer target to rescue p53-mediated apoptosis. To achieve the aim of developing MDM2 inhibitors, VS strategies were used to screen potential leads. In part II, information about protein-protein interactions and the challenges of designing inhibitors of protein-protein interactions are discussed.

Part I MDM2 and the Ubiquitin Proteasome System

1.1 Ubiquitin Proteasome System (UPS)

The **U**biquitin **P**roteasome **S**ystem (UPS) plays a number of key roles in controlling cell growth and proliferation, including progression of the cell cycle, tumour suppression, and induction of the inflammatory response (Glickman & Ciechanover, 2002; Hershko & Ciechanover, 1998; Koepp et al., 1999; Pickart, 2001b; Rock & Goldberg, 1999; Weissman, 2001). UPS is a well-defined multistep pathway that processes the ubiquitin modification of proteins. The enzymes involved include ubiquitin (Ub), ubiquitin activating enzyme (E1), ubiquitin conjugating enzyme (E2), ubiquitin protein ligase (E3) and the 26S proteasome (Figure 1-1A) (Hershko et al., 1983; Peter et al., 1998; Pickart & Eddins, 2004). In the first step, E1 adenylates the C-terminus of Ub in an ATP-dependent process, forming the E1-AMP~Ub intermediate. Subsequently, this activated ubiquitin is transferred to the catalytic domain of E1, forming the E1~Ub thioester intermediate. A second ubiquitin binds to the adenylation domain of E1, becoming the E1-AMP~Ub intermediate. This doubly loaded E1 is now recognised by E2. The ubiquitin bound to the catalytic site of E1 is then transferred to the active site cysteine residue of E2 through transesterification and forms an E2~Ub thioester intermediate. In the third step, E3 binds with its substrate protein and interacts with ubiquitin-charged E2. Subsequently, the terminal glycine carboxylate group of ubiquitin is linked in an amide isopeptide linkage to an ε–amino group of a lysine residue on the substrate protein, or to a lysine residue of a ubiquitin already attached to the substrate protein (Hershko et al., 1983; Passmore & Barford, 2004; Pickart, 2001b).

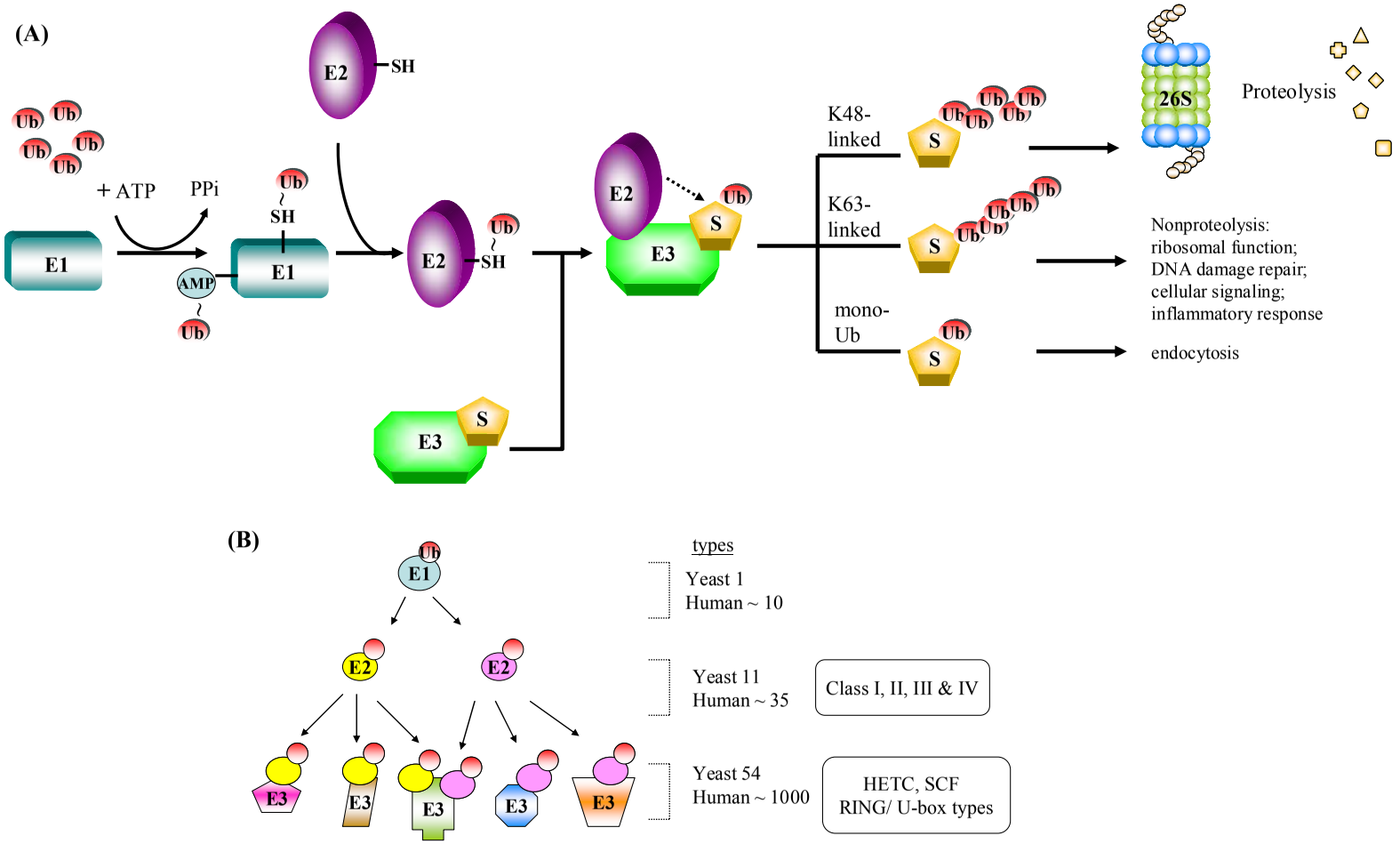

Figure 1-1: The Ubiquitin-Proteasome System (UPS). (A) As described in the textt, E1, E2, E3 and ubiquitin (Ub) are sequentially involved in the UPS sequentially. At the end, the fate of the ubiquitinated substrate is determined by the linkage type of attached ubiquitin chain. (B) In yeast or human cells, there are few E1(s), four classes of the E2(s) (class I, II, III and IV) and a large number of E3(s) (HECT domain and RING/U-box domain- type).

Ubiquitinated proteins have different cellular fates that depend on the topology or the number of the substrate-conjugated ubiquitins and the subcellular localisation of the substrate (Figure 1-1B) (Pickart, 2000). For instance, substrates marked with a Lys48-linked (K48-linked) polyubiquitin chain are targeted for proteolysis by the multisubunit ATP-dependent 26S proteasome (Hershko & Ciechanover, 1998; Hochstrasser, 1996; Thrower et al., 2000). Substrates conjugated with a Lys63-linked (K63-linked) polyubiquitin chain are directed for non-proteolytic signalling, such as ribosomal function, DNA repair and inflammatory response (Deng et al., 2000; Hoege et al., 2002; Hofmann & Pickart, 1999; Spence et al., 1995; Spence et al., 2000). Some proteins bound with one or a few ubiquitins are directed for endocytosis (Kim et al., 2007; Hicke, 1999). It has been noted that disregulation in ubiquitination results in pathological syndromes, including tumour development, viral infection, inflammation and neurogenesis deficiency (Lam et al., 2000; Joazeiro et al., 1999; Matsuura et al., 1997; Petroski, 2008; Scheffner et al., 1990; Staub et al., 1997).

Reviews show that there are few E1s, limited numbers of E2s and large numbers of E3s involved in ubiquitination pathways (Hershko & Ciechanover, 1998; Hochstrasser, 1996). Although the numbers of E2s are limited, each E2 interacts with several E3s. Similarly, each E3 interacts with one or more E2s (van Wijk & Timmers, 2010). Moreover, E3s play important roles in the determination of the substrate specificity. Those complicated combinations of E2-E3 complexes provide delicate cellular regulation to enable cells to deal with different conditions. Moreover, E3s play important roles in the determination of the substrate specificity.

.

1.1.1 Ub: Ubiquitin

As the name suggests ubiquitin or ubiquitin-like proteins (UBLs), such as Sumo and Nedd8, are ubiquitous in cells and play critical roles in the determination of the fate of cellular proteins (Herrmann et al., 2007; Kerscher et al., 2006). Ubiquitin (Ub) is a 76-amino-acid residue protein. Sumo and Nedd8 are 103- and 76-amino acid proteins, respectively. Ubiquitin has 57% identity to Nedd8 and 18% identity to Sumo (Figure 1-2A). Ubiquitin and UBLs share a common structural fold, called the β-grasp (Figure 1-2B) and have similar biochemical mechanisms to modify proteins. For instance, the last C-terminal residue of Ub and Nedd8 and the last third residue of Sumo is a glycine which is involved in the interaction of thioester bond formation between the carboxyl-terminal glycine (G76 in Ub and Nedd8, G99 in Sumo) attached to the active cysteine residue of the E1 or E2 upon the thioesteration (Lois & Lima, 2005; Wenzel et al., 2010). An isopeptide bond forms between the amino acid group of the lysine residue of target protein (or ubiquitin). The canonical ubiquitin-chain is the Lys48 linked-polyubiquitin chain that is recognised and degraded by the 26S proteasome (Hershko & Ciechanover, 1998). Furthermore, several topologies of ubiquitin chains have been characterised (Pickart, 2001a) and shown to play a number of roles in different cellular functions (Table 1-1). For example, the Lys48-linked or the Lys11-linked and Lys29-linked polyubiquitin chain attached target proteins are degraded by the 26S proteasome. In the nonproteolytic pathway, Lys6-linked and Lys63-linked mono-ubiquitin or polyubiquitin chains play distinct roles in regulatory modifications.

Table 1-1: Distinct topologies of the ubiquitin chain and their cellular functions.

topology of ubiquitin chain	mono/poly	function
Lys48-linked, Lys11-linked, Lys29-linked	poly-	**proteolytic pathway**
Lys6-linked, Lys33-linked, Lys63-linked	mono-/ poly-	**Non-proteolytic pathway** membrance trafficking, endocytosis, signal transduction, DNA repair signalling, the stress response, histone function, transcription

(A)

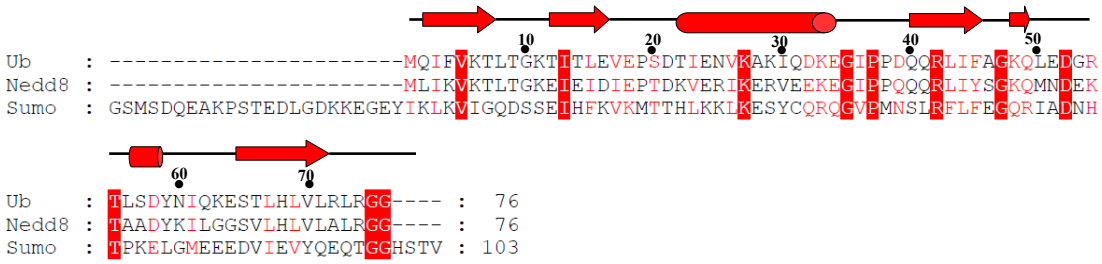

Identity (%)	Ub	Nedd8	Sumo
Ub			18
Sumo		21	
Nedd8	57		

(B)

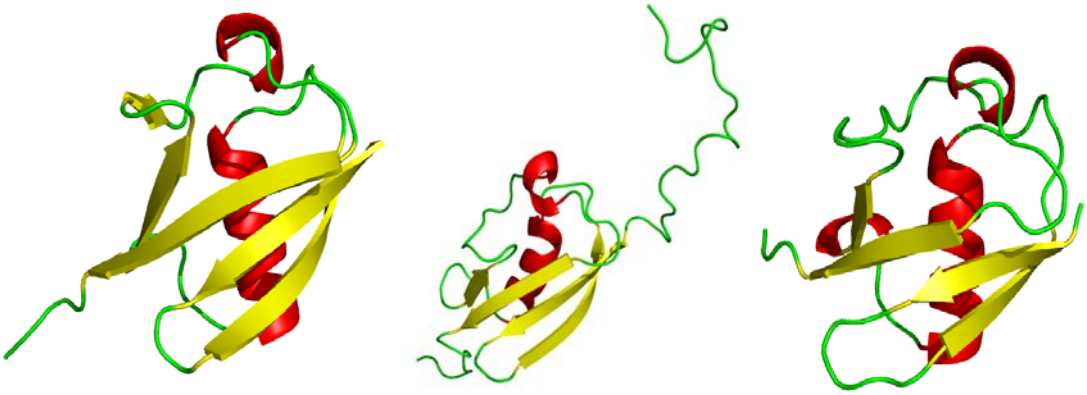

Ubiquitin
(1UBQ)

SUMO
(1A5R)

Nedd8
(1NDD)

Figure 1-2: Sequences and structures of Ubiquitin and Ubiquitin-like proteins (Ubls). (A) Sequence alignments of Ubiquitin, Sumo, and Nedd8. Identical residues are shown in white letters and conservative substitutions are shown in red. Secondary structure elements within these proteins are denoted above the sequences (based on the structure of ubiquitin, PDB code: 1UBQ). Red cylinders represent α-helices and arrows represent β-sheets. Numbering refers to the ubiquitin sequence. (B) Structures are highly conserved, and are principally comprised of a β-grasp fold (yellow). The structure of Ubiquitin, Sumo and Nedd8 are rendered of a using Pymol. α-helixes, β-sheets, and loops are coloured in red, yellow and green, respectively. Ubiquitin (left panel, PDB code: 1UBQ) (Vijay-Kumar et al., 1987), Sumo (middle panel, PDB code: 1A5R) (Bayer et al., 1998) and Nedd 8 (right panel, PDB code: 1NDD) (Whitby et al., 1998).

1.1.2 E1: Ubiquitin activating enzyme

In most organisms, ubiquitin activating enzyme (E1) is an essential enzyme to activate ubiquitin or UBLs for the entire downstream ubiquitination/ sumolyation/ neddylation pathway (Haas & Rose, 1982; McGrath et al., 1991). Although there are several types of E1s (monomers, homodimers and heterodimers) (Table 1-2), the conserved E1 functions are to activate ubiquitin (UBLs) in an ATP-dependent mechanism and transfer activated ubiquitin to E2 proteins (Haas & Rose, 1982; Hershko et al., 1983). In general, the structures of the E1s can be dissected into several domains (Schulman & Harper, 2009): the adenylation domain, inactive adenylation domain, the ubiquitin fold, and the catalytic Cys domain (Figure 1-3). Fully loaded E1 contains two activated ubiquitins: an adenylate-linked ubiquitin (UBL(A)) and a thioester-linked ubiquitin (UBL(T)). Initially the adenylation domain of E1 is responsible for the adenylation of ubiquitin to generate an ubiquitin~adenylate intermediate (UBL(A)). The adenylate-linked ubiquitin (UBL(A)) acts as a donor to facilitate the thioester formation of the ubiquitin to a conserved active site cysteine of E1 (Haas & Rose, 1982; Schulman & Harper, 2009). Sequentially, a UBL(A) is transferred to the activated Cys in the catalytic domain to form a thioester bond, forming the activated ubiquitin~E1 complex (UBL(T) ~ E1). Once an E2 binds to the ubiquitin fold domain of a doubly loaded E1, it stimulates the transfer of UBL(T) to E2 and forms a E2~Ub complex via a thioester bond (Walden et al., 2003).

Table 1-2: Ubiquitin activating enzyme (E1) family. There are several species in different oligomeric states: monomer, homodimer, and heterodimer.

Species	E1s
monomer	UBA1 ; UBA6; UBA7
homodimer	MoeB or TriF; UBA4 (MOCS3 in human); UBA5; ATG7
heterodimer	SAE1-UBA2; NAE1-UBA3

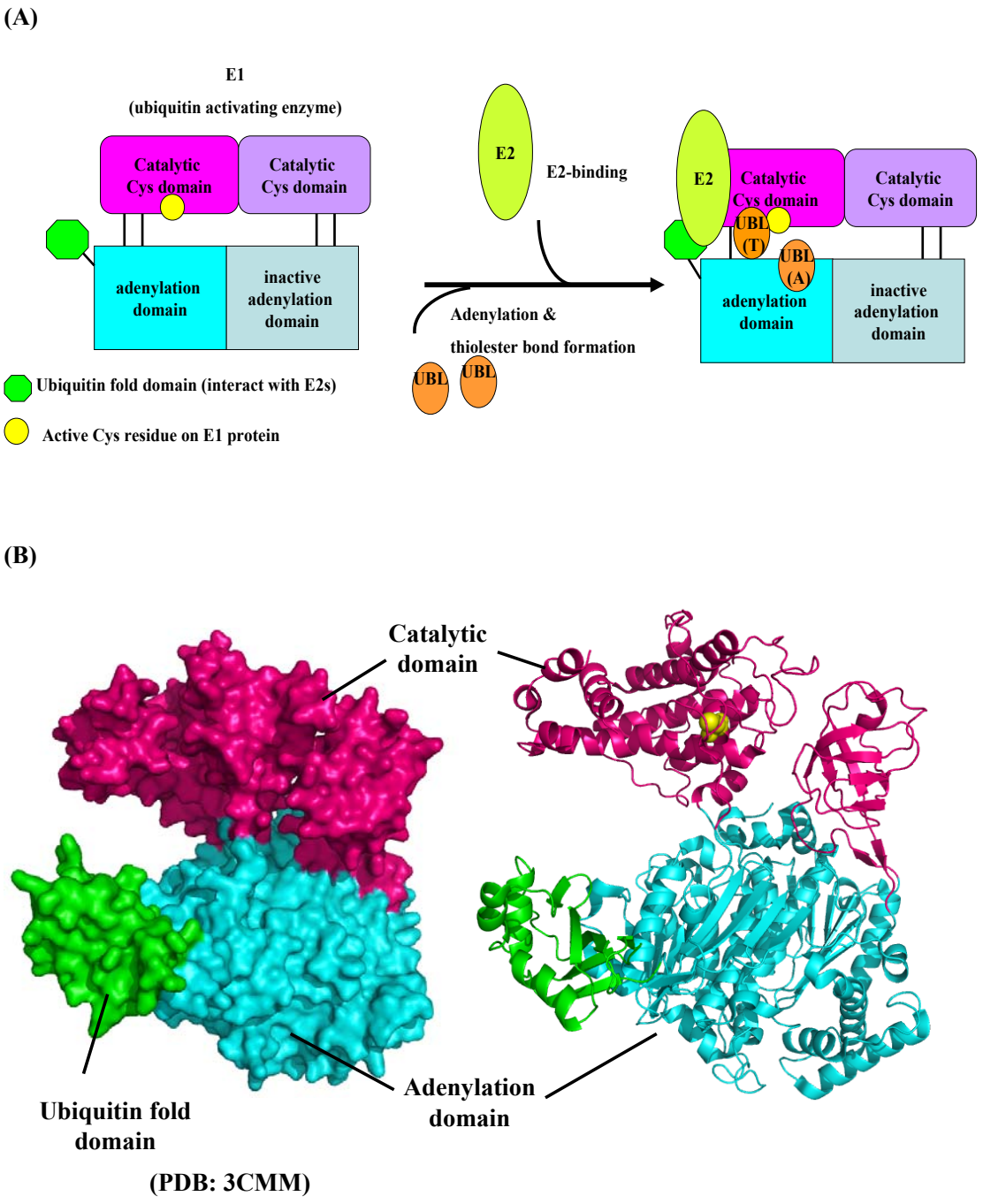

Figure 1-3: The ubiquitin activating enzyme (E1). (A) General structural compositions of the E1s and the roles of the E1s: adenylation of ubiquitin, thioesterification, and binding to the E2. (B) One example of the structure of the E1 proteins: yeast, UBA1 (PDB code: 3CMM)(Lee & Schindelin, 2008). The structure on the left is presented in surface representation, that on the right is shown in cartoon representation. Distinct domains of UBA1 are coloured as follow: catalytic domain in magenta, adenylation domain in cyan and ubiquitin fold domain in green. The active cysteine residue on UBA1 is depicted as a yellow sphere.

1.1.3 E2: Ubiquitin conjugating enzyme

The E2s act as carriers of Ub from E1 to the different E3-substrate complexes. An E2 protein interacts with an E1 and forms a thioester conjugate with the C-terminus of Ub (the E2~Ub intermediate). The charged E2 (E2~Ub) binds to an E3 and transfers the attached Ub to the E3 or the substrate. Recent studies reveal that the E2s also determine the types of mono-ubiquitin chain and polyubiquitin chain of the lysine linkage (Christensen et al., 2007; Roderigo-Brenni & Morgan, 2007; Windheim et al., 2008). E2s are central to the UPS system, playing numerous roles including interaction with E1, ubiquitin/ UBLs, and different E3s, the diverse functions of E2s being reflected in their relative abundance. This relative abundance reveals why determining the mechanisms of E2-mediated interactions have been the focus of so much research activity with more than 35 E2 proteins identified in the human genome (*van* Wijk & Timmers, 2010).

- ***Topology of E2 Ubc domain***

There are over 90 structures of E2s available to date in the PDB (Wenzel et al., 2011). All E2s have an evolutionarily conserved catalytic ubiquitin-conservation domain, Ubc domain, consisting of approximate 150 residues (Cook et al., 1993; Huang et al., 1999; Jiang & Basavappa, 1999; Miura et al., 1999; Worthylake et al., 1998; Zheng et al., 2000). The Ubc domain has a compact structure formed by α2, a short 3_{10} helix and four antiparallel β–sheets, surrounded by α1 on one side and α3 and α4 on the other side (Figure1-4). The catalytically active cysteine, a highly conserved residue in all E2s for the catalysis of ubiquitin, is located in a shallow groove surrounded by residues in the long loop (L5) that connects β4 and the short 3_{10} helix. Those residues surrounding the catalytically active cysteine of E2 are also highly conserved. For example, there is an HPN motif which usually is located about ten residues preceding the catalytically active cysteine residue (Wenzel et al., 2011). The HPN motif plays a structural role in maintaining the E2 active site.

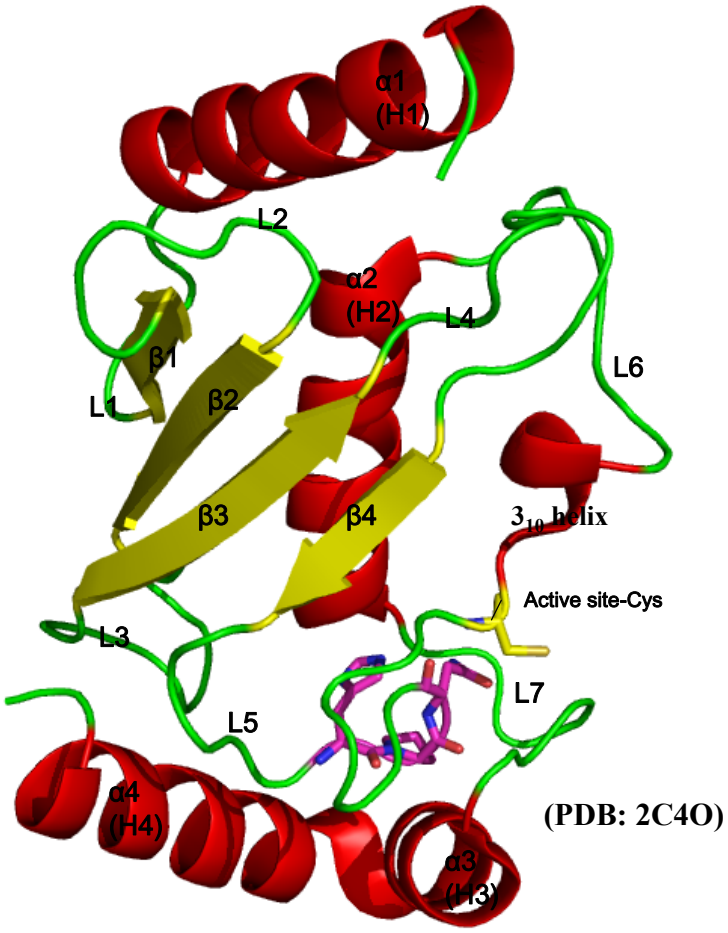

Figure 1-4: Ubiquitin-conjugating enzyme (E2). An E2 Ubc domain consists of four α-helices, four antiparallel β–sheets, and a short 3_{10} helix. An active cysteine residue (yellow sticks) is responsible for the interaction with Gly76 of Ub. The HPN motif is also depicted in magenta sticks. This E2 structure is UbcH5b protein (PDB code: 2C4O).

- ***Four classes of E2s***

Although all E2s share a highly conserved topology of the Ubc domain, the sizes and specific biological functions of E2s are distinct (*van* Wijk & Timmers, 2010; Winn et al., 2004). Some E2s have N- or C- terminal extensions to the Ubc domain, which play important roles in their specific interactions with partner proteins. There are four E2 families classified on the basis of the presence of the additional fragments. Class I E2s have only a Ubc domain, such as the UbcH5 family, UbcH7, UbcH9 and Ubc13 (Giraud et al., 1998; Houben et al., 2004; *van* Demark et al., 2001; Zheng et al., 2000); Class II E2s contain a Ubc domain plus a N-terminal extension, such as UbcH10 (Lin et al., 2002; Summers et al., 2008). Class III E2s comprise an Ubc domain plus a C-terminal extension, such as cell division cycle 34 (CDC34) (Ceccarelli et al., 2011); and Class IV E2s have a Ubc domain plus both an N- and C-terminal extensions, such as E2–230K and BIRC6.

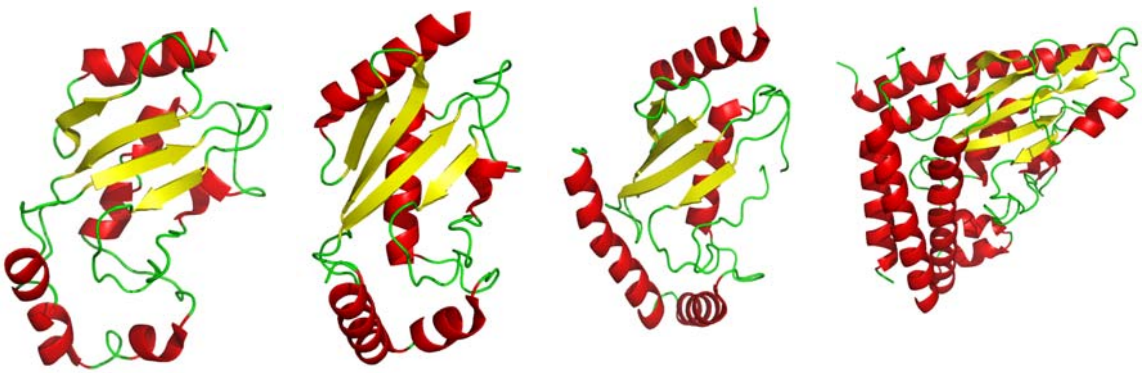

Class I	Class II	Class III	Class IV
UbcH7	UbcH10	CDC34	BIRC6
(1FBV)	(1I7K)	(3RZ3)	(3CEG)

Figure 1-5: Structures of four classes of E2s. Each representative E2 protein is as following: Class I-UbcH7 (PDB code: 1FBV); Class II- UbcH10 (PDB code: 1I7K); Class III- CDC34 (PDB code: 3RZ3) and Class IV- BIRC6 (PDB code: 3CEG). All E2 proteins have a conserved Ubc domain (detail in the text).

- ***Interaction surfaces of the E2s***

Functions and mechanism of E2s have been described (Wenzel et al., 2011) that suggest the entire surface of E2 is involved in protein-protein interactions (Figure 1-6). The canonical E2-mediated interactions include the following (Figure 1-6): the H1/L4/L6 motif of the E2 Ubc domain is responsible for the E3 interaction (in region A) (Zhang et al., 2005), and the H1/L1/L2 motif is the E1-binding site (in region B) (Huang et al., 2005). The E1- and E3-binding sites on the E2 surface overlap. The active site cysteine residue is responsible for the formation of a thioester bond with ubiquitin (in region C) (Sakata et al., 2010). Recently, many non-canonical E2-interactions have been observed, for example, the backside of an E2 is found to interact with ubiquitin or sumo molecules (in region D) (Brzovic et al., 2006). The C-lobe of a sumo E2 (Ubc9) is found to bind the substrate RanGAP1 (in region E) (Reverter & Lima, 2005).

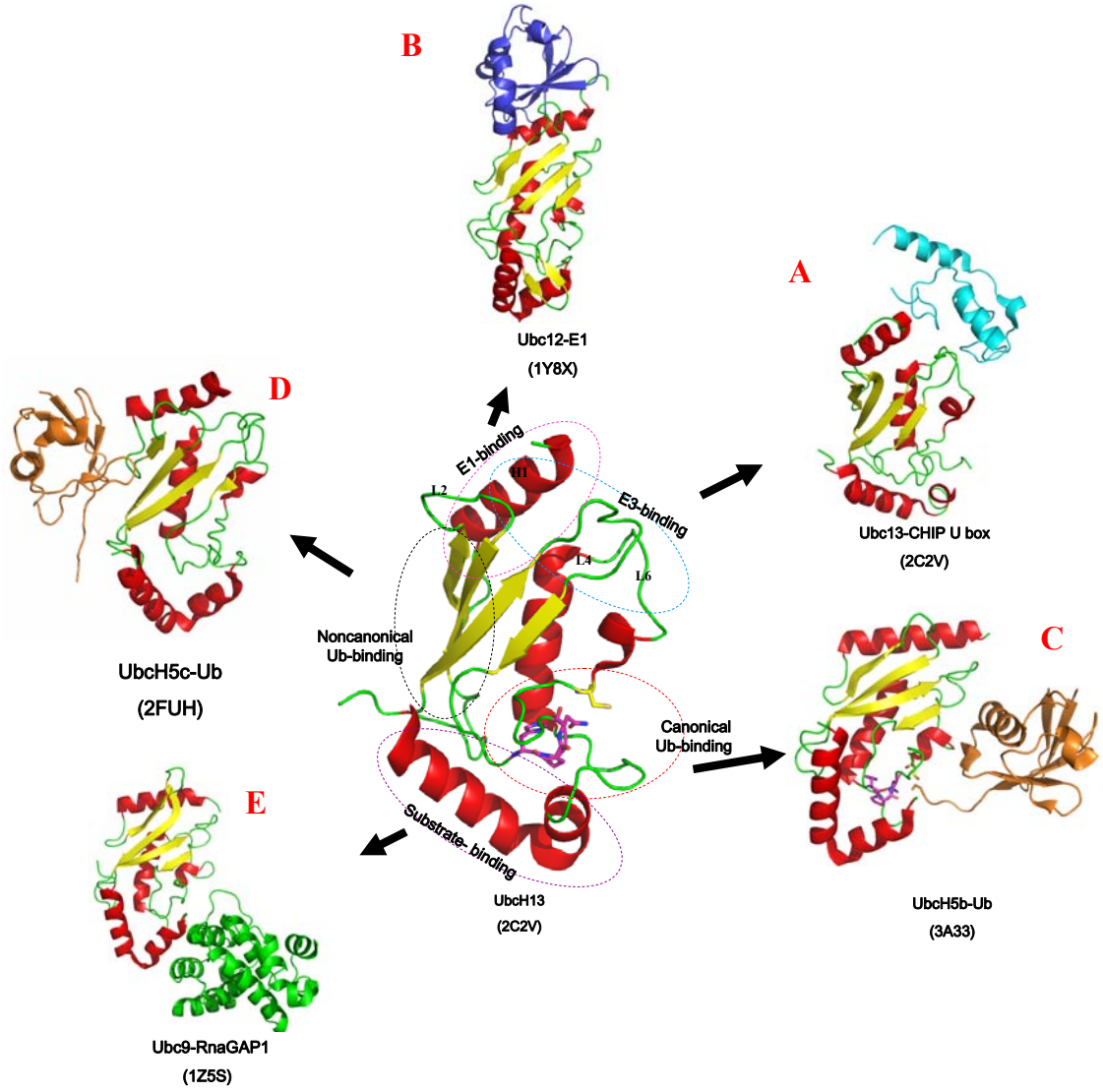

Figure 1-6: E2s and the E2-partners. Each motif on the E2 surface responsible for the interaction with a distinct binding partner is shown. Canonical E2-mediated interactions are presented as below: the E2-E3 complex is shown in the Ubc13-CHIP U-box complex (region A); the E1-E2 complex is seen in the Ubc12-E1 complex (region B); the E2-Ub covalent conjugate is seen in the UbcH5b-Ub complex (region C). Noncanonical E2-mediated interactions are seen in the noncovalent UbcH5c-Ub complex (region D) and the Ubc9-RanGAP1 (region E) complex.

1.1.4 E3: Ubiquitin protein ligase

In the ubiquitination pathway, E3s coordinate the interactions of multiple proteins. The function of E3 ligase in the ubiquitination system involves in the binding of E2 protein to transfer the ubiquitin to its substrate. E3s can also ubiquitinate themselves (autoubiquitination) by adding ubiquitin to their own lysine residues. E3s are involved in the binding of charged E2 (Ub-E2), the binding of the substrate, the transfer of Ub to the substrate, and the covalent ligation of one or more Ub(s) to the lysine residue of the substrate (Deshaies, 1999; Deshaies & Joazeiro, 2009; Kamadurai et al., 2009).

Productive ubiquitination depends on the efficient interactions of the E3 and its cognate E2 in addition to those with substrate. Many studies have found that E2 or E3 are modified and regulated by additional factors before ubiquitination is induced (Deng et al., 2000; Hofmann & Pickart 1999; Lahav-Baratz et al., 1995; Rajapurohitam et al., 1999). For example, the binding of a small molecule can allosterically regulate E3 function (Worrall et al., 2009). One of the most common mechanisms is phosphorylation (Feldman et al., 1997; Skowyra et al., 1997; Yaron et al., 1998). The interaction of the E3-substrate regulated via phosphorylation is coupled with the activity of cyclin-dependent kinase (CDK), which mediates the cell cycle (Deshaies, 1999; Koepp et al., 1999; Page & Hieter, 1999).

A large number of E3s have been found and have been grouped into distinct families dependent upon the characteristics of their domains, including HECT domain, PHD domain, U-box/RING domain and multisubunit SCF domain (Deshaies, 1999; Huibregtse et al., 1995; Loricke et al., 1999). Sequences or structures of those distinct E3s families are unrelated (Borden, 2000; Huang et al., 1999; Zheng et al., 2000). The mechanisms of E3-mediated ubiquitination are distinct (Figure 1-7): the HECT domain E3s mediate covalent catalysis for ubiquitin transfer (Huibregtse et al., 1995) and the RING/U-Box and SCF E3 acts as scaffolds for the transfer of ubiquitin to the substrate (Ardley & Robinson, 2005; Deshaies & Joazeiro, 2009).

(A)

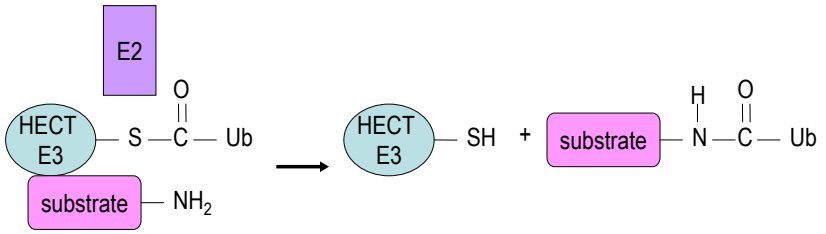

(B)

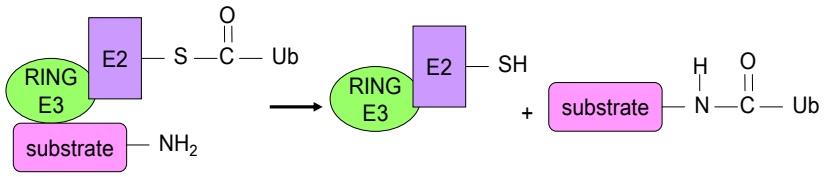

Figure 1-7: Two types of E3-mediated ubiquitination mechanisms. (A) HECT domain E3-mediated and (B) RING/U box domain or PHD domain E3s-mediated ubiquitination.

1.1.4.1 HECT domain E3

One family of the E3s is the HECT domain family (homologous to E6-AP carboxyl terminus), that consists of ~ 350 residues. There are many HECT domain E3s, such as E6-AP, Ras5, Itch and Toml (Beaudenon et al., 1999; Huibregtse et al., 1997; Qui et al., 2000; Saleh et al., 1998; Scheffner et al., 1993). The HECT domain E3s often consist of several sub domains (Figure 1-8): the unique N-terminal domain (N-lobe) is for the binding of specific substrate(s), while the C-terminus (C-lobe) is for mediation of covalent catalysis with the Ub-E2 conjugate and processing the ubiquitination (Huibregtse et al., 1993; Kumar et al., 1999). One of the significant features of the HECT domain is that a strictly conserved cysteine residue is located ~35 residues upstream of the C-terminus (C-lobe) (Huibregtse et al., 1995; Kamadurai et al., 2009). The mechanism of HECT E3s-mediated ubiquitination is through covalent catalysis: the formation a thioester intermediate of the conserved cysteine residue on HECT E3s with the activated ubiquitin on E2 (Huibregtse et al., 1995) (Figure 1-7A), followed by the ubiquitin being transferred to the substrate. Previous reports have shown that the cognate E2s of all HECT domain E3s are Ubc4, UbcH5, UbcH7 or UbcH8 (Duncan et al., 2000; Huang et al., 1999; Huibregtse et al., 1997; Kumar et al., 1997; Nuber et al., 1996).

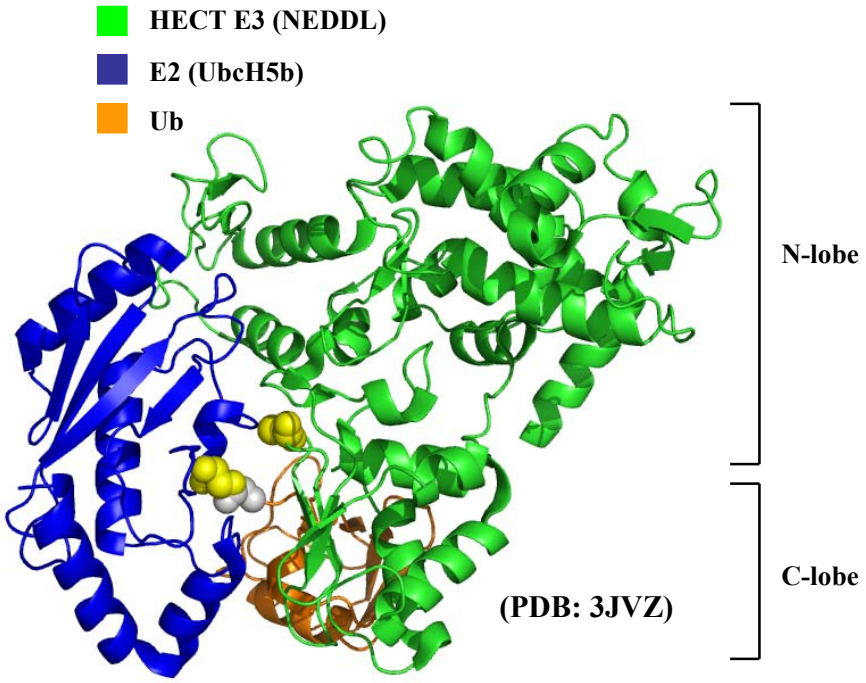

Figure 1-8: The structure of the Ub-UbcH5a-HECT (NEDD4L) complex. Active residue, Cys 922 (NEDD4L HECT domain), and active site Cys85 (UbcH5b) are coloured in yellow spheres. Both cysteine residues are responsible for the interaction with the glycine of ubiquitin. Ubiquitin Gly76 is depicted in gray spheres. (PDB code: 3JVZ) (Kamadurai et al., 2009).

1.1.4.2 RING domain E3s

One dominant family of the E3s are proteins with a **RING** finger domain (**R**eally **I**nteresting **N**ew **G**ene). RING finger domains have a set of cysteine and histidine residues which coordinate two zinc ions in a cross-brace structure and form a characteristic globular conformation (Borden, 2000; Loricke et al., 1999). Unlike the HECT domain E3s, the RING domain E3s act as scaffolds to interact with E2s and bring the ubiquitin closer to the substrate (Figure 1-7B) (Borden, 2000; Joazeiro & Weissman, 2000). Compared to the HECT domain E3s, the RING E3s can autoubiquitinate and this mechanism plays an important role in the down-regulation of E3 to maintain normal physiological function (Fang et al., 2000; Joazeiro & Weissman, 2000; Lorick et al., 1999). RING-type E3s are modular: the RING domain interacts with the E2 and facilitates the ubiquitination of the substrate, other subunits within the proteins are responsible for the binding of the substrate. Hundreds of RING finger proteins have been found and are implicated in different cellular functions (Deshaies, 1999; Joazeiro & Weissman, 2000). It is not clear whether all RING finger proteins have E3 ligase activity; however, a large number of RING finger proteins are E3

ligases, including single-subunit E3s such as c-Cbl-1, cIAP2, MDM2 (Mace et al., 2008; Kostic et al., 2006; Zheng et al., 2000) and multiple subunit E3s such as SCF E3 ligase, VCB E3s (Deshaies, 1999; Page & Hieter, 1999; Tyers & Jorgensen, 2000; Wei & Sun, 2010). The distinct features of these two types of the RING E3s are described as bellow.

- ***Multiple-subunit E3s***

The multiple-subunit E3s, such as the SCF E3s (Skp1-Cullin-F-box protein), the VCB E3s and the APC E3s, consist of several proteins, including an essential small RING E3 protein Rbx1 (approximately 100 residues) (Deshaies, 1999; Page & Hieter, 1999; Tyers & Jorgensen, 2000). In the scaffold model of the SCF E3s or the VCB E3s, Rbx1 plays a critical role to coordinate the Fbox protein/Cul1/E2-Ub (in the SCF E3s) and pVHL/Cul2/E2-Ub (in the VCB E3s) (Figure 1-9) (Kamura et al., 1999; Skowyra et al., 1999).

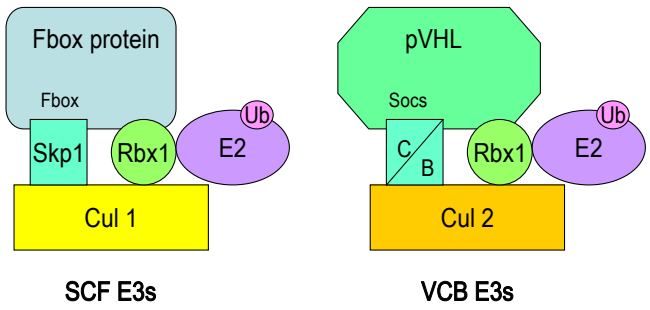

Figure 1-9: Multi-subunit E3s architecture. SCF E3s contain an Fbox Protein, Skp1, Cul1 and Rbx1. VCB E3s including pVHL, Cul2, Elo C/B and Rbx1. Rbx1 plays a role in the co-ordination with E2 proteins and other proteins to become active E3s. Fbox and pVHL are responsible for substrate-binding.

- ***Single-subunit E3s: RING/U-box E3s***

Single-subunits E3s are modular: one subunit is the RING or U-Box domain, other subunits are responsible for substrate binding. The fold of a RING-type E3 ligase is a unique cross-brace zinc-binding scheme (Figure 1-10), for example MDM2 (Linke et al., 2006; Kostic et al., 2006; Haupt et al., 1997), c-Cb1 (Zheng et al., 2000), IAPs (Mace et al., 2008). The U-Box domain adopts a similar conformation to that of the RING domain (Figure 1-10), for example CHIP U-Box (Zhang et al., 2005). One significant difference is that stabilisation of the conformation of the U-box is provided by electrostatic and hydrophobic interactions (Zhang et al., 2005). Many single-subunit E3s often interact with a partner protein and form

a heterodimer or homodimer, such as MDM2 homodimer, MDM2/MDMX heterodimer (Kubbutat et al., 1997; Haupt et al., 1997; Stad et al., 2000), c-Cbl homodimer (Waterman et al., 1999), BARD1/BRCA1 (Brzovic et al., 2001), Bmi-Ring1b heterodimer (Buchwald et al., 2006) and inhibitors of apoptosis (IAPs) homodimer (Mace et al., 2008). Dimerisation interactions of the MDM2/MDMX dimer (PDB: 2VJE) were contributed by β3 and the C-terminal residues of one monomer with the β2 of the other monomer (Linke et al., 2008). Other RING-type E3 ligases, such BRCA1-BARD and Bmi-Ring1b, form heterodimers through their N-and/or C-terminal helices preceding the RING domains (Brzovic et al., 2001; Buchwald et al., 2006).

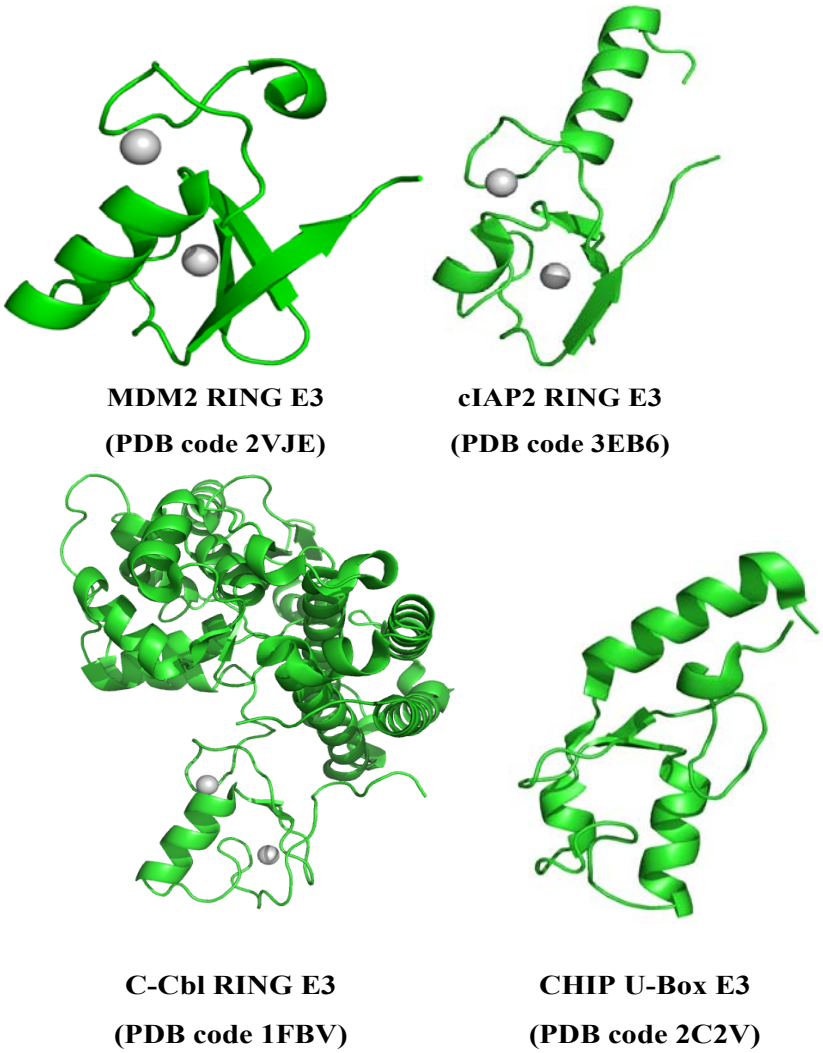

Figure 1-10: Single subunit RING/U-Box E3s. MDM2, cIAP2 and c-Cbl are RING E3s, and two zinc ions (gray spheres) play roles in stabilising the conformation of the RING domain. CHIP U-Box E3 has a similar architecture stabilised by hydrophobic interactions.

1.1.5 MDM2 E3 ligase is a oncoprotein

1.1.5.1 Biological roles of MDM2

- ***MDM2 –related diseases***

MDM2 (murine double minute 2) is a well characterised oncoprotein that regulates the level of p53 through transrepression and ubiquitination (Grier et al., 2006; Iwakuma & Lozano, 2003; Ko & Prives, 1996; Momand et al., 1992; Oliner et al., 1993). MDM2 transrepresses p53 by binding to the transactivation domain of p53 and inhibits p53-mediated transcription, resulting in the disruption of cell cycle arrest or apoptosis (Shmueli & Oren, 2004; Stommel & Wahl, 2004; Yang et al., 2004). MDM2 also regulates p53 through its E3 ligase activity ubiquitinating p53 for further proteolysis (Brooks. & Gu, 2006; Honda & Yasuda, 2000). It has been demonstrated that amplification of the MDM2 gene is observed in human tumours that contain wild type p53 (Juven-Gershon & Oren, 1999; Momand et al., 1998), overexpression of MDM2 induces chromosome instability in tumors that contain wild type p53 (Carroll et al., 1999). It has been found that tumours containing a single nucleotide polymorphism (SNP309) in the MDM2 promotor accelerates SP1-dependent MDM2 transcription, the increased concentration of MDM2 protein results in subsequent attenuation of p53-dependent transcription and apoptosis (Arva et al., 2005; Bond et al., 2004). It has been shown that the level of MDM2 increases in tumour cells, such as soft tissue sarcoma (Bartel et al., 2001; Toledo & Wahl, 2006). Furthermore, many tumours contain alternatively spliced MDM2 variants including human breast, ovarian, bladder and astrocytic neoplasms tumours, and those MDM2 variants lack the p53-binding domain (Dang et al., 2002; Hori et al., 2000; Matsumoto et al., 1998; Sigalas et al., 1996).

- ***MDM2-binding partners***

MDM2 proteins also have a number of protein-protein interaction partners, distinct complexes each having their specific biological functions (Daujate et al., 2001; Ganguli & Wasylyk, 2003; Momand et al., 2000). Several reports have demonstrated that the ARF-MDM2 complex promotes p53 stability (Honda & Yasuda, 1999; Sherr & Weber, 2000; Zhang et al., 1998). ARF, a tumor suppressor protein, binds to MDM2 and blocks the nucleo-cytoplasmic shuttling of MDM2 sequestering MDM2 in the nucleolus (Tao & Levine, 1999; Zhang & Xiong, 2001). p300/CBP (CREB-binding protein) acetylates p53 and activates the transactivation function of p53 (Gu & Roeder, 1997). In contrast, it has been described that the MDM2-p300/CBP-p53 ternary complex inhibits p300-mediated acetylation of p53 (Ito et al., 2001; Kobet et al., 2000). In the Ras signaling pathway, Ras

promotes the transcriptional activation of MDM2 (Ries et al., 2000). L11 is also found to bind to MDM2 and sequester MDM2 in the nucleolus (Lohrum et al., 2003). It has been demonstrated that MDM2 is phosphorylated on Ser395 by ATM-mediated phosphorylation and the p53 function is rescued (Maya et al., 2001). Akt kinase can enhance the nuclear translocation of MDM2, and inhibit the interaction of MDM2 with ARF and also promote the MDM2 E3 activity upon the enhancement of the interaction of MDM2 with p300/CBP (Ashcroft et al., 2002; Ogawara et al., 2002; Zhou et al., 2001). It has been demonstrated that Numb (specifying cell fate during development) is degraded by MDM2 (Juven-Gershon et al., 1998; Yogosawa et al., 2003). Androgen receptor protein (AR), a transcription factor, interacts with MDM2RING domain and is ubiquitinated and degraded by MDM2 (Lin et al., 2002). Furthermore, it has been shown that MDM2 also interacts with E2F1 to stimulate cell proliferation (Loughran & La, 2000). MDM2 may also play roles in ribosomal biogenesis and translation regulation in the cell via an interaction with the ribosomal protein, L5 (Elenbaas et al., 1996; Marechal et al., 1994). MDMX (or MDM4), a MDM2 homologue, is also found to regulate p53 (Böttger et al., 1999; Shvarts et al., 1996) and it also has been shown that the MDM2-MDMX heterodimer has stronger E3 activity (Badciong & Hass, 2002; Marine et al., 2007). Many tumours have been found to be related to the overexpression of MDM2, and some contain MDM2 variants and mutated p53. Therefore, MDM2 has become a very exciting and popular drug target in recent years (Shangary & Wang, 2009).

- ***the flexibility of MDM2***

Structural studies show that the binding cleft of the MDM2 hydrophobic domain is flexible and can adapt to the different shapes of the peptides and small molecules with some significant changes seen upon ligand binding (Bowman et al., 2007; Dastidar et al., 2008; Stoll et al., 2001; Wallace et al., 2006; Vassilev et al., 2004). There is dynamic communication between each domain to determine its substrate binding and ubiquitination ability (Nicholson & Hupp, 2010; Schon et al., 2004). Recent studies also describe that MDM2-dependent transrepression activity can be mediated by RING-mediated allosteric modulation (Poyurovsky et al., 2003; Shimizu et al., 2002; Wawrzynow et al., 2009). Mutations in the RING domain of MDM2 that disrupt zinc coordination have a higher affinity for the BOX-I transactivation domain of p53 and transrepression of p53 function (Wawrzynow et al., 2009).

1.1.5.2 Composition of modular MDM2

MDM2 is a RING-type E3 protein. Similar to the canonical RING-E3 ligase proteins, MDM2 is also a modular protein which interacts with its cognate E2 and binds to the substrate. MDM2 is 491 amino acids long and is a multi domain protein (Figure 1-11) composed of the following: a lid region (residues 16-23), a hydrophobic pocket (residues 29-128); a nuclear localization signal (NLS) (residues 181-185), a nuclear export signal (NES) (residues 191-199), an acidic domain (200-299); a zinc-finger domain (300-332), a nucleolar localisation signal (NoLS) and the C-terminal RING domain (residues 438-478). Each domain has its own function and binding partners as shown in Figure 1-12.

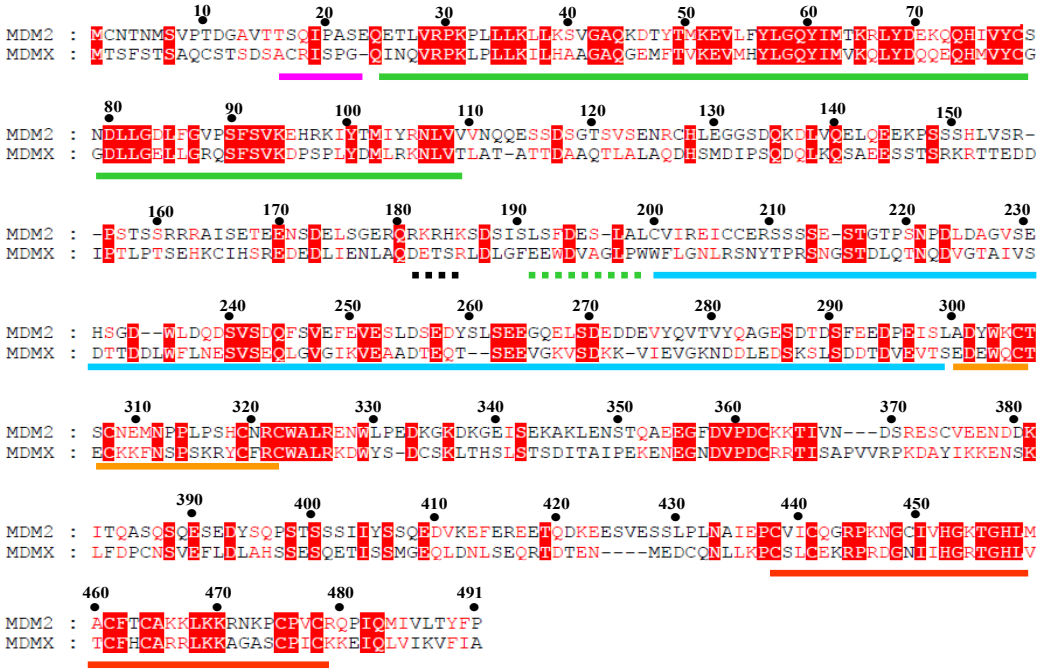

Figure 1-11: Sequence alignments of MDM2 and its analogous protein, MDMX. Identical residues are shown in letters enclosed in filled red boxes. The numbering and distinct domains above the alignments correspond to the MDM2 sequence. Hydrophobic domain marked with green bar, lid motif (pink bar), the nuclear localization signal (black dashed bar), the nuclear export signal (green dashed bar), acidic domain (cyan bar), zinc finger domain (orange bar) and RING domain (red bar).

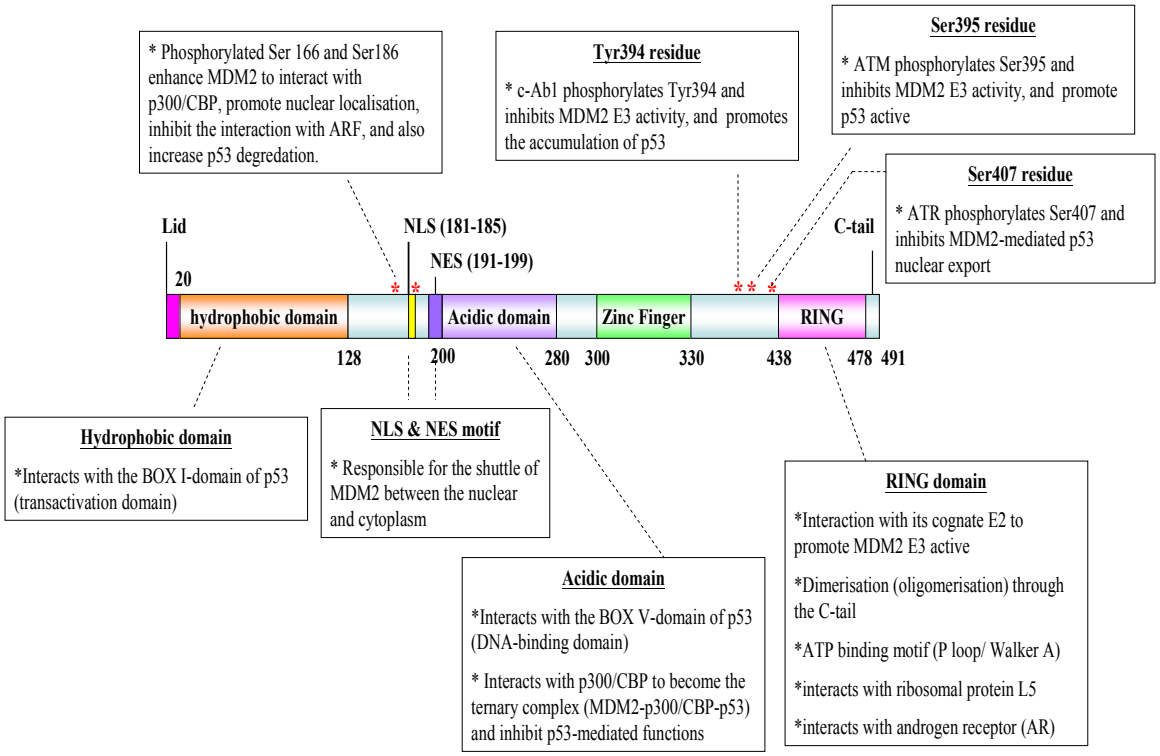

Figure 1-12: Schematic representations of modular MDM2. Each domain on MDM2 interacts with different binding partners and plays different roles in cellular regulation.

- ***MDM2 hydrophobic domain***

The hydrophobic pocket at the N-terminus of MDM2 is formed by residues 25-109, there is a deep groove formed by 14 aromatic and hydrophobic residues (Kussie et al., 1996). This deep groove plays a critical role in interactions with the BOX-I transactivation domain of p53 (Chi et al., 2005; Kussie et al., 1996; Schon et al., 2002; Schon et al., 2004). Biochemical studies have confirmed that this MDM2-p53 interaction is essential for the transrepression of p53 and disruption of the p53-dependent transcriptional machinery (Oliner et al., 1993; Stommel & Wahl, 2005; Thut et al., 1997). Crystallography data shows that an amphiphatic p53 α-helix peptide (residues 17-29) binds into the deep cleft on the N-terminal hydrophobic domain of MDM2 (Figure 1-13) (Kussie et al., 1996). Especially, p53 residues (F19/W23/L26) provide significant interactions with MDM2. Site-directed mutagenesis experiments reveal that mutations of the above residues reduce the binding affinity of p53 to MDM2. Because the p53-MDM2 interaction shows a tight "lock and key" configuration (Kd from 50 to 500 nM) (Schon et al., 2002), a large number of anti-p53-dependent cancer drugs are designed to disrupt the p53-MDM2 interaction (Hu & Hu, 2008; Shangary & Wang, 2009; Tovar et al., 2006; Vassilev et al., 2004).

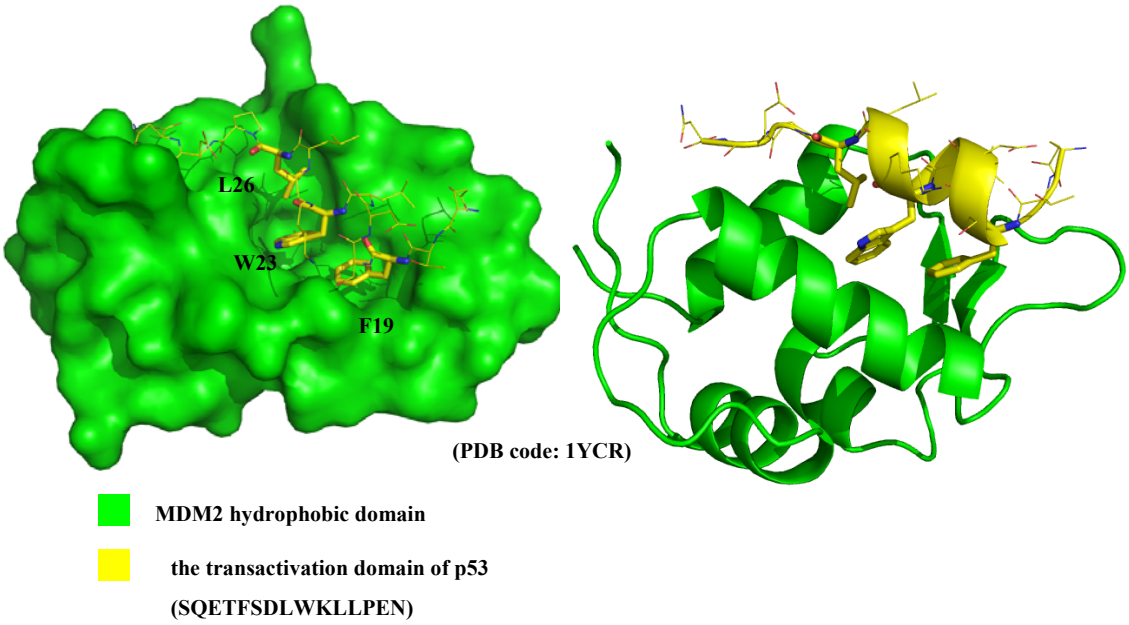

Figure 1-13: The structure of the MDM2-p53 complex. The hydrophobic domain of MDM2 is shown in green and the transactivation domain of p53 is shown in yellow (PDB code: 1YCR). Three critical residues (F19/W23/L26), which provide major interactions to the residues around the cavity of MDM2 hydrophobic domain, are depicted in sticks.

- ***MDM2 Lid motif, NLS, & NES***

There is a PI3-kinase-like phosphorylation site at Ser17 on the lid motif (or pseudosubstrate motif, aa 16~23) of MDM2 (Mayo et al., 1997). The MDM2 lid motif plays a critical role in the control of the "open-close switch" conformation to favour/inhibit the binding of the p53 into the MDM2 hydrophobic groove in a phosphorylation-dependent manner (Uhrinova et al., 2005; Worrall et al., 2010). Biochemical studies and a quantitative fluorescence-based dye binding assays show that MDM2 phosphomimetic mutant, S17D, opens the lid over the MDM2 hydrophobic groove, stabilising the p53-MDM2 interaction (McCoy et al., 2003; Worrall et al., 2009; Worrall et al., 2010). The nuclear localisation signal (NLS) and nuclear export signal (NES) play roles in the transportation of MDM2 and MDM2-bound p53 in the cytoplasm or nucleus to regulate MDM2 and p53 functions (Freedman & Levine, 1998; Roth et al., 1998).

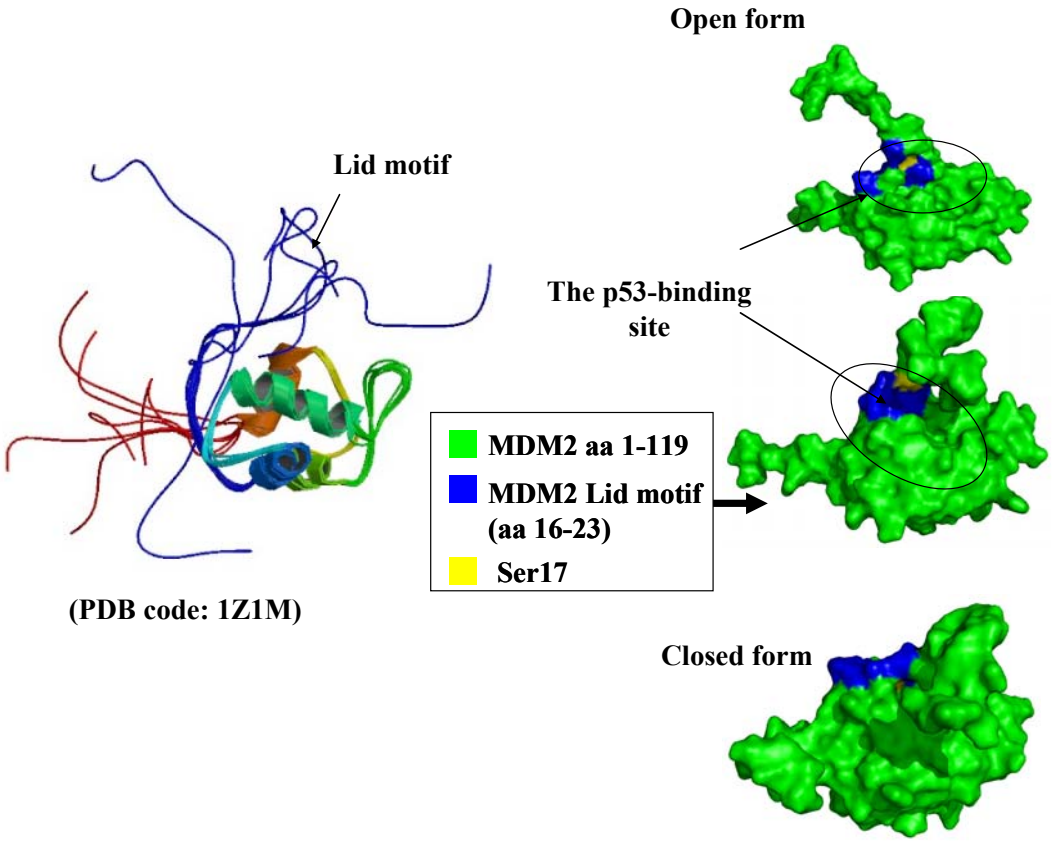

Figure 1-14: Structure of MDM2 flexible Lid motif. Left panel: NMR structure of MDM2 N-terminal domain (PDB: 1Z1M) reveals that the flexibility of MDM2 lid motif (blue line). Right panel: Distinct MDM2 lid conformations (open/close) are shown presented in surface representations, the p53-binding site is highlighted by a black circle, the lid motif is coloured in blue and Ser17 is depicted in yellow.

- ***MDM2 acidic domain***

The acidic domain of MDM2 interacts with the BOX-V peptide derived from the DNA binding domain of p53 (Wallace et al., 2006). MDM2 acidic domain is critical for the poly-ubiquitination of p53 (Argentini et al., 2001; Meulmeester et al., 2003). MDM2 lacking the acidic domain that overlap that overlaps the p300/CBP-binding domain can monoubiquinate p53, but fail to degrade p53 (Zhu et al., 2001). This domain is quite flexible, and as yet no structure has been published.

- ***MDM2 C4 zinc finger domain***

The X-ray structure of MDM2 C4 zinc-finger domain has been solved (PDB code: 2C6A) and it has been shown that this domain plays a critical role in the inhibition of cell growth and in the regulation of Gl cycle arrest (Brown et al., 1998; Yu, et al, 2006). This domain

adopts a compact globular zinc ribbon conformation, four residues (Cys305, Cys308, Cys319 and Cys322) interact with a single zinc ion to maintain the integrity of this domain (Figure 1-15). In follicular lymphomas and liposarcomas, missense mutations in the MDM2 C4 zinc finger domain have been found to be Cys305Phe and Cys308Tyr, respectively (Schlott et al. 1997; Tamborini et al. 2001). These mutants may be responsible for effects seen on the overall stability of the protein.

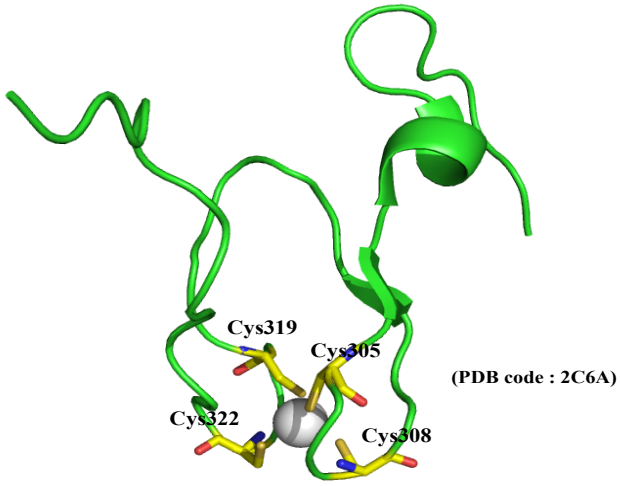

Figure 1-15: MDM2 C4 zinc finger domain (PDB: 2C6A). Four cysteine residues, Cys305, Cys308, Cys319, and Cys322 (shown as yellow sticks) co-ordinate with zinc. The single zinc ion is shown as a white sphere.

- ***MDM2 RING domain***

MDM2 has a RING-type E3 ligase domain, of approximately 60 residues, which is found at the C-terminal zinc-binding domain (Boddy et al., 1994; Fang et al., 2000). Similar to other RING domain E3s, MDM2RING has a compact ββαβ fold, a small hydrophobic core, and contains two essential zinc ions (Figure 1-16). In recent years, structures of both the MDM2 homodimer (PDB code: 2HDP) and MDM2-MDMX heterodimer (PDB code: 2VJE) have been published (Kostic et al., 2006; Linke et al., 2008). Both structures show that each subunit of the MDM2-MDM2 homodimer or MDM2-MDMX heterodimer coordinates two zinc ions in a sequential manner and in an anticooperative binding mode. The conformation of each MDM2 RING subunit is stabilised by the two zinc ions in a C2H2C4 cross-brace zinc binding topology: one C4 zinc binding site (C438C441C461C464) and one H2C2 zinc binding site (H452H457C475C478). The MDM2 RING domain also contains an RNA-binding motif and it has been found that addition of RNA stimulates ubiquitination (Elenbaas et al., 1996; Lai et al., 1998). It has been noted that MDM2 contains an ATP binding motif

(448GCIVHGKT455), Walker A or P loop, which plays a role in intracellular localisation, and ATP-dependent chaperone activity and also mediates the tetramerisation of p53 (Poyurovsky et al., 2003; Stevens et al., 2008; Wawrzynow et al., 2007). ATP-bound MDM2 is preferentially localised in the nucleolus, and one MDM2 mutant (K454A) results in the upregulation E3 ligase actitivty promoting the degradation of p53 (Poyurovsky et al., 2003). The last eight residues at the MDM2 C-terminus (Figure 1-16) have been found to be essential for dimerisation (Boddy et al., 1994; Fang et al., 2000; Kostic et al., 2006; Linke et al., 2008).

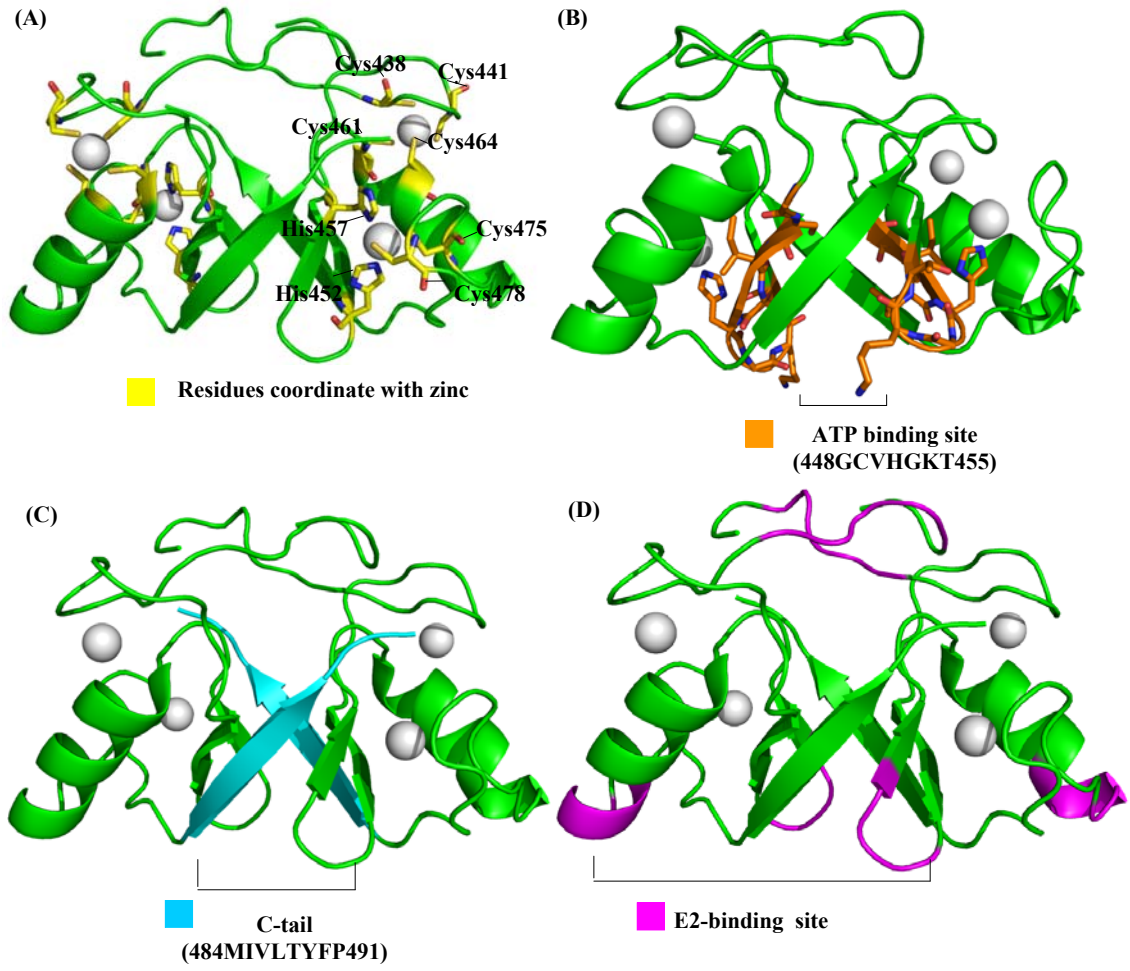

Figure 1-16: Crystal structure of dimeric MDM2 RING domain, residue 432-491, (PDB code: 2HDP). (A) Residues coordinate with zinc are highlighted in yellow sticks. (B) Residues located in the ATP-binding site are shown in orange sticks. (C) The C- terminal eight residues (in cyan) are responsible for the dimerisation. (D) Residues located in the E2-binding site are highlighted in magenta. Zinc ions are shown as grey spheres.

1.1.6 Tumour suppressor protein: p53

1.1.6.1 Biological roles of p53

p53 is a tumour suppressor protein that functions to protect cells from malignant transformation (Lane, 1992; Levine, 1997; Vogelstein et al., 2000; Vousden & Prives, 2009). In more than 50% of human cancers, p53 is found to be mutated and inactivated (Hollstein et al., 1994). p53 regulates cell cycle arrest and apoptosis through post-translational modifications of p53 to induce p53-dependent gene expression (Krummel et al., 2005; Xu, 2003). Those p53-responsive genes express proteins involved in numerous signal transduction pathways (Figure 1-17). A number of reports have noted that the mechanisms of p53 activation are regulated by several post-translational modifications: ubiquitination, phosphorylation, acetylation, sumolyation, neddylation, and methylation (Brooks & Gu, 2003; Brooks & Gu, 2006; Chuikov et al., 2004; Fraser et al., 2010; Rodriguez et al., 1999; Xirodimas et al., 2004). Tumour suppressor protein, p53, behaves as a specific DNA-binding protein or transcription factor regulating those genes that mediate DNA amplification, cell cycle arrest, apoptosis, and cellular senescence when cells are damaged (Ashcroft et al., 2000; Harris & Levine, 2005; Vogelstein et al., 2000; Vousden & Lu, 2002).

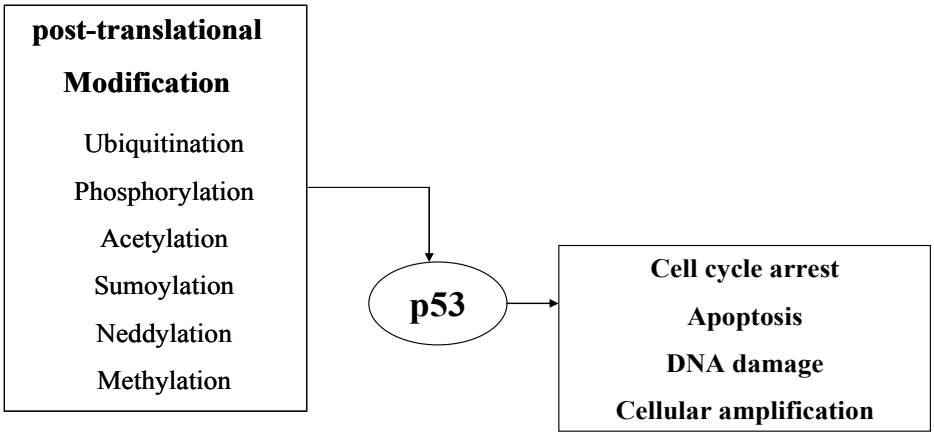

Figure 1-17: Biological roles of p53. p53 is regulated by several modifications, for example ubiquitination, phosphorylation, acetylation, sumolyation, neddylation and methylation. p53 also is responsible for several tasks including cell cycle arrest, apoptosis, DNA damage and cellular amplification.

- ***p53-binding partners***

There are two core mechanisms to control the level and function of p53 in stressed cells (Table 1-3): positive regulation (stabilisation or stimulation of translation) and negative regulation (repression of the transcription or ubiquitination/ degradation) (Dornan & Hupp, 2001; Lu, 2005; Toledo & Wahl, 2006; Lavin & Gueven, 2006). For DNA damage responses, positive regulation to mediate p53 is through its transcriptional coactivator, p300/CBP to stimulate DNA-dependent mediated acetylation (Brooks & Gu, 2003; Shimizu& Hupp, 2003) and activating gene expression by forming a complex with chromatin remodelling factors (Barlev et al., 2001; Dornan et al., 2003). Moreover, activation of p53-mediated transcriptional regulation of various genes involved in apoptosis or cell cycle arrest is controlled by an ATM-CHK2-depedent pathway (Banin et al., 1998; Ljungman & Lane, 2004; Meek, 2004; Shieh et al., 2000). Numerous studies have showed that ARF ($p14^{ARF}$ in humans and $p19^{ARF}$ in mouse) can induce p53 upon the inhibition of MDM2 activity (Kamijo et al., 1998; Pomerantz et al., 1998; Sherr, 2001; Zhang et al., 1998; Zhang & Xiong, 2001). Furthermore, several ribosomal proteins, such as L11 and L23, stabilise p53 by inhibiting MDM2 activity (Dai et al., 2004; Zhang et al., 2003). Ribosomal protein, L26 stimulates the translational expression level of p53 upon binding to the 5'-untranslated region of p53 (Takagi et al., 2005). HAUSP (the herpes virus-associated ubiquitin-specific protease), one of DUBs (deubiquitin enzymes), stabilises p53 and promotes p53-mediated apoptosis and cell cycle arrest (Li et al., 2002; Li et al., 2004; Hu et al., 2002). p53 function is negatively regulated by a number of E3 proteins, including MDM2, COP1, Pirh2, and ARF-BP1 (Brooks & Gu, 2006; Chen et al., 2005; Dornan et al., 2004; Ghosh et al., 2003; Leng et al., 2003). These complicated and delicate protein-protein interactions provide evidence for the hypothesis that cellular proteins can exist in distinct combinations under different environmental conditions.

Table 1-3: Positive and negative regulators of p53.

Positive regulators of p53	Negative regulators of p53
p300/CBP	MDM2
ATM-CH2 depedent pathway	MDMX
ARF	COP1
Ribosome protein (L11/L23/L26)	Pirh2
HAUSP	ARF-BP1

* Only some regulators of p53 are listed here.

1.1.6.2 The interactions between MDM2-p53

MDM2 is the predominant oncogenic E3 ligase for p53. MDM2 mediates the abundance of p53 in the cell through several protein-protein interactions (Figure 1-18): (1) MDM2 acts a transrepressor to mediate p53-mediated transcription through the binding of the N-terminal hydrophobic domain (Hy) of MDM2 to the transactivation domain (BOX-I domain, Thr^{18}-Asp^{29}) of p53 (Momand et al., 1992; Oliner et al., 1993; Shimizu and Hupp, 2003). It has been shown that disruption of the interaction between the hydrophobic domain of MDM2 and the BOX-I activation domain of p53 can rescue p53 function (Dornan & Hupp, 2001; Lin et al., 1994; Liu et al., 2001). (2) The acidic domain interacts with the DNA binding domain (BOX-V) of p53 (Shimizu et al., 2002; Wallace, et al., 2006). A peptide derived from the S9-S10 linker region in the DNA-binding domain of p53 is able to inhibit the ubiquitination of p53 by MDM2 (Shimizu et al., 2002). (3) MDM2 is a RING–type E3-ligase that ubiquitinates p53 and induces degradation of p53 by the 26S proteasome (Arva et al., 2005; Kubbutat et al., 1997; Haupt et al., 1997; Honda et al., 1997; Michael and Oren, 2003). Furthermore, recent reports indicate that MDM2 acts as an ATP-dependent molecular chaperone to regulate p53 (Burch et al., 2004; Wawrzynow et al., 2007). MDM2 has become an attractive drug target for p53-related cancer therapy by disruption of the p53-MDM2 protein-protein interaction or inhibition of MDM2 E3 ligase activity.

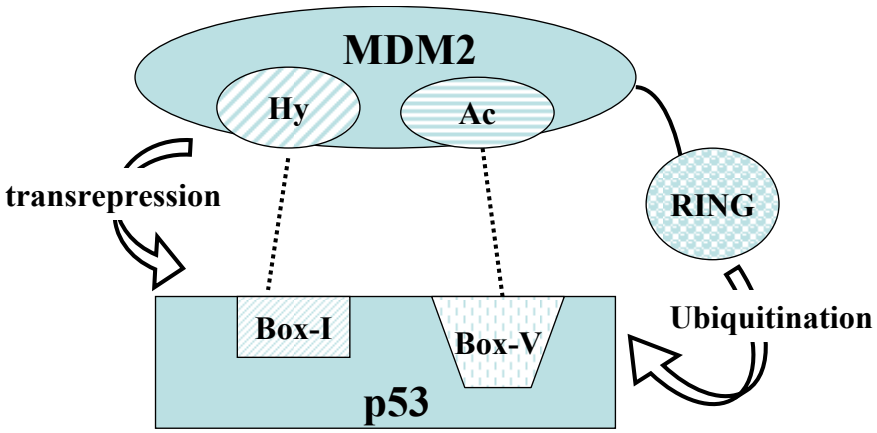

Figure 1-18: MDM2-p53 interactions. Hydrophobic domain (Hy) of MDM2 interacts with the transactivation domain (BOX-I) of p53. Acidic domain (Ac) of MDM2 interacts with the DNA-binding domain (BOX-V) of p53. The MDM2 RING domain is responsible for the ubiquitination of p53.

Part II Antagonists/Agonists of Protein-Protein Interaction

1.2.1 Protein-Protein Interaction (PPI): the challenges

Protein-Protein interactions (PPI) play important roles in biological functions by regulating proteins, such as kinases (protein phosphorylation), proteases (proteolysis), or glycosylases (glycosylation). Recently, PPIs became attractive pharmaceutical targets, after the complete genome sequence became available. However, PPIs are challenging targets for the design of small-molecule inhibitors (Arkin & Wells, 2004; Cochran, 2000; Dömling, 2008; Ma et al., 2003; Teague, 2003) because the majority of PPI interfaces are widely spread over the surfaces of proteins forming a flat interface (Nooren & Thornton, 2003). Historically, small molecules inhibitory for a number of enzymes were designed based upon known bioactive small molecules (neurotransmitters) or ligands. Because the structures of those small molecules are known, they provide a template for the design of new antagonists. However, this approach is not applicable in the case of the majority of PPIs. Drugs that can act as the starting template for the design of small molecules of PPI are rare. One of the few examples is Cyp A/ CsA and FKBP/ FK506, providing the templates for further drug design (Schreiber & Crabtree, 1992; Yang et al., 2007). A major problem is still the difficulty of identifying a druggable site in most PPIs. Numerous mutagenesis experiments and structural studies are used to define the binding interface and verify residues critical for binding in the PPIs, revealing that the binding residues are also often found in discontinuous parts in the protein sequence. For example, with the well characterised E2-E3 protein-protein interaction (Figure 1-6), residues in H1/L4/L6 in E2 interact with residues in E3.

Many reports have shown that a “typical” PPI interface has an approximate surface area of 700 ~ 1600Å and includes approximately 170 atoms, which may be from both main chains and side chains (Lo et al., 1999; Stites, 1997; Jones & Thornton, 1996). At the interface, aromatic residues and arginine residue are often present, and hydrophobic surfaces promote complex formation (Clackson & Wells, 1995). Moreover, hydrogen bonds, salt bridges and van der Waals interactions are also frequently observed in PPIs. The PPI interface is large and it is unlikely that every part of the interface is an ideal site for small-molecule binding.

Drug like molecules have been found to follow the so called “Lipinski’s rules of five” (Lipinski et al., 1997), suggesting that greater drug efficacy will be achieved if molecules have the following properties: (1) The molecular weight is less than 500 Daltons. (2) The

LogP value is less than 5. (3) The molecule has less than 5 hydrogen bond donor. (4)The molecule has less than 10 hydrogen bond acceptors. The ideal pharmaceutical agents would have the following characteristics: few side effects, *in vivo* efficacy, good bioavailability, solubility and no toxicity (Ajay et al., 1998; Bemis & Murcko, 1996; Bemis & Murcko, 1999; Lipinski et al., 1997).

Although a number of PPI antagonists have been developed and are in clinical trials (Dömling, et al., 2000), identifying PPI antagonists is still a very challenging task. There are no universal principles governing the features of PPIs. Some PPI interfaces are more accessible and antagonists can readily bind to these interfaces whereas some PPIs contain surfaces which are buried and therefore not readily accessible. The PPI antagonists developed to date have diverse features (and modes of action) (Figure 1-19). Some antagonists are competitive antagonists which bind to the PPI binding site on the interfaces. For example, Nutlin, one of the best characterised molecules, binds to the hydrophobic domain of MDM2 to interfere with binding of the p53. In some cases, allosteric PPI antagonists bind to other areas remote from the interface, resulting in conformational changes of one protein, thus interfering with the interaction with the partner protein. For example, agonists act as modules to (de)polymerise the tubulin cytoskeleton (Luque & Freire, 2000; Jordan, 2002). *de novo* prediction of a potential druggable site is very difficult and therefore that the design of small molecule inhibitor for PPI is very challenging. However, the study and discovery of small molecule inhibitors of PPIs is important as many PPIs are implicated in tumourognesis.

There are numerous methods to identify the "consensus" characteristics of the "hotspot" (the potential binding site for small molecules), which is comprised of subset of the interface that may provide high binding abilities (Bogan & Thorn, 1998; DeLano, 2002; Ma et al., 2003). For example, crystallisation of proteins with various organic solvents is used to characterise the binding site (Mattos & Ringe, 1996), nuclear-magnetic resonance (NMR) analysis of proteins with a library of small molecules can be used to verify the potential binding motif (Fejzo et al., 1999; Shuker et al., 1996), or computational analysis can be performed to determine the anatomy of cavities in protein pockets in a potential binding site (Liang et al., 1998). Recently, a number of PPI antagonists/agonists have been discovered by combinations of several techniques, including (1) Direct screening methods for PPI antagonists: phage display, and high-throughput screening (HTS) with libraries of small

molecules (Schaffer et al., 2003; Sidhu et al., 2003). (2) Virtual screening methods for PPI antagonists: utilising structural information of the PPI interface generated from structural studies (NMR, X-ray crystallography), and combinations of computational analysis to identify the hotspots on PPI or virtual screening (VS) strategies searching for the potential PPI antagonists (Ma et al., 2003).

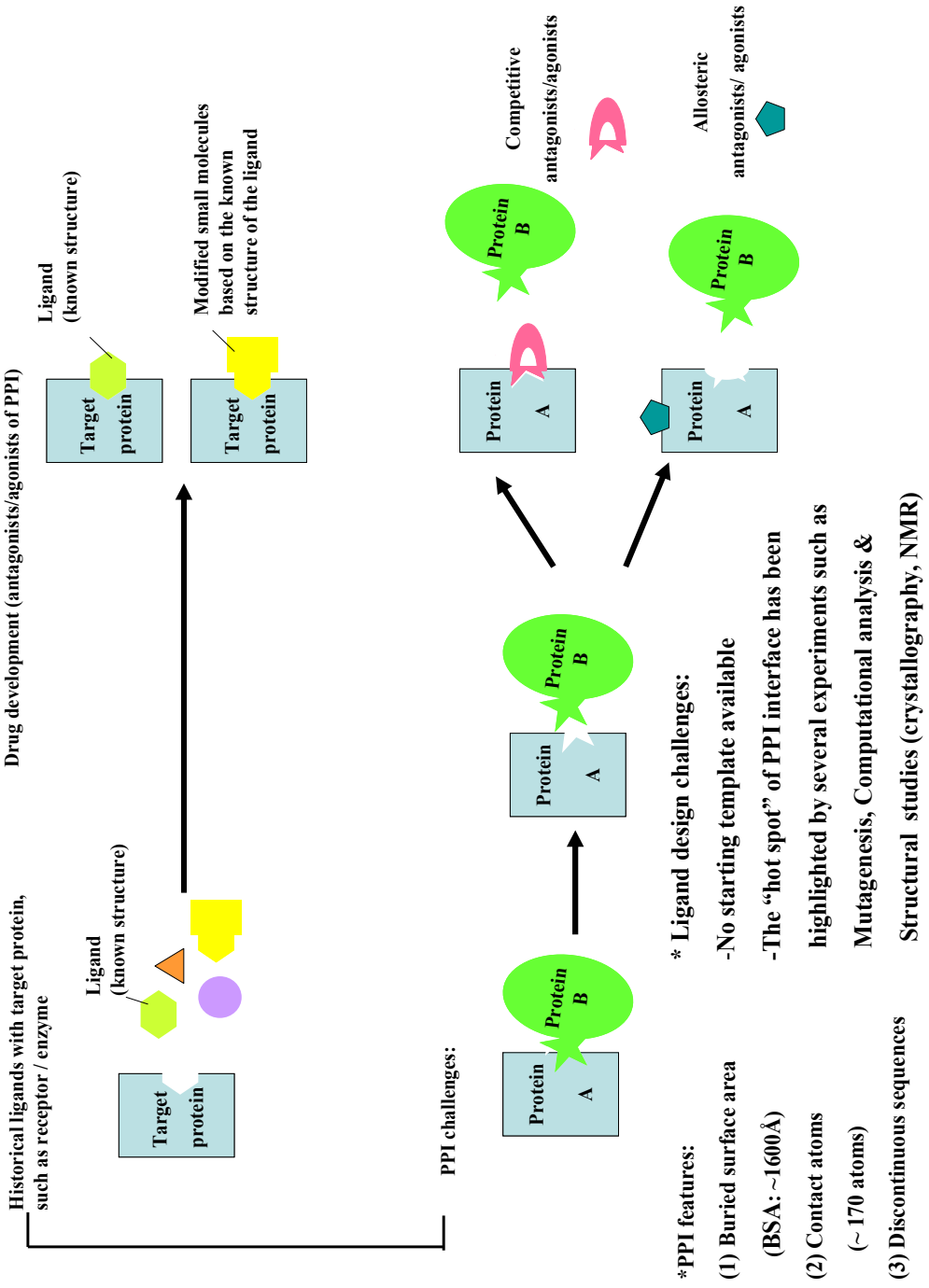

Figure 1-19: Developments and challenges of antagonists/agonists of PPI. Details introduced in the text.

1.2.2 Virtual screening (VS) and database mining approaches

There are various strategies used to identify drug leads, including high throughput screening (HTS) and virtual screening (VS) *in silico*. Numerous studies showed that *in vitro* or *in vivo* HTS methods have a number of straightforward advantages to characterise the effects of small molecules on the target protein. However, HTS methods also have a number of disadvantages including cost and time taken to perform the experiments. VS is a technique which uses simulation methods to predict the characteristics of small molecules or to pre-calculate (estimate) binding affinities between small molecules and the drug target. Compared to high-throughput screening, VS is economical and able to simulate the rational binding modes of selected small molecules from a large chemical database (in our project, millions of compounds) in a short time. VS therefore has many advantages as the first step of drug discovery for PPI antagonists/agonists, since most PPIs lack any template that could be used for the rational design of small molecule inhibitors. After new PPI antagonists/agonists have been selected by VS, their effects can be evaluated by *in vitro* or *in vivo* assays.

The VS approach can be both protein structure-based and ligand-based. Protein structure-based VS approach is based on the knowledge of the target receptor selecting potential ligands that have affinities to the receptor, such an approach is used in our in-house programme, LIDAEUS (Taylor et al., 2008). Ligand-based VS and database mining methods search for new small molecules which might have some of the characteristics required and this approach is used in our in-house programme, UFSRAT.

To date, no known ligand to the MDM2 RING domain has been characterised. To achieve our aims of developing our MDM2/UbcH5a antagonists/agonists, we set up a VS pipeline which combines several programmes including EDULISS, UFSRAT, LIDAEUS, and AutoDock (Figure 1-20) (introduced in more detail in the following section). Several potential small molecules were selected by VS that can affect MDM2-mediated ubiquitination of p53, the first such methods are reported. Results of VS to find MDM2/UbcH5a antagonists/agonists are presented in Chapter 6.

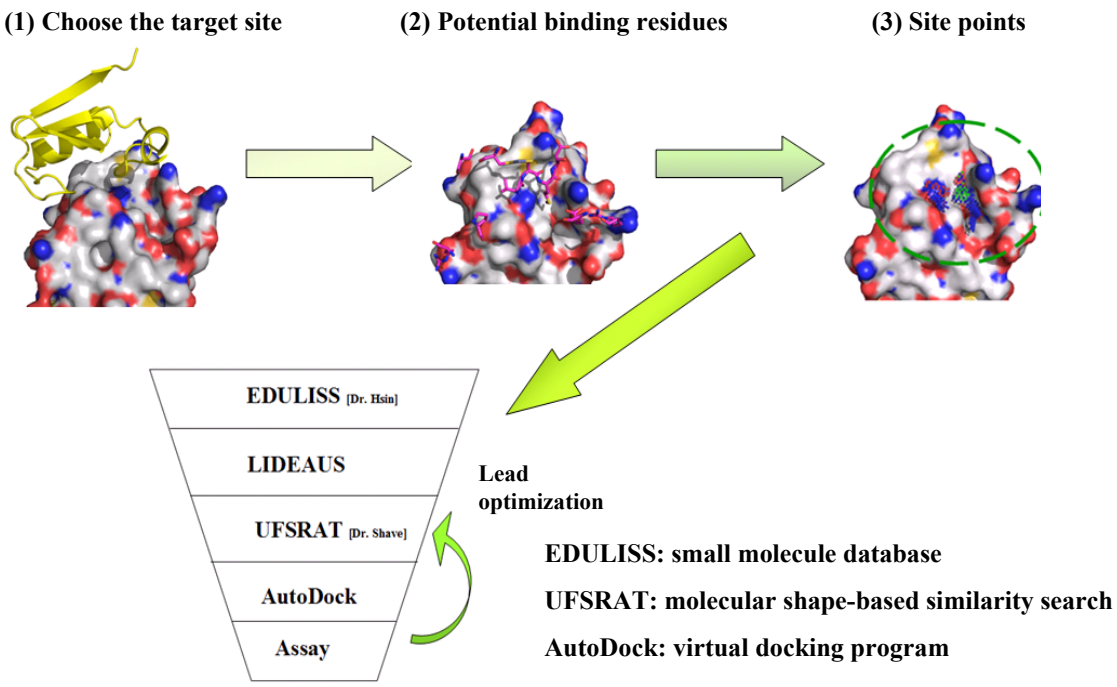

Figure 1-20: The selection process undertaken in virtual screening. Step 1 is to choose the target site of interest. Step 2 is to determine the starting molecule (potential binding residues) that was found to interact with the target site. Step 3 is to create the dots required for simulation on the basis of the distances or/ types of atoms using UFSRAT or LIDAEUS. Step 4 is to start the virtual screening runs, including the EDULISS, LIDAEUS, UFSRAT, AutoDock and biochemical assay. More detail is provided in the text.

- ***EDULISS (EDinburgh University Ligand Selection System)***

EDULISS is a recently developed relational database (http://eduliss.bch.ed.ac.uk/) (Hsin et al., 2011). To date, in EDULISS, there are more than 5 million commercially available compounds sourced from 28 suppliers. Within the database, the following information is available on each compound, including structural, physiochemical, and pharmacophoric properties. EDULISS is a powerful data-mining program because each molecule is stored with its 3D structure along with over 1600 calculated descriptor values (molecular descriptors), such as topology, geometry, physicochemistry and toxicology. EDULISS also stores information on interatomic distances between various atoms in each molecule. This feature is useful for the Interatomic Pharmocophore Profiles (IPP) that defines the characteristics required for the interatomic distance of hydrogen bond donor and acceptor atoms, halogens, phosphorous and sulphur atoms (Hsin et al., 2011). These features are also useful to extract subgroups that have similarly shaped molecules or fit the specific pharmacophore properties required.

As shown in Figure 1-21, in our project those compounds selected conform to Lipinski's rule of five and are readily available from the suppliers, Sigma and Specs.

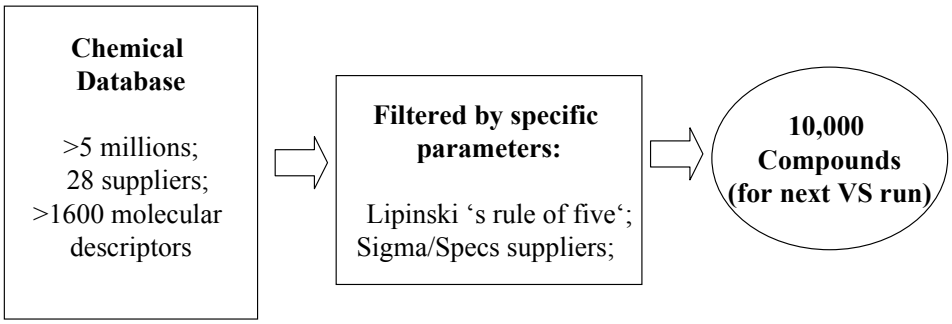

Figure 1-21: The concept of EDULISS. Selections of molecular descriptors, such as Lipinski's rule of 5 or suppliers, act as filters to sieve out potential molecules. One of advantages is to reduce the number of candidate molecules and therefore save computational time in the VS run.

- ***UFSRAT (Ultra Fast Shape Recognition with Atom Types)***

UFSRAT is a ligand-based virtual screening program to search for small molecules on the basis of molecular similarity to known ligands (Developed by Dr. Shave et al., http://opus.bch.ed.ac.uk/ ufsrat/index.php). Molecular similarity is an important concept to biologists and chemists. The overall concept is that similar molecules are supposed to have similar properties and behave in a consistent manner. One significant application of molecular similarity is in rational drug design, especially in medicinal chemistry and in the pharmaceutical industry. Once there is a known binder/ligand, which can be used as a starting molecule, new potential binders may be synthesised by adding or removing chemical groups or atoms from the starting scaffold (Bender & Glen, 2004; Dimasi, 2001).

The concept of UFSRAT is that consideration is given to both shape and atom type descriptors within a molecule (Figure 1-22). In UFSRAT- molecular similarity is important and atoms of certain type in a common position contribute to higher similarity scores. This is important to ensure that similar interactions occur in a candidate molecule as in a query molecule. Each descriptor is assigned a value. Similarity ($0 < \text{score} < 1$) between two molecules is that the values of the geometrical distribution of a candidate molecule against that of the query molecule. UFSRAT had been successfully used in our project (See Chapter 6, the antagonists of MDM2-MDM2 dimerisation) and in addition to the study of inhibitors

of 11β –hydroxysteroid dehydrogenase (11βHSD1) and the immunophilin protein FKBP (FK506 Binding Protein) (Dr. Shave's thesis, 2009).

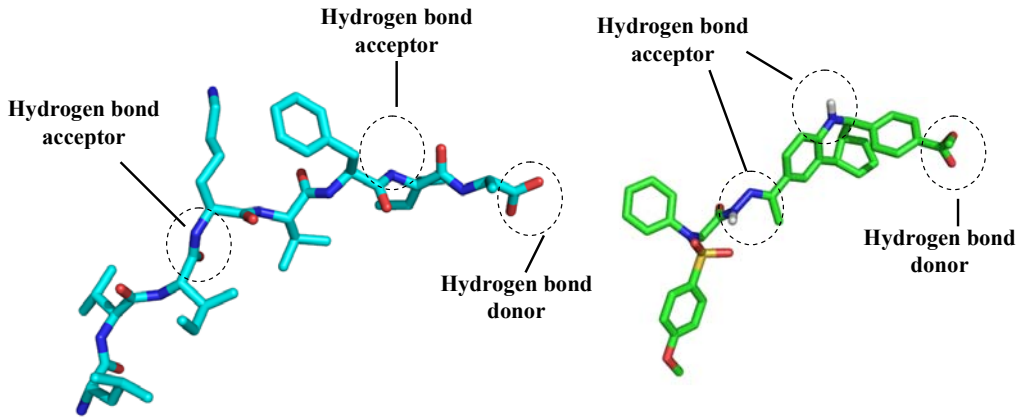

Figure 1-22: A query molecule (blue) and a candidate molecule (green) UFSRAT predicted similarity. Dash circles highlight some atom types in the common positions, presumably contributing to similar interactions with the target. Selected candidate molecules also keep the same atom types as the query molecule. Hydrogen bond donors are coloured in red, hydrogen bond acceptor are coloured in blue.

- ***LIDAEUS (Ligand Discovery At Edinburgh University)***

LIDAEUS is our in-house simulation program which uses a structure-based VS program for the docking and mining of molecules into the target receptor (Dr, Taylor Paul; Shave et al., 2008). LIDAEUS has been successfully used in the study of inhibitors of human cyclophilin-A (CypA) and FKBP (Taylor et al., 2008; Wu et al., 2003). LIDAEUS is a user-oriented, highly adaptable and modular rigid body docking program. Prior to using LIDAEUS, a PDB file of a receptor-ligand complex is required to generate the virtual maps. This map is used to generate the binding pocket and define a set of site points (atoms of a known ligand) that act as a starting template for small molecule similarity screening. The pipeline of LIDAEUS includes the following four steps: Preen, Pose, Score, and Sort (Figure 1- 23). "Preen" defines site points, which are generated by LIDAEUS, and are coloured according to their molecular characteristics: hydrogen bond donors (red), hydrogen bond acceptors (blue) and hydrophobic atoms (white). The site points act as a starting template for the design of small molecules to the target site of interest. "Pose" is a procedure to fit the molecules onto the set of the site points generated in many ways. "Score" is used to estimate the energies of the molecules position that position over the site points in the binding pocket. "Sort" outputs the top scoring ligands on the basis of the simulated binding energies generated in the Score step.

The top scoring ligand candidates are presumed to have similar interactions with the target protein to that of the known ligands, and hence provide another level of selectivity prior to evaluation of the test ligands using biochemical or biophysical analysis.

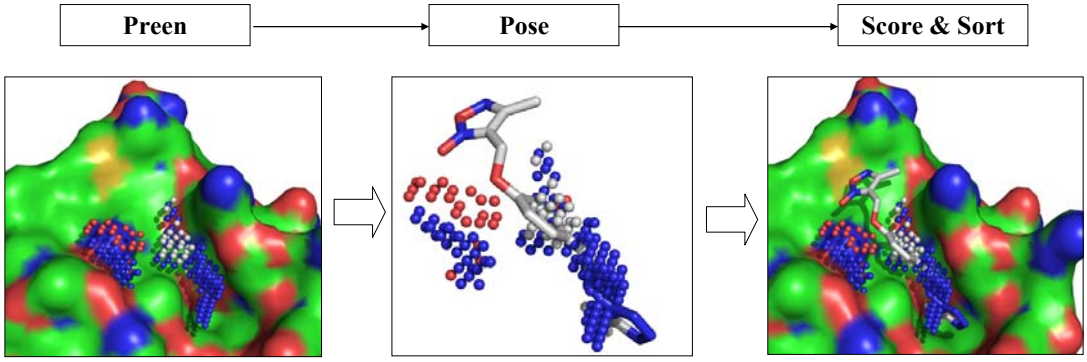

Figure 1-23: Steps involved in LIDAEUS. LIDAEUS includes four steps: Preen, Pose Score & Sort (Taylor et al., 2008). The target is coloured in green surface representation. Sites points of a starting template are coloured on the basis of atom types: hydrogen bond donor (red), hydrogen bond acceptor (blue) and hydrophobic atom (white). A candidate molecule is shown in stick form.

Further detail on UFSRAT and LIDAEUS are available in Steven R. Shave's thesis (2009) "The development of high performance structure and ligand based virtual screening techniques, and also in Daphne Kan's thesis (2007) "Studies of protein-ligand interactions and the discovery of new cyclophilin inhibitors." (University of Edinburgh)

- ***AutoDock***

The basic concept of AutoDock is to predict how a small molecule binds to the target receptor of known 3D structure (http://autodock.scripps.edu/). Major advantages of AutoDock are rapid grid-based energy evaluation and an efficient search of torsional freedom. AutoDock is a package of automated docking tools: AutoGrid, AutoDock and AutoDockTools (Goodsell et al., 1996; Morris et al., 2009; Norgan et al., 2011; Sotriffer et al., 2000). "AutoGrid" is designed to pre-calculate grids that describe the target protein. Four steps are required in an AutoDock calculation: (1) coordinate file preparation using "AutoDockTool"; (2) creating grid parameters and pre-calculation of atomic affinities and the torsional degree of freedom of side chains using "AutoGrid"; (3) docking the ligands to the receptor using "AutoDock" on the basis of free energy calculation; and (4) Analysis of the results using AutoDockTools which is a tool to analyse ligand-receptor docking calculations and visualisation of the atomic affinity grids (Morris et al., 2008). This feature is

important for synthetic chemistry to facilitate optimisation of small molecules resulting in higher binding affinity with the receptor. Application of AutoDock to our project is described in greater detail in Chapter 6.

1.3 Aim of the project: Discovery of MDM2 Antagonists

MDM2 plays a critical role in the regulation of the p53 level in cells. About 50% of human tumors are related to mutations or deletions in the p53 gene. Human cancers that have wild type p53 proteins overexpress MDM2, which inhibits p53-mediated transcription or degradates p53 by ubiquitination. Hence, inhibitors of p53-MDM2 or of MDM2-mediated ubiquitination are attractive strategies to rescue p53 function for potential cancer therapies (Lauria et al., 2010; Patel & Player, 2008).

To date, only a few small molecules found to inhibit MDM2 E3 ligase activity have been identified (Lai, et al., 2002; Yang, et al., 2005). There are large numbers of inhibitors found to interrupt the MDM2-p53 interactions (Weber, 2010). One well characterised inhibitor is Nutlin. Nutlin, a BOX-I mimetic, has been proved to have high affinity with the hydrophobic domain of MDM2, and activates p53-dependent transcription *in vitro* and *in vivo* (Vassilev, 2004; Vassilev et al., 2007; White et al., 2006). The mechanism of Nutlin resulting in the rescue of p53 function has been widely studied. An early hypothesis suggested that when Nutlin binds to the hydrophobic domain of MDM2 it would prevent interaction between p53 and MDM2, and p53 would not be ubiquitinated. In fact, Nutlin does inhibit the interaction of p53 and MDM2, but does not block ubiquitination of p53 (Wallace et al., 2006). The 12.1 peptide (MPRFMDYWEGLN) shows similar behaviour and is able to inhibit the p53-MDM2 interaction but does not attenuate the MDM2-mediated ubiquitination to p53 (Böttger et al., 1996; Wallace et al., 2006).

Recently, the MDM2 RING domain has attracted significant effort in drug design due to its E3 ligase activity. The goal is to disrupt MDM2 E3 ligase activity directly. There are two alternative target sites on the MDM2RING domain: (1) **the C8-binding site** (for the dimerisation) and (2) **the E2-binding site**. It has been found the MDM2 RING domain proteins are more active as dimers rather than monomers. Therefore, if small molecules having higher affinities with the C8-binding site can be designed; MDM2 will exist as monomers and will have weaker E3 ligase activity. Interaction with the E2 protein is

essential to trigger E3-mediated ubiquitination. Therefore, if small molecules bind to the E2-binding site of the E3 protein or the E3-binding site of E2, ubiquitination pathways are interrupted.

In this project, we characterised the interactions between MDM2 and its partner UbcH5a. In an attempt to provide new therapies for MDM2-mediated tumours, a virtual screening strategy (VS) was applied to design new potential drugs that could affect MDM2 E3 ligase activity. The interaction between UbcH5a and MDM2 is essential for the ubiquitination mechanism. Therefore, the interaction between MDM2 and UbcH5a provides a potentially druggable site, providing opportunities to design small molecules that disrupt the interactions. Numerous reports indicate that dimerisation of MDM2 affects its E3 ligase activity. This provides an alternative druggable site (Figure 1-24): the C8-binding site. Overall, in this project, we will focus on three potential drug targets: (1) the UbcH5a-binding site of MDM2, (2) the MDM2-binding site of UbcH5a, and (3) The C8-binding site of MDM2. The aim is to screen potential MDM2 antagonists to inhibit MDM2 E3 activity.

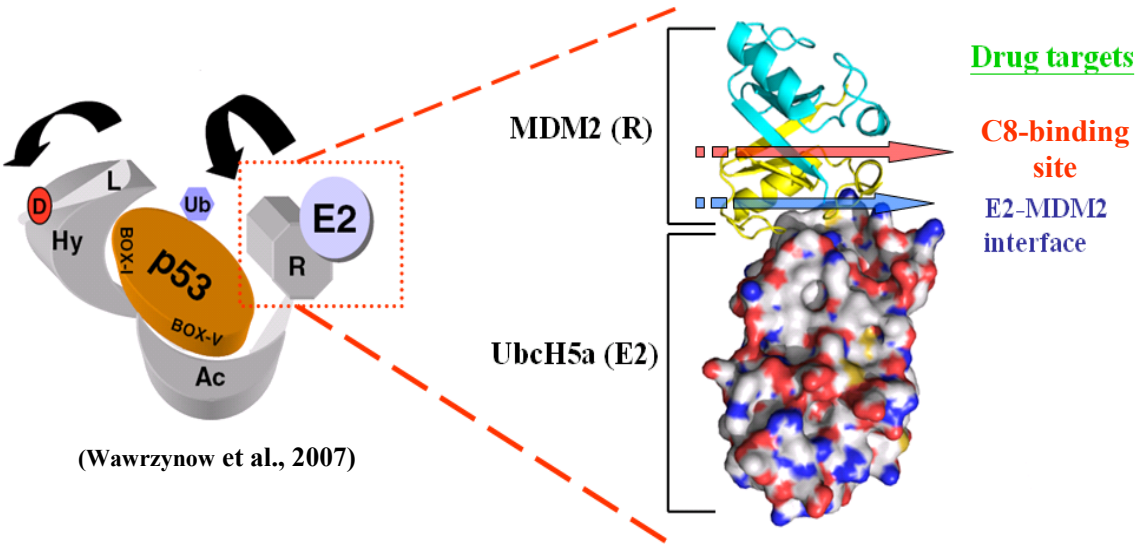

Figure 1-24: The aims of the project. (1) The study of UbcH5a-MDM2RING domain interaction (dashed red square). (2) Search for new small molecules to inhibit MDM2 E3 ligase activity upon the interruption the UbcH5a-MDM2 interaction or MDM2 dimerisation. Left figure is the model of the full length MDM2-p53 interaction through hydrophobic domain (Hy), and acidic domain (Ac) to allosterically regulate MDM2-mediated ubiquitination (more detail in Wallace et al., 2006). Right figure is the model of MDM2-UbcH5a interaction. MDM2RING-MDM2RING is shown as a cartoon. UbcH5a is shown in surface representations. The arrows (red & blue) are the druggable sites of interest. The MDM2-UbcH5a complex model was built based on the known crystal structure of the cIAP2UbcH5b complex (PDB: 3EB6).

2 Expression and Purification of MDM2 RING and UbcH5a

This chapter described the strategies behind the expression and purification of MDM2RING (residues 386-491), MDM2RING△C (residues 386-478) and UbcH5a (residues 1-147). Following our optimisation of the purification procedures, the purity of each protein routinely was greater than 95%. These purified proteins were used for further biophysical and biochemical studies (Chapter 3) and structural studies (Chapter 4), and also as drug targets to study the effects of peptide 9 selected by K. Ball's group and of small molecules selected by the virtual screening system (Chapter 5 and 6).

2.1 Introduction

MDM2 is an E3 ligase protein which plays a critical role in determining the level of p53 in cells. It is a modular protein and its RING domain possesses E3 ligase activity. Here, we have produced and purified two constructs: MDM2RING (residue 386-491) and MDM2RING△C (residues 386-478). There are two published structures of MDM2RING proteins, MDM2/MDM2 homodimer (PDB ID: 2HDP) and MDM2/MDMX heterodimer (PDB_ID: 2VJE). However, there is no structure of a complex of MDM2 with a partner protein, for example UbcH5a. It has been proved that the interaction between E2-E3 is essential for the ubiquitination pathway. There are several structures of an E2-E3 complex available, which show that the E2-binding site of the E3 protein is quite expanded around the E3 surface. Previous studies have shown that the binding affinity between MDM2RING and its partner UbcH5 is too weak to be detected by ITC or pull-down methods: perhaps under these experimental condition, small MDM2 RING domain (residues 432-491), which may lack sufficient interaction for the UbcH5a-binding. One of our initial aims was to obtain the crystal structure of MDM2-UbcH5a, and the protein-protein interaction affinity is therefore a critical factor in determining if we can achieve this goal. A larger MDM2RING construct (residue 386-491) may have higher affinities with UbcH5a, therefore increasing the likelihood of obtaining the crystal structure of the MDM2-UbcH5a complex. In this project, we designed an MDM2RING construct, comprised of residues 386-491. MDM2 C-terminal tail fragment plays a critical role in oligomerisation of the protein and is also required for MDM2 E3 activity. A number of papers have shown that MDM2RING△C exists as a monomer and loses its E3 ligase activity. Therefore, we also made a construct, MDM2RING△C, consisting residues 386-478, as a negative control in our studies. MDM2RING, MDM2RING△C and UbcH5a were successfully produced and purified in this project. Amino acid sequences of those proteins are shown in the Figure 2-1 (MDM2RING & MDM2RING△C) and Figure 6-11 (UbcH5a). Pure proteins are essential for crystallisation, NMR analysis and biophysical characterisation, such as dynamic light scattering (DLS), thermal denaturation assay (TDA), circular dichroism (CD), and fluorescence anisotropy (Chapter 3, 4, 5 & 6). We also carried out *in vitro* ubiquitination experiments to test if our purified proteins are active.

2.2 Cloning

2.2.1 Cloning: MDM2RING & MDM2RING△C

The principle of cloning is that the coding gene of the protein was inserted into the expression vector, pET15b, and then transformed into *Escherichia coli* BL21(DE3) expression system. pET15b (Novagen Co.) contains a T7 promoter upstream at the multiple cloning sites (as protein expression sites) (Figure 2-1B). pET15b has a *lac* operator, which strictly controls the T7 promoter. BL21(DE3) is a modified *Escherichia coli*, which can express T7 polymerase. To produce the target protein, isopropyl β-D-1-thiogalactopyranoside (IPTG) is used to induce the expression of T7 polymerase, which binds to T7 promoter and triggers the expression of the inserted gene and produces the target protein. Advantages of the pET15b vector are that it possesses an N-terminal His · Tag, following a thrombin cleavage site, both of which facilitate protein purification (Figure 2-2).

2.2.2 Material and Methods: Cloning

MDM2 (murine double mutant 2) (Accession number Q00987) residues 386-491 (MDM2RING) and residues 386-478 (MDM2RING△C) were cloned into the expression vector pET15b (Novagen Co.) that carries a His · Tag and a thrombin cleavage site (Figure 2-2). In PCR reactions, the templates were plasmids containing the full length *mdm2* gene which were gifts provided by Kathryn Ball's group. PCR reaction mixtures included the plasmid templates (5 ng), forward primer (1 nmole), reverse primer (1 nmole), ATP, reaction buffer, T7 polymerase (1 Unit, Sigma Co.) and ddH_2O up to final volume of 30 μl. PCR reaction conditions were: 95℃, 5 minutes; 30 cycles of 95℃, 30 seconds, 72℃, 45 seconds, and 37℃, 60 seconds; 37℃, 5minutes. The PCR products were checked on a 1.2% agarose gel.

To obtain the constructs containing the RING domain of MDM2, primers were designed to amplify MDM2 RING, and MDM2 RING△C as shown below:

MDM2RING	
NdeI_386F	5'-GGAATTCCATATGTCACAATCACAAGAAAGTGAA-3'
BamHI_491R	5'-CGCGGATCCTAGGGGAAATAAGTTAGCACAAT-3'
MDM2RING△C	
NdeI_386F	5'-GGAATTCCATATGTCACAATCACAAGAAAGTGAA-3'
BamHI_478R	5'-CGCGGATCCTAACATACT GGGCAGGGCTTATT-3'

All the forward primers contained an *Nde*I restriction site and the reverse primers included a *Bam*HI restriction site. For cloning, the PCR products and expression vectors pET15b were treated by *Nde*I and *Bam*HI enzymes for 1 hour at 37℃. Those treated samples were loaded onto a 1.2% agarose gel to separate cleaved samples from the uncleaved samples. The bands of the expected sizes were cut out of the agarose gel and purified using a gel extraction kit (QIAGEN, Co.). Next, we used a Rapid DNA ligation Kit (Roche Co.). The ligation mixture included purified cleaved pET15b, cleaved PCR products, ligase, and ligation buffer. Ligation mixtures were incubated for 5 minutes at room temperature. Following ligation, mixtures were transformed to the competent cells used for cloning and plasmid production, DH5α. Competent cells were put on ice for 15 minutes, followed by heat shock at 42℃ for 90 seconds, and the cells were put back on ice quickly for another 15 minutes. The transformed cells were incubated at 37℃ with shaking at 250 rpm for 1 hour and then spread on LB plates (+100 μg/ml carbenicillin) and incubated at 37℃ overnight. A single colony was picked for DNA sequencing. Sequences of all constructs have been confirmed by sequencing.

Figure 2-1: Cloning of MDM2 RING constructs. (A) Schematic diagram presenting the domain architecture of MDM2. The RING domain starts from C438 to C478. The secondary structure of MDM2 RING domain exists as β1β2α1β3. The zinc binding residues are labeled with red asterisks (*). The sequences (G448CIVHGKT G456) shown in green and underlined are the ATP binding motif, Walker A. In our project, two constructs were generated: MDM2RING (residues 386 ~ 491) and MDM2RING△C (residues 386 ~ 478). (B) The cloning vector used in this project is pET15b (Details available from Novagen Co.).

(A)

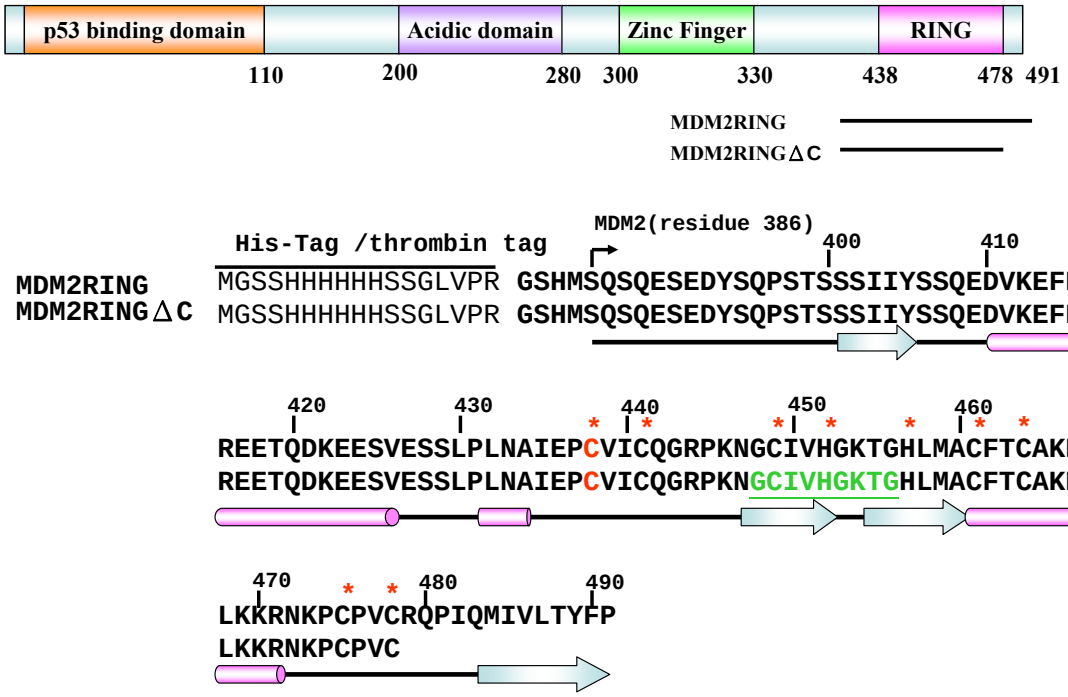

(B)

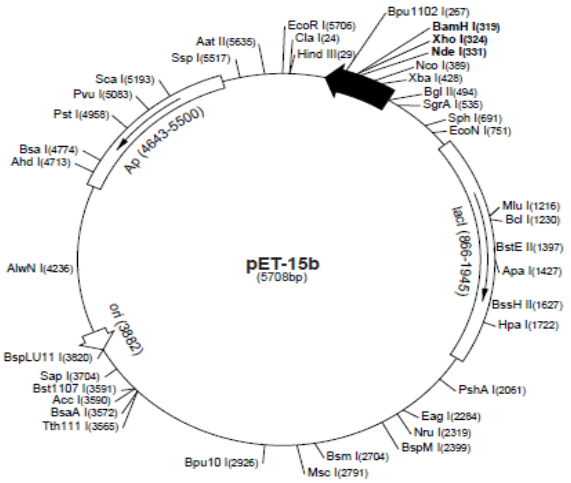

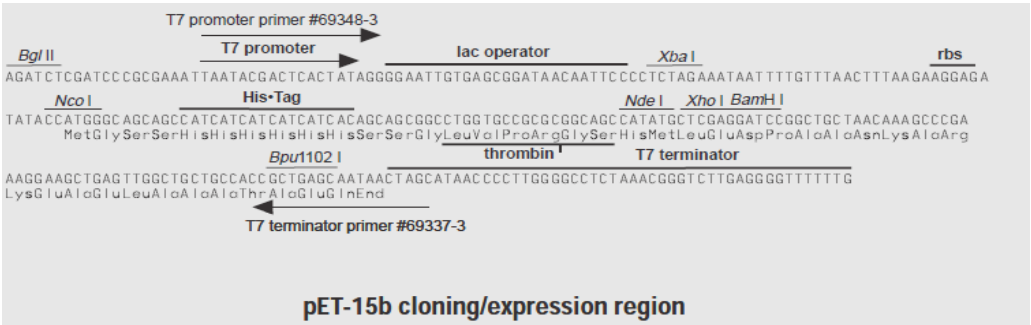

pET-15b cloning/expression region

2.2.3 Results and Discussion: Cloning

In this work, we designed and constructed two MDM2 RING domain proteins, MDM2RING (residues 386-491), and MDM2RING △C (residues 386-478). Specific primers were designed for the cloning. After optimisation of PCR conditions, the fragments of MDM2RING and MDM2RING△C were successfully amplified (Figure 2-2A). The sizes of the PCR products shown on the agarose gel were as expected the sizes of MDM2RING and MDM2RING△C, respectively, 387 and 346 bps. For cloning, those PCR products and the vectors, pET15b, were treated by these two restriction enzymes (*Nde*I / *Bam*HI) following by separation of cleaved and uncleaved fragments on a 1.2 % agarose gel. Cleaved fragments of the PCR products were purified and inserted into the expression vector, pET15b.

Those MDM2RING ligates (pET15b-MDM2RING or pET15b-MDM2RING △C) were treated by two restriction enzymes (*Nde*I and *Bam*HI) to confirm whether the molecular sizes of those clones were what we expected. The MDM2RING ligates were treated by *Nde*I / *Bam*HI and analysed on 1.2 % agarose gel. The size of the smaller fragment was about 300 ~ 400 bps and the size of the larger one was about 5000 ~ 6000 bps. The sizes of those two fragments were similar to the size of MDM2RING (372 bps) and pET15b (5708 bps). Constructs have been checked by sequencing and were the correct sequence.

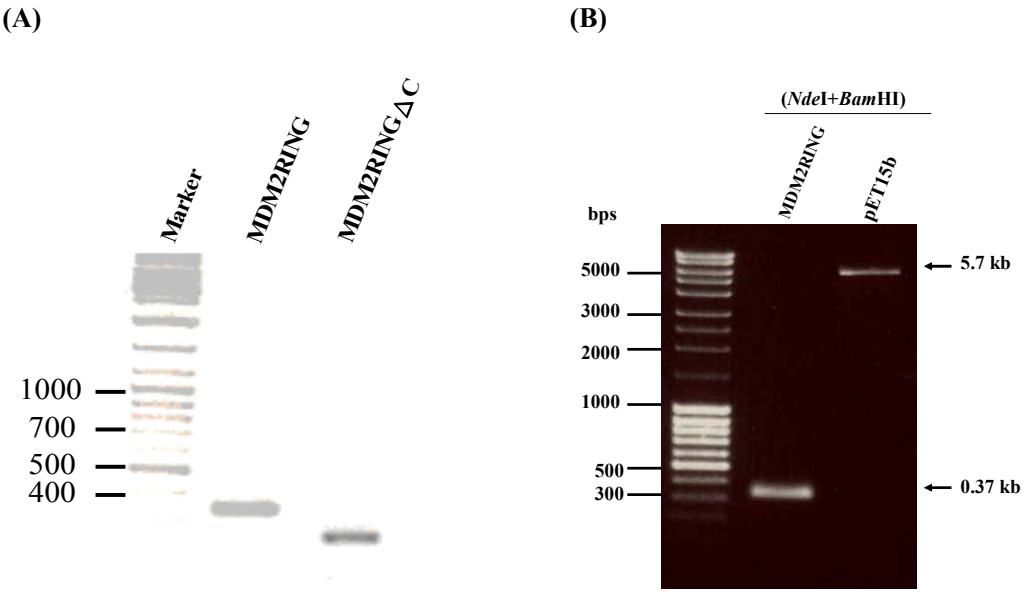

Figure 2-2: Cloning of MDM2 RING domain: MDM2RING and MDM2RING△C. (A) PCR products are checked on the 1.2% agarose gel. PCR reactions: 95℃, 5minuts; 30 cycles of 95℃,

30 seconds; 72℃, 45 seconds, and 37℃, 5 minutes. The sizes of those PCR products are respectively 387 bps (MDM2RING) and 346 bps (MDM2RING△C). (B) Constructs of pET15b-MDM2RING are digested by the restriction enzymes *Nde*I/*Bam*HI. The size of the smaller fragment is approximately 300 ~ 400 bps, similar to the expected size of 372 bps. The larger fragment (~ 5.7 kbps) is pET15b. Those constructs have been confirmed by sequencing.

2.3 Protein expression

High yields of pure proteins are required for protein crystallisation, NMR and biophysical experiments. We successfully cloned MDM2RING and MDM2RING △ C into the expression vector, pET15b. UbcH5a plasmid, a kind gift, from Professor Kathryn Ball, was cloned into pET15b. The pET expression system utilise IPTG-induced expression of the target protein. Recombinant protein expression is affected by various factors including: induction temperature, concentration of IPTG used, time post induction or the requirement for additives. Those factors can determine both the yield and quality of the over-expressed recombinant proteins. Therefore, a number of expression trials are required to determine optimal expression conditions.

2.3.1 Materials and Methods: Protein Expression

- ***Protein Expression***

A single colony was used to inoculate 5 ml LB (+ 100 μg/ml carbenicillin) followed by incubation at 37℃ overnight with agitation at 250 rpm. The overnight cell culture was transferred into fresh LB broth (+ 100 μg/ml carbenicillin) using a 1:40 inoculum ratio and was incubated at 37℃ for 1.5 ~ 2 hours until the O.D.600 reached 0.6 ~ 0.8. IPTG to a final concentration of 1 mM was added to the cell culture followed by incubation at 37℃ for another 5 hours to express the protein of interest. Cells were harvested by centrifugation at 8,000 xg for 30 minutes. Cell pellets were frozen in liquid nitrogen and stored at -80 ℃. UbcH5a was expressed as above. Because MDM2RING and MDM2RING△C are zinc-binding proteins, 100 μM ZnAcetate was added to cell cultures 15 minutes before the addition of 1 mM IPTG.

- ***SDS-PAGE***

SDS-PAGE, sodium dodecyl sulphate polyacrylamide gel electrophoresis, is a common technique to separate proteins based on their electrophoretic mobility. In this work, 15% SDS-PAGE was used to observe the purity of our target proteins. The recipes of each SDS-PAGE we used were shown below: separation gel [4X Tris-SDS, pH8.0 (4.65 ml), 30% acrylamide (9.3 ml), sterile H_2O (4.65 ml), 10% APS (15 µl) and TEMED (5 µl)] and stacking gel [8X Tris-SDS, pH6.8 (6.25 ml), 30% acrylamide (3.25 ml), sterile H_2O (1.5 ml), 10% APS (15 µl) and TEMED (5 µl)]. Sample (15 µl) was mixed with 2X loading dye (15µl) and heated at 95℃ for 5 minutes before loading into the gel.

2.3.2 Results & Discussions: Protein expressions

In this work, many expression trials were carried out to increase the level of expressions of the proteins, such as different expression cells, temperatures, and IPTG-induction times (Figure 2-3). MDM2RING, MDM2RING△C and UbcH5b, were expressed by 1 mM IPTG at 18℃ and 37℃, respectively, for different induction times. The level of the expression of the protein was detected using 15% SDS-PAGE. Results showed that, at an induction temperature of 18℃, MDM2RING was not expressed even after inducing for 3 ~ 5 hours, but only started to be over-expressed after being induced overnight (Figure 2-3B). Because MDM2RING is a zinc-binding protein, the addition of zinc metals should be beneficial to allow the protein to adopt the correct structure while it is expressed. However, for some cells, the addition of zinc metals may damage cell growth and reduce protein expression. Here, our results show that addition of zinc metals did not affect the protein expression (Figure 2-3B). MDM2RING was induced after 3 hours at 37℃. The expression levels of the cells induced for 5 hours or overnight did not increase significantly. The molecular weight of 6xHis-MDM2RING and 6xHis-MDM2RING△C are respectively, 14.3 kDa, and 12.7 KDa. The intense protein bands on the 15% SDS-PAGE gels are the over-expressed proteins. The estimated molecular weights of those bands were higher than expected, perhaps as a result of negative charged surface or the conformation of denatured proteins reduced the motilities of 6xHis-MDM2RING and 6xHis-MDM2RING△C. Another protein, UbcH5a, was cloned into pET15b, which has a 6XHis tag and thrombin cleavage site at its N-terminus. 6xHis-UbcH5a, contains 168 amino acids and its predicted molecular weight is 18.9 kDa. Expression trials on His-tagged UbcH5a produced bands of the correct estimated weight when analysed by SDS-PAGE (Figure 2-3D).

Solubility is critical for structural studies and biological characterisation. Overexpressed proteins may be incorrectly folded and can form inclusion bodies, therefore controlling how much soluble protein is produced is very important. The cell pellets were resuspended in lysis buffer, followed by sonication (10s x 10 cycles, at 10-sec intervals) on ice, the soluble and insoluble proteins were separated by centrifugation at 13,000 xg for 30 minutes. Total protein and soluble fractions were tested on 15% SDS-PAGE gels. The results showed that here MDM2RING△C, had the majority in a soluble form (Figure 2-3C).

Figure 2-3: Expression of purification of MDM2RING, MDM2RING△C, and UbcH5a. (A) Expression trails of MDM2RING transformed into different host cell types, respectively, to BL21(DE3), BL21(pLys) Rosetta(DE3)(pLys) and Rosetta(DE3)(RIPL). IPTG is added to a final concentration of 1 mM and the cells grow for 3 hours and overnight (O/N) at 37 ℃. (B) MDM2RING is induced by the addition of 1 mM IPTG at incubated for 3, 5, and 16 hours, respectively, at 18℃ and 37℃. (C) Solubility tests of overexpressed proteins. More than 95% expressed proteins are soluble. "T" presented total proteins and "S" meant soluble proteins. (D) Overexpression of UbcH5a. Arrows in those figures show over-expressed target proteins.

(A)

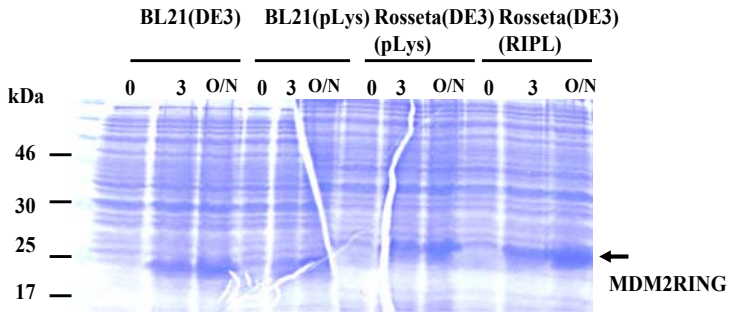
BL21(DE3)
BL21(pLys)
Rosseta(DE3) (pLys)
Rosseta(DE3) (RIPL)
kDa
0 3 O/N 0 3 O/N 0 3 O/N 0 3 O/N
46
30
25
17
MDM2RING

(B)

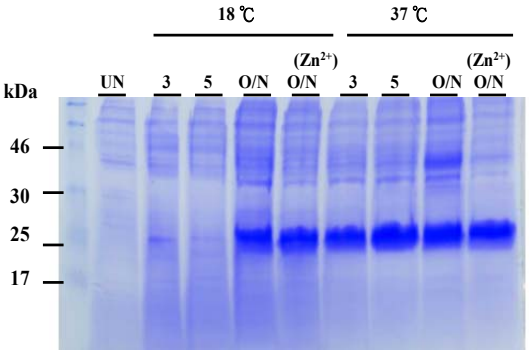
18 ℃
37 ℃
kDa
UN 3 5 O/N (Zn2+) O/N 3 5 O/N (Zn2+) O/N
46
30
25
17

(C)

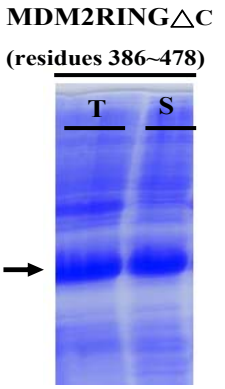
MDM2RING△C
(residues 386~478)
T
S


6xHis Tag
Thrombin Tag
MDM2RING

6xHis Tag
Thrombin Tag
MDM2RING△C

(D)

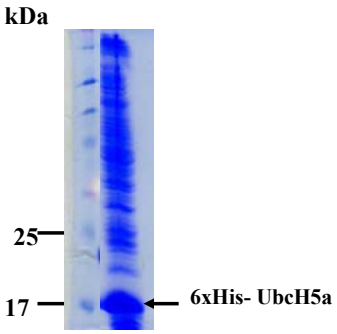
kDa
25
17
6xHis- UbcH5a


6xHis Tag
Thrombin Tag
UbcH5a

2.4 Protein Purification Strategy

Several purification techniques were combined to achieve the goal of producing high yields of highly pure target proteins. The protein purification strategy consisted of immobilised metal affinity chromatorgraphy (IMAC), desalt chromatography, thrombin cleavage, benzamidine affinity chromatography and size exclusion chromatography (SEC) (Figure 2-4). First, we utilised the IMAC column to remove most of the contaminating proteins. Thrombin was used to remove the fusion tag from the target protein. To increase protein purity and homogeneity, benzamidine and size exclusion chromatography were used.

Three proteins, MDM2RING, MDM2RING△C and UbcH5a were successfully purified. In this section, the basis of each chromatographic technique used in the work will be introduced and the results of each purification presented. In summary, for each protein we were able to achieve approximately 95% purity. All the columns used were purchased from GE Healthcare and detailed information of those columns is available from this website (http://www. gelifesciences.como). Thanks to the EPPF staff in the University of Edinburgh for their valuable advice and assistance during the work.

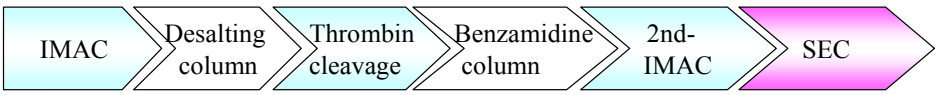

Figure 2-4: Overview of protein purification strategies used. Each method is introduced in great detail in the text the following sections.

2.4.1 Immobilised Metal Affinity Chromatography (IMAC)

- ***The basis and applications of IMAC***

IMAC, immobilised metal affinity chromatography, is a method to achieve purification by the coordination of the His · Tag to metal ions, such as Ni, Co, Zn, Fe and Cd. Proteins have a variety of amino acids, especially histidine, which bind to divalent metal ions. However, to increase the efficiency of purification, a recombinant protein usually has a fusion tag, such as a His-Tag. In this work, all of our constructs (MDM2RING, MDM2RING△C and UbcH5a) are fused with a 6xHis-Tag (His-Tag), which has strong affinities with divalent metals.

IMAC columns contain immobilised chelating groups, such as sepharose, which are cross-linked to the agarose beads. Those immobilised chelating groups are charged with divalent metal ions, such as nickel and cobalt, which of both have high affinity with histidine residues and are commonly used for IMAC purification (Yip et al., 1989).

In this work, cell pellets were treated by sonication or French press, and proteins were released from the cells. Cell lysate is a mixture of our fusion proteins (with His · Tag), other proteins without His · Tag, nucleotides, RNA and other metabolites. To separate the target protein from the cell lysate mixture, IMAC is a convenient and effective method. As shown in Figure 2-5A, our proteins with His · Tag bound tightly to the IMAC column. Other proteins and mixtures passed through the IMAC column to the waste fraction. To elute the target protein, several methods are available such as competitive elution or pH adjustment. In this current work, competitive elution was used by the addition of an excess amount of imidazole, which has stronger affinity with the nickel, allowing the target protein to be eluted from the IMAC column.

- ***MDM2RING and MDM2RING△C were purified by IMAC***

Cell pellets of MDM2RING and MDM2RING△C were resuspended in binding buffer A [50 mM Tris, 500 mM NaCl, 10 μM Zn Acetate, 2 mM DTT, 20 mM imidazole, pH 7.8]. Cells were lysed by pulsed sonication (10s x 10cycles, at 10-sec intervals) on ice. Cell lysate was then centrifuged at 22,000 xg for 30 minutes at 4 ℃. The resulting supernatant was filtered through 0.45 μm filters to remove small particles that may block and damage the column. IMAC was used as the first step for the purification of the histidine tagged protein. An IMAC Sepharose 6 Fast Flow column was charged with excess nickel sulfate (NiSO4) according to manufacturers' protocol, followed by three washes in binding buffer A. Filtered sample was loaded onto a 5 ml IMAC column at a flow rate of 1 ml/min. Binding buffer A [50 mM Tris, 500 mM NaCl, 10 μM Zn Acetate, 2 mM DTT, 20 mM imidazole, pH7.8] and elution buffer B [50 mm Tris, 500 mM NaCl, 10 μM Zn Acetate, 2 mM DTT, 750 mM imidazole, pH7.8] were prepared for IMAC purification. Imidazole gradient elution was used to elute the His-Tag gel proteins.

MDM2RING and MDM2RING△C were purified to approximately 95% after the first purification step by IMAC (red arrows, Figure 2-5 A & B). Two steps were used to elute the proteins: the first step of the purification method was to remove the majority of contaminating proteins using a low concentration of imidazole containing about 60 mM imidazole. The second step used imidazole gradient elution (8% to 100% buffer B) to elute the target proteins. At this stage, about 10 ~ 15 mg 6xHis-MDM2RING and 6xHis-MDM2RING△C were produced from 1 L cell culture.

Figure 2-5: Purification using IMAC. MDM2RING (A) and MDM2RING△C (B) are purified using an IMAC Sepharose 6 Fast Flow column charged with Ni^{2+}. Unwanted proteins are removed at 8 % buffer B (~60 mM imidazole). MDM2RING and MDM2RING△C are eluted by imidazole gradient (8 to 100 % buffer B). SDS-PAGE analysis of several fractions from the purification shows that greater than 95% purity was achieved for the target protein. Red arrows indicate the target proteins. M: Marker; S: total protein.

(A)

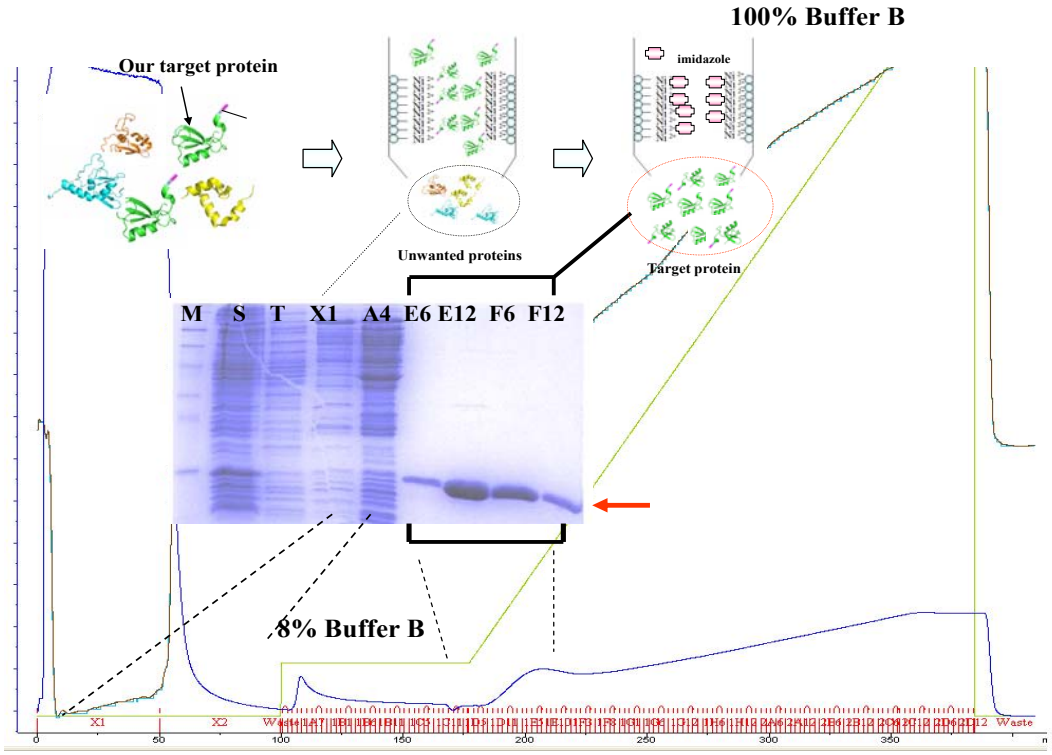
100% Buffer B
Our target protein
imidazole
Unwanted proteins
Target protein
M S T X1 A4 E6 E12 F6 F12
8% Buffer B

(B)

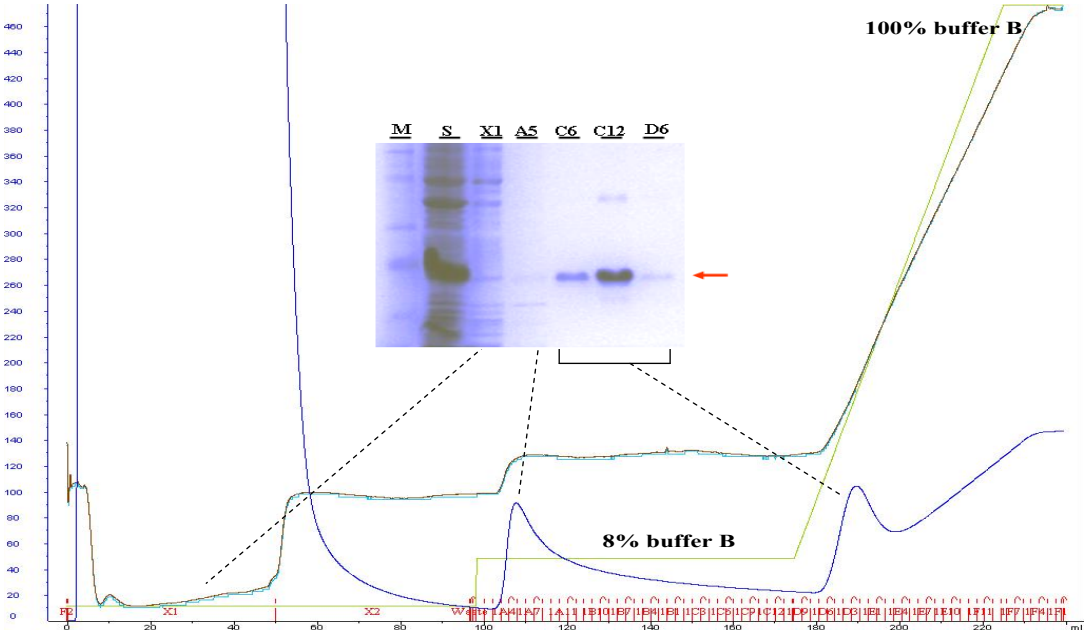
100% buffer B
M S X1 A5 C6 C12 D6
8% buffer B

2.4.2 Desalting chromatography

Desalting chromatography is a fast, simple one step process to remove low molecular weight substrates that may interfere with subsequent purification, the stability or activities of the target proteins. The desalting column resin, Sephadex, made by cross-linked dextran with epichlorohydrin, is commonly used. There are several types of Sephadex available to separate different sizes of molecules. In general, Sephadex G-25 is well suited for the separation of globular proteins (M.W. >5,000 Daltons) from other smaller molecules such as salts or imidazoles (M.W. <1,000 Daltons). A desalting column was often used to remove imidazole and exchange the sample into the desired buffer for further purification or activity studies. In this current work, a HiPrep 26/10 desalting column was used to buffer exchange our sample into the desired buffer [20 mM Tris, 150 mM NaCl, 10 μM Zn Acetate, 2mM DTT, pH 7.2] for the subsequent experiment, thrombin cleavage. Buffer exchange was necessary as enzymatic activity of thrombin is low in a high concentration of salt and imidazole.

2.4.3 His · tag removed by thrombin cleavage

To avoid the effects of those tags that may interfere with the protein activity, some vectors, such as pET15b, are designed to attach a thrombin-specific recognition site between the His · Tag and the target protein (Figure 2-1B). Thrombin (EC 3.4.21.5) is a "trypsin-like" serine protease and its molecular weight is 36 kDa. Thrombin can recognise sequences "LVPRGS" and cleaves between Arg and Gly (Chane et al., 1985; Law et al., 1984). After the sample is treated with thrombin at the optimal conditions, fusion tag moieties will be cleaved off from target proteins.

To reduce the possibility that a His · tag moiety may interfere with biophysical characterisation or might inhibit crystallisation, the His · Tag was removed from MDM2RING and MDM2RING△C by thrombin cleavage. Following IMAC and desalting steps, thrombin was added to samples of both 6xHis-thrombin-MDM2RING and 6xHis-thrombin-MDM2RING△C. The efficiency of thrombin cleavage depends on the amounts of the enzymes, the reaction time, and incubation temperature. Preliminary experiments were carried out to find the optimal conditions to achieve complete digestion. 6xHis-MDM2RING was completely cleaved by 1, 2, 2.5, 5 and 10U thrombin at 20℃ for 4 hours, while the

complete digestion of 6xHis-MDM2RING was achieved with 5U and 10U thrombin at 4℃ for 16 hours. SDS-PAGE results showed the higher molecular weight band was 6xHis-thrombin-MDM2, and the smaller was cleaved MDM2RING (Figure 2-6A). Considering the stability and activity of the proteins, the optimal condition for thrombin cleavage was determined to be 5U thrombin for 16 hours at 4 ℃. Another protein, MDM2RING△C was also obtained using the same conditions as above (Figure 2-6B). Following thrombin digestion, a benzamidine column was used to remove thrombin from the samples.

(A)

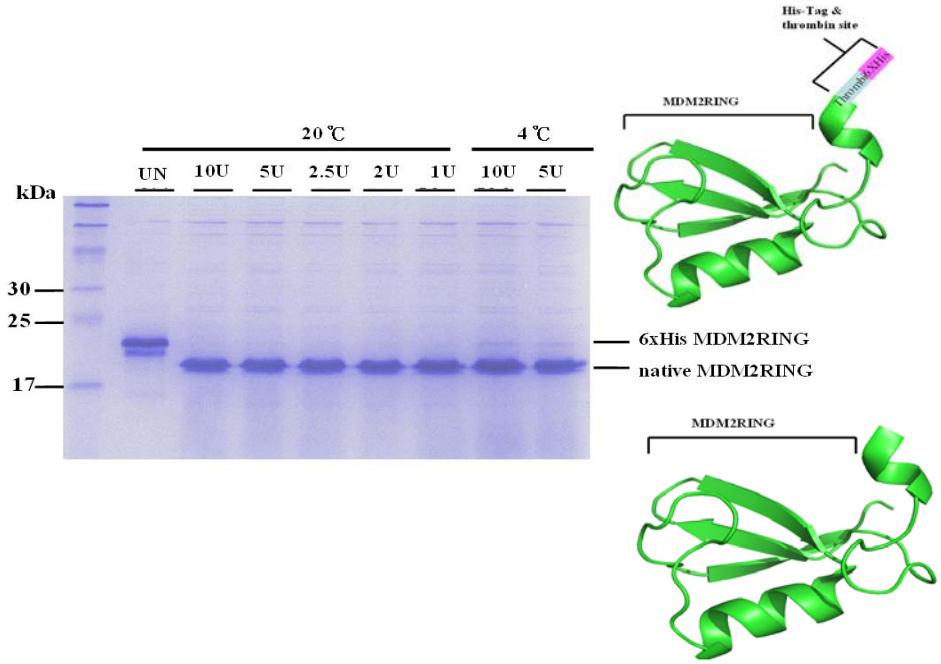

(B)

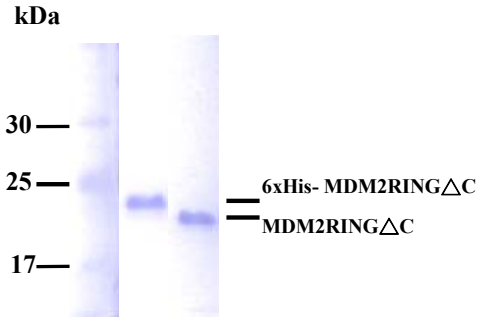

Figure 2-6: SDS-PAGE analysis of the thrombin cleavage trials. (A) 6xHis-MDM2RING is completely cleaved with all the amounts of thrombin tested at 4℃ for 16 hours or at 20 ℃ for 4 hours. In the right panel, the structure in green shows MDM2RING and the cyan and magenta rectangles are thrombin cleavage site and 6xHis-Tag. (B) 6xHis- MDM2RING△C is also completely cleaved by thrombin at the optimal condition: incubation with 5 U thrombin at 4℃ for 16 hours.

2.4.4 Benzamidine Column

Benzamidine is known as a strong and specific thrombin inhibitor. A HiTrap Benzamidine FF (high sub) column used in this work is made of highly cross-linked 4% agarose with p-aminobenzamidine (pABA). To stop the thrombin cleavage reaction, samples in the thrombin cleavage buffer were transferred to the benzamidine buffer [50 mM Tris, 500 mM NaCl, 10 μM Zn Acetate, 2 mM DTT, 20 mM imidazole, pH8.0]. The samples were then loaded onto the benzamidine column, the cleaved protein of interest collected in the flow-through, and the thrombin bound to the column. The samples were loaded onto an IMAC column again to remove uncleaved 6X His-thrombin moieties. Native target proteins can be collected in the flow-through fraction. Subsequently, native proteins were loaded onto a size exclusion column, Sephacryl S-200HR.

2.4.5 Size Exclusion Chromatography (SEC)

2.4.5.1 The basis and applications of SEC

Size exclusion chromatography (SEC, also known as gel-filtration chromatography) is a technique to separate molecules based on the size (more accurately, the hydrodynamic volume) when they pass through the SEC medium. SEC media covers the molecular range from 100 to 80,000,000 Daltons. Therefore, SEC is well suited for the separation of macromolecular complexes, such as proteins, polysaccharides, or nucleic acids. The porosity of the SEC medium is chosen according to the molecular weight of the protein of the interest. In this work, Hi-Prep Sephacryl S-200HR was used for the purification of MDM2RING and MDM2RING△C, while Superdex 75 was chosen for the purification of UbcH5a. Small molecules can diffuse into interior of the smaller pores and therefore, are retained for longer through the whole column compared to larger molecules. Larger molecules are eluted faster and are therefore separated from smaller molecules.

- ***SEC profiles of MDM2RING & MDM2RING△C***

In the purification strategies used throughout this project, SEC was the last purification step used to increase sample purity and provide an estimate of the molecular size of the target protein. HiPrep Sephacryl S-200HR was used in the SEC purification of MDM2RING and MDM2RING△C. The resolution range of Sephacryl S-200HR is 5,000 ~ 250,000 Daltons.

The buffer used in the SEC purification was 20 mM Tris (pH7.5), 150 mM NaCl, 10 μM Zn Acetate and 2mM DTT.

The molecular weights of monomeric MDM2RING and monomeric MDM2RING△C were estimated to be 12.4 kDa and 10.8 kDa, respectively, according to their amino acid compositions. The SEC profiles of MDM2RING showed two major peak fractions (Figure 2-7A). Molecules in the first peak were eluted at V_{ret} (the retention volume) of 40ml, and the molecular weights were greater than 250 kDa. The second fraction was eluted at Vrent = 65 ml, and the molecular weight were estimated at about 26 kDa. To confirm if both fractions contained MDM2RING, SDS-PAGE analysis was carried out. The result revealed that the sizes of both products were the same. The SEC profile of MDM2RING showed that MDM2RING might exist as a dimer (V_{ret} = 65 ml) or higher oligomers (V_{ret} = 40ml) (high order structured oligomers or aggregates). Another protein, MDM2RING△C eluted as a single species (eluted at V_{ret} = 70 ml), and its molecular weight was estimated to be 22 kDa according to the SEC profile (Figure 2-7B). The result revealed that MDM2RING△C was a dimer.

(A) MDM2RING

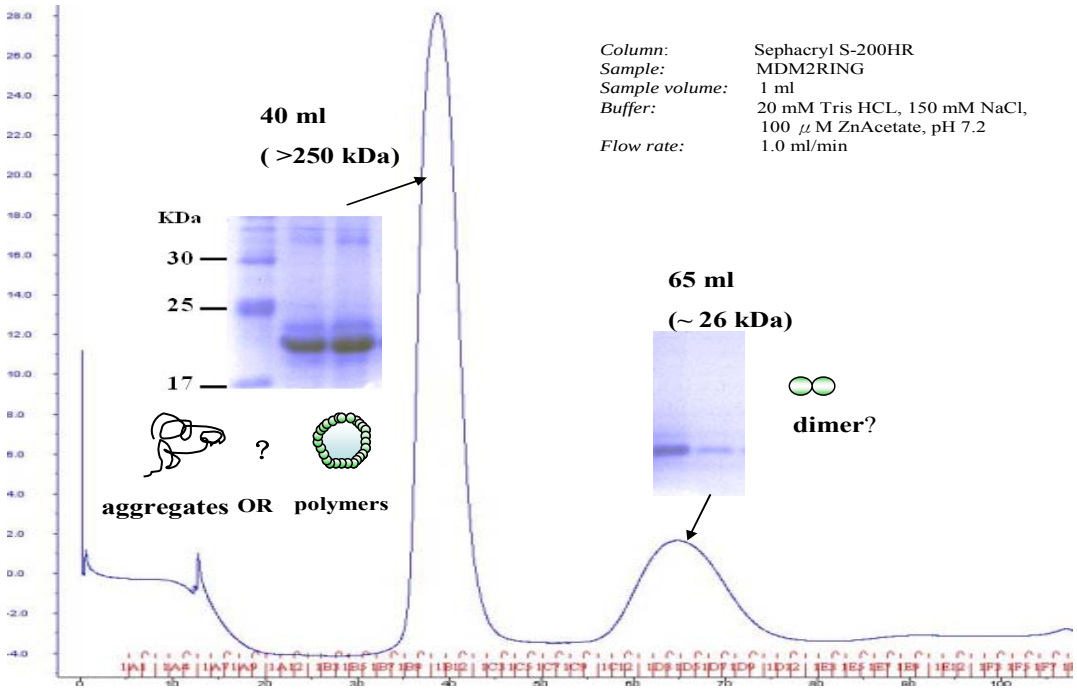

(B) MDM2RING△C

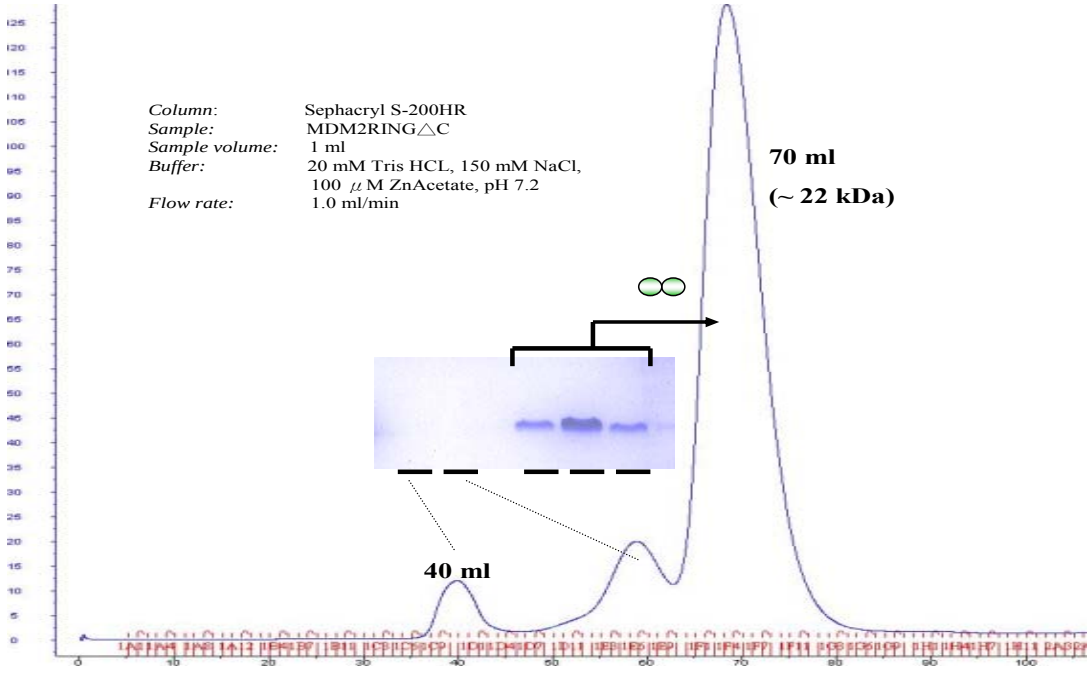

Figure 2-7: Purification using SEC. MDM2RING (A) and MDM2RING△C (B) are purified using Sephacryl S-200HR. (A) There are two major peaks on the SEC profile of MDM2RING. The molecular weight of the fraction in the first peak is larger than 250 kDa. Second peak is 26 kDa. (B) There is one species (~ 22 kDa) in the SEC profile of MDM2RING△C.

Our SEC profiles showed that MDM2RING existed as a dimer or multimers and MDM2RING△C, a MDM2RING lacking the last 13 amino acids, was a dimer. Differences in the oligomeric states between MDM2RING and MDM2RING△C revealed that the last C-terminal 13 residues were involved in the oligomerisation. These results were consistent with previous reports which indicate that the C-terminus of RING-type proteins is responsible for the dimerisation/ oligomerisation of RING-E3 ligases, such as cIAP2, and BRCA1 (Brzovic et al., 2001; Mace et al., 2008). Because a proportion of MDM2RING2 eluted in the void volume, further experiments were carried out to confirm whether the protein exist as non-specific aggregates or specific high molecular supramolecules (Chapter 4). Previous report showed that GST-MDM2 (400–484) is monomeric (Poyurovsky et al., 2007). In contrast, our MDM2RING△C (386-478) is a dimer. It is possible that the dimeric MDM2RING△C was due to the interactions between the longer N-terminal fragments (residue 386-400). Further support for the hypothesis can be found in the basis of published crystal structures of other E3 ligases: dimerisation of the cIAP2 RING homodimer and BRCA1/BARD1 RING heterodimer (Brzovic et al., 2001; Mace et al., 2008) are through the interactions of their N-terminal and C-terminal fragments.

In summary, MDM2RING and MDM2RING△C were more than 95% pure after the SEC. Dimeric MDM2RING and MDM2RING△C were used in further biophysical and structural studies, as well as in activity assays.

2.5 Purification of 6xHis-UbcH5a

UbcH5a was cloned into an expression plasmid (pET15b), producing 6xHis-UbcH5a. Its molecular weight is 18.9 kDa and its pI value is estimated to be 7.94. The purification protocol used two steps IMAC and SEC. Two buffers were used in the IMAC step: buffer A (20 mM Tris, 150 mM NaCl, 20 mM imidazole, pH7.2), and buffer B (20 mM Tris and 150 mM NaCl, 750 mM imidazole, pH7.2). A Sepharose 6 Fast Flow column (IMAC) was used first to remove the majority of the contaminating proteins, achieved by a wash of 8% buffer B (~ 60 mM imidazole). The target protein, 6xHis-UbcH5a was eluted with a gradient elution step, 8% to 100% Buffer B, (20 mM to 750 mM imidazole). The protein was greater than 95% pure following the first step (Figure 2-8A). Subsequently, Superdex^{TM} 75 (10/300 GL) was used as the second purification step to remove imidazole from the sample and also further increase the purity. The buffer used in SEC was 20 mM Tris, 150 mM NaCl (pH7.2).

The SEC profile of 6xHis-UbcH5a showed that one single peak (V_{ret} equivalent to 13.8 ml) with an estimated molecular weight of 20 kDa (Figure 2-8B). The result revealed that 6xHis-UbcH5 is a monomer. In the expression and purification protocols described, 6 mg 6xHis-UbcH5a was produced from 1 L cell culture.

(A) IMAC

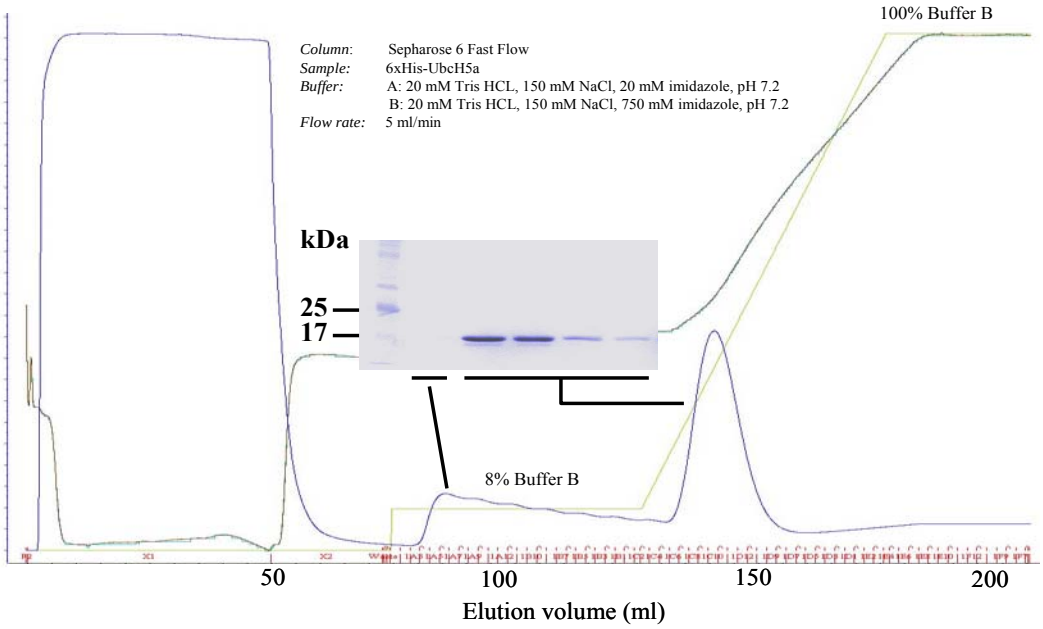

(B) SEC

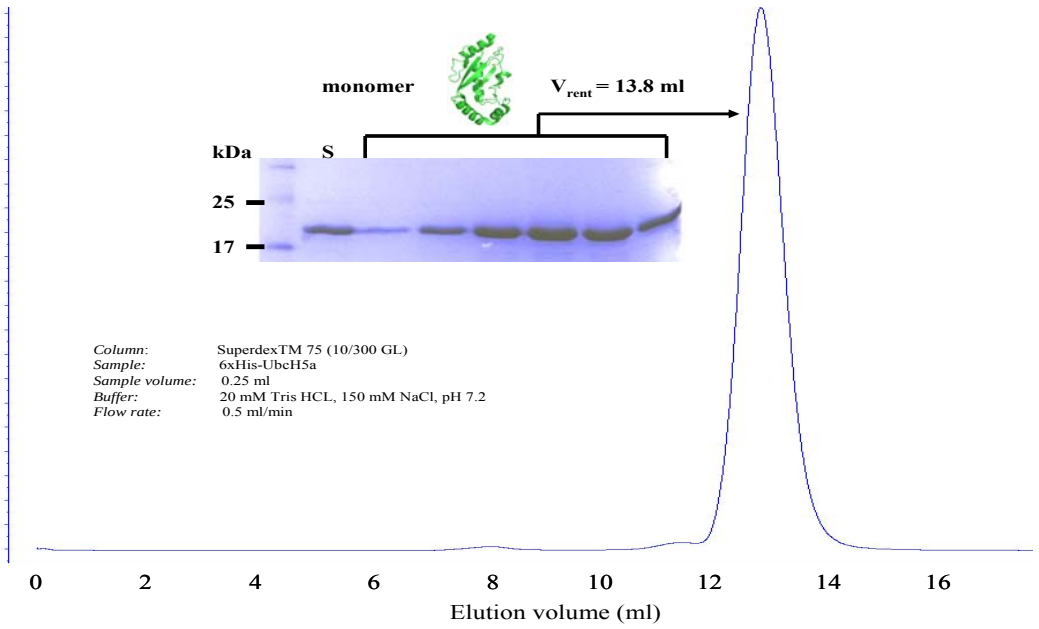

Figure 2-8: Two step purification of 6xHis-UbcH5a. (A) IMAC Sepharose 6 Fast Flow column charged with Ni^{2+} and (B) SuperdexTM 75 (10/300 GL). SDS-PAGE analysis of the eluted fractions reveal that the purity is greater than 95%.

2.6 Matrix-Assisted Laser Desorption/ionisation Flight-of-Time Mass Spectrometry (MALDI-TOF MS)

2.6.1 The basis and applications of MALDI-TOF MS

Matrix-Assisted Laser Desorption/ionisation Time-of Flight Mass Spectrometry (MALDI-TOF-MS) is commonly used, and is a sensitive ionisation mass spectrometry technique to determine the mass of biomolecules, such as proteins, nucleotides, sugars or organic molecules (Tanaka. et al., 1988; Karas et al., 1987). Moreover, MALDI-TOF-MS is also often applied to detect modification of molecules such as phosphorylation or methylation. In this current work, MALDI-TOF-MS was used to measure the mass of our constructs, MDM2RING, MDM2RING△C and UbcH5a.

MALDI-TOF MS is a combination of two methods: an ionisation mechanism (MALDI) and a mass analyser (TOF). MALDI is one method to ionise the molecules and TOF is one type of mass spectrometry commonly used to determine the mass of molecules via a time measurement (Wollnik, 1993).The basic principle of MALDI-TOF-MS is that the molecules are ionised to become charged molecules which are accelerated by an electric field through a vacuum channel at different velocities to reach the detector. The advantage of MALDI is that the matrix facilitates vaporization and ionisation of the molecules and also protects the molecules from being destroyed by the laser beam. The m/z (mass/ charge ratio) determines time taken for ions to travel through the flight tube.

In this section, the equipment used was a Voyager DE STR MALDI-TOF MS (Applied Biosystems Co.). The first step involves ionisation of the protein sample. A laser beam hits the sample previously spotted onto a metal plate together with a small quantity of matrix, typically, sinapic acid (3,5-dimethoxy-4-hydroxycinnamic acid), which then results in a transfer of the energy from the laser beam, via the matrix, into the sample (Beavis & Chait, 1989 a & b). The sample is therefore ionised, into a number of different charges by various ionisation mechanisms (Knochenmuss, 2006). Because the parameters of the flight distance and the strength of electric field are known, the mass of the molecule can be calculated.

2.6.2 Results and Discussions: MALDI-TOF MS

MALDI-TOF MS experiments were used to determine an accurate molecular mass for purified MDM2RING, MDM2RING△C and UbcH5a. 0.5 µl protein sample was spotted on to a gold mass spectrometry specific plate and then 0.5 µl sinapic acid matrix was added to enhance the ionisation of the sample. After the drop dried, the MS plate was loaded into the Voyager DE STR MALDI-TOF MS, and the analysis started.

The MALDI-TOF MS profile of MDM2RING showed that there was one strong ion peak (at m/z = 12852.3) and one weak ion peak (at m/z = 6432.3) (Figure 2-9A). The former peak was assumed to be the species with one proton ($[MDM2RING+1H]^{1+}$) and the latter peak was the species with two protons ($[MDM2RING+2H]^{2+}$). The experimental molecular weight of MDM2RING was 12.85 kDa similar to the theoretical molecular weight, 12.47 kDa (Calculated using Protein Calculator v3.3, a website that estimates the mass of a protein according to its primary amino acid composition (http://www.scripps.edu/~cdputnam/protcalc.html)). The MALDI-TOF MS profile of MDM2RING△C also revealed one strong ion peak (at m/z = 10872.8) and one weak ion peak (at m/z = 5432.2), suggesting that the experimental molecular weight was 10.93 kDa, similar to the theoretical molecular weigh of MDM2RING△C, 10.74 kDa (Figure 2-9B). The MALDI-TOF MS profile of 6x-UbcH5a showed that there was one dominant peak (at m/z = 18785.1), indicating that the experimental molecular weight was 18.8 kDa, similar to the theoretical molecular weight, 18.9 kDa (Figure 2-9C).

MALDI-TOF MS data revealed that there was one species in each sample. The calculated molecular mass suggested that both MDM2RING and MDM2RING △ C existed as monomers. These results were not consistent with the SEC profile results, which showed that MDM2RING proteins were dimers or higher order structured oligomers and that MDM2RING△C was a dimer. These differences may be due to the different means of characterisation. Proteins might tend to be detected as monomers by MALDI-TOF MS, as they are charged by a high voltage laser which may disrupt the dimer-dimer interactions resulting in only monomers being observed in the experiment. According to the MALDI-TOF MS data, the experimental molecular weight of each purified monomers, MDM2RING, MDM2RING△C and 6xHis-UbcH5a was as expected (Table 2-1).

(A) MDM2RING

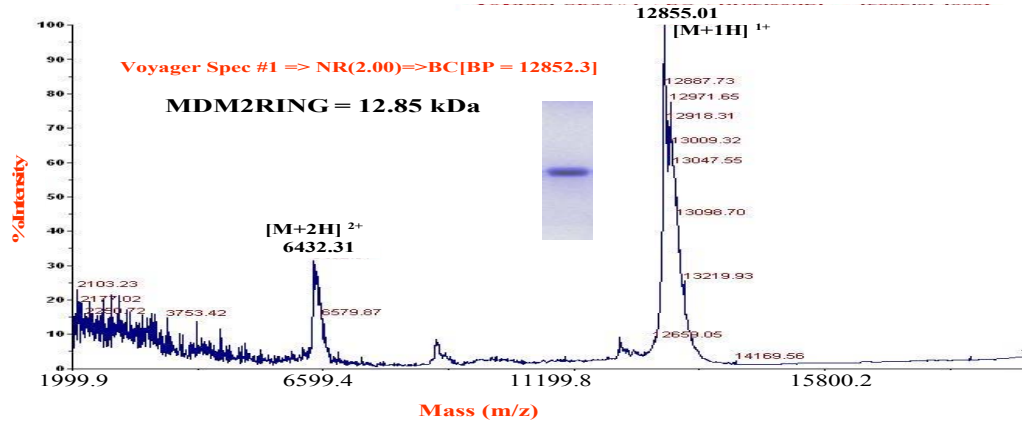

(B) MDM2RING△C

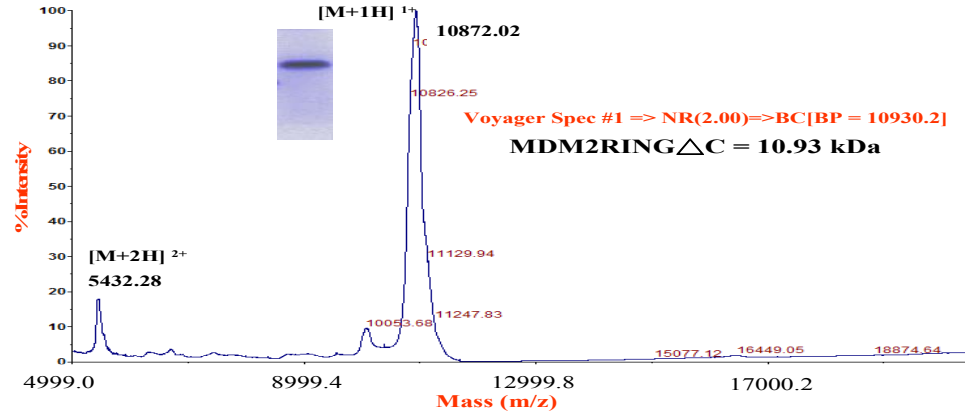

(C) 6xHis-UbcH5a

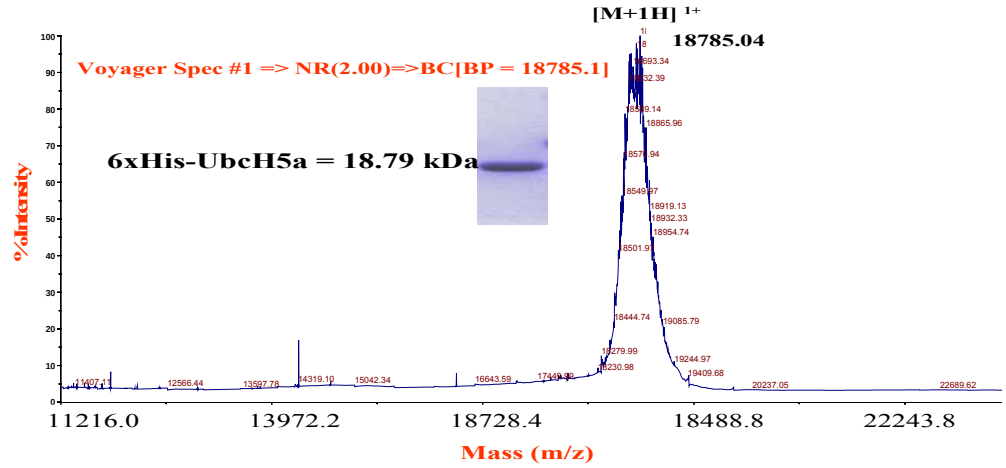

Figure 2-9: The molecular weight of purified MDM2RING, MDM2RING△C and 6xHis-UbcH5a determined by MALDI-TOF mass spectrometry. (A) MDM2RING is 12.85 kDa. (B) MDM2RING△C is 10.93 kDa. (C) UbcH5a is 18.79 kDa.

Table 2-1: Molecular weights of three constructs obtained using different methods.

	Molecular Weight (kDa)			
Constrcut	on-gel	theoretical*	MALDI-TOF MS	SEC
MDM2RING (386-491)	20~ 25	12.47	12.85	~ 26; > 250
MDM2RING△C (386-478)	20 ~ 25	10.74	10.93	~ 22
6xHis-UbcH5a	~ 17	18.9	18.8	~ 20

* Theoretical molecular weight was estimated using Protein Calculator v3.3 on the basis of primary amino acid sequences.

2.7 Conclusions

To sum up, the purity of three proteins, MDM2RING (residues 386-491), MDM2RING△C (residues386-478) and UbcH5a were more than 95%. On the SEC profiles, there were two major species in MDM2RING, dimeric and higher molecular weight oligomers, while MDM2RING△C existed predominately as a dimer. The yields of dimeric MDM2RING and dimeric MDM2RING△C from 1L cell culture were approximately 0.6 mg, and 3 mg, respectively. The SEC profile of UbcH5a demonstrated that UbcH5a is a monomer, and the yield was about 6 mg from 1L Cell culture. The MALDI-TOF MS methods confirmed that the molecular weight of each protein was as we expected. Following optimisation of the purification protocol, the three proteins of interest were highly purified and can be used for further biochemical, biophysical and structural studies.

3 Biochemical and Biophysical Characterisation of MDM2RING and UbcH5a

In this chapter, several methods were used to study the biochemical, biophysical and structural characteristics of MDM2RING and UbcH5a (as outlined in Figure 3-1). *in vitro* ubiquitination assays were used to test whether MDM2RING, residues 386-491, and MDM2RING△C, residues 386-478, have E3 ligase activity and can ubiquinate p53 (Section 3.1). To understand the oligomerisation state of those proteins, dynamic light scattering (DLS) and size exclusion chromatography (SEC) were used (Section 3.2). The thermal denaturation assay (TDA) has been used for identification of the folded state of proteins and to provide an assessment of the thermal stability of these proteins (Section 3.3). Circular dichroism spectroscopy (CD) also has been applied to study whether those proteins are folded or unfolded, and also to monitor the thermal stability (Section 3.4). Further structural studies using crystallization, negative staining transmission electron microscopy (TEM) and nuclear magnetic resonance (NMR) are described in Chapter 4.

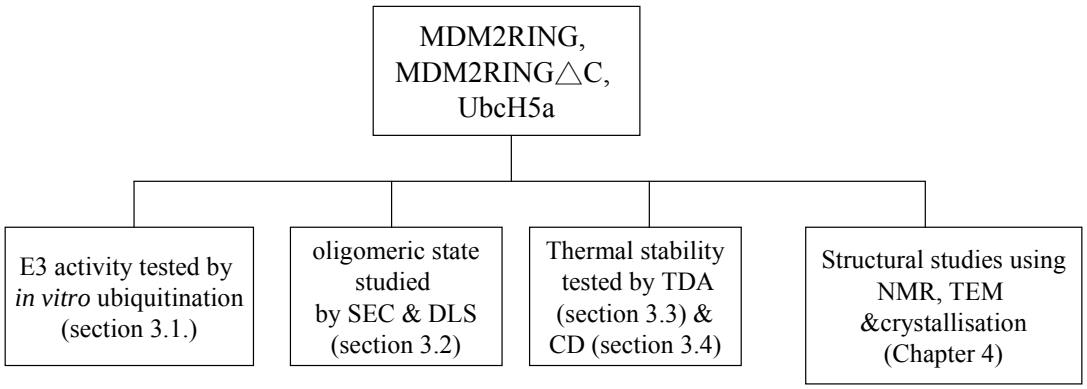

Figure 3-1: The work flow of analyses applied in the characterisation studies of MDM2RING, MDM2RING△C and UbcH5a in this thesis.

3.1 *in vitro* ubiquitination

3.1.1 the basis of *in vitro* ubiquitination

Ubiquitination is a critical mechanism in cells (described detail in Chapter 1). Several proteins are involved: E1 (ubiquitin activating protein), E2 (ubiquitin conjugating protein), E3 (ubiquitin kinase protein) and Ub (ubiquitin) (detail introduced in Chapter 1). To test the E3 ligase activity of MDM2 protein, we carried out an *in vitro* ubiquitination reaction. MDM2 has a RING domain, which possesses E3 ligase activity; therefore, the *in vitro* ubiquitination assay data is an indicator which confirms whether our MDM2RING has proper E3 ligase function. As with *in vivo* ubiquitination, the reaction mixture contains E1 (Ube1), E2, E3 and Ub proteins. In addition, ATP, substrates (such as p53), CK (creatine kinase) and CP (creatine phosphate) are also needed for the reaction. For the first step of ubiquitination, ATP is critical to activate Ub and induce the interaction of Ub and E1 protein. To maintain the concentration of ATP throughout the reaction, CP and CK are added to produce ATP from ADP. Following successful ubiquitination, the substrate will be modified with mono- or poly-ubiquitins (Figure 3-2). In this work, the E3 ligase activity of MDM2 was characterised by the extent of p53 ubiquitination. After the ubiquitination reaction, the sample was analysed using gradient SDS-PAGE, ubiquitinated p53 were detected by western blotting (Figure 3-2B). Antibody D01 (against p53) was used to detect p53 and ubiquitinated p53.

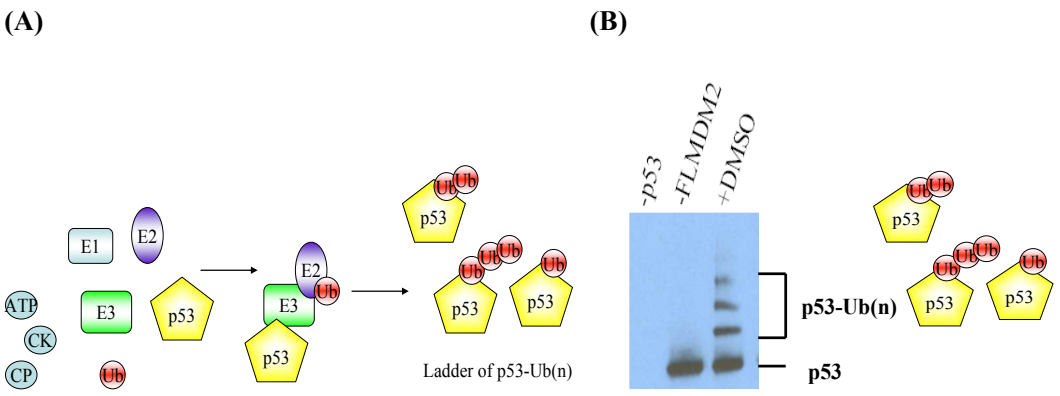

Figure 3-2: *in vitro* ubiquitination assay. (A) Schematic representation of the *in vitro* ubiquitination assay. (B) MDM2RING protein shows E3 activity and ubiquitinated p53. 10 ng FLMDM2 is used in this experiment.

3.1.2 Materials and Methods: *in vitro* ubiquitination assay

The protocol for an *in vitro* ubiquitination assay is as below (for 16 reactions): 366 µl H_2O, 10 µl 1M Hepes (pH8) (stored in fridge), 2.4 µl 1M $MgCl_2$, 2µl 10% Triton X, 0.2 µl 1M DTT, 0.4 µl 1M benzamidine, 3.2µl 10mg/ml ubiquitin, 6µl ATP 0.2M , and mix them gently by inversion (remove bubbles on cap). 4 µl 1M CP (creatine phosphate) and 2µl 10mg/ml CK (creatine kianse) were added into the reaction solution, and mixed gently by inversion. Next, 0.7 µl E1 Ube1 (0.55 mg/ml; 5µM; 110 kDa, purchase from Bioscience Co.) and 0.48 µl E2 UbcH5a (2.5 mg/ml) were added and mixed gently. Finally, the substrate was added for example p53 (0.5µg), and E3 ligase (0.2 µl/reaction, 120 ng). 22 µl reaction solution was aliquoted into each tube, and incubated at 30℃ for 10 minutes.

To stop the reaction, 22 µl loading dye was added to each sample, followed by heating at 95℃ for 5 minutes. Then samples were then put on ice before being loaded onto a ready made gradient gel, NuPAGE 4~12% (Invitrogen Co.). For each gel, a prestained marker (5 µl/well) was loaded into one well, and 20 µl of each sample was loaded. The tank was filled with NuPAGE buffer (diluted to a 1 X stock). The gel was run at 180 Volts for 2 hours. Following electrophoresis, western blotting was used to transfer the proteins from the gel to nitrocellulose membrane using 130 volts for 1 hour. 1L transfer buffer contains 100 ml (10X transfer buffer), 200 ml methanol, and 700 ml H_2O.

The membrane was blocked using 5% milk in a 1X PBST (100ml 10X PBST, 1ml Tween 20 in 900ml H_2O) and put on the shaker at room temperature for 20 minutes. The membrane was given three five minutes washes in PBST. The primary antibody used was D01, an anti-p53 antibody, diluted 1 in 5000 in 1XPBST+5% milk. 3 ml of the diluted primary antibody was used for each membrane. After incubation with 1°-Ab, D01, for 1 hour at room temperature (or overnight in the cold room), the membrane was washed three times in 1X PBST each time for 5 minutes. The secondary antibody (A26, anti-mouse) was diluted 1 in 2000 in 1XPBST + 5% milk. 3ml diluted 2°-Ab was added to each membrane, and the blot incubated on the bench for 1 hour. The membrane was given three times five minute washes in 1XPBST. Chemiluminescent development reagent (TCL: ECL =1:1 (v:v)) was prepared and mixed, prior to adding it to the membrane for 1 minute followed by detection using photographic film.

3.1.3 Results and Discussion: *in vitro* ubiquitination

- ***MDM2RING, residues 386-491, ubiquitinates p53***

The *in vitro* ubiquitination method has been widely used to study the function of E3 ligases. The *in vitro* ubiquitination methodology used in this thesis has been developed in Kathryn Ball's group (Wawrzynow et al., 2009), showing that FLMDM2 has E3 ligase activity to ubiquitinate p53 (Figure 3-2B). Several reports have shown that FLMDM2 can bind p53 through interactions with the N-transactivation and acidic domains, and facilitate p53 ubiquitination (Moll & Petrenko, 2003; Uldrijan et al., 2007; Wawrzynow et al., 2009). Previous work also showed that MDM2RING can autoubiquitinate itself (Kostic et al., 2006; Linke et al., 2008; Poyurovsky et al., 2007), however, there is no report yet to indicate that MDM2RING can ubiquitinate p53.

Our construct MDM2RING, residues 386-491, can ubiquitinate p53, suggesting that MDM2RING may contain a putative p53 binding site. Moreover, on the basis of previous reports (Goldberg et al., 2002; Maya et al., 2001; Khosravi et al., 1999; Shinozaki et al., 2003), MDM2 residue Tyr394 (phosphorylated by c-Abl) or Ser395 (phosphorylated by ATM) or Ser407 (phosphorylated by ATR) inhibits MDM2 E3 activity and activates p53 function. Phosphorylated MDM2 has been shown to attenuate the cytoplasmic export of p53. It is still probable, however, that phosphorylated MDM2 changes its conformation which disfavours p53-binding. Alternatively, phosphate competes with p53 to bind to this motif. Presumably, if our MDM2RING has a new p53 binding site within the N-terminal fragment proceeding the RING domain, our MDM2RING should bind and ubiquinate p53. As we expected, *in vitro* ubiquitination assay results showed that our MDM2RING (residue 386-491), could ubiquitinate p53 (Figure 3-3). These data demonstrated that there must be a motif in our MDM2RING constructs that interacts with p53 and facilitates MDM2-mediated ubiquitination of p53.

To test the hypothesis that this new p53 binding motif was located in the N-terminal fragment of MDM2RING, one deletion construct, MDM2RING△C (residue 386-478) was chosen to test its E3 ligase activity. If the new p53-binding motif was positioned in the N-terminus of MDM2RING, it should be possible to detect ubiquitinated p53. As shown in Figure 3-3, MDM2RING△C did have E3 ligase activity against ubiquitinated p53, demonstrating that a new p53-binding motif must be at the N-terminus of MDM2RING.

Although the exact p53-binding site still needs to be identified, these data provide additional evidence that the N-terminus of MDM2RING is essential for MDM2-dependent ubiquitination of p53.

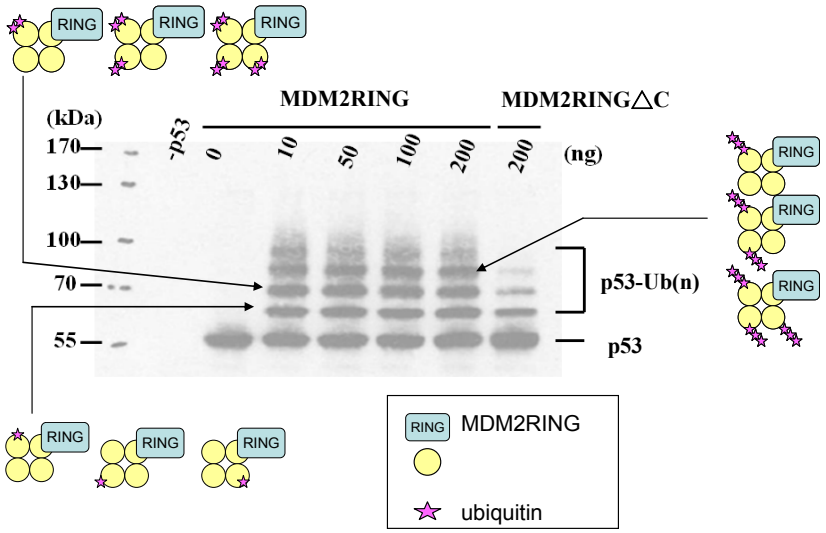

Figure 3-3: *in vitro* ubiquitination studies of the MDM2RING or MDM2RING△C-mediated ubiquitination of p53. Ubiquitination reactions are assembled with p53, E1, and E2 in the presence of MDM2RING or MDM2RING△C. Unmodified (p53) and ubiquitinated p53 (p53-Ub(n)) are detected using antibody DO-1.

- ***MDM2RING has higher E3 ligase activity than MDM2RING△C***

Titration experiments with MDM2RING showed that 10 ng MDM2RING had similar E3 activity to than seen with 200 ng MDM2RING△C (Figure 3-3). To determine the minimum amount of MDM2RING required for an *in vitro* ubiquitination assay, titration experiments were carried out ranging from 1 ng to 500 ng of MDM2RING. Results showed that 1, 5, 10, 50, and 100 ng MDM2RING had similar E3 ligase activities (Figure 3-4), whilst 200 ng and 500 ng protein showed reduced E3 activity. Consistent with previous report (Poyurovsky et al., 2007), it is of note that MDM2RING (residues 400-491) has stronger E3 ligase activity at low concentrations than high concentrations.

Moreover, Figure 3-3 showed that MDM2RING has stronger E3 ligase activity than MDM2RING△C (Figure 3-3), indicating that 200 ng of MDM2RING△C had weaker E3 ligase activity compared to that seen with the same amount of MDM2RING (200 ng). These results are consistent with previous studies noting that the C-terminus of MDM2RING plays an important role in E3 activity (Fang et al., 2000; Kawai et al., 2007).

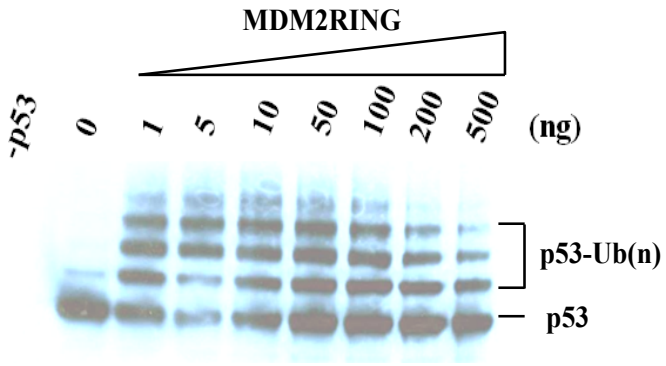

Figure 3-4: The E3 ligase activity of FLMDM2 and MDM2RING using *in vitro* ubiquitination assay. Titration experiments of MDM2RING are used to test its E3 ligase activity in the range of 1 to 500 ng.

- ***the potential role of the MDM2RING N-terminus for E2-binding***

The larger MDM2RING△C construct has E3 ligase activity, inconsistent with other studies that indicate that MDM2 C-terminal mutants or deletions lose their E3 activity (Line et al., 2006). For example, full length MDM2△7 (residue 1-484), full-length MDM2Y489A or full-length MDM2F490A lose their E3 activity (Poyurovsky et al., 2007; Uldrijan et al., 2007). One possible explanation is that our MDM2RING△C construct has an extended N-terminal domain which might provide necessary contacts with its cognate E2 protein, UbcH5a, facilitating the ubiquitination reaction. Based on the crystal structure of cIPA2-UbcH5b, cIAP2 proteins have interactions with their E2 partners through two regions: the N-terminus and C-terminus (Mace et al., 2008). Previous report indicated that the last five C-terminal residues are essential for MDM2 E3 ligase (Linke et al., 2008). Their MDM2 mutants (residues 432-479) or MDM2F490A mutant lost E3 ligase activity. Compared to previous MDM2 constructs, our MDM2RING△C (residues 386-478) has a longer N-terminal fragment, suggesting that the additional residues may play a key role in E2-binding. Additionally, evidence comes from the crystal structure of the c-Cbl-Ubc13 complex, in which a linker preceding the U-type E3 domain seems to be responsible for the interactions with Ubc13 (Zheng et al., 2005) (Figure 3-5). The linker is between c-Cbl N-terminal TKB domain and C-terminal RING-type E3 domain including two intermolecular hydrogen bonds between C-Cbl Glu369 and UbcH7 Arg5 and c-Cbl Glu366 and UbcH7 Arg15. The c-Cbl linker contains several polar and charged residues. Corresponding residues in MDM2 are also polar and charged, and this observation may explain why our MDM2RING△C is E3 active as the N-terminal region provides additional interaction with the E2 protein (Figure 3-

5). Moreover, it has been noted that MDM2RING (residues 400-491) could autoubiquitinate itself, but MDM2RING deletion (residues 400-484) lost its E3 activity (Poyurovsky et al., 2007). Taken together, our data suggest that an uncharacterised extended N-terminus (residues 386-400) in our MDM2RING△C may play an unidentified role in contributing to maintenance of MDM2RING△C E3 ligase activity.

(A)

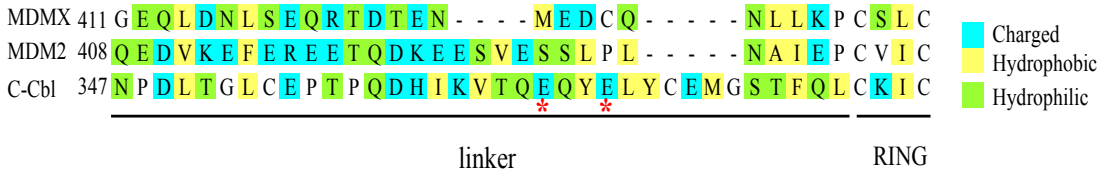

(B)

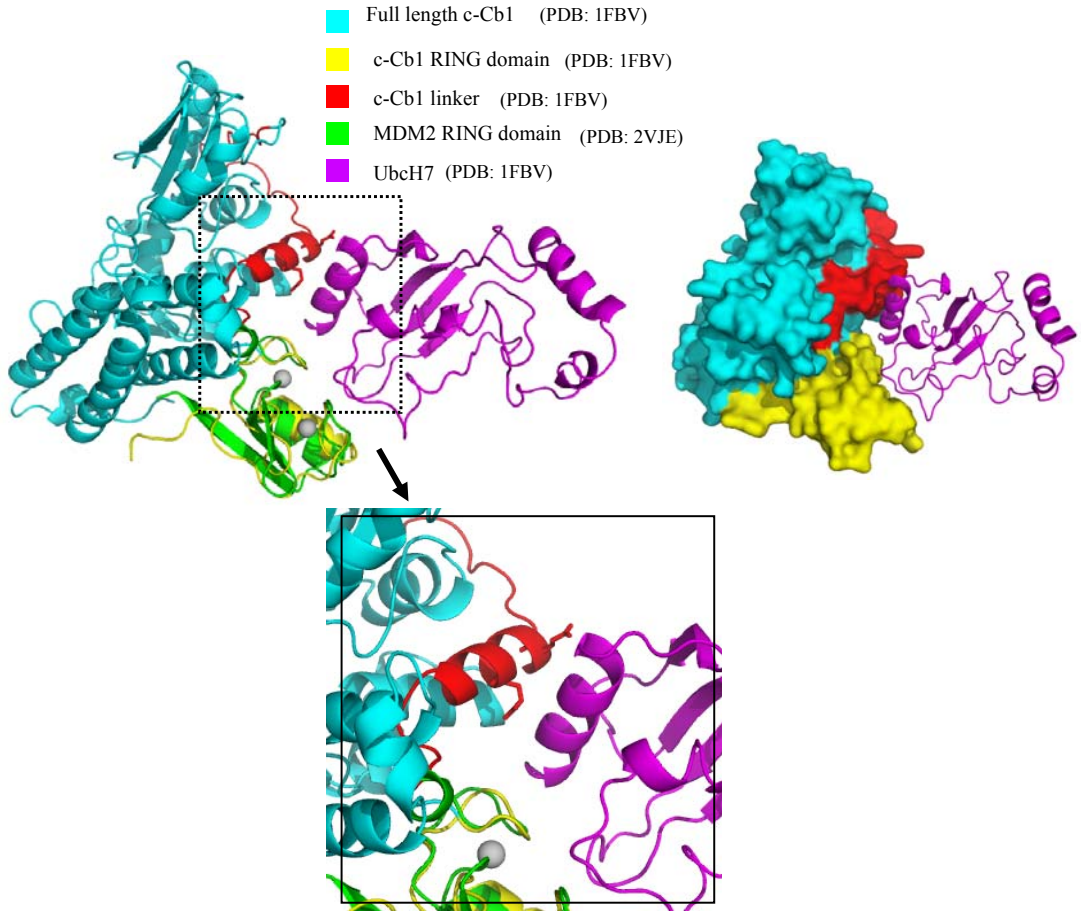

Figure 3-5: The role of the N-terminal fragment of RING/U-type E3 ligases. (A) Sequence alignment of c-Cbl linker and the N-terminal fragment proceeding MDM2/MDMX RING domain. Those fragments contain several polar and charged residues. c-Cbl residues forming H-bonds with UbcH7 are highlighted by a red star. (B) MDM2 RING (green) domain is superimposed onto the cCbl RING domain (yellow) of the cCbl-UbcH7 complex (PDB code: 1FBV). c-Cbl RING domain and the linker interact with UbcH7.

- ***a hypothesis of MDM2RING-mediated ubiquitination of p53***

It has been widely noted that the N-hydrophobic domain (i) and acidic domain (ii) in MDM2 play essential roles in the interactions with p53 (Fang et al., 2000; Wallace et al., 2006). A careful analysis of the literature coupled with the new finding discussed in this work has allowed a new hypothesis to be proposed: a new motif preceding the N-terminal fragment of the RING domain (iii) is also critical for p53-binding (Figure 3-6). Both our MDM2RING and MDM2RING△C constructs could ubiquitinate p53, and this suggests that the motif responsible for the p53-binding must be located in the N-terminal fragment preceding the RING domain, rather than the C-terminus. Additional supporting evidence for our hypothesis comes from another MDM2RING construct, residues 396-491, which also ubiquitinates p53. Moreover, it has been noted that MDM2S386D can ubiquitinate MDMX, but not p53 (Cheng, et al., 2009).

In our model, tetrameric p53 interacts with the hydrophobic domain (Hy), and the acidic domain (Ac) of MDM2 and induces a conformational change, subsequently opening the third p53-binding site to process the ubiquitination of p53 (Figure 3-6A). For the MDM2RING-mediated ubiquitination, the third p53-binding site in MDM2RING is easily accessible for p53-binding (Figure 3-6B). Additionally, combined with our previous analysis of the sequence and structural alignments of MDM2 and c-Cbl, the N-terminal motif preceding the MDM2RING may play a role in the interaction with its cognate E2 (UbcH5a) as seen in the c-Cbl linker. Taken together, we proposed that the interaction of p53 with a third binding motif (iii) may be essential to bring MDM2RING domain (charged-UbcH5a attached) close to the substrate and facilitate the transfer of ubiquitin to p53 (Figure 3-6A & B). This model provides a putative explanation for FLMDM2-mediated and MDM2RING-mediated ubiquitination of p53. Consideration of MDM2 proteins easily becoming oligomers, we also propose a model of the interactions between the oligomeric MDM2 RING proteins with UbcH5a and tetrameric p53 (Figure 3-6C). However, these proposals await further experiments to identify the exact new motif responsible for the interaction with p53.

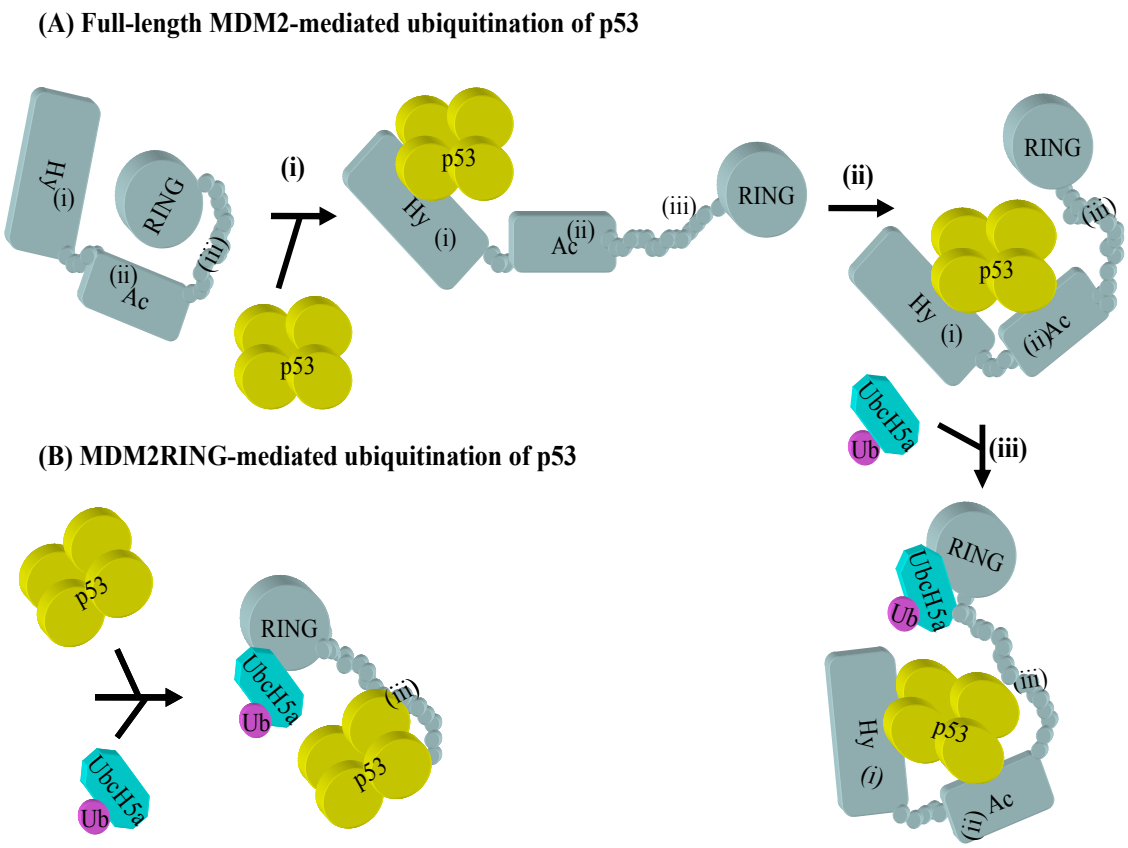

(C) the interaction between oligomeric MDM2 RING proteins with UbcH5a and p53

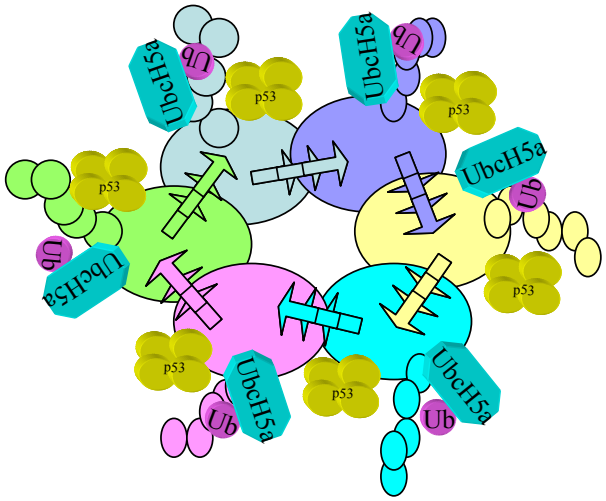

Figure 3-6: The proposed model of the p53-MDM2-UbcH5a-Ub complex. (A) Full-length MDM2-mediated ubiquitination of p53. Three binding sites on MDM2: hydrophobic domain (i), Acidic domain (ii) and the N-terminal fragment of MDM2RING (a linker, iii). (B) MDMRING-mediated ubiquitination of p53 is achieved through binding of MDM2 linker (iii) to bring the p53 and the charged-UbcH5a (Ub-UbcH5a) closer to facilitate the transfer of Ub. Hy: hydrophobic domain; Ac: acidic domain; RING: RING domain; Ub: Ubiquitin. (C) the interaction between oligomeric MDM2 RING proteins with UbcH5a and p53

3.2 Oligomeric state studies using dynamic light scattering

3.2.1 The Principle of dynamic light scattering

Dynamic light scattering (DLS) is used to measure the hydrodynamic size and polydispersity of molecules and particles, including proteins and nanoparticles, in solution. DLS is also referred to as Quasi-Elastic Light scattering (QELS) or Photon Correlation Spectroscopy (PCS) and was first used the 1960s (Berne and Pecora, 1976; Brown, 1993; Earnshaw and Steer, 1983; Johnson and Gabriel, 1994). The principle of DLS is that the laser beam passes through a focusing lens hits the moving particles in solution, resulting in light scattering at all angles while the light hit the particles (Figure 3-7). Generally, to simplify the effect of the scattered light, there is only one detector on the instrument at 90 degrees to record the scattered light. The scattered light passes through coherence optics and is detected by a photomultiplier, also called the digital correlator, which is designed to immediately convert the intensity fluctuations of the light signal into electrical pulses. The electric pulse data is analysed automatically.

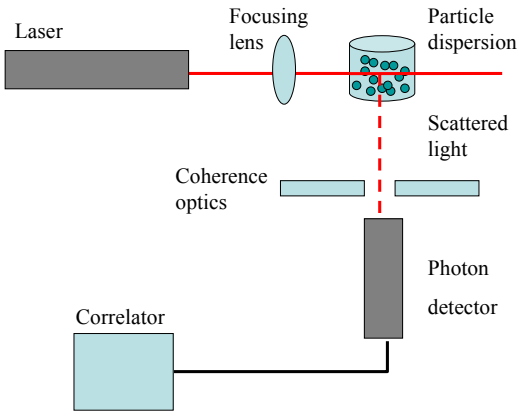

Figure 3-7: The diagram illustrates the basic mechanism of the dynamic light scattering (DLS) instrument. The size of the sample is able to be measured according to the intensity fluctuation of light signal (detail introduction in the text).

The advantages are that sample concentration can be low and the sample can be recovered. DLS is used to measure the diameter of the hypothetical hard sphere of a particle. However, protein molecules are dynamic and non-spherical. Therefore, the measured diameter is the apparent size of the dynamic particle (the hydrodynamic diameter). Therefore, DLS can be used to determine the oligomeric state of proteins according to the measured hydrodynamic sizes. For small proteins, DLS may be less accurate when compared to classical light scattering. However, it is still a convenient preliminary method to determine the size of the samples in solution, the stability of the proteins in various buffer conditions, and also useful for preliminary screens to determine the optimum conditions for crystallography (Jia et al., 2005; Wilson, 2003). In this section, the DLS analysis is performed on a Zetasizer APS instrument designed by Malvern Co. Furthermore, to avoid noisy signals produced by aggregates, the sample was filtered by the syringe filter (0.22 μm) prior to loading into the well. A minimum of 60 μl at 0.5 mg/ml was required for each sample to be analysed.

3.2.2 Oligomeric states of MDM2RING

- ***Hydrodynamic diameter of MDM2RING by SEC and DLS***

There were several peaks in the SEC profile of MDM2RING, when purified using a Sephacryl S-200HR column. The two major peaks were at a V_{ret} of 40 ml (>160 kDa), and at V_{ret} of 65 ml (20 ~ 40 kDa) (Figure 3-8A). The theoretical molecular weight of monomeric MDM2RING was 12.47 kDa. The SEC profile suggested that MDM2RING might exist as higher molecular weight oligomers and as tetramer or dimer. To further characterise the oligomeric state of MDM2RING, dynamic light screening (DLS) was used.

The concentration of protein required for DLS is at least 0.5 mg/ml. The second major peak from the Sephacryl S-200HR column was collected and the protein concentrated to 40 μM (=0.5mg/12470 daltons). The measured hydrodynamic diameter of 40 μM MDM2RING was 6.7 nm (67 Å) (Figure 3-8B). According to the known crystal structure of the MDM2-MDMX heterodimer (PDB code: 2VJE), the hydrodynamic diameter of a monomer is approximately 33.8 ~36.1 Å, and that of the dimer is approximately 33.7 ~ 47.7 Å (Figure 3-8C). Therefore, 40 μM MDM2RING did not exist as either a monomer or a dimer. Moreover, the calculated molecular weight of MDM2RING by DLS is 58 ~60 kDa, the data therefore suggested that MDM2RING may exist as a hexamer.

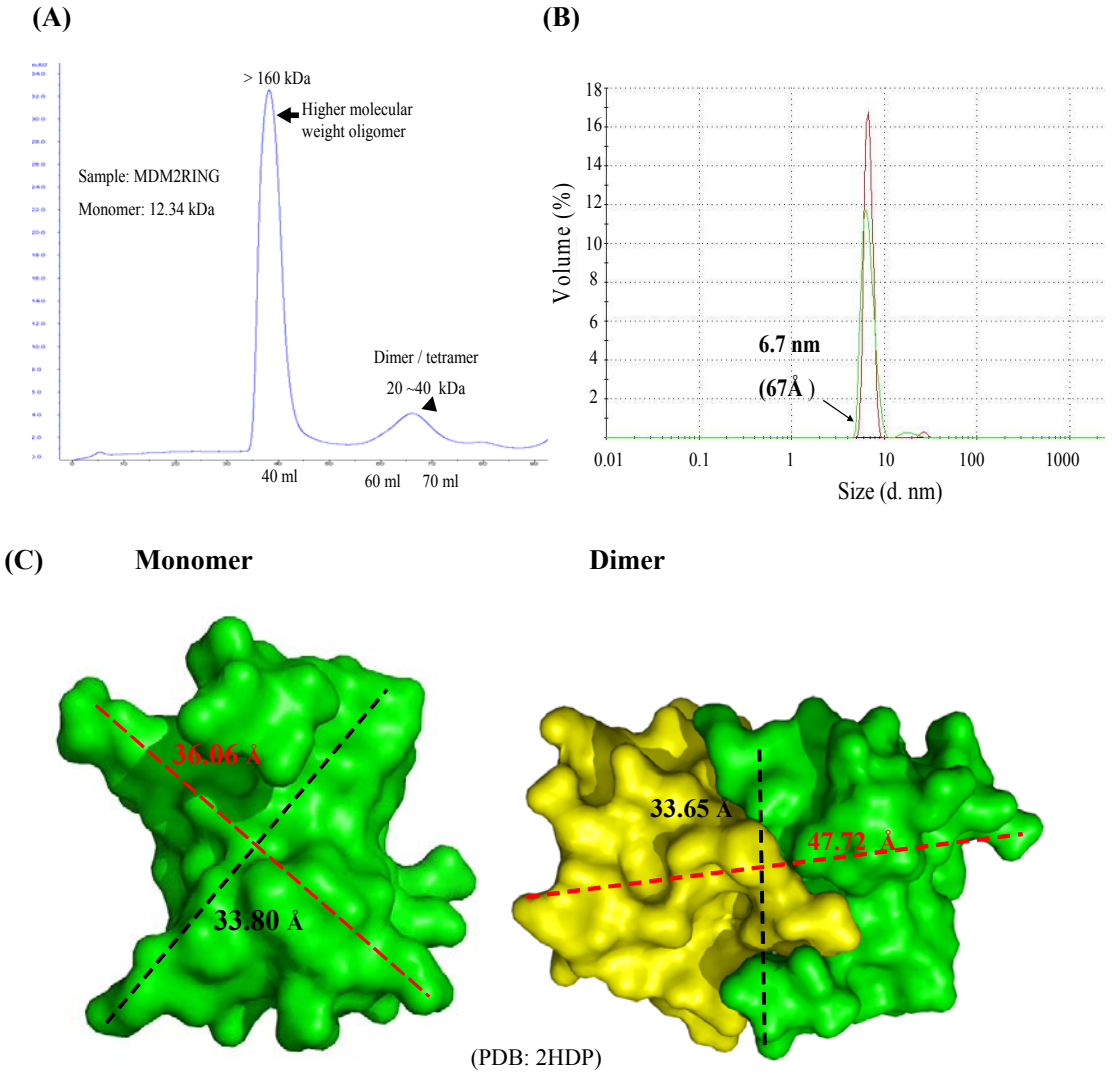

Figure 3-8: Oligomeric states of MDM2RING are measured by dynamic light scattering. (A) The SEC data show that there are two major populations of MDM2RING: higher molecular weight oligomers MDM2 at V_{ret} = 40 ml (>160 kDa) and dimer/tetramer MDM2RING at V_{ret} = 65 ml about 20 ~ 40 kDa. (B) DLS data show that the experimental hydrodynamic diameter and the estimated molecular weight of the eluted protein solutions from the fraction (V_{ret}=65 ml) is 6.7 nm and 58~60 kDa, respectively. The concentration of the tested MDM2RING is 40 µM. (C) The hypothetical hydrodynamic diameter of monomeric MDM2RING or dimeric MDM2RING/MDMXRING is shown based on the crystal structure of MDM2-MDMX heterodimer (PDB code: 2VJE).

- ***Concentration-dependent oligomerisation of MDM2RING***

During the purification of MDM2RING, we observed a concentration-dependent oligomerisation of the protein as seen in the SEC profiles when using a superdex 200 column (Figure 3-9A). At low concentrations, 0.3 mg/ml (24 µM) or 1.0 mg/ml (80 µM) MDM2RING, the major peak eluted at about 15ml ($M.W._{estm.}$ = 25 ~ 30 kDa) (Figure 3-9A,

red & gray lines). When MDM2RING was concentrated to 1.7 mg/ml (136 μM) or 1.9 mg/ml (152 μM), there were two major peaks on the size exclusion profile: one at 15 ml whilst higher molecular weight oligomers eluted at 10.7 ml ($M.W._{estm.}$ > 440 kDa) (Figure 3-9A, cyan and blue lines). The SEC data therefore suggests a concentration dependent oligomerisation of MDM2RING resulting in a very high proportion of multimers being produced at concentrations above 100 μM.

To confirm the SEC data with respect to the concentration-dependent oligomerisation seen, DLS was used. Different concentrations of MDM2RING (42.6 μM, 82.0 μM and 163.9 μM) were used. DLS data shown in Figure 3-9B indicated that the hydrodynamic diameter of the 42.6 μM and 82.0 μM MDM2RING samples were both approximately 7 nm with a predicted molecular weight of 68 kDa. As we expected, concentrated proteins (163.9 μM) formed larger particles (>1000 kDa).

Differences were seen in the calculated molecular weights of MDM2RING as detected by SEC and DLS. One reason was that DLS detects the particles in solution in a mobile state, and was sensitive to any particle in the solution. The DLS technique is more sensitive to larger particles rather than small molecules, such as our constructs. Because the small particles are easily affected by Brownian motion, it is not easy to obtain an accurate molecular weight of the small particles at lower concentrations. However, results obtained from SEC and DLS both showed that MDM2RING became higher molecular weight oligomers at higher concentrations. This finding is similar to that of another group that also showed their construct, MDM2RING easily aggregates (or oligomerises) at a concentration higher than 120 μM (Kostic et al., 2006). We maintained our purified MDM2RING at less than 100 μM during the whole analysis.

(A) Size exclusion chromatography (superdex 200)

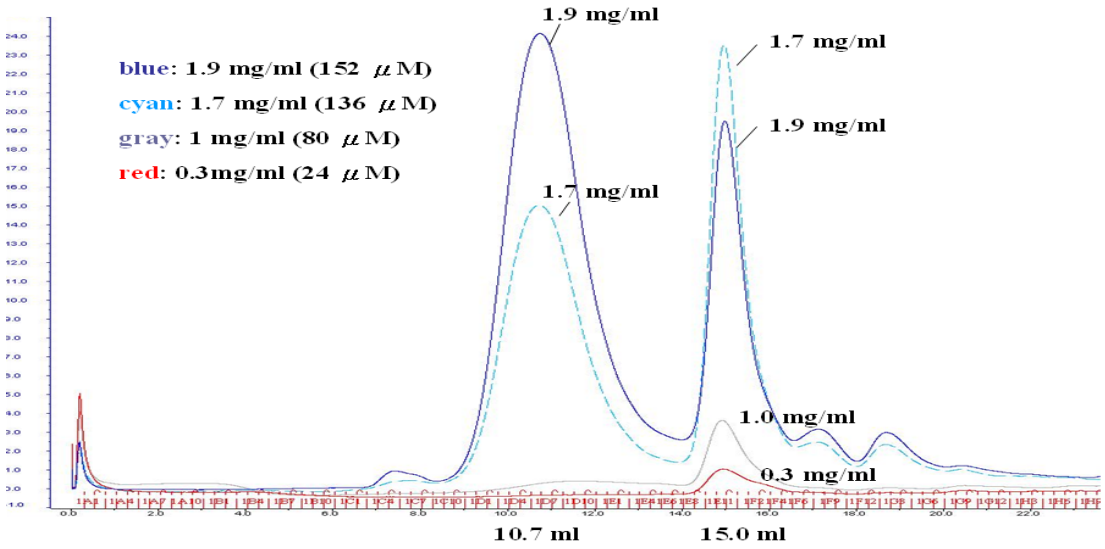

(B) Dynamic light scattering

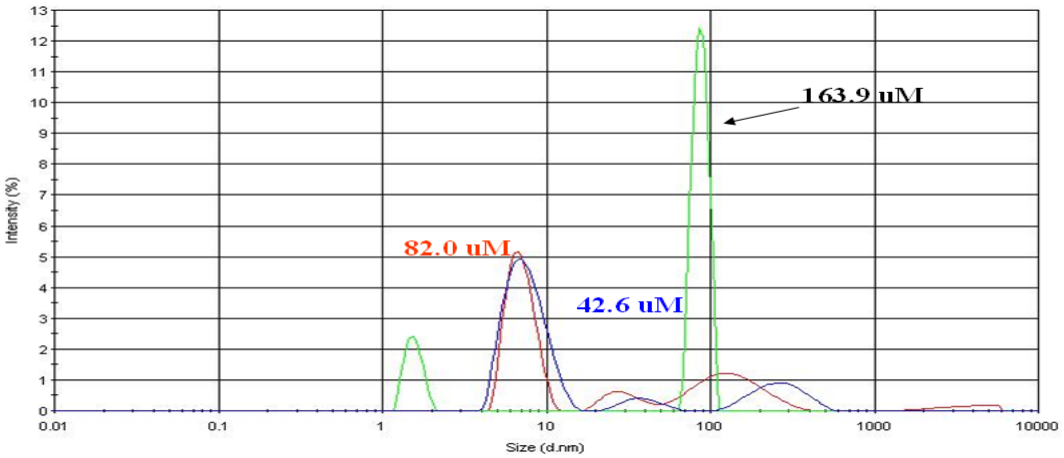

Figure 3-9: The oligomeric state of MDM2RING appears concentration-dependent when analysed by size exclusion chromatography (SEC) and dynamic light scattering (DLS). (A) A greater proportion of proteins are eluted in the void fraction when a more concentrated sample of MDM2 RING protein is applied to the superdex200 column. Red curve: 24 μM, gray curve: 80 μM, cyan curve: 136 μM and blue curve: 152 μM. (B) The results from dynamic light scattering indicated that highly concentrated MDM2RING easily become higher oligomers. MDM2RING 42.6 μM and 82.0 μM exist as lower molecular weight entitles (~ 68 kDa), and became higher molecular weight oligomers at a concentration of 163.9 μM.

3.2.3 Oligomeric states of MDM2RING△C

MDM2RING△C protein is a dimer based on the SEC data (Figure 2-7B). To test whether the MDM2RING△C protein also tends to become aggregated at higher concentrations (as seen with the MDM2RING), we analysed concentrated MDM2RING△C (~ 200 μM) by DLS. The result showed that the hydrodynamic diameter of MDM2RING△C was approximately 4.4 nm, with a predicted molecular size of 22~28 kDa. Monomeric MDM2RING△C theoretically was 10.88 kDa based on its amino acid sequence. These results suggest that MDM2RING△C exists as a homo dimer even at higher protein concentrations (Figure 3-10A). To clarify if the concentration of NaCl in the buffer affects the oligomeric status of MDM2RING△C, we also tested MDM2RING△C in different ionic strengths buffers, such as 50 mM and 150 mM NaCl (Figure 3-10B). Data showed that there were no differences in the size distribution of MDM2RING△C in both buffers. In summary, the differences seen in the oligomeric states of MDM2 RING△C and MDM2RING showed that the C-terminal thirteen amino acids play a critical role in the concentration-dependent oligomerisation of MDM2 RING protein.

(A)

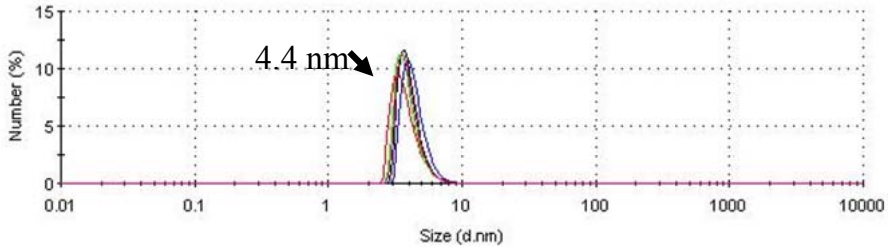

(B)

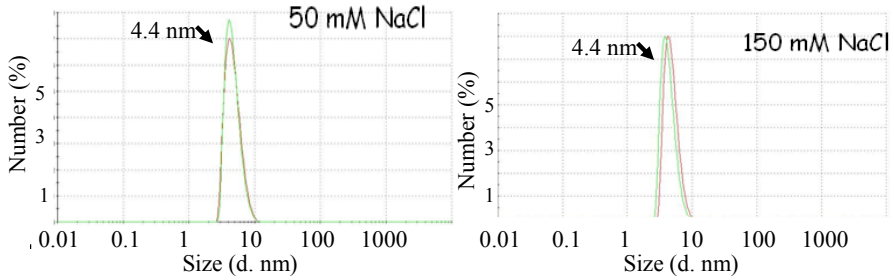

Figure 3-10: A high concentration 200 μM of MDM2RING△C protein are analysed by DLS (A), comparing two different ionic strength buffers (B). The predicted molecular weight suggests that MDM2RING△C was dimeric (~ 22 kDa) and not affected by change in ionic strength of the buffer.

3.2.4 Oligomeric states of UbcH5a

The oligomeric state of UbcH5a was analysed by various methods, such as gel filtration chromatography, MALDI-TOF mass spectrometry and dynamic light scattering, and these results revealed UbcH5a was monomeric. There was single peak on gel filtration chromatography, with an estimated molecular weight of 20 kDa (Chapter 2, Figure 2-8B). A single major peak is seen with MALDI-TOF mass spectrometry (Chapter 2, Figure 2-8C) with an estimated molecular weight of approximate 18.8 kDa. We also used dynamic light scattering to further characterise the oligomeric status of UbcH5a and to test the stability of UbcH5a in the storage buffer (50 mM Tris, 150 mM NaCl, pH7.2). DLS data showed that the hydrodynamic diameter of UbcH5a was 3.95 nm, and the molecular weight was approximate 18 kDa. Consistent with our previous analysis, DLS data (Figure 3-11) demonstrated that UbcH5a existed as a monomer even at higher concentrations (2 mg/ml), suggesting UbcH5a is stable in this storage buffer.

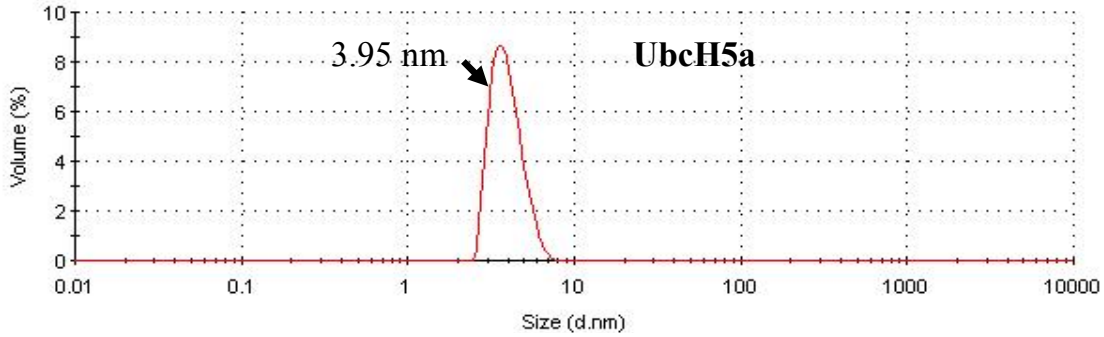

Figure 3-11: The oligomeric status of UbcH5a was analysed by dynamic light scattering. Purified UbcH5a at a concentration of 2mg/ml in storage buffer (50 mM Tris, 150 mM NaCl, pH7.2) was analysed and showed that its calculated hydrodynamic diameter is 3.9 nm with an estimated molecular weight of approximately 18 kDa.

3.3 Thermal Denaturation Assay (TDA)

3.3.1 The Principle of TDA

The thermal denaturation assay (TDA), also called thermal fluorescence assay (TFA) or thermal shift assay (TSA), is an efficient and simple technique to study the thermal stability of proteins. This technique has broad applications in screening for protein stability in different buffers with additives or salts to determine the optimal buffer for any given protein. It is critical to maintain the stability of proteins in an appropriate buffer to enable further

studies, such as biophysical characterisation, bioactivity, and structural studies, including NMR and crystallography (Chung, 2007; Ericsson et al., 2006). TDA is also a fast and efficient method to test the interaction of proteins and potential ligands (Lo et al., 2002; Pantoliano et al., 2001). Thermal stabilities of apo-protein and protein-ligand complexes are different. Moreover, several reports have shown that the melting temperatures (Tm) obtained by TDA are consistent with other techniques including circular dichroism (Kelly & Price, 1997), and differential scanning calorimetry (Freirey, 1995). The Tm value, the melting temperature of the protein, is defined as the temperature at which the amounts of folded and unfolded proteins are equal in solution. The Tm value acts as an indicator of the stability of the protein. Compared to other methods, some of the advantages of TDA are that only a small amount of protein is required per experiment (1~15 μg) and that the experiment can be carried out on a commercially available real-time PCR machine, making the technique accessible to laboratories without ready access to highly specialised equipment. The technique is also relatively high throughput using a 96 well format plate with an average run time of less than an hour.

The basic principle of the thermal denaturation assay is the detection of fluorescence emitted by a fluorophore bound to folded and unfolded proteins (Figure 3-12). A hydrophobic environmentally sensitive fluorophore, such as Sypro Orange (yellow star, Figure 3-12), is commonly used to monitor protein unfolding (Ericsson et al., 2006). The Sypro Orange probe is easily quenched in an aqueous environment within the folded protein. When the protein starts to undergo thermal unfolding as the temperature increases, hydrophobic region of the unfolding protein are exposed. Sypro Orange preferentially binds to hydrophobic regions of unfolded proteins, resulting in a significant increase in fluorescence emissions. After the fluorescence intensity reaches a maximum, the fluorescence intensity starts to decrease as the complex of denatured protein and Sypro Orange probe precipitates. The melting transition curves reveal differences in the fluorescence intensity of the folded vs. the unfolded protein as a function of temperature..

3.3.2 Material and Methods: TDA

1~15 μg protein and 5X Sypro Orange dye, a fluorescent dye, were added to each well of a 96-well thin-wall PCR plate (Bio-Rad), the final volume of the sample was 50 μl. The plate was sealed with Optical-Quality Sealing Tape (Bio-Rad). The experiment was performed on an iCycler iQ Real Time PCR Detection System (IQ5) (BioRad): the experimental set up

was as described below: 1℃ increment per 30s hold time with temperature intervals from 20 ~ 90℃. The data were automatically analysed to provide a value for the melting point (Tm). All samples were analysed in triplicate to generate reliable data.

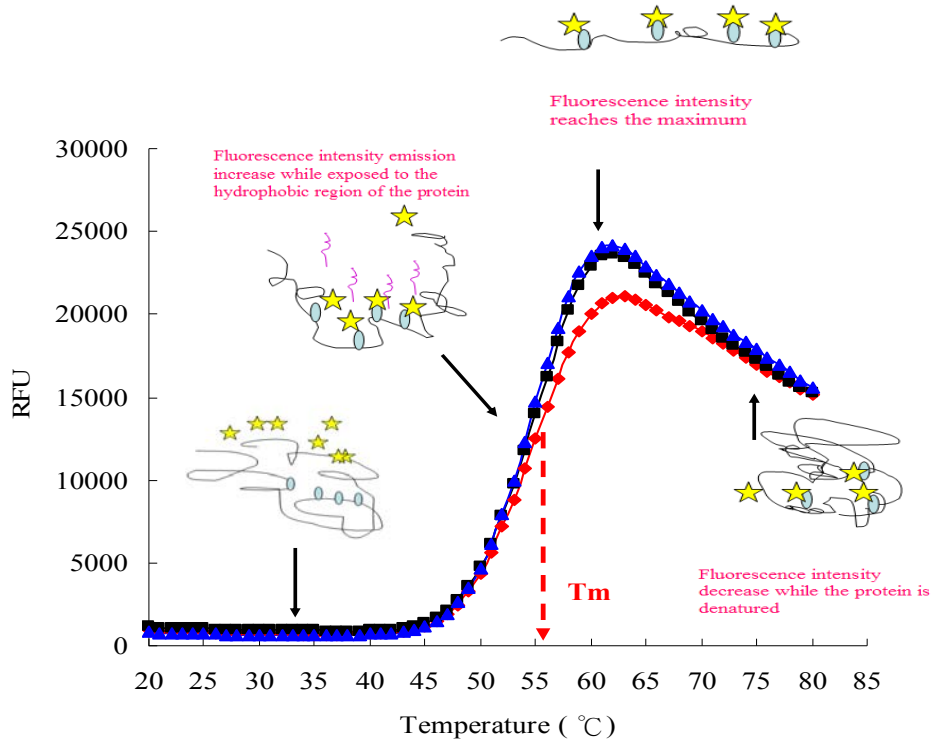

Figure 3-12: The principle of TDA method. Fluorescent dye, Sypro Orange (yellow stars), preferentially bind to hydrophobic residues (cyan ellipses), which usually are buried within the protein. As the temperature increases, the proteins unfold, exposing hydrophobic residues, allowing the Sypro Orange to bind to the hydrophobic residues, resulting in an increase in the fluorescence signals detected. The fluorescence intensities decrease when the proteins become denatured and aggregated at high temperatures. The red dashed line indicates the Tm value, the melting temperature referred to as the midpoint of the unfolding transition of a protein.

3.3.3 Results & Discussions: TDA

- ***MDM2RING is a metal-binding protein***

TDA results showed that there was no clear melting transition curves observed for MDM2RING. Besides, initially, high fluorescence intensities were observed that dropped gradually after the temperature increased (Figure 3-13A). Fluorescence intensities of 500 RFU were detected at the start of the analysis for 10 μM MDM2RING. No clear melting

transition curves may be due to the high hydrophobicity of the metal-binding protein. The solution structure of MDM2 homodimer showed that MDM2 RING domain is folded tightly through interactions with two zinc ions (Kostic et al., 2006; Linke et al., 2008), possibly resulting in MDM2RING being thermally stable and being difficult to unfold as the temperature increases. At high temperature, precipitated MDM2RING might shield the hydrophobic part and Sypro Orange dye also denatured; therefore, there was no detectable increase in fluorescence intensity. In order to confirm the assumption that our MDM2RING is folded and tightly interacts with zinc ions, we added excess EDTA to chelate the zinc ions from MDM2RING, and test the thermal stability of MDM2RING in the buffer with EDTA. Two zinc ions have been noted to play a structural role in MDM2RING (Figure 3-14): the first zinc binding site is formed by Cys438, Cys441, Cys 461 and Cys 464, and the second one is formed by His452, His457, Cys475 and Cys478. Therefore, without the zinc ions, MDM2RING should have less structural integrity, resulting in the hydrophobic part of MDM2RING being easily exposed as the temperature increases. Sypro Orange could then bind to an exposed hydrophobic part of the unfolding MDM2RING, producing a rise in fluorescence intensity.

As expected, in the presence of EDTA, our TDA studies of MDM2RING showed that there was a clear melting transition curve. Tm for MDM2RING in the presence of excess EDTA (about 10 fold) was approximately 47.6℃ (Figure 3-13B). If MDM2RING initially is an unfolded protein, there will be a similar melting transition curve of MDM2RING seen in solution with or without EDTA (Figure 3-13A). Because there was a clear melting transition curve observed after the addition of EDTA, these results confirmed that MDM2RING is a folded zinc binding protein, as addition of EDTA which chelates the zinc ions from MDM2RING resulted in MDM2RING becoming more flexible and easily unfolded at higher temperatures; allowing the melting transition curve to be observed.

(A) 10 µM MDM2RING

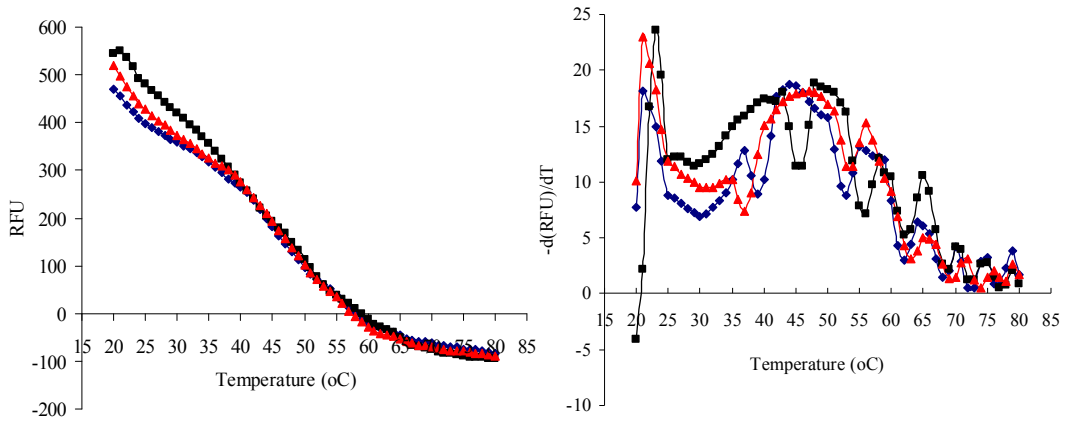

(B) 10 µM MDM2RING + 100 µM EDTA

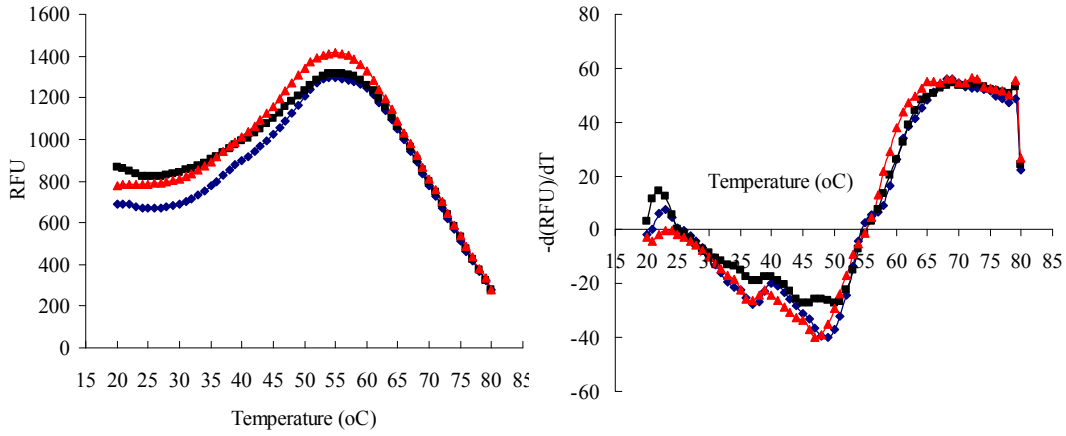

Figure 3-13: The thermal stability of MDM2RING was analysed by TDA. (A) 10 µM MDM2RING was analysed using TDA and showed no clear transition melting curve. (B) After addition of a 10 fold excess of EDTA to MDM2RING, a Tm value for MDM2RING of approximately 47.6 ℃ was calculated. The panel on the left illustrates the fluorescence intensities, the panel on the right shows the value of –d(RFU)/dT as a function of the temperature. All samples were tested in triplicate (as shown by the black, red and blue curves).

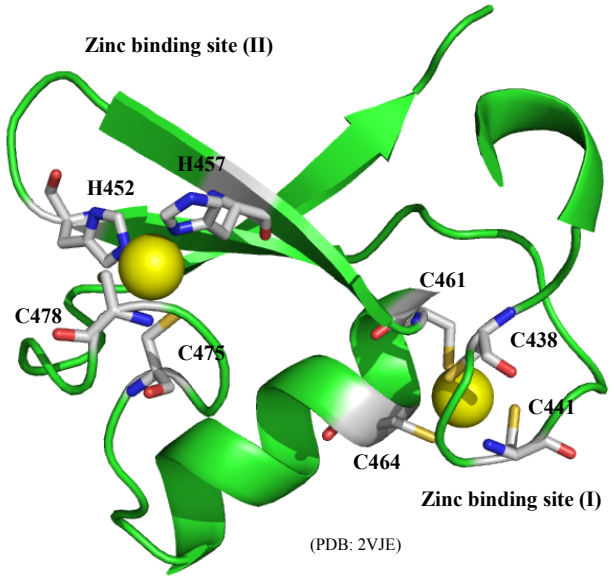

Figure 3-14: Zinc ion binding coordination in MDM2RING. The solution structure is one subunit of MDM2 dimers (PDB code: 2VJE). First zinc binding site (I) is formed by Cys438, Cys441, Cys461 and Cys464 while the second one (II) is formed by His452, His457, Cys475 and Cys478. Zinc is depicted as yellow spheres. Those zinc-binding residues are coloured in white stick representations.

- ***MDM2RING is an ATP-binding protein***

It has been noted that MDM2 RING domain contains an ATP binding motif. ATP-bound MDM2 is preferentially located in the nucleolus (Poyurovsky et al., 2003). By definition, binding of ATP to the protein may induce a conformational change in the protein and shift the Tm value of MDM2RING. In this work, we tested the thermal stability of MDM2RING by TDA, with the addition of ATP and with or without EDTA. Although there was no clear melting curve shown by apo-MDM2RING, we wanted to test if ATP might bind to MDM2RING to make MDM2RING unfold and provide a transition melting curve.

Results showed that addition of ATP had no effect on the data obtained (Figure 3-15A). However, on addition of EDTA and ATP, there was a clear melting transition curve seen. The Tm obtained for the mixture (5 μM MDM2RING + 500 μM ATP + 5 mM $MgCl_2$ and 50 μM EDTA) was about 62.0℃(Figure 3-15B). This compares with a Tm of 47.6℃ for MDM2RING and EDTA. Thus addition of ATP gives a thermal stability upward shift of approximately 14.4℃. (Figure 3-16). Such a significant increase in Tm provides clear evidence that not only there is an interaction between ATP and MDM2RING, but also

demonstrated that stabilization of MDM2RING is enhanced by ATP. Consistent with previous reports, it has been shown that ATP-binding to MDM2 is structurally dependent, and the affinity of ATP to MDM2 was approximate 0.77 µM (Priest et al., 2010). ATP plays diverse roles in mediating the function of MDM2 including regulation of sub-cellular compartmentalization of MDM2 (Poyurovsky et al., 2003), acting as molecular chaperone for p53 (Wawrzynow et al., 2007), and enhancing MDM2-mediated inhibition of the DNA-binding function of E2F1 (Stevens et al., 2008). In summary, these TDA studies provide biophysical data showing that MDM2RING contains metal ions and also revealed that ATP interacts with and stabilises MDM2RING.

(A) 5 µM MDM2RING + 500 µM ATP + 5 mM $MgCl_2$

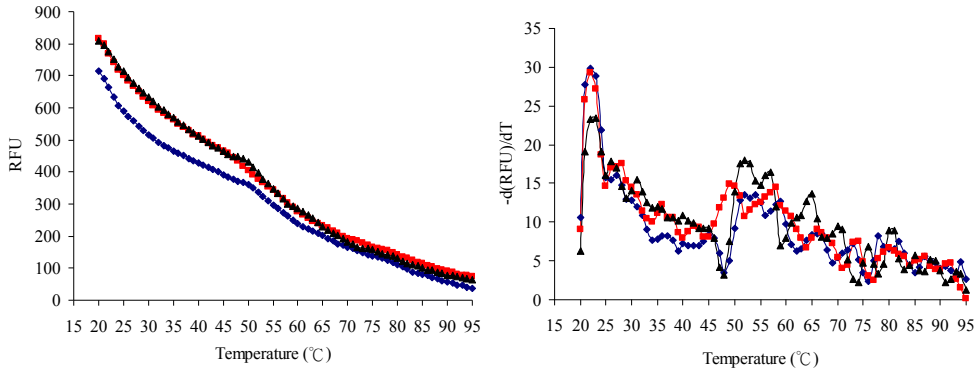

(B) 5 µM MDM2RING + 500 µM ATP + 5 mM $MgCl_2$ + 50 µM EDTA (61.96℃)

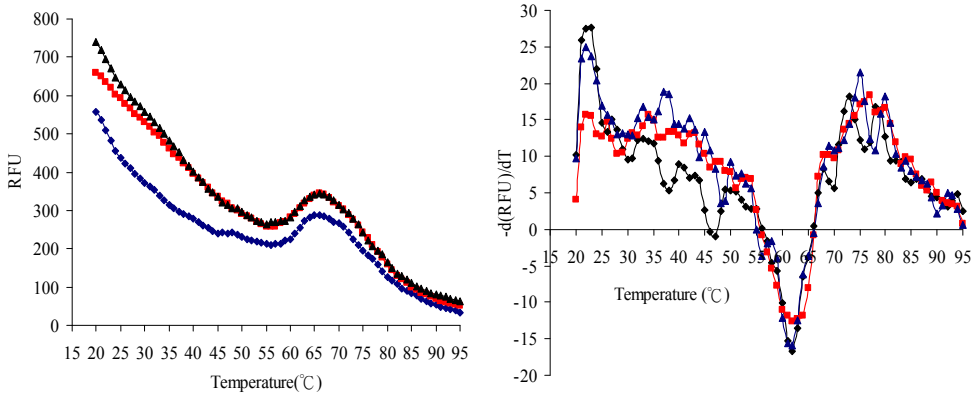

Figure 3-15: TDA studies of MDM2RING in the presence of ATP with and without EDTA. (A) 5 µM MDM2RING + 500 µM ATP + 5 mM $MgCl_2$. (B) 5 µM MDM2RING + 500 µM ATP + 5 mM $MgCl_2$ + 50 µM EDTA. There is detectable thermal melting curve while both ATP and EDTA were present in the sample. All samples were tested in triplicate.

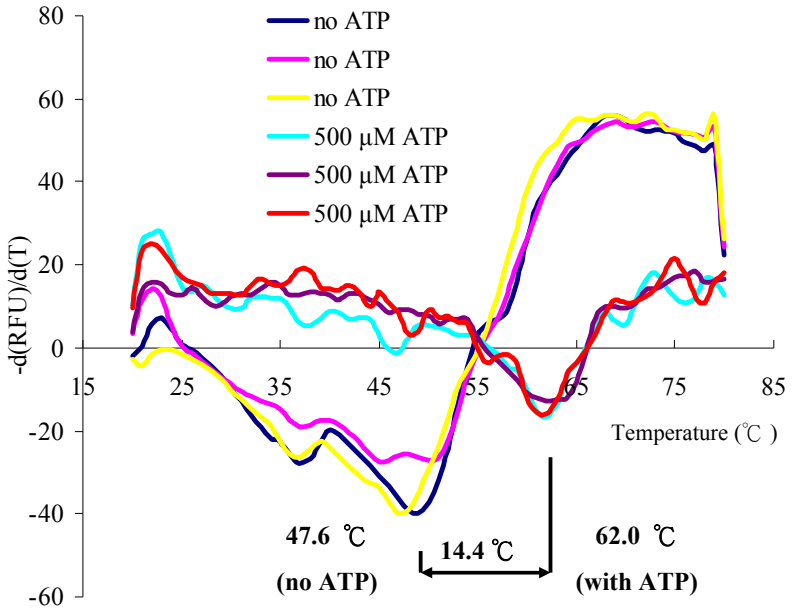

Figure 3-16: Comparison of the Tm values of MDM2RING with and without ATP. Compared to the Tm value detected in the absence of ATP, a dramatic increase of 14.4 ℃ is observed, in the presence of ATP, suggesting that ATP binds to and stabilizes MDM2RING.

- ***Thermal stability of UbcH5a***

Our thermal denaturation studies of UbcH5a showed a clear melting transition curve (Figure 3-17). Data demonstrated that after purification, UbcH5a is a folded protein with a melting temperature (Tm) of 55.4℃ (Figure 3-17 A). This result also revealed that UbcH5a is stable at the reaction temperature (30℃) used in the *in vitro* ubiquitination assay.

To test whether there is an interaction between UbcH5a and MDM2RING, 5 µM UbcH5a and 10 µM MDM2RING was incubated for 30 minutes prior to TDA analysis. The assumption was that if there was an interaction between these two proteins, the Tm of UbcH5a may change. In the presence of MDM2RING, TDA results showed that there was a downward/negative shift from 55.4℃ (apo-UbcH5a) to 53.7℃ (UbcH5a-MDM2RING) (Figure 3-17C). Differences in Tm provide evidence that there was interaction between the two proteins, and the downward Tm shift suggests that MDM2RING-binding destabilised the conformation of UbcH5a. This finding suggests that the conformational change in UbcH5a induced by MDM2-binding is necessary for the release of ubiquitin from E2 to the substrate. However, further analysis is needed to confirm this hypothesis.

(A) 5 µM UbcH5a

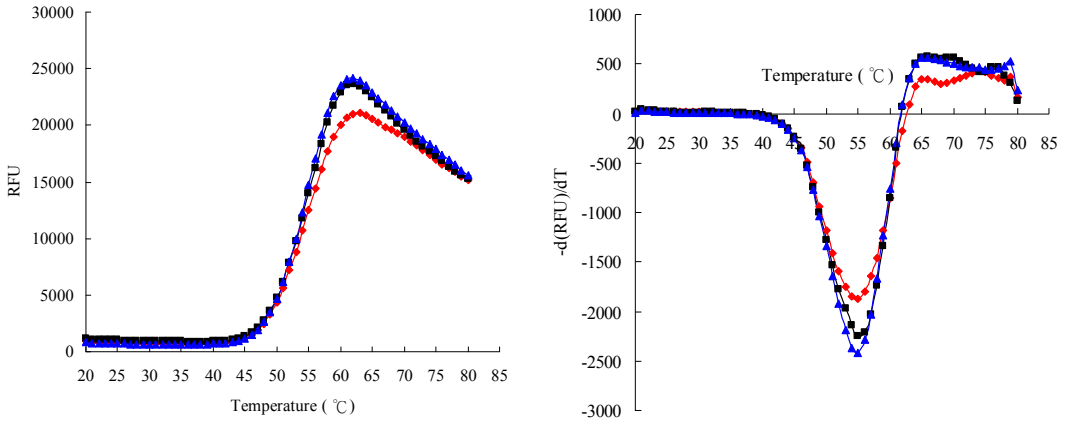

(B) 10 µM MDM2RING + 5 µM UbcH5a

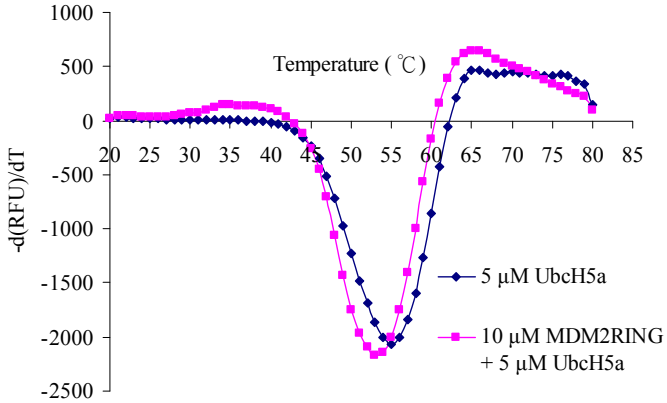

Figure 3-17: Comparison of the Tm of apo-UbcH5a and UbcH5a-MDM2RING using TDA. (A) & (B) showed that the Tm of 5 µM UbcH5a is 55.4℃. (C) The Tm of 10 µM MDM2RING + 5 µM UbcH5a was about 53.4℃ (magenta line), and the Tm of apo-5 µM UbcH5a was 55.4℃ (blue line). All samples were tested in triplicate.

3.4 Circular Dichroism (CD)

3.4.1 The Principles of CD

The basic principle of circular dichroism (CD) technology is that plane-polarised light passing through chiral molecules produce differential absorbance for right- and left-handed circular polarised light. For achiral molecules, there is no CD signal and generate plane-polarised radiation. For chiral molecules, at some wavelengths, the CD signal is generated as elliptically polarised light. Ellipticity (θ), in dimensions of millidegrees, is commonly used as a CD measurement unit. For proteins the peptide bond in isolation is a chromophore which the nπ* transition is at ~220 nm and ππ* transition ~190 nm. Generally, a CD spectrum of a protein is mainly recorded in the UV region, because protein polypeptide backbones produce dominant peaks in the far UV region (from ~260 nm to ~ 190 nm). Information on protein conformation is generated based on the chiral features of the three-dimensional secondary structure. As shown in Figure 3-18, α-helix structures produce one positive CD peak at ~190 nm and two negative CD peaks at ~222 nm and ~208 nm; β-sheet structure produce one negative CD peak at ~215 nm and one positive CD peak at ~195 nm. Proteins are composed of different secondary structure elements of α-helix, β-sheet and β-turns. Therefore a CD spectrum can be considered as a sum of spectra contributed by each secondary structure type of the protein sample. The CD data may give a meaningful interpretation of overall secondary structure of the protein sample.

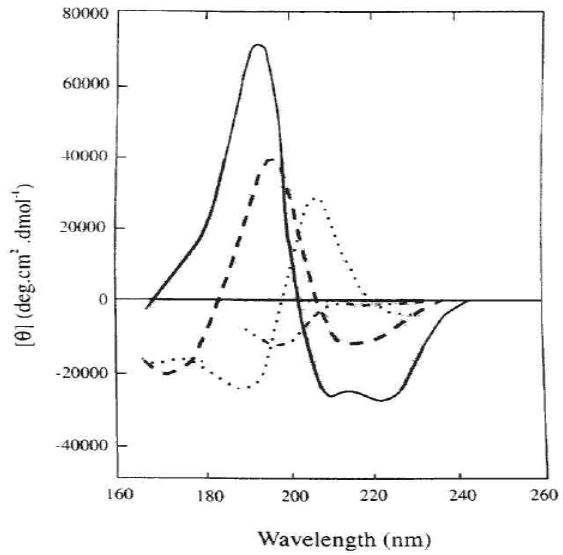

Figure 3-18: The Far UV CD spectrum of four proteins. The solid line represents a α–helical protein; dashed line is the spectrum of a β–sheet protein; dotted lines and short lines are the spectrum of unfolded proteins (Johnson et al., 1990).

In this work, the CD method was used to primarily demonstrate that these protein clones, overexpressed and purified for all experiments were folded, and also to measure the thermal stability. Solvents should be carefully selected as their absorption properties vary and some chemicals, such as chloride and Tris molecules, show strong absorption at the far UV region and affect the quality of CD data (Kelly & Price, 2000). Therefore, the CD buffer used was PBS and sodium fluoride (NaF), instead of the characterisation Tris buffer and NaCl used in other biophysical experiments.

3.4.2 Materials and Methods: CD

The CD spectra were collected using a Jasco J800 with a 10 mm pathlength cuvette. Prior to the experiments, UbcH5a was dialysed into a suitable buffer (20 mM PBS, 150 mM NaF, pH7.5) for the CD analysis. A protein concentration of 0.12 mg/ml UbcH5a was used for the CD measurements. Both samples were measured using the following experimental parameters: bandwidth 1 nm; response 1 s; measurement range 185 – 285 nm; scanning speed 20 nm/min; scan 10 times; temperature 25℃. For thermal denaturation experiments, each sample was tested using the same experiments parameters as previously described. Each sample was incubated at a specific temperature for 15 minutes before collecting the CD spectra for five repeated scans. Experimental temperatures were 25, 35, 45, 55, 65, and 75℃. All CD spectra were analysed using Dichroweb (http://dichroweb.cryst. bbk.ac.uk/html/ home.shtml) (Whitmore & Wallace, 2004), and the CONTIN program using reference set7.

3.4.3 Results & Discussions: CD

- ***UbcH5a is folded***

Because CD directly monitors the secondary structures of proteins, CD experiments were conducted to assess whether our purified UbcH5 was folded. As shown in Figure 3-19, it was clear that the CD spectrum of UbcH5a has minima at 208 nm and 222 nm and a maximum in the range of 190~195 nm, revealing that Ubc5Ha is a folded protein with a mixture of α-helical and β-sheet structures (Figure 3-19). The secondary structure contents of UbcH5a analysed using Dichroweb, and the COTIN program with reference set 7 showed that the secondary structure of UbcH5a contained an average content of 31.4 % α-helix and 19.3% β-sheet. Our far-UV CD data of UbcH5a secondary structure was similar to the X-ray structure data of UbcH5a (2C4P) (30 % α-helix and 18% β-sheet) (Table 3.1), suggesting that our UbcH5a is folded correctly.

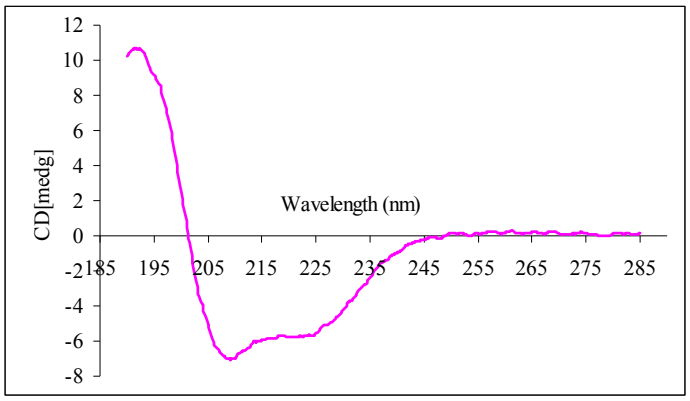

Figure 3-19: Analysis of the folding state of UbcH5a by Far-UV CD spectroscopy. Secondary structure contents of UbcH5a (0.12 mg/ml) is studies using the circular dichroism analysis. Data are recorded on 25 ℃ at the wavelength 185 nm ~ 285 nm. CD data are analysed using Dichroweb. The spectrum is an average of representatives of ten scans.

Table 3-1: Secondary structure content of UbcH5a was analysed using CD data and X-ray structure.

	α-helix	β-sheet
CD data	31.4%	19.3%
X-ray	30%	18%

The spectra were analysed at the Dichroweb sever using the CONTIN algorithm and the reference 7 dataset

- ***Thermal stability of UbcH5a using CD***

The stability of protein is correlated with its conformation; hence heat treatment of protein will change the tertiary structure of the protein. The change in the CD spectra as a function of temperature was used to monitor the thermal stability of UbcH5a. In these experiments, CD spectra were collected at the wavelength 185 ~ 285 nm at different temperatures, 25, 35, 45, 55, 65, and 75℃ (Figure 3-20A). As shown in Figure 3-16A, at the temperatures of 25, 35, 45, 55℃, there were similar far-UV CD spectra seen, indicating that UbcH5a was stable at 55℃. Increasing the temperature to 65℃, the far-UV CD spectra of UbcH5a was significantly changed, showing that UbcH5a lost its native conformation and was denatured at 65℃. Using the information we obtained from these data, we analysed the data of the CD spectra obtained at 208nm and 222 nm for studies of the unfolding state of proteins, because there were broad CD minima at these two wavelengths, indicative of α-helical content (Figure 3-20B). We also monitored the changes of the CD spectra at 216 nm, as an indicator of β-sheet content (Figure 3-20B). All CD data suggest that the conformational change of UbcH5a started at 55 ℃. The midpoint of thermal melting temperature (Tm) of UbcH5a using CD at all three wavelengths was about 60 ℃ (Figure 3-16B). The difference between the Tm measured using TDA (56.4 ℃) (Figure 3-20A) and CD may be due to the buffer conditions. It has been noted that the stabilities of proteins are buffer-dependent. In the CD spectroscopy experiments, sodium fluoride (NaF) was used to avoid the noisy signals resulting from sodium chloride (NaCl). The buffer system was 20 mM PBS instead because the Tris buffer may produce some noisy signals. Overall, both Tm values measured using TDA and CD revealed that UbcH5a is a thermally-stable protein. Importantly, during our *in vitro* ubiquitination experiments, the reaction is incubated at 30℃, and UbcH5a was stable at that temperature.

(A)

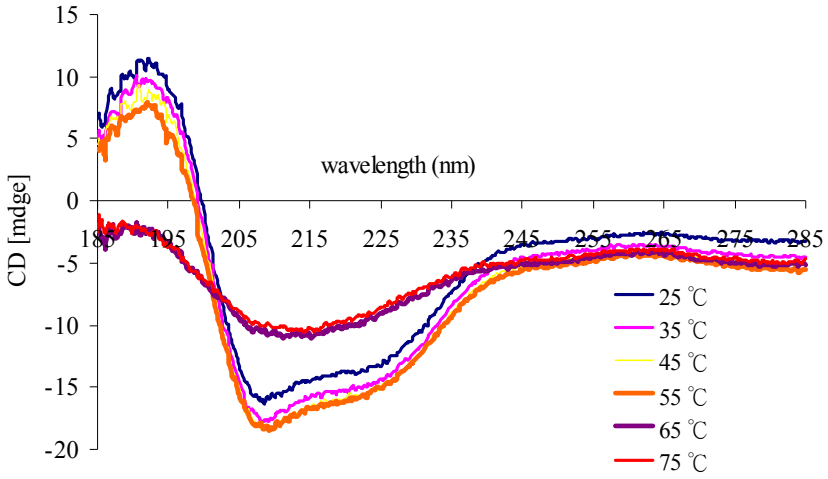

(B)

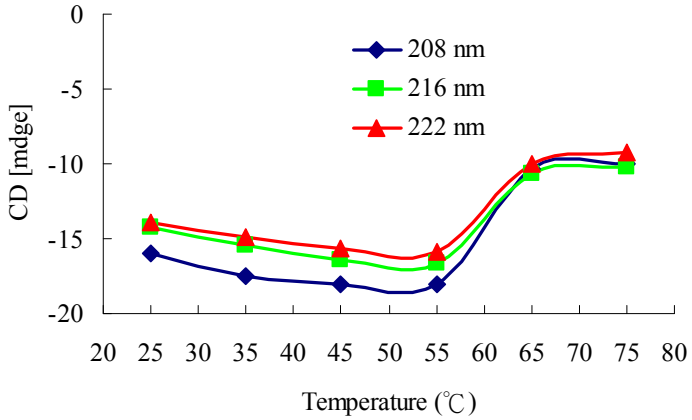

Methods	Tm (℃)
TDA	56.4
CD	60

Figure 3-20: The thermal stability of UbcH5a analysed on circular dichroism. (A) 0.12 mg/ml UbcH5a is used on this assay. Different colours represent different temperatures. While increasing the temperature, the changes of the CD spectra are observed. (B). The changes of the CD spectra of UbcH5a are observed at three wavelength, 208 nm (blue), 216 nm (green) and 222 nm (red).

3.5 Conclusions

The *in vitro* ubiquitination assay data showed that our purified MDM2RING and MDM2RING△C are E3 active and MDM2RING has stronger E3 activity than MDM2RING△C. MDM2RING and MDM2RING△C can ubiquitinate p53 which suggests that there is a new p53-binding site within our MDM2RING construct. Additionally, according to the dynamic light scattering and size exclusion chromatography data, the oligomeric states of MDM2RING were concentration-dependent whereas MDM2RING△C exists as a dimer at all concentrations. Thermal denaturation data of MDM2RING revealed that zinc binding plays a role in the folding and stability of MDM2RING. Moreover, the thermal denaturation data also provides evidence that ATP interacts and stabilises MDM2RING.

UbcH5a was a stable monomer as confirmed by size exclusion chromatography and dynamic light scattering. According to the circular dichroism analysis, it showed that the secondary structure of UbcH5a consisted of 19.3 % β-sheet, 31.4% α-helix and 49.3% loop or random coil. The thermal stability of UbcH5a was also verified by a thermal denaturation assay and circular dichroism analysis, showing that the thermal melting temperature (Tm) were determined to be 56.4℃and 60℃, respectively.

4 Structural studies of MDM2RING, MDM2RING △ C and UbcH5a

Crystallisation trials were set up for the following proteins, MDM2RING (residues 386- 491), MDM2RING △ C (residues 386-478), and the MDM2RING-UbcH5a complex. 1-dimensional nuclear magnetic resonance (1D-NMR) was used to investigate the folded state of these protein constructs. To study the interaction of MDM2 and UbcH5a, we used 2-dimensional heteronuclear single quantum coherence NMR (2D-^{1}H,^{15}N HSQC NMR) to monitor chemical shifts in ^{15}N-UbcH5a following the addition of MDM2RING △ C. Furthermore, we used negative-staining transmission electron microscopy to study the structure of the higher oligomers of MDM2RING.

4.1 Macromolecular Crystallisation

4.1.1 The principles of crystallisation

To determine the structure of macromolecules, including proteins and nucleic acids by X-ray diffraction, the production of high quality crystals is pivotal. However, finding favourable conditions for crystallisation has always been a bottleneck in the structure determination process, because useful crystals grow only under specific conditions, frequently at the boundary between nucleation and metastable zones (Durbin & Feher, 1996). If the conditions produce too many nuclei, no high-quality crystals grow, instead, microcrystals, or amorphous precipitate is generated. Protein-protein interactions in a crystal are very complex, achieving the thermodynamically metastable state, known as supersaturation, is difficult. Supersaturated proteins are within the nucleation or metastable zones (introduced in greater detail in the following paragraph). Therefore, one of the pivotal steps in crystallisation is the control of nucleation.

Optimisation of crystallisation conditions is usually achieved following the guidance of the crystallisation phase diagram (Chayen, 2004; Chayen, 2005). Figure 4-1 shows a crystallisation phase diagram that includes four distinct zones presenting different supersaturation states. (i) In the highest supersaturation zone (precipitation zone), all macromolecules aggregate. (ii) At the zone of moderate saturation (nucleation zone), spontaneous nucleation will occur. (iii) At the zone of lower supersaturation, known as the metastable zone (just below the nucleation zone), crystals may grow and no further nucleation will take place. This condition is favourable for crystal growth. (iv) At the zone of under-supersaturation, macromolecules are fully soluble and no crystallisation will occur. Crystal quality is dependent on several parameters, including concentration of macromolecule, buffer composition, pH, incubation temperature, the degree of stability/homogeneity of the macromolecule and many other parameters (McPherson, 2004). Several methods have been developed to achieve supersaturation of the macromolecular solution inducing nucleation and generating crystals suitable for X-ray diffraction analysis (McPherson, 1999). Currently, vapour diffusion is the most popular crystallisation method.

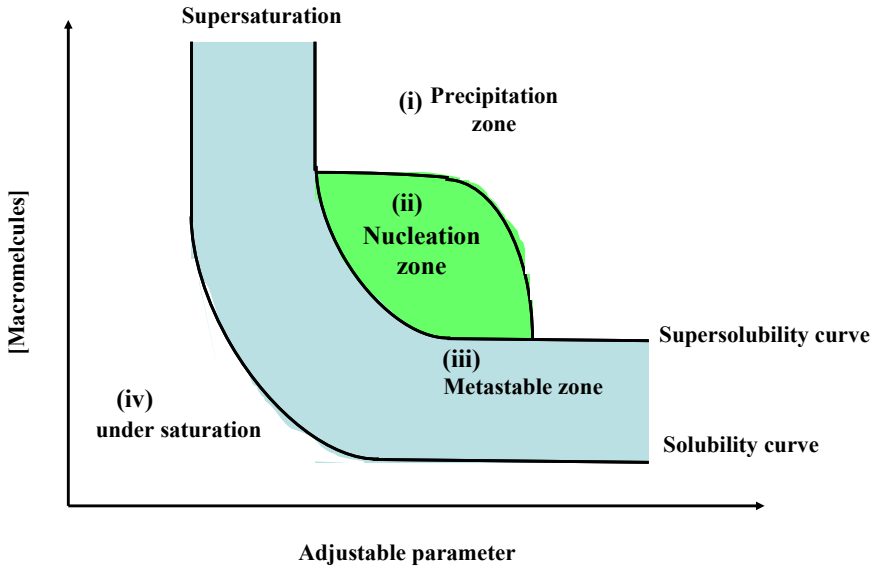

Figure 4-1: The crystallisation phase diagram. As described, there are four zones representing different supersaturation states: (i) precipitation zone, (ii) nucleation zone, (iii) metastable zone, and (iv) under saturation. Nucleation and subsequent crystal growth often take place within the nucleation and metastable zones, respectively, as protein concentration changes over time.

● ***The vapour diffusion method***

There are two common variations of the vapour diffusion method: hanging and sitting drops (Figure 4-2). The mother liquor (a mixture of crystal growth reagents) is in the well. A drop is in suspended (hanging) or supported (sitting) and contains protein solution (usually between 0.5 ~ 20 µl) mixed with the same volume of mother liquor. In the sealed system, equilibrium is achieved by the evaporation of water or volatile reagents from the drop, resulting in an increase in the concentration of the protein reaching a supersaturated state and hopefully forming crystals. Many rounds of screening, continually optimising parameters including protein concentration, precipitants/additives used may be required to produce well diffracting crystals.

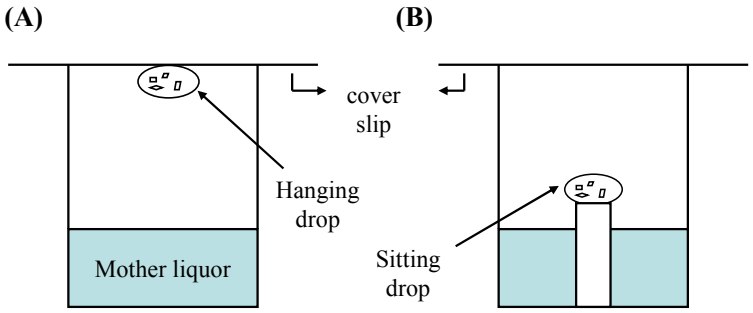

Figure 4-2: Vapour diffusion methods. Illustration of the two most commonly used methods in crystallisation (A) hanging drop preparation & (B) sitting drop preparation.

4.1.2 Materials & Methods: crystallisation

In this work, the vapour diffusion method was used. Glass coverslips used were siliconised followed by a water wash. The well contained 500 µl mother liquor (crystallisation buffer). 1 µl protein solution was pipetted onto the treated coverslip and 1 µl of mother liquor was pipetted onto the protein solution. The coverslip was then inverted, placed over the reservoir and sealed as shown in Figure 4-2A. The plates were stored at two temperatures 4 and 18℃. Microscopy was used to monitor the drops.

4.1.3 Results & Discussions: Crystallisation

The published crystallisation conditions for MDM2-MDMX heterodimers (Linke et al., 2008) were used first, in an attempt to produce crystals of MDM2RING and MDM2RING△C. It has been noted that different constructs can behave very differently and may not produce crystals under the same conditions. A number of commercially available crystallisation screening kits including Crystal Screen I & II, PEG/Ion Screen (HR2-126) and Natrix Screen (HR2-116) (Hampton Research Hamilton-Screen Kits). The kits have been developed from analyses of the protein structure database and are comprised of variations of the most successful conditions found in the PDB. Meanwhile, we also systematically varied a number of parameters including protein concentration, type and concentration of precipitants including ammonium sulfate (AS), pH and percentage of glycerol in the mother liquor. After several rounds of screening, microcrystals were grown but unfortunately were of insufficient quality for further studies.

Crystallisation trials using UbcH5a in complex with MDM2RING were set up, once again using the commercial available screens. Many hundreds of crystallisation trials were set up, a few crystals were seen with one buffer condition (0.2 M ammonium acetate, 0.01M calcium chloride dihydrate, 0.05 M sodium cacodylate trihydrate (pH6.5), and 10% w/v polyethylene glycol 4000) (Figure 4-3). However, the microcrystals were not of sufficient quality for X-ray diffraction studies.

The screening trials produced one potential lead for any further attempts to crystallise the UbcH5a-MDM2RING complex. In the future, further optimisation of crystallisation conditions will be necessary to obtain good quality crystals for X-ray diffraction. Cloning of multiple constructs of the target proteins could be attempted to find proteins with greater stability to increase the chance of producing high quality crystals.

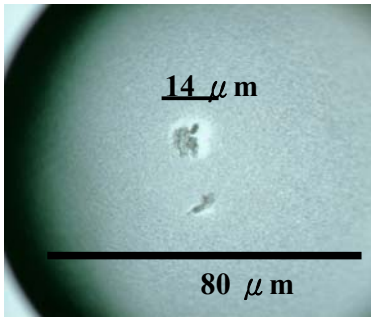

Figure 4-3: Crystallisation of the MDM2RING-UbcH5a complex. Crystal grows from10% w/v polyethylene glycol 4000, 0.2 M ammonium acetate, 0.01 M calcium chloride dihydrate, 0.05 M sodium cacodylate trihydrate pH6.5, at 18℃. Those microcrystals are with dimension approximately 4 μm.

4.2 Negative Staining Transmission Electron-Microscopy (negative staining TEM)

4.2.1 The basis and applications of negative staining TEM

Negative staining TEM (transmission electron microscopy) is one technique available to observe the ultrastructure of macromolecules, such as cells, viruses or larger proteins (Ohi et al., 2004). The resolution of light microscopy is limited to approximately 0.25 μm whilst with TEM resolution down to 0.2 nm can been achieved. Negative staining is a mild technique to enhance contrast, highlighting the structures of macromolecules in the image produced. Therefore, in negative staining TEM, protein is deposited on to a carbon-coated copper grid, followed by staining with a negative stain solution, such as 1-3% uranyl acetate. The images of the topography of the macromolecules are recorded by a CCD camera (charged-coupled device camera). The images generated by TEM of the stained sample provide pictures of the morphology of the specimen. TEM images of soluble proteins display the particles in bright field sharply contrasting with the dark environment surrounding them (Figure 4-4). Because the energy of the electron beams is absorbed by heavy metals used in the stain, the dark regions in the images represent the environment surrounding the sample or aggregates. Brighter areas represent soluble proteins. Conversely, particles of insoluble aggregates were also viewed as in the dark field. In this thesis, negative staining TEM method was used to study the topography of the high molecular weight MDM2RING.

4.2.2 Materials & Methods: negative-staining TEM

To ascertain whether large-molecular-weight MDM2RING (Figure 4-4A) was present as aggregates or as a supramolecular assembly, negative staining TEM was used. Firstly, copper grids, as a supportive membrane for the samples, were coated with a carbon film. Then, the carbon-coated copper grid was discharged as the carbon becomes hydrophobic after some time. The samples (0.1 mg/ml MDM2RING (usually 2.5 μl)) were then deposited onto the discharged carbon-coated copper grid under low pressure in a vacuum chamber. Then the sample on the grid was washed with two drops (2.5μl) of deionised water, and stained with two drops of the heavy metal salt reagent, 1% uranyl acetate. Electron micrographs were recorded on a CCD camera at a magnification of 20,000X with a Phillips CM120 Biotwin (http://coil.bio.ed.ac.uk/TEM.html) operating on 200 kV.

4.2.3 Results & Discussions: Negative staining TEM images of the high molecular weight form of MDM2RING

Figure 4-4A shows that two forms of MDM2RING are eluted by gel filtration using a Sephacryl S-200 HR column. The molecular mass of the high molecular weight form present in the void volume is presumed to be greater than 660 kDa (void volume = 40 ml). The dimeric form (with an elution volume of 65 ml) has an estimated molecular weight of 26 kDa. To ascertain whether the protein in this fraction were aggregates or soluble proteins (supramolecular assembly), negative staining TEM was applied.

TEM images showed that each MDM2RING particle displayed a regular donut-like structure (Figure 4-4B, insets). The width of the particles viewed in one dimension were 7~15 nm. The diameter of the high molecular weight form of MDM2RING particles was approximately 7.4 x 11.1 nm (white arrow, in Figure 4-4B).To some extent, the different appearances of the particles might also be due to the different viewing angles. The heterogeneity in shape and size might be due to differential absorption of the protein onto the grid or the presence of different subunits in the supramolecular assembly. It has been noted that MDM2RING (residues 432-491) and other RING domain proteins, such as Z protein or BRCA1/BARD1, tend to become supramolecular assemblies at high concentrations (Kentsis et al., 2002; Poyurovsky et al., 2007). Consistent with previous reports, negative staining TEM provided evidence that our high molecular weight form of MDM2RING are not aggregates; instead, they exist as regular donut-like proteins in a larger supramolecular assembly.

The molecular weight of MDM2RING was greater than 660 kDa as estimated from the size exclusion profile (Figure 4-4A). Since the theoretical molecular weight of monomeric MDM2RING is 12.47 kDa, this suggests that the high molecular weight MDM2RING fraction is composed of a mixture of larger complexes of at least 50 subunits. Since the negative staining TEM images showed that high molecular weight MDM2RING was detectable as a soluble regular donut-like shaped protein, an important step was to clarify whether high molecular weight MDM2RING still has E3 ligase activity. Using *in vitro* ubiquitination (see Chapter 3), the data showed that MDM2RING (supramolecular assembly, large) was E3 active (Figure 4-4C). To understand if there are different levels of E3 ligase activities between the two forms of MDM2RING (larger and small), 100 ng of each

MDM2RING form was tested. Results showed that the small MDM2RING form has higher E3 ligase activity than larger MDM2RING, as more ubiquitinated-p53 ladders were detected. This result was consistent with a previous report (Poyurovsky et al., 2007), which also indicated that small MDM2RING (residues 432-491) is more E3 active than large MDM2RING (residue 432-491). From a biological viewpoint, the equilibrium between small and large MDM2 proteins may play a critical role in determining the degree of ubiquitination in cells. When more dimeric MDM2 exists, p53 or other MDM2-binding substrates may be more readily ubiquitinated and degraded.

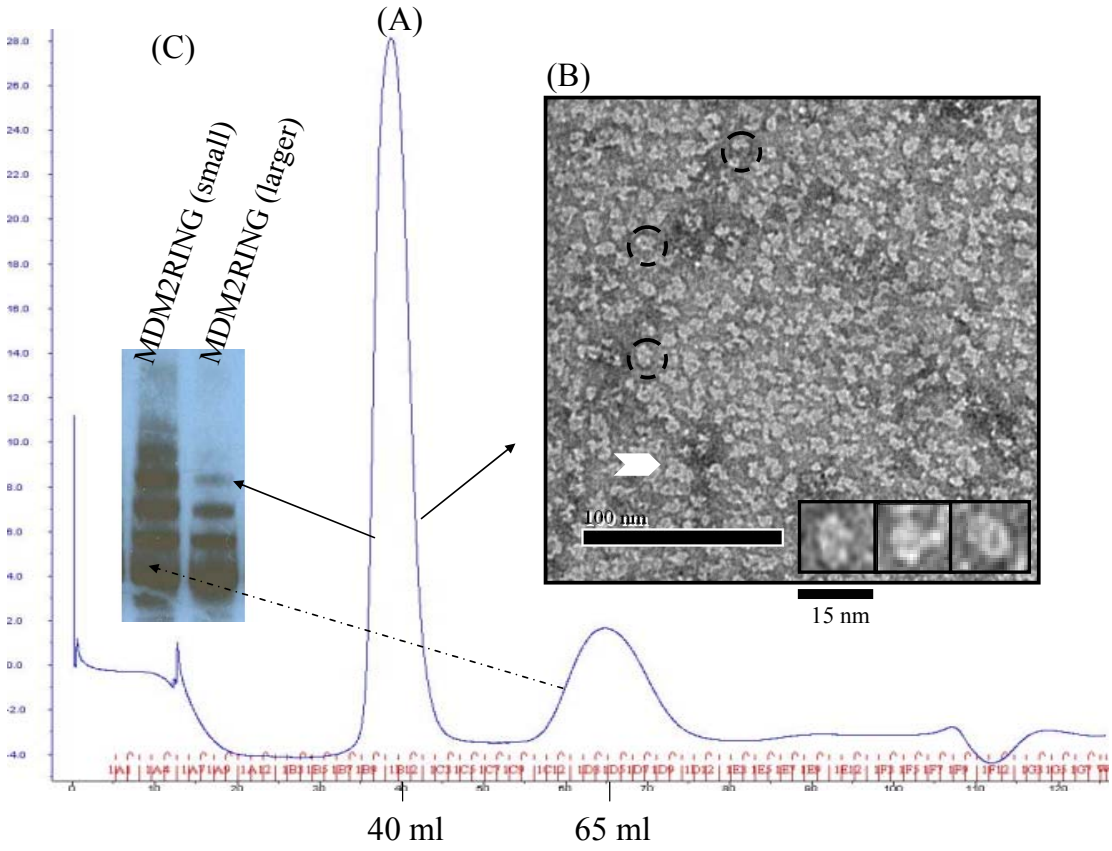

Figure 4-4: Characterisation of larger-molecular-weight MDM2RING. (A) The molecular weight of large-molecular-weight MDM2RING is estimated to be greater than 660 kDa. (B) Negative staining TEM images of MDM2RING are recorded at a magnification of 20,000X. MDM2RING is deposited onto a carbon-coated copper EM grid and stained with 1% uranyl acetate before being visualised using transmission EM. The arrow highlights one particle of approximately 7.4 x 11.1 nm. Scale bar = 100 nm. Inset: high molecular weight MDM2RING forms a regular donut-like structure. The frame size of the magnified particles in a gallery is 15 nm. (C) Data from *in vitro* ubiquitination confirms that the high-molecular-weight MDM2RING has E3 ligase activity.

4.3 Nuclear magnetic resonance (NMR) spectroscopy

4.3.1 The basis and applications of NMR spectroscopy

- ***NMR spectroscopy***

NMR spectroscopy, **N**uclear **M**agnetic **R**esonance spectroscopy, is a technique to obtain chemical, physical, and structural information on molecules of interest. The resonance frequency that is detected by NMR spectroscopy is proportional to the magnetic field applied to a nucleus. The motion of the electrons is induced by the external magnetic field and produces a small magnetic field to the nucleus. The electron distribution of a nucleus (e.g. ^{1}H, ^{13}C and ^{15}N) varies according to the local geometry (binding partners, bond lengths, angles between bonds). The change in the effective magnetic field experienced by a nucleus causes the resonance frequencies to shift. Over the last few decades, NMR chemical shift perturbation methods have been successfully used to obtain the structure of macromolecules (Rehm et al., 2002; Yee et al., 2002; Yee et al., 2006) and for mapping the residues involved in the protein-protein or protein-ligand interactions (Brzovic et al., 2006; Coles et al., 2003; Kalus et al., 1997; Shuker et al., 2006). One of the limitations of NMR spectroscopy is the overlap of the signals that results if the macromolecules are too large. Therefore, NMR is suitable to study small proteins (<25 kDa), such as one domain of a larger protein. Compared to crystallography, NMR provides structural information on a macromolecule closer to physiological conditions in solution with additional information on stability, solubility and conformation. NMR is also an alternative method to obtain structural information from macromolecules that are refractory to crystallisation. Moreover, recently, NMR has become a powerful tool in the pharmaceutical industry to study the interactions between protein target and small molecule ligands (Lepre et al., 2004; Moore, 1999; Viegas et al., 2009).

In our project, we used 1-dimensional NMR (1D-NMR) to monitor whether UbcH5a and MDM2RING△C are folded and then applied 2-dimensional heteronuclear single quantum coherence NMR (2D-HSQC NMR) to study the structural and conformational changes of ^{15}N-UbcH5a with or without MDM2RING△C (in this chapter) or with selected ligands (Chapter 5). Residues involved in protein-protein interactions or in ligand-receptor interactions are easily determined by chemical shift changes of the cross-peaks.

4.3.2 Materials & Methods: 1D & 2D NMR

NMR experiments discussed in this thesis were performed using a Bruker AVANCE 600 MHz spectrometer for the 1D-NMR experiments and a Brucker AVANCE 800 MHz spectrometer for the 2D-HSQC NMR (Edinburgh Biomolecular NMR Unit). NMR data were collected using the Topspin interface. The CCPNMR software suite Analysis 2.1.1 was used for data analysis.

- ***1D NMR: sample preparations***

For 1D-NMR experiments, UbcH5a, MDM2RING and MDM2RING△C, respectively, were purified as described in Chapter 2. High concentrations of salts, such as NaCl, affect NMR experiments; therefore, samples were buffered exchanged into an "NMR buffer" with lower ionic strengths (50 mM NaCl, 20 mM Tris, pH7.2) prior to the experiments. A 500 µl sample (containing 10% (v/v) deuterated water (D_2O)) at a protein concentration of 50 µM was required for each NMR experiment. D_2O was used to produce a deuterium lock signal to enable the correction of inhomogeneity in the magnetic field. Samples were transferred into a 5-mm NMR tube (Wilmad HighPrecision), data recorded at a temperature of 300 K.

- ***^{1}H, ^{15}N-HSQC 2D-NMR: sample preparations***

For ^{1}H, ^{15}N-HSQC experiments, isotopically labelled samples were prepared as follows. A single colony of His • tagged-MDM2RING△C or UbcH5a was picked and used to inoculate 12.5 ml LB medium (with carbenicillin, at 100 µg/ml) followed by overnight incubation at 37℃ with shaking at 250 rpm. Cells were centrifuged, the LB medium discarded and the pellets washed gently three times using minimal medium [1X M9 salt solution including 8.4 mM Na_2HPO_4, 4.8 mM NaH_2PO_4, 1.8 mM NaCl]. This procedure is to reduce the amount of unlabelled nitrogen in the sample which may produce noisy signals in the ^{1}H, ^{15}N-HSQC NMR data. Then for the scale-up incubation, cell pellets were resuspended using 500 mL specific grow medium to label the nitrogen atoms [1X M9 medium, 0.8 mM $(^{15}NH_4)_2SO_4$, 1 mM Mg_2SO_4, 50 µM $CaCl_2$, 0.5% (w/v) ^{15}N-labelled Isogro (Sigma), 50 µg/ml thiamine and 1% PTM1 salts]. Cells were grown at 37℃ with shaking at 250 rpm for approximately 6 ~ 8 hours until an $O.D._{600}$ of 0.8 was reached. IPTG to a final concentration of 1 mM was added to the growth medium and the cells were incubated for another 16 ~ 20 hours at 20℃. At this stage cells grew slowly as the growth medium is low in nutrients. Cells were collected and

flash frozen. The ^{15}N-labelled samples were purified using the purification procedure outlined in Chapter 2. The ^{15}N-labelled His • tagged-MDM2RING△C and UbcH5a were concentrated to 0.5 mg/ml and 1 mg/ml, respectively. For 2D-NMR experiments, 500 μl samples containing 25 μM purified ^{15}N-labeled samples and 10% (v/v) D_2O (the same buffer for 1D experiments) were transferred into a 5-mm NMR tube and data recorded at a temperature of 300 K.

4.3.3 Results & Discussions: 1D & 2D NMR

- ***1D ^{1}H NMR spectrum of UbcH5a***

In one-dimensional ^{1}H NMR spectra, there are three major chemical shift regions giving an indication as to the folding state of a protein (Rehm et al., 2000): (1) the amide region; (2) the aromatic region; and especially (3) the methyl group region (between 1 ~ -1ppm). In Figure 4-5, the 1D ^{1}H NMR spectrum of UbcH5a showed distinct cross-peak dispersions with sharp linewidths. Strong Peaks at 3.5 ~ 4 ppm were derived from the Tris in the buffer. Several distinct peaks were detected between 6~11 ppm, representing amide/aromatic regions, indicative of folded UbcH5a. Moreover, several peak shifts were detected around 0 ppm, and the signals were generated from the buried methyl groups. Those peaks further confirmed that there are soluble UbcH5a proteins in solution.

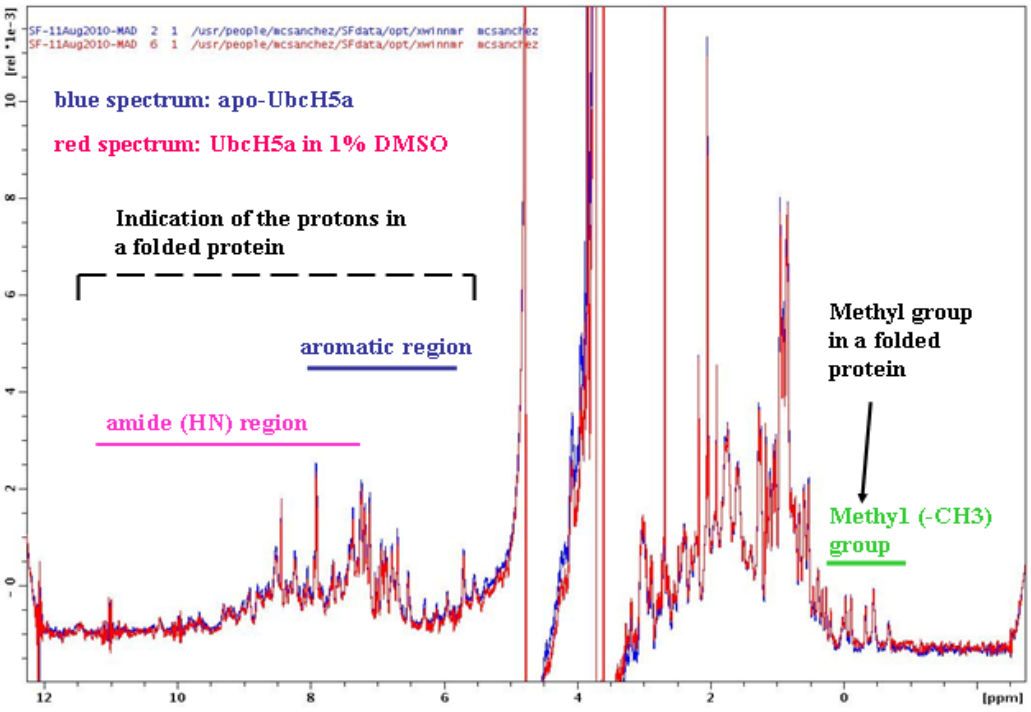

Figure 4-5: 1D ^{1}H-NMR spectrum of UbcH5a. 50 µM non-labeled UbcH5a (in 20 mM Tris buffer, 50 mM NaCl, pH 7.2.) is recorded at 600 MHz at a temperature of 300 K. Data are processed using "Topspin". Blue peaks represent the NMR spectrum of apo-UbcH5a. Red peaks represent the NMR spectrum of UbcH5a in solution (containing 1% DMSO).

- ***1D-NMR spectrum of His • tagged-MDM2RING△C***

In Figure 4-6, the 1D-NMR spectrum of His • tagged-MDM2RING△C showed a minor peak in the methyl group region (~ 0.5 ppm) and a few peaks shifts in the amide/aromatic regions (6.5 ~ 9 ppm). The pattern of this type of 1D-NMR spectrum may indicate the protein is aggregated. Broader linewidths (around 8~8.5 ppm) are correlated to the tumbling rate of a molecule in solution, such as non-specific aggregation or higher-order oligomers (Hill & DeGrado, 2000). On the basis of the 1D ^{1}H NMR spectrum of His • tagged-MDM2RING△C (Figure 4-6), it is difficult to distinguish whether proteins are forming properly folded or the NMR signal is caused by folded proteins with a high molecular weight. The previous biophysical studies on the **non** His • tagged- MDM2RING△C construct (Chapter 3) showed that the protein formed a dimer in solution. In order to study the His • tagged construct, which appear to have higher molecular weight, two-dimensional ^{1}H, ^{15}N-HSQC NMR, was used for further study.

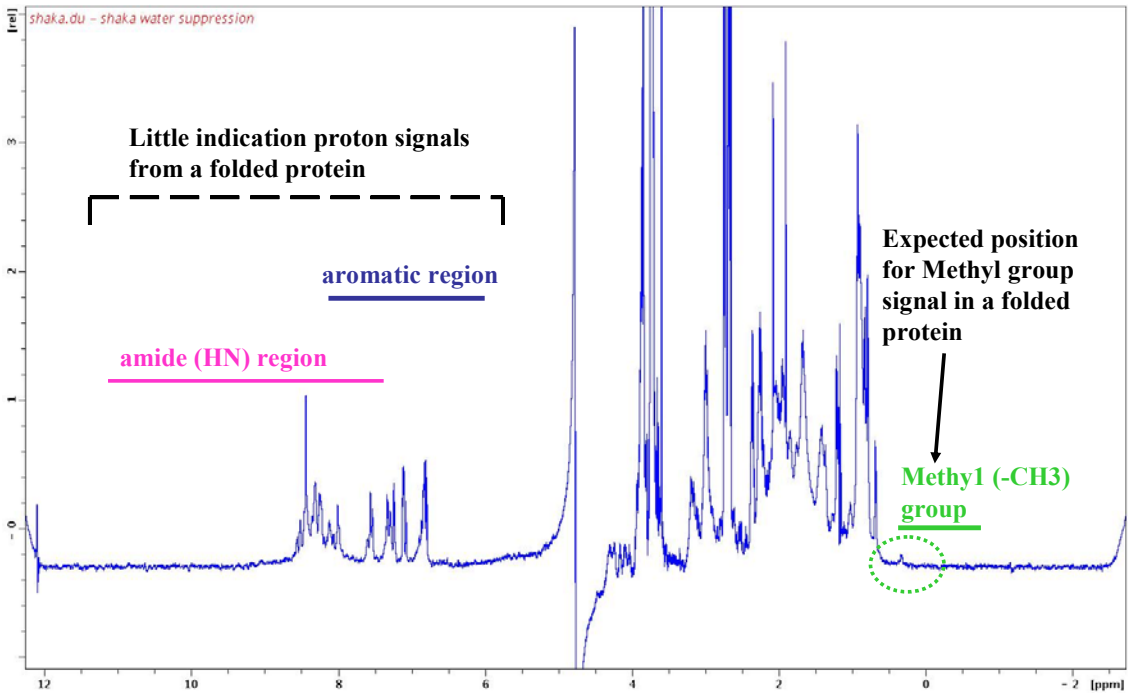

Figure 4-6: 1D ^{1}H NMR-spectrum of His • tagged-MDM2RING△C. 100 µM non-labeled His • tagged- MDM2RING△C (in 20 mM Tris buffer, 50 mM NaCl, pH 7.2.) was analysed at 600 MHz at a temperature of 300 K. Data are processed using "Topspin".

- ***2-dimensional heteronuclear single quantum coherence NMR (2D HSQC NMR)***

HSQC-NMR (Heteronuclear Single Quantum Coherence NMR) is one of a number of 2-dimensional NMR techniques (Bodenhausen & Ruben, 1980). The signals from a protein on a 1D-NMR spectrum are overlapping and it is difficult to distinguish the peaks. Therefore, alternative NMR techniques are required to provide better resolution of the NMR spectrum of a macromolecule. HSQC-NMR becomes significant for protein NMR which can be performed using isotopically labelled protein. For example, 2D-[^{1}H, ^{15}N] HSQC NMR spectrum provides more "frequency space" and fewer overlapping cross peaks in a 2D dataset compared to 1D ^{1}H NMR. Each cross-peak represents a ^{1}H (x-axis) and ^{15}N (y-axis) chemical shift of each backbone NH proton in a protein. The dispersion of each cross-peak is determined by the amino acid identity and its local magnetic environment (which corresponds to its neighbouring amino acids). A 2D-[^{1}H, ^{15}N] HSQC NMR spectrum of a protein produces a unique of "protein fingerprint".

[^{1}H, ^{15}N]-HSQC-NMR is a cheap and quick experiment, and therefore, it has become the first choice technique to study conformational changes in the folded *versus* unfolded state (Dyson et al., 2004; Hanoulle et al., 2009), wild-type *versus* mutant protein (Boeckler et al., 2008; Chatterjee & Hosur et al., 2006; Tevelev et al., 1996), or apo-protein versus protein-ligand complex (Johnson et al., 2000). If the protein is folded, each cross-peak is distinguished and there is a correlation between the number of cross-peaks and the number of amino acids. For the ligand-binding experiments, to compare the HSQC spectra of the labelled protein in the absence and presence of the ligand, changes in chemical shifts of the cross-peaks indicate residues responsible for in the binding interaction.

- ***2D- $^{1}H,^{15}N$- HSQC NMR spectrum of ^{15}N-His • tagged-MDM2RING△C***

2D-HSQC NMR spectrum of ^{15}N-His • tagged-MDM2RING△C showed that it is largely unfolded because it had poor cross-peak dispersions (Figure 4-7). Most amide ^{1}H chemical shifts were dispersed at a narrow range (8.0 ~8.5 ppm) and some were at 7 and 7.5 p.p.m (Figure 4-7), showing that those peaks originate from flexible residues of the protein. In addition, data supported by the DisMeta results (Figure 4-7B) showed that a disordered segment was located in the N-terminal 52 residues (residues 386-438) of MDM2RING△C. The DisMeta Server (www-nmr.cabm.rutgers.edu/ bioinformatics/ disorder) was developed by the NESG (The Northeast Structural Genomics Consortium), and offers several sequence-based structural tools for the predictions of unknown proteins of unknown structure (Rossi et al., 2010).

To sum up, the ^{1}H, ^{15}N-HSQC NMR spectrum of His • tagged-MDM2RING△C suggested that this protein is largely unfolded. However, the biochemical studies showed that native MDM2RING△C has E3 ligase activity (Figure 3-3). Furthermore, the ESI-MS analysis showed that native MDM2RING△C is folded (Figure 5-7). Taken together, the data suggested that additional His • tag could readily induce this protein to become improperly or partially unfolded.

(A)

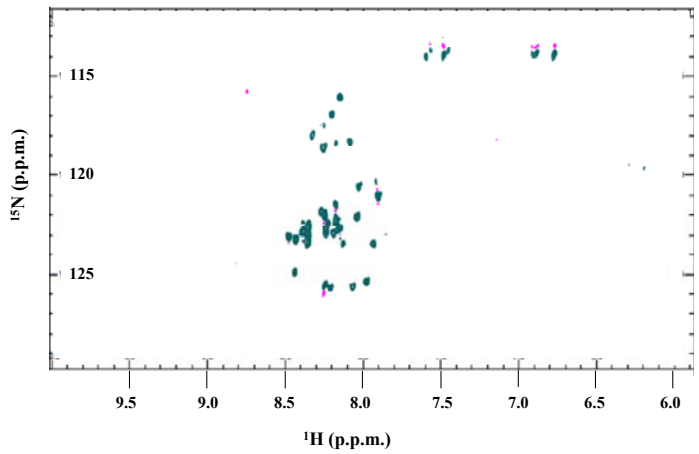

(B)

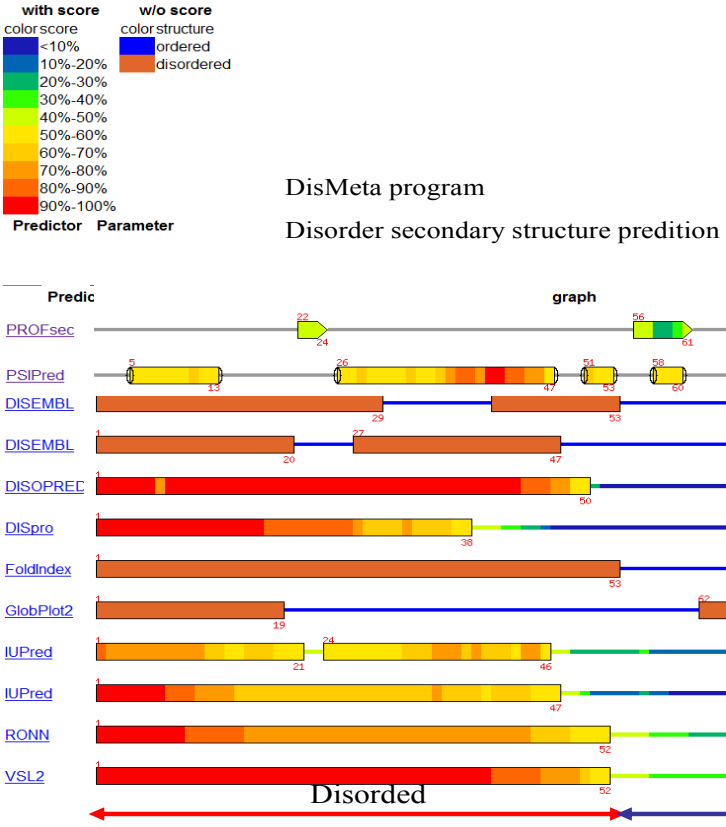

Figure 4-7: $^{1}H,^{15}N$-HSQC NMR spectrum of His・tagged-MDM2RING△C. (A) A spectrum of 50 μM His・tagged-MDM2RING△C (in 90% buffer/10%D_2O (v/v)) was recorded at 800 MHz at a temperature of 300 K. (B) The output from the DisMeta sever shows that the N-terminal 53 amino acids (residues 386-438) of His・tagged-MDM2RING△C are predicted to be disordered.

- ***2D- $^{1}H,^{15}N$-HSQC NMR spectrum of UbcH5a***

^{1}H, ^{15}N-HSQC-NMR experiments were used to monitor the folded state of the protein and to compare any change in chemical shifts of the proteins with and without ligand. A ^{1}H, ^{15}N-HSQC NMR spectrum of UbcH5a was recorded, and the resulting cross-peaks were properly dispersed, indicating that UbcH5a is folded (Figure 4-8). The spectrum from a ^{15}N-HSQC NMR experiment alone is not enough to determine the structure; other techniques are required. There is an alternative method to make the backbone assignment of UbcH5a, comparison with previous published NMR spectra of the same proteins. Published chemical shift assignments for an UbcH5a (NMR accession number: 6584), referred to as "UbcH5a$_{ref}$", was used as a reference to assign our UbcH5a (Figure 4-8). The amino acid sequence of UbcH5a$_{ref}$ is very similar to that of our construct UbcH5a except two residues (K51F and S62F) have been mutated and residues at the N terminus, not part of the core UbcH5a, are different (Figure 4-8A).

The spectra of the known solution structure of UbcH5a$_{ref}$ and our UbcH5a were similar (Figure 4-8B). Differences in the positions of the peaks were due largely to the samples being in different buffer solutions because the positions of the cross-peaks in a NMR spectrum are solvent dependent. The buffer for UbcH5a$_{ref}$ NMR experiments was (150 mM KCl, 20 mM KPi (pH 7.0), 10 mM $ZnCl_2$, 5% D_2O); however, our protein did not produce good data in this buffer. Therefore, our UbcH5a was stored in Tris buffer for the NMR experiments. Although the peak positions were slightly different, the overall dispersion of the cross-peaks was similar. Manual assignments of each cross-peak to a specific residue in UbcH5a was guided by the assignments of the known structure of UbcH5a$_{ref}$. We tried to assign about 109 residues (65% of total residues) of our UbcH5a. Manually-optimised NMR assignment of our UbcH5a was ready to be used as a reference for further studies into the interactions of ^{15}N-UbcH5a with MDM2RING△C (discussed in the following section) or ^{15}N-UbcH5a with a ligand (Chapter 5).

(A)

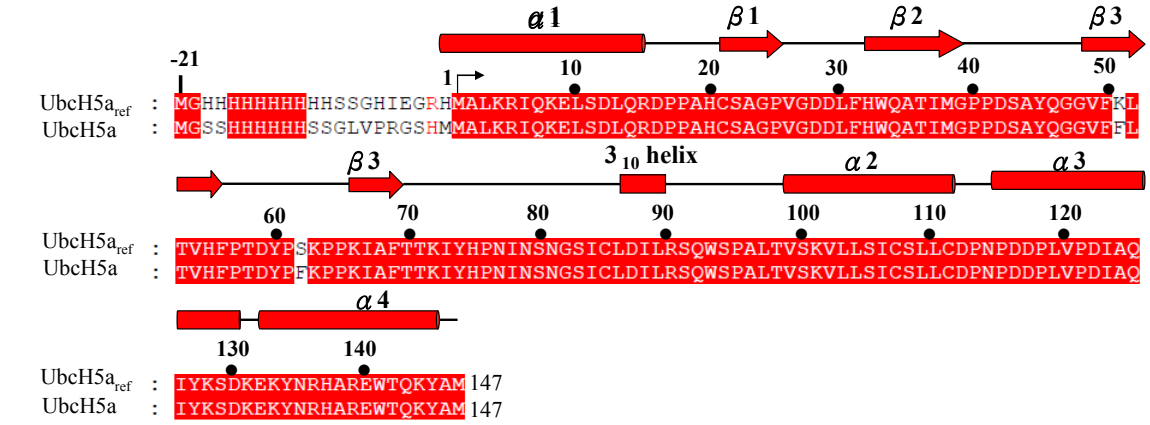
α1
β1
β2
β3
-21
1
10
20
30
40
50
UbcH5a$_{ref}$: MGHHHHHHHHSSGHIEGRHMALKRIQKELSDLQRDPPAHCSAGPVGDDLFHWQATIMGPPDSAYQGGVFKL
UbcH5a : MGSSHHHHHHSSGLVPRGSHMMALKRIQKELSDLQRDPPAHCSAGPVGDDLFHWQATIMGPPDSAYQGGVFFL
β3
3 10 helix
α2
α3
60
70
80
90
100
110
120
UbcH5a$_{ref}$: TVHFPTDYPSKPPKIAFTTKIYHPNINSNGSICLDILRSQWSPALTVSKVLLSICSLLCDPNPDDPLVPDIAQ
UbcH5a : TVHFPTDYPFKPPKIAFTTKIYHPNINSNGSICLDILRSQWSPALTVSKVLLSICSLLCDPNPDDPLVPDIAQ
α4
130
140
UbcH5a$_{ref}$: IYKSDKEKYNRHAREWTQKYAM 147
UbcH5a : IYKSDKEKYNRHAREWTQKYAM 147

(B)

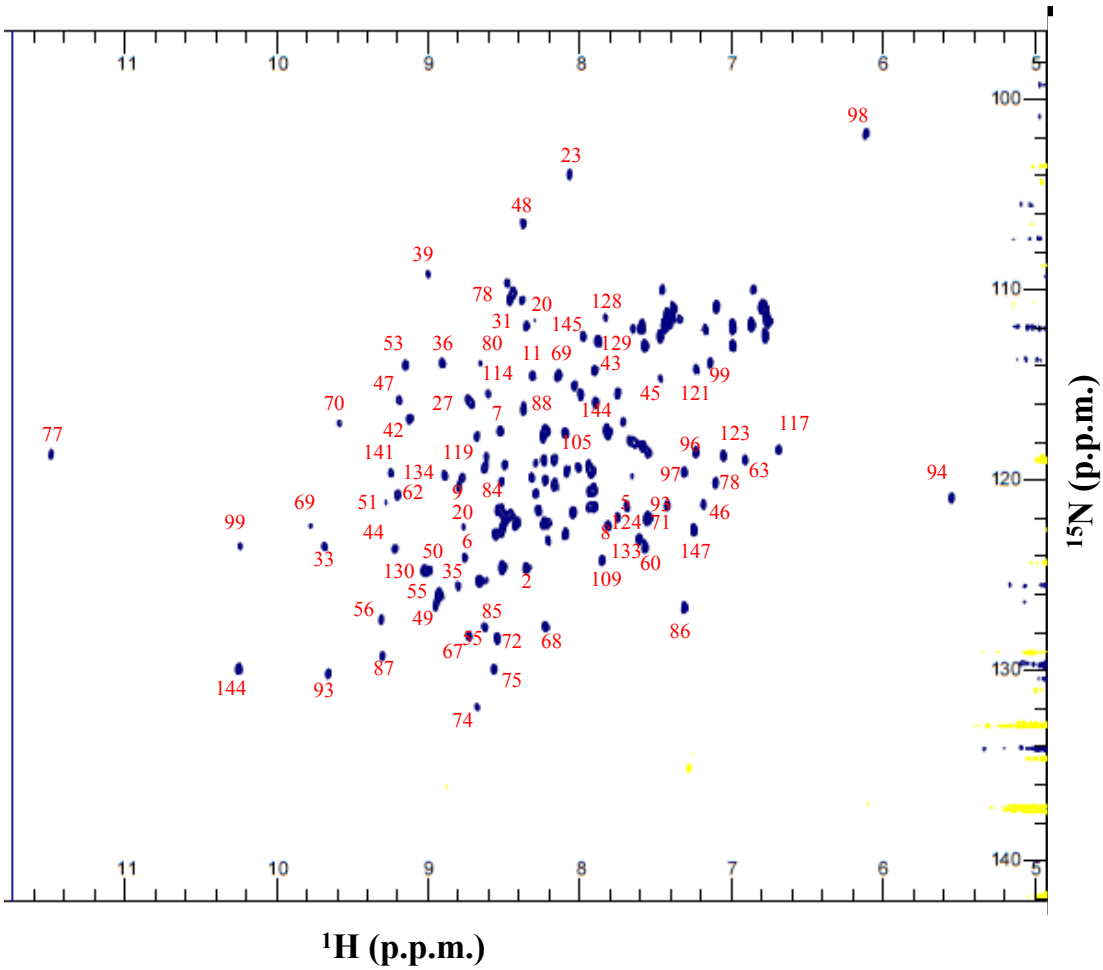
11
10
9
8
7
6
5
100
110
120
130
140
^{15}N (p.p.m.)
^{1}H (p.p.m.)

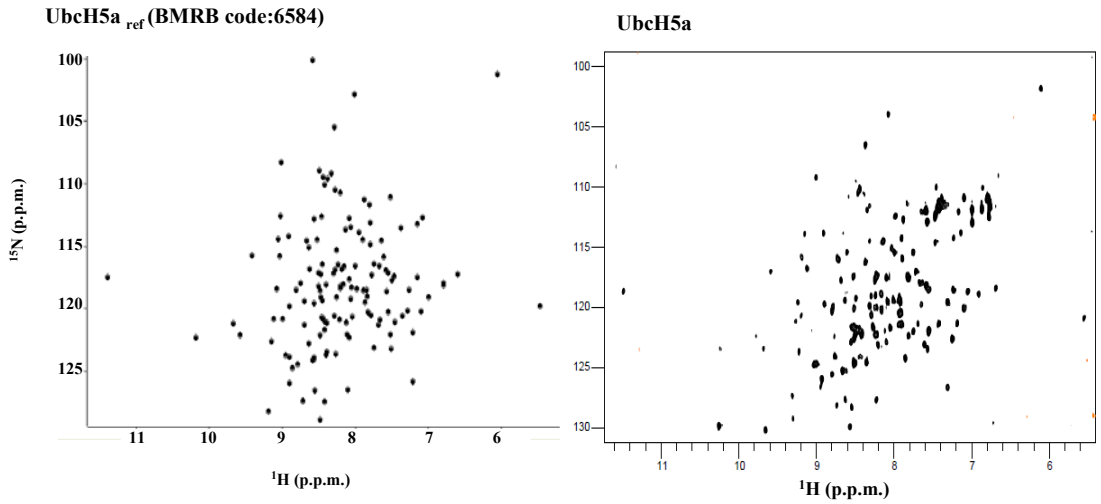

Figure 4-8: $^{1}H,^{15}N$-HSQC NMR spectrum of UbcH5a. (A) Sequence alignment of $UbcH5a_{ref}$ (BMRB code: 6584) and our constructs, UbcH5a. (B) The NMR spectrum of our construct, UbcH5a, (right panel) was recorded at 300 K in the NMR buffer [20 mM Tris, 50 mM NaCl, pH7.2] on an 800 MHz NMR spectroscopy. Using $UbcH5a_{ref}$ (left panel) as a reference, 65% of UbcH5a residues are identified and labelled as shown (page 112). HSQC spectra of both proteins show similar cross-peaks dispersions.

- ***The HSQC spectrum of ^{15}N-UbcH5a in the presence of MDM2RING△C***

NMR data of ^{1}H, ^{15}N-UbcH5a (25 μM) in the presence of MDM2RING△C showed that there were no shifts of cross-peaks; instead, a decrease in the signal intensities of the cross-peaks was observed (Figure 4-9). The molecular weight of apo-UbcH5a is 18 kDa, and the molecular weight of the UbcH5a-MDM2RING△C complex is approximately 40 kDa. The larger size of the complex increased the tumbling time, meaning less signals detected in a reasonable amount of time, resulting in substantially reduced signal intensity being recorded. This data provided evidence that MDM2RING△C interacted with UbcH5a. Corresponding residues of UbcH5a that had no or lower level signal intensities were depicted on the spectrum (Figure 4-9). After the addition of a 4 fold amount of MDM2RING△C (100 μM), the relative signal intensity of each residue on ^{15}N-UbcH5a was reduced (Figure 4-10). Signal intensity of each peak reduced in most cross-peaks. Signal intensities of residues that completely disappeared were Phe31, Tyr74, Asn77 Ser101, and Ile106. Relative signal intensities of cross-peaks only remaining less than 25% (compared to the signal intensities of

cross-peaks on the apo-^{15}N UbcH5a) were Arg5, Leu10, Ser11, Val54, Phe69, Ile78, Ile84, Ser94, Thr98, Asn114 and Lys144.

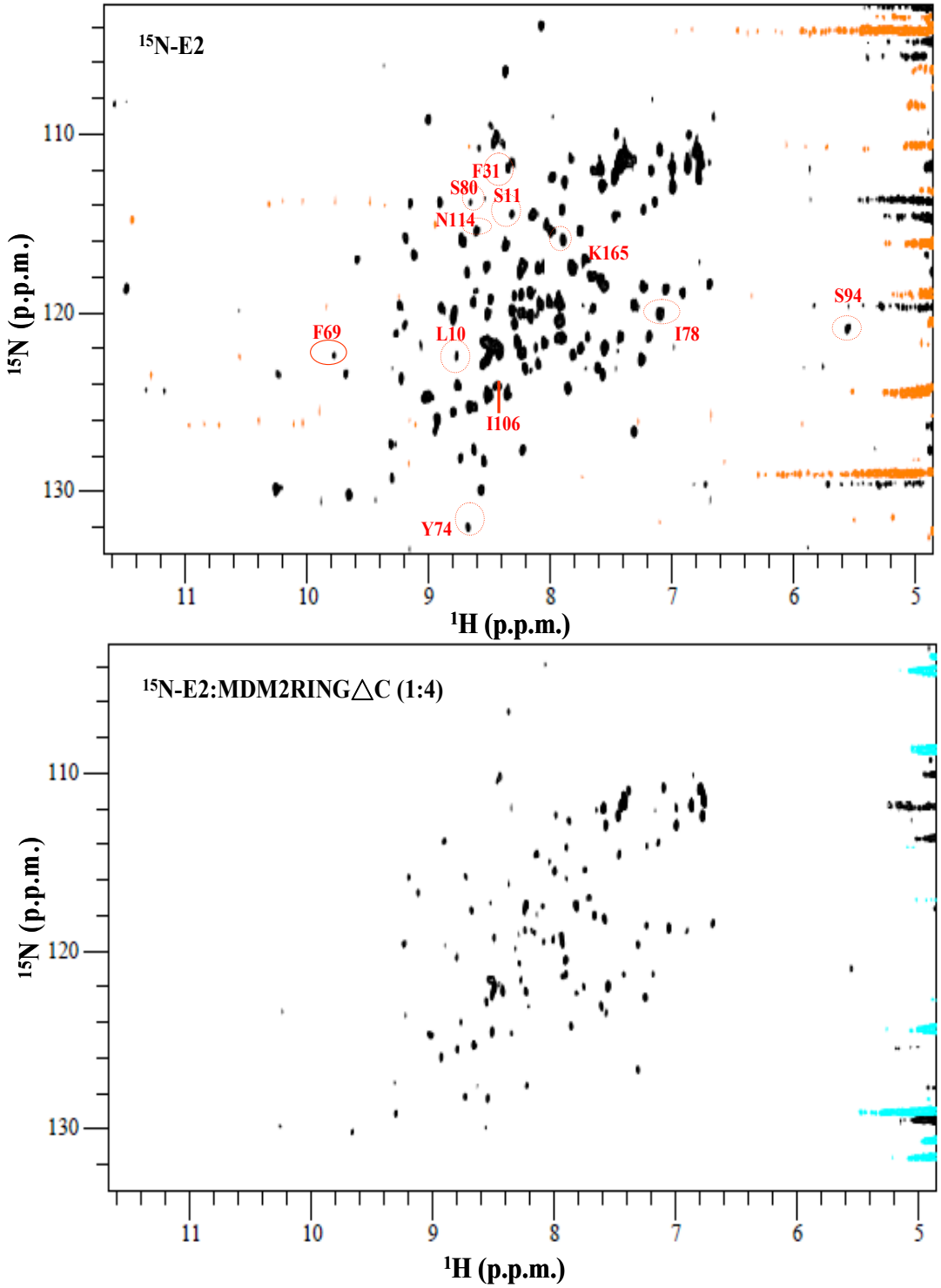

Figure 4-9: ^{1}H,^{15}N-HSQC NMR spectra of ^{15}N-UbcH5a in the absence/presence of MDM2RING△C. Upper panel is the HSQC spectrum of apo-^{15}N-UbcH5a (50 µM). Lower

panel is the HSQC spectrum of ^{15}N-UbcH5a (50 μM) in the presence of MDM2RING△C (200 μM). Signal intensities of all cross-peaks are reduced in the presence of MDM2RING△C. Resonances no longer visible in the lower spectrum are circled and labelled in the upper panel.

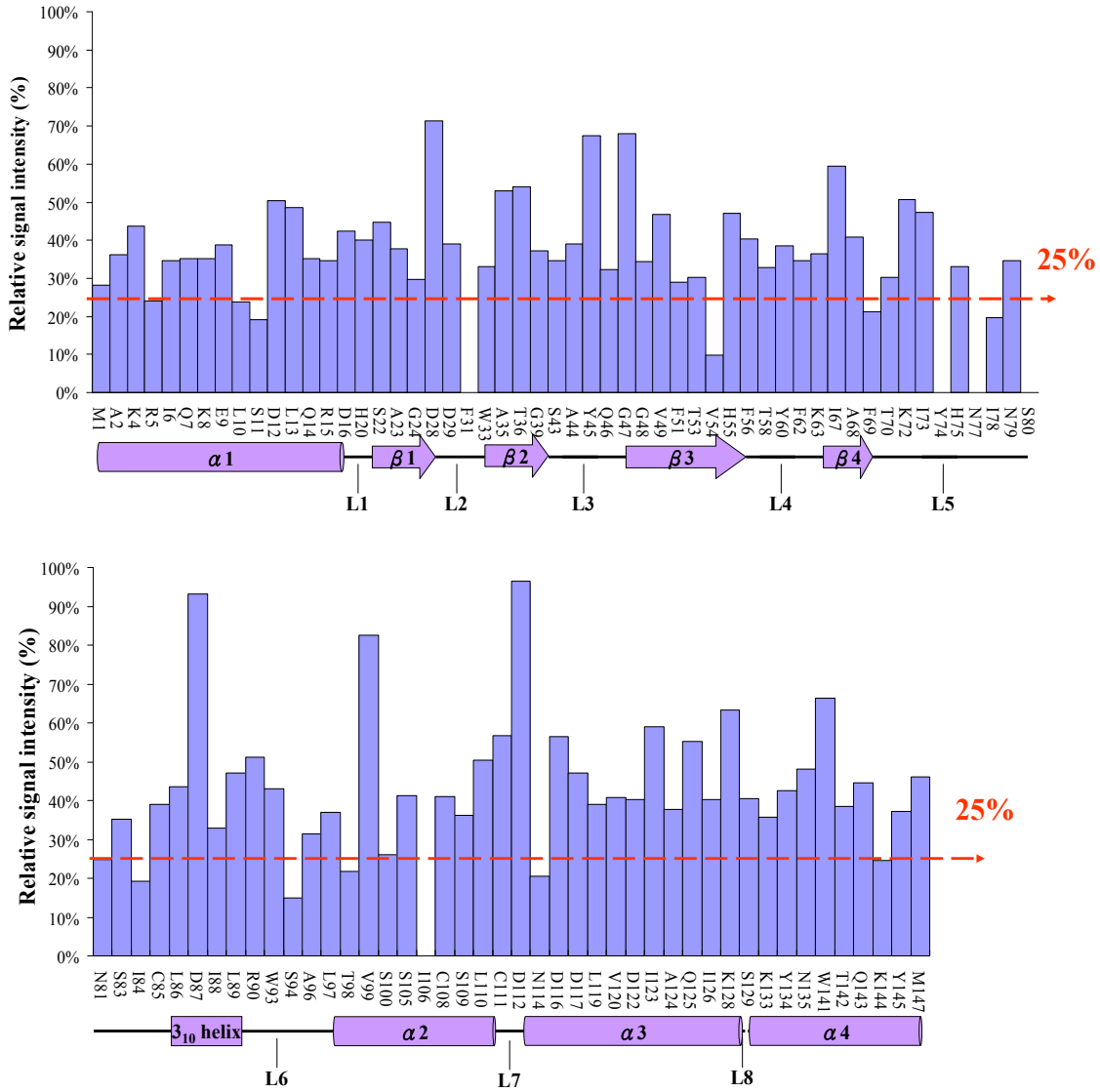

Figure 4-10: Relative signal intensity of each peak of UbcH5a (25 μM) in the presence of MDM2RING△C (100 μM). Each assigned cross-peak representing each residue of UbcH5a is labelled, and the relative signal intensity observed in the presence of MDM2RING△C compared to apo-^{15}N-UbcH5a is plotted in the bar chart. The secondary structure of UbcH5a is shown below the sequence.

- ***Residues involved in the MDM2RING△C interaction were mapped on the structure of UbcH5a***

Residues which may be involved in the interaction with UbcH5a were mapped onto the structure of UbcH5a (Figure 4-11), showing that some of those residues were positioned in the canonical E3-binding site, including Arg5, Leu10, Ser11 (at the α1) and Phe31 (L2, the loop between the β1 and β 2).

Our NMR data in the presence of MDM2RING△C showed that a peak representing Asn114 decreased in intensity (less than 25% remaining). Previous reports have found that Asn114 plays a role in regulating the exposure of the groove near the active cysteine residue (Cys85) to allow access of the acceptor ubiquitin (Sakata et al., 2010). Combining the published crystal structural data of the UbcH5a~Ub intermediate with our current NMR data, these observations suggested that on binding, MDM2RING△C may have a allosteric effect on the orientation of N114 (Figure 4-11) affecting ubiquitin binding. In addition, a previous report that showed mutations of Lys8, Ile37, Leu89, Ile106, Asn114 weakened the UbcH5b-CONT4 mediated ubiquitination (Ozkan et al., 2005). Consistent with this notion, signal intensities of peaks representing these residues (except un-assigned Ile37), of UbcH5a were reduced or diminished (Figure 4-10) after the addition of MDM2RING△C, providing evidence that these residues play a role in communication between the MDM2RING△C and UbcH5a. A hypothesis has been proposed that E3-binding to UbcH5a or the thioester-bond ubiquitin-binding to UbcH5a may allosterically induce communication between the E3-binding site and the active site of UbcH5a (Ozkan et al., 2005). The observation from our NMR data was consistent with this hypothesis.

In summary, NMR data showed that UbcH5a interacts with MDM2RING△C. Since the E2-E3 interaction is essential for ubiquitination (Deshaies & Joazeiro, 2009), this HSQC NMR data supports our previous hypothesis that there is interaction between MDM2RING△C and UbcH5a, because the *in vitro* ubiquitination data showed (Figure 3-3) that MDM2RING△C is E3 active.

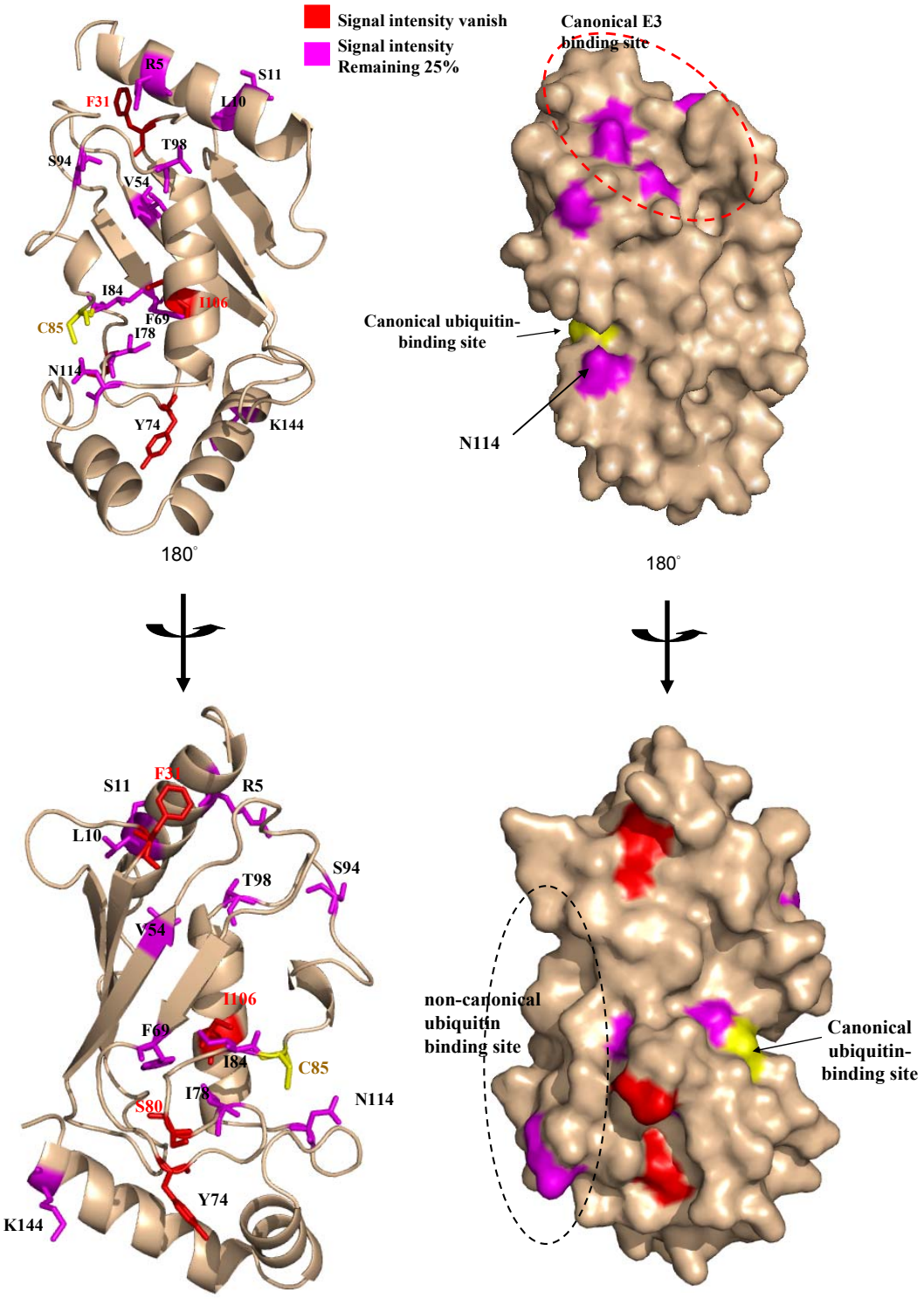

Figure 4-11: Mapping of the perturbed residues on UbcH5a upon binding to MDM2RING△C. Residues (The intensity of peaks completely diminished) are coloured in red, and residues (with less than 25% remaining signal intensity) are shown in magenta. The active cysteine (Cys85) is coloured in yellow. Ribbon and surface diagrams are both provided.

4.4 Summary

In this work, we carried out crystal trials to screen the optimal conditions to form UbcH5a-MDM2RING△C and UbcH5a-MDM2RING complex. Unfortunately, no suitable crystals have yet been produced for diffraction studies. According to the DisMeta results, MDM2RING (residue 386-491) or MDM2RING△C (residues 386-478) has flexible segments at the N-terminal 52 residues. Note that a flexible region often complicates structural determination by suppressing crystal formation or generating a poor dispersion of the NMR spectrum. Hence, in the future experiments for the structural determination, using NMR or X-ray crystallography, it would be better to make new constructs in which the disordered sequences are removed, to increase the stability of the ordered core of a folded protein.

^{15}N-UbcH5a has a good quality NMR spectrum, and signal intensity reduction of ^{15}N-UbcH5a was observed in the presence of MDM2RING△C, suggesting that there was interaction between MDM2RING△C and UbcH5a. Mapping the peaks which had reduced signal intensity (Figure 4-11) showed that some residues were located at the canonical E3-binding site, and other residues play roles in communication of the E3-binding and the active site of UbcH5a upon allosteric regulation.

Negative staining transmission electron-microscopy provided evidence that the structure of the purified fraction of higher oligomers of MDM2RING is a supramolecular assembly (regular donut-like particles), consistent with other group findings (Poyurovsky et al., 2007). Moreover, *in vitro* ubiquitination data demonstrated that the higher oligomers of MDM2RING had E3 ligase activity.

5 Biophysical Studies of the interaction of the MDMX C-terminal peptide with MDM2 and UbcH5a

MDM2 is an attractive drug target against p53-related tumours. It has been shown that MDM2 regulates p53 through transrepression and ubiquitination. A number of small molecules have been developed to inhibit MDM2-mediated transrepression function by disruption of p53-binding onto the hydrophobic domain of MDM2. Recently, a potential inhibitory peptide, peptide 9, has been found (K. Ball's group, unpublished data). It has been shown that peptide 9 binds to FLMDM2 and inhibits MDM2 E3 ligase activity; however, the mechanism is unclear. Moreover, peptide 9 was synthesised based upon the C-terminal twelve amino acids (KEIQLVIKVFIA) of MDMX. From previous reports, the C-terminal amino acids of MDMX binds to the C8-binding site; therefore, presumably peptide 9 binds to MDM2RING in a similar way. In this work, we studied the interaction between peptide 9 and MDM2 using a number of techniques, including intrinsic tryptophan fluorescence, thermal denaturation assay, fluorescence anisotropy, and electrospray ionisation mass spectrometry.

5.1 The initial finding: peptide 9

A potential peptide inhibitor, peptide 9 was identified by K. Ball's group (courtesy of Dr. Susanne Patterson, unpublished data) and was found to have an identical sequence to the C-terminal 12 residues of MDMX. Results of both *in vitro* and *in vivo* pulldown experiments showed that peptide 9 interacted with FLMDM2 (Figure 5-1A). The MDMX C-terminal twelve residues, KEIQLVIKVFIA, has been synthesised and called "peptide 9" (Figure 5-1B). The crystal structure of the MDM2/MDMX heterodimer showed that peptide 9 may interact with FLMDM2 through **the C8-binding site** of the RING domain (Figure 5-1B). Several groups (Kawai et al., 2007; Poyurovsky et al., 2007) and our previous data (discussed in Chapter 3) have proved that dimerisation/ oligomerisation is critical for MDM2 E3 ligase activity. If peptide 9 binds and disrupts the dimerisation of MDM2, it is likely that monomeric MDM2 will lose its E3 ligase activity. As expected, *in vitro* ubiquitination data show that 10 μM peptide 9 completely inhibited the E3 activity of FLMDM2, and also inhibited the E3 activity of MDM2RING (Figure 5-1C). Moreover, a truncated peptide, KEIQLVIKVF, lacking last two amino acids, showed no inhibition of MDM2 E3 ligase activity (Dr. Susanne Patterson, unpublished data), suggesting that the truncated peptide cannot bind to FLMDM2, and the last two amino acids, Ile489 and Ala490, are critical for the interaction with MDM2.

Figure 5-1: The interaction of peptide 9 and MDM2. (A) *in vitro* and *in vivo* peptide pulldown experiments reveal that peptide 9 interacts with FLMDM2. (data from Dr. S. Patterson). p1: peptide 1; p9: peptide 9. DMSO is used as a negative control. (B) MDMX C-tail bound to the C8-binding site of MDM2 RING domain. The crystal structure is from PDB structure 2VJE. (Left) MDMX RING domain is shown in cyan. MDMX C terminal-tail is shown in stick representations (magenta) (C= white; O = red; N = blue; S = yellow). MDM2 is shown in surface representations (white).peptide 9 is synthesised based upon the MDMX C-terminal twelve residues; therefore, peptide 9 is assumed to bind to the C8-binding site of MDM2. (C) *in vitro* ubiquitination assays of FLMDM2 (left) and MDM2RING (right) show that peptide 9 inhibits their E3 activity. Reactions are resolved by gradient SDS-PAGE, and detected by autoradiography using p53 antibodies (D01).

(A)

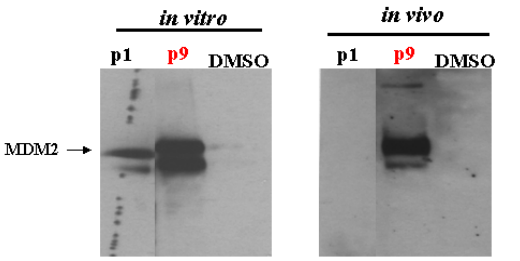

peptide 1 _ CSLCEKRPRDGNIIHGRTGH
peptide 9 _ KEIQLVIKVFIA

(Data courtesy of Dr. S. Patterson)

(B)

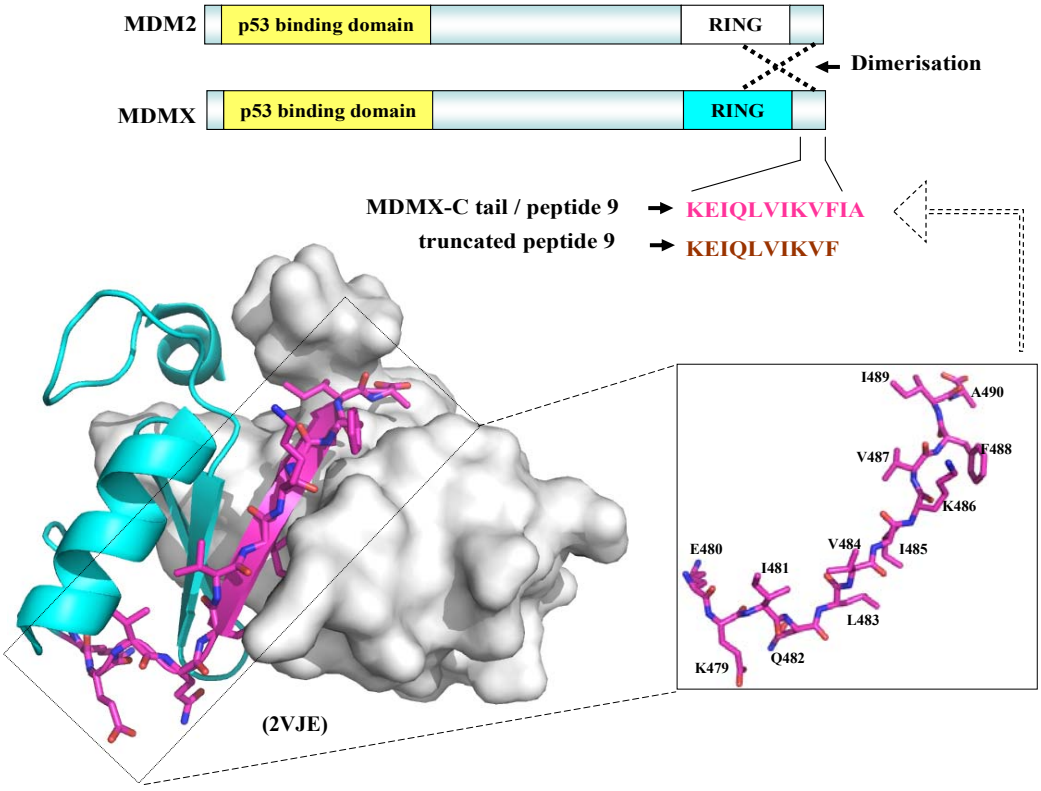

(C)

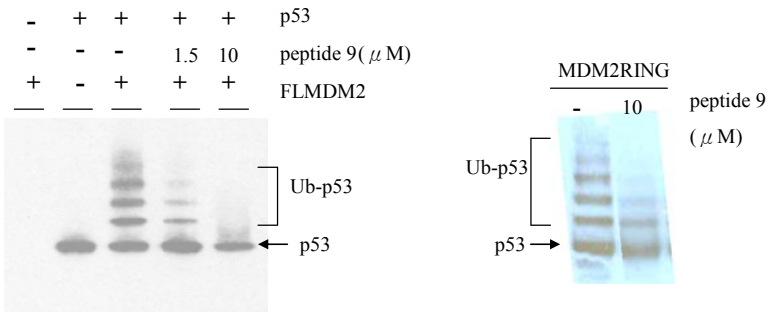

5.2 peptide 9-binding changes the conformation of FLMDM2

Peptide 9 is synthesised according to the C-terminal twelve amino acids of MDMX and has been shown to inhibit MDM2 E3 ligase activity (Figure 5-1C). To support our hypothesis that peptide 9 binds to and induces conformational change in FLMDM2, we used intrinsic tryptophan fluorescence and measured the emission fluorescence spectra of apo-FLMDM2, FLMDM2-peptide 9, and FLMDM2-truncated peptide (Figure 5-2).

5.2.1 The principle of intrinsic tryptophan fluorescence

Intrinsic tryptophan fluorescence is a well-characterised and convenient method to detect changes in protein conformation under different conditions including pH, temperature, ligand-bound state or as a result of mutagenesis experiments (Crang & Rumsby, 1979; *van* Duffelen et al., 2004; Ramalingam et al., 2008). The fluorescence intensity of a folded protein is derived from the contributions from the intrinsic fluorescence of its constituent amino acids. Proteins contain three aromatic amino acids which exhibit fluorescence: tryptophan, tyrosine and phenylalanine. These three amino acids have different absorption and emission wavelengths. Tryptophan is a stronger emitter and has a higher quantum yield than tyrosine and phenylalanine. When a ligand binds to a target protein, it may induce conformational changes within the target protein. The local environment of tryptophan residues within the target protein may change, resulting in changes in the intrinsic tryptophan fluorescence spectrum between apo- and ligand-bound proteins.

5.2.2 Methods and Materials: intrinsic tryptophan fluorescence

Tryptophan intrinsic fluorescence experiments were carried out using a FLUOROMAX-3 (HORIBA Jobin Yvon) spectrofluorometer. All measurements were carried out at 25 ℃. Each sample contained 1 ml solution in each eppendorf with 10 μM FLMDM2 in the buffer (25 mM HEPES, pH 7.5, 50 mM KCl, 2 mM DTT, 10 μM $ZnSO_4$, 5% (v/v) glycerol) as used in previous experiments (Wawrzynow et al., 2009). 10 μM FLMDM2 with 10 μM peptide 9 or 10 μM truncated peptide was incubated on ice for 5 minutes prior to transfer of the mixture to 1 cm path length Quartz cuvette. The sample was allowed to equilibrate for 15 minutes before intrinsic fluorescence intensities were measured. For detection of tryptophan intrinsic fluorescence, experimental parameters were: excitation wavelength (λ_{exc}) set to 295 nm, intrinsic fluorescence emission spectra (λ_{emi}) was collected over the range of 300 to 400

nm, and the bandwidth set to 5 nm. The data were corrected by subtraction of buffer fluorescence. All samples were measured in triplicate.

5.2.3 Results and discussion: intrinsic tryptophan fluorescence

FLMDM2 contains four tryptophan residues: W245, W303, W323 and W329 (Figure 5-2A). W245 is in the acidic domain and the other three residues are within the zinc finger domain. Hence, although there is no structure of FLMDM2 available, intrinsic tryptophan fluorescence is a useful technique to study the structural integrity of FLMDM2, the FLMDM2-peptide 9 complex and the FLMDM2-truncated peptide complex (Figure 5-2B). Our results showed that the maximum fluorescence intensity of apo-FLMDM2 (green line, Figure 5-2B) was 369950.7 cps with a λ_{max} peak at 343 nm as seen in earlier experiments (Wawrzynow et al., 2009). Following incubation of 10 μM truncated peptide with FLMDM2, the tryptophan fluorescence spectrum of the mixture was similar to that seen with apo-FLMDM2. The maximum fluorescence intensity is 356956.0 cps at 342.5 nm (blue line, Figure 5-2B), showing that the truncated peptide did not induce any conformational change in FLMDM2. These results are consistent with previous data showing that there is no binding between truncated peptide and FLMDM2 (Dr. Susanne Patterson, unpublished data). When 10 μM peptide 9 was incubated with FLMDM2, the tryptophan spectrum of FLMDM2-peptide 9 obtained showed that the maximum fluorescence intensity has increased to 411609.34 cps with a λ_{max} peak at 340 nm (red line, Figure 5-2B). A significant increase in the intensity of the signal suggests that peptide 9 induced a perturbation in the folded state of FLMDM2. The blue shift (from 343 nm to 340 nm) also suggested that peptide 9 interacts with FLMDM2 and induces a conformational change in FLMDM2. The major shift of the λ_{max} peak to a shorter wavelength means binding of peptide 9 may induce the reorientation of the tryptophan residues of FLMDM2 to adopt a more nonpolar environment. There is another minor emission peak at 358 nm, possibly contributed by one of the four tryptophan residues within FLMDM2.

Previous reports indicate the C-terminus of MDM2 or MDMX is essential for the dimerisation of MDM2/MDM2 homodimer or MDM2/MDMX heterodimer (Poyurovsky et al., 2007). Because our peptide 9 has the same sequence as that of the MDMX C-terminal twelve amino acids, the binding site of peptide 9 to FLMDM2 is proposed to be located in the C8-binding site of MDM2 RING domain as seen in the model structure (Figure 5-1B). FLMDM2 contains four tryptophan residues which are located in a flexible region. The blue

shift to a shorter wavelength provides evidence that peptide 9 induces structural changes in FLMDM2. However, the actual binding site of peptide 9 to FLMDM2 is as yet unclear. Further studies are required to determine whether the changes in intrinsic fluorescence were caused by the direct interaction of peptide 9 with tryptophan or by an allosteric effect.

In summary, our tryptophan intrinsic fluorescence data were consistent with previous data (Figure 5-1), and provide evidence that peptide 9 bound to FLMDM2, inducing a conformational change in FLMDM2 to buried the tryptophan in more hydrophobic environment. Our findings also suggest that the last two amino acids of peptide 9, Ile489 and Ala490, were critical for the interaction with FLMDM2.

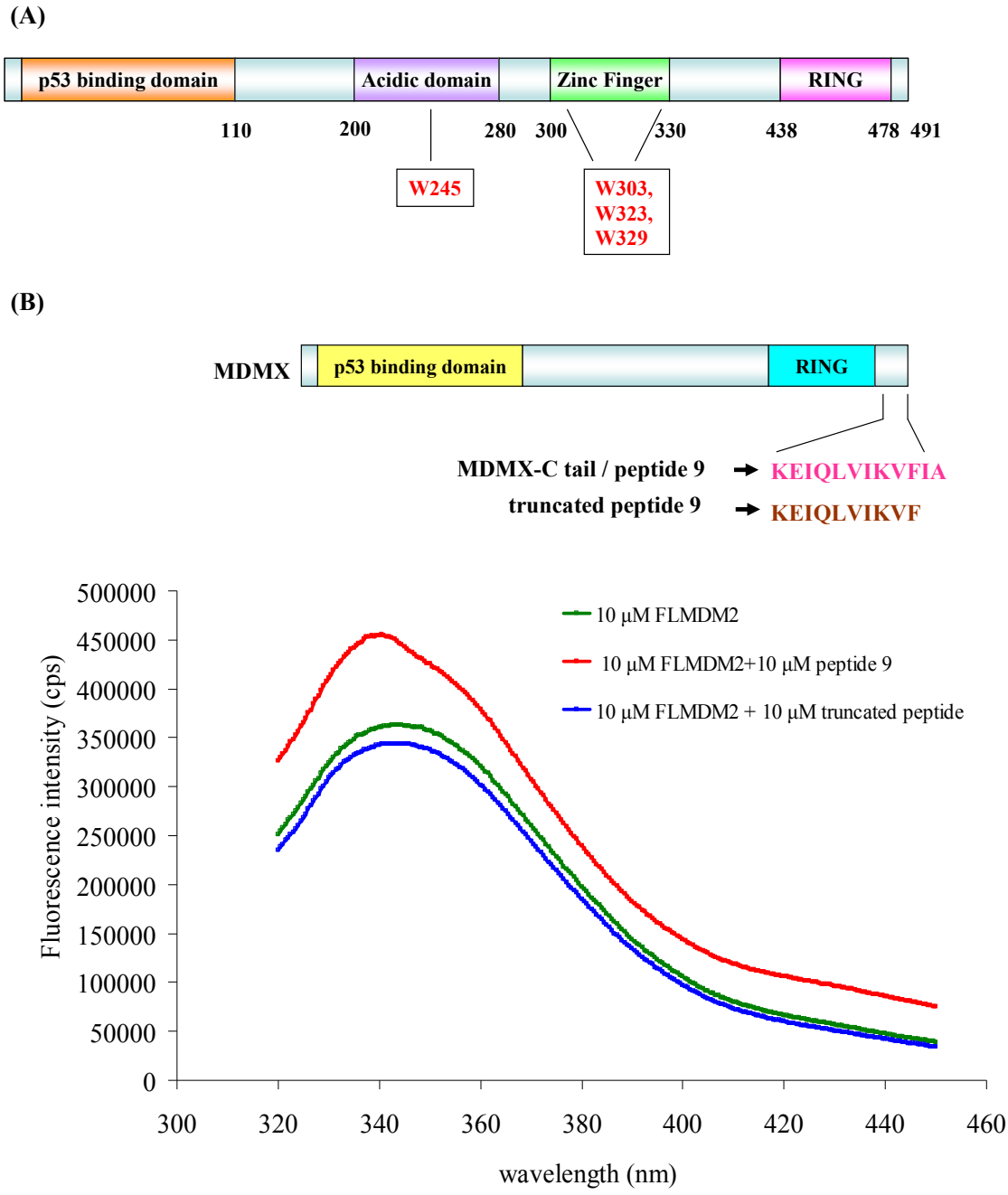

sample	λmax [nm]	Fluorescence max [cps]
10 µM FLMDM2	343.0	369950.7
10 µM FLMMDM2 + 10 µM truncated peptide	342.5	356956.0
10 µM FLMMDM2 + 10 µM peptid 9	340.0	411409.3

Figure 5-2: peptide 9 induced a conformational change in FLMDM2. (A) FLMDM2 has four tryptophan residues (highlighted in red in the sequence): one is located in the acidic domain, with three in the zinc finger domain. (B) Intrinsic tryptophan fluorescence spectra of FLMDM2 (green), FLMDM2-truncated peptide (blue), FLMDM2- peptide 9 (red).

5.3 The putative peptide 9-binding site: the C8-binding site of MDM2RING

Previous studies confirmed that peptide 9 bound to FLMDM2 and inhibited its E3 activity (Figure 5-1, 5-2). The next question we asked was what is the peptide binding site within FLMDM2? Our initial assumption was that the MDM2 RING domain was likely to be the binding site for peptide 9 (a MDMX C-terminus). The crystal structure of the MDM2/MDMX heterodimer (PDB: 2VJE) showed that the MDMX C-terminus interacts with the C8-binding site of MDM2 RING domain (Figure 5-1B).

In general, the interaction interface is a critical determinant of protein-protein affinities: a greater buried surface provides higher binding affinities (Hoeflich & Ikura, 2002). A newly built structure of the MDM2-peptide 9 complex (Figure 5-3A) was generated based on the crystal structure of MDM2-MDMX (PDB: 2VJE). Here, peptide 9 was assumed to bind in the same way as the last twelve C-terminal residues of MDMX. This modelled structure was used as a template for the calculation of the buried surface areas (BSA) of the MDM2-peptide 9 interaction using the PISA program (Protein Interfaces, Surfaces, and Assemblies), that is available to calculate the buried surface based on coordinate data from the PDB (http://www.ebi.ac.uk/msd-srv/ prot_int/pistart.html). The results showed that in the MDM2-peptide 9 complex, the buried surface area of peptide 9 and MDM2 within the complex were, respectively, 503.1 $Å^2$ and 444.7 $Å^2$ (Table 5-1). The buried surface of peptide 9 amounted to 88% of the accessible surface of the complex. Generally, if the ligand fits well in the binding site of the target, buried surface areas of both ligand and target should be similar (Wu et al., 2000).

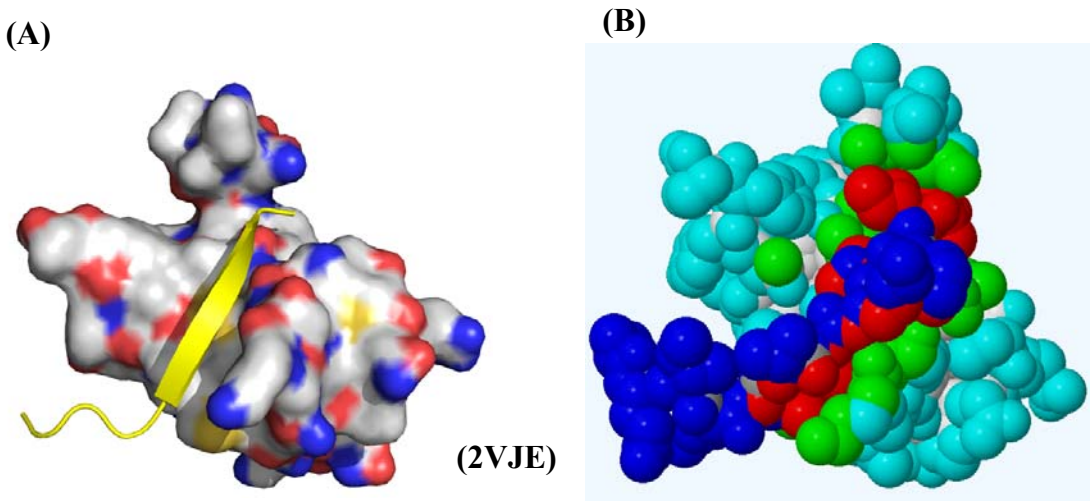

Figure 5-3: Three dimensional structure of the putative peptide 9 binding site within the C8-binding site. (A) peptide 9 (a MDMX C-terminal twelve amino acids) is highlighted in yellow and MDM2RING is shown in surface representation coloured according to atom types (C= white; O = red; N = blue; S = yellow). (B) The structure of the peptide 9-MDM2 complex, same as (A), generated using the PISA program. MDM2 is shown in cyan spheres and peptide 9 is coloured according to the contribution of each residue to the buried surface areas of the MDM2-peptide 9 complex. (Contribution: green, high; red, medium, and blue: low). Both figures are based on the crystal structure of MDM2-MDMX (PDB: 2VJE).

Table 5-1: The buried surface areas (BSA) of MDM2-peptide 9 and MDM2-truncated peptide are calculated using PISA program. The CPS and the number of H-bonds were also shown.

	Buried sureface area (Å²)			
	peptide	MDM2	CPS	H-bond
MDM2-peptide 9 (KEIQLVIKVFIA)	503.1	444.7	0.71	8
MDM2-truncated peptide (KEIQLVIKVF)	311.8	282.0	0.06	5

*CPS is a parameter from PISA which gives a measure of the significance of the interaction.

Interaction interface studies also revealed that the last two residues, Ile and Ala, were critical for the interaction of MDM2 with peptide 9. There were eight intermolecular H-bonds in the MDM2-peptide 9 complex (Figure 5-4B): Lys486-amide to Lys454-oxygen; Lys486-oxgen to Thr455-Og1; Lys486-oxgen to Leu458-amide; Phe488-amide to Gly456-oxygen; Phe488-oxgen to Leu458-amide, Ile489-oxygen to Asn433-Nd2; Ala490-oxygen to Lys446-Nz; and Ala490-amide to Leu458-oxygen. Results also showed that the last 8 residues of peptide 9 contributed most to the complete buried surface areas (Figure 5-4A). Buried surface areas between the truncated peptide and MDM2 in the complex, were respectively, 311.8 $Å^2$ and 282.0 $Å^2$ (Table 5-1). However, the truncated peptide interacted with MDM2 through only five H-bonds (Figure 5-4B). Moreover, the last two residues in peptide 9, Ile and Ala, contributed approximately 43% of the buried surface areas in the complex and also provided three H-bonds (Figure 5-4A). Those results could explain why the truncated peptide lost binding ability in our intrinsic fluorescence experiments. Moreover, the CPS value of MDM2-peptide 9 and MDM2-truncated peptide 9 were 0.713 and 0.06 (Table 5-1). The CPS values range from 0 to 1 and a higher score means a greater likelihood of complexation. This provides additional support for the importance of the last two residues of peptide 9 in the interaction with MDM2 (Table 5-1). In summary, according to our analysis of buried surface areas in the MDM2RING-peptide 9 complex, the C8-binding site of MDM2RING is likely to be the binding site for peptide 9.

Figure 5-4: The putative peptide 9 binding site is in the C8-binding site of MDM2RING domain. (A)The sequence and the putative secondary structure of peptide 9 are shown. The bar graph above the sequences of the peptide presents the buried surface area of each peptide 9 residue complexed with MDM2RING. (B) The corresponding residues contributed to the H-bonds between MDM2-peptide 9 (upper left panel) and MDM2-truncated peptide (upper right panel). MDM2 is shown in white surface representation and the residues shown in cyan surface are involved in the H-bond interaction. Both peptides are shown in magenta cartoon and residues involved in the H-bonds are highlighted in yellow sticks. The H-bonds are also shown in dashed red lines.

(A)

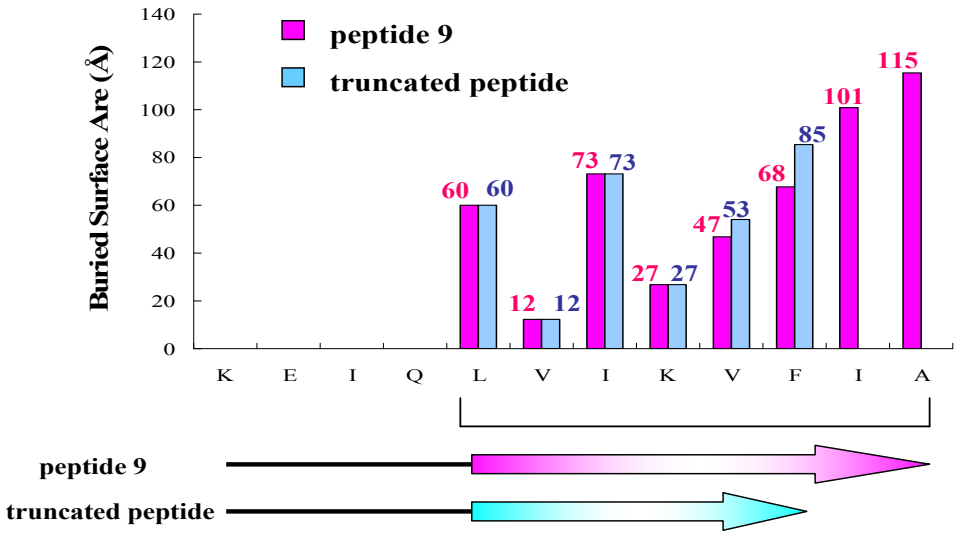
Buried Surface Are (Å)
140
120
100
80
60
40
20
0
peptide 9
truncated peptide
60 60
12 12
73 73
27 27
47 53
68 85
101
115
K E I Q L V I K V F I A
peptide 9
truncated peptide

(B)

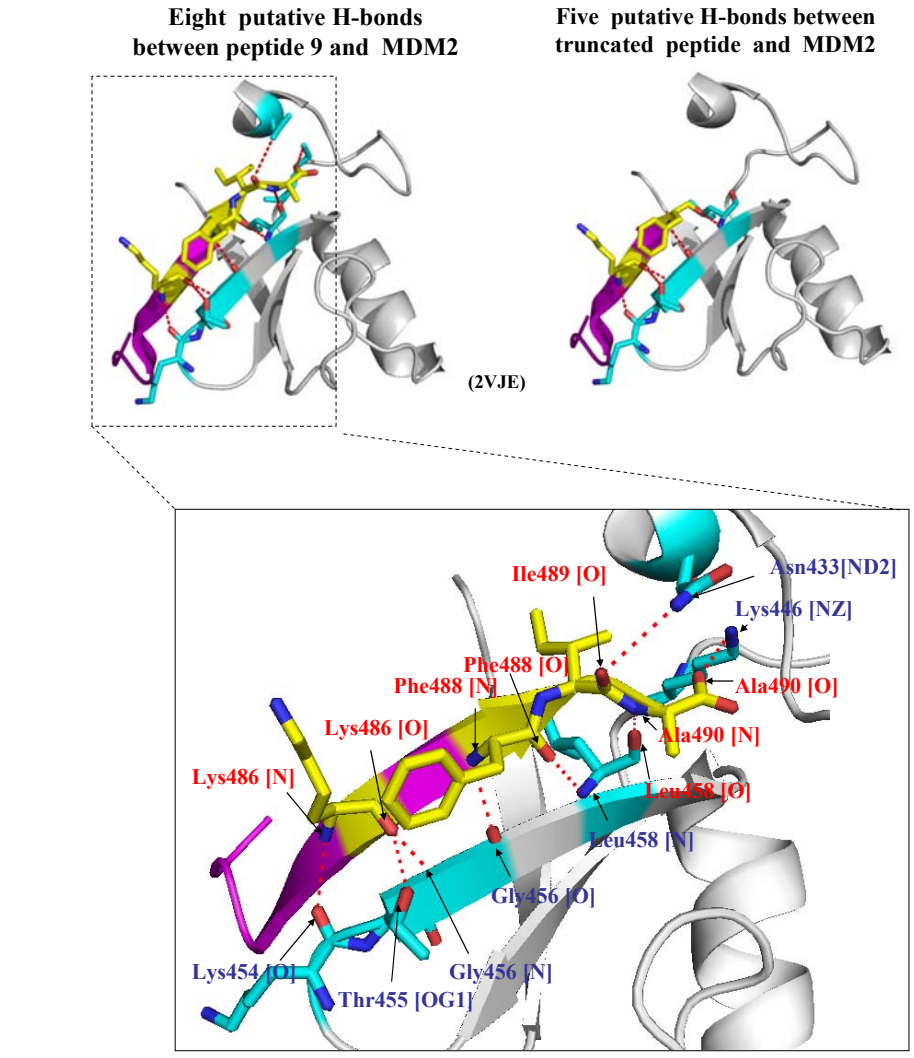
Eight putative H-bonds between peptide 9 and MDM2
Five putative H-bonds between truncated peptide and MDM2
(2VJE)
Ile489 [O]
Asn433[ND2]
Lys446 [NZ]
Phe488 [O]
Phe488 [N]
Ala490 [O]
Lys486 [O]
Ala490 [N]
Lys486 [N]
Leu458 [O]
Leu458 [N]
Gly456 [O]
Lys454 [O]
Gly456 [N]
Thr455 [OG1]

5.4 Does peptide 9 really bind to the C8-binding site of MDM2RING?

A previous report shows that the MDM2 RING domain can allosterically regulate the conformation of MDM2 (Wawrzynow et al., 2009). Additional supporting data was obtained from our intrinsic tryptophan fluorescence experiments with FLMDM2-peptide 9 (section 5.2) and the analysis of the buried surface areas of the MDM2-peptide 9 complex (section 5.3). The data suggested that the C8-binding site of MDM2 could be the binding site for peptide 9. To evaluate this assumption, studies of the interaction of MDM2RING and peptide were required. MDM2RING (residues 386-491), contains no tryptophan residues; therefore intrinsic tryptophan fluorescence experiments are not appropriate to study this interaction. An alternative approach was required to study the interaction of peptide 9 with MDM2RING or MDM2RING△C. MDM2RING△C (residues 386-478) was also chosen here because it lacks the C-tail and may therefore have an accessible C8-binding site for the binding of peptide 9. A number of techniques were used: fluorescence anisotropy to study the affinity of peptide 9 to MDM2RING, and electrospray ionisation mass spectrometry (ESI-MS) to analyse whether peptide 9 bound to MDM2RING.

5.4.1 The principles of fluorescence anisotropy

The principle behind fluorescence anisotropy is to monitor fluorescence intensities of the fluoroprobe-labeled ligand apo- and holo- molecules (Figure 5-5). Free fluoroprobe-labeled ligands can be peptides or small molecules. Free fluoroprobe-labeled ligands have a very fast relaxation time and show low anisotropy, because the tumbling rate is fast. However, when the fluoroprobe-labeled ligands bind to their targets, such as proteins, the tumbling rate of the larger complex becomes slower; resulting in an increase in the fluorescence emission (high anisotropy). The fluorescence anisotropy assay has been widely used to measure the binding affinity of protein to ligands (Brown et al., 2008; Harker et al., 2009; Hernandez-Valladares et al., 2010). The binding affinity of a ligand to the target can be calculated from the fluorescence intensity change of fluorescently-labeled ligands as a function of protein concentration (Figure 5-5). To confirm our hypothesis that peptide 9 binds to the C8-binding site, we used fluorescence anisotropy assays to monitor the binding affinities of peptide 9 with two MDM2RING domain constructs, MDM2RING and MDM2RING△C.

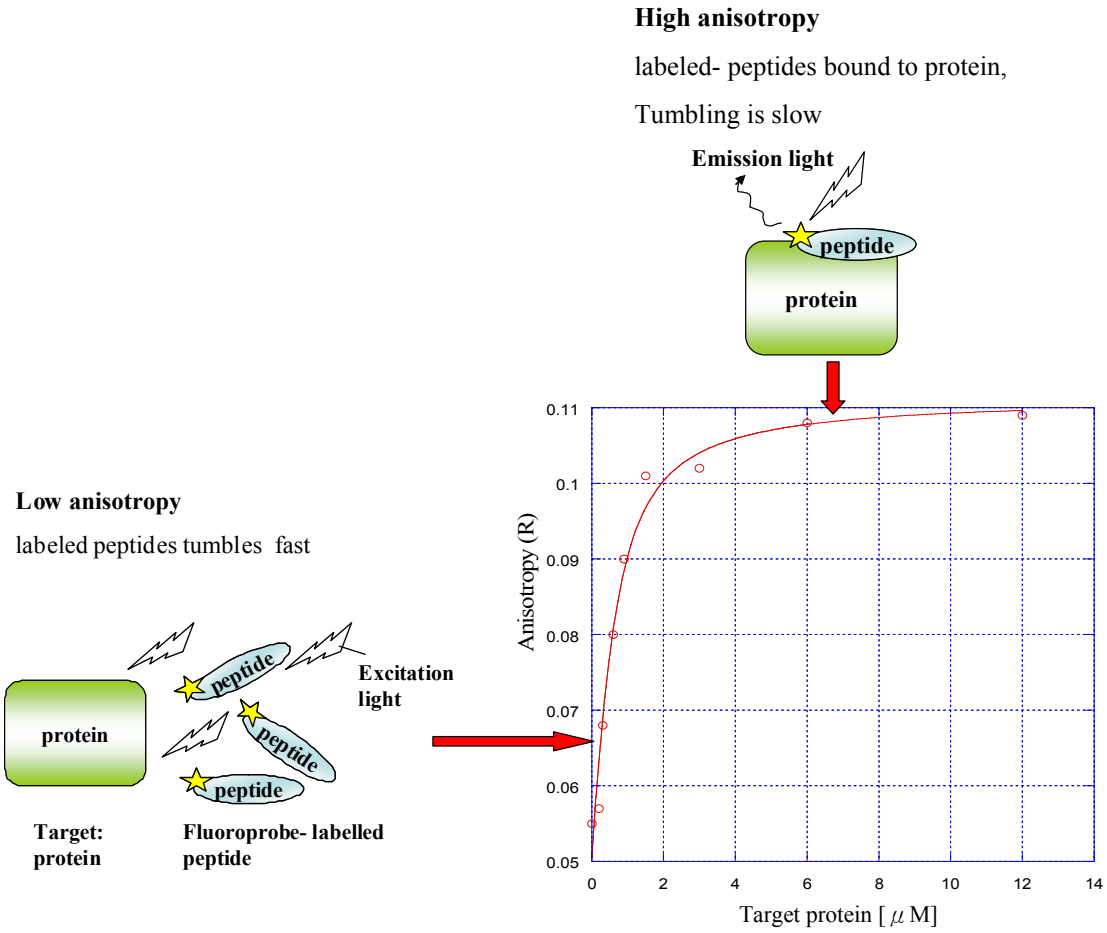

Figure 5-5: The basis of fluorescence anisotropy. The detection of the fluorescence intensity depends on the tumbling rates of the fluoroprobe -labeled molecule. The fluoroprobe is shown as a yellow star. When more fluoroprobe-labeled ligands bind to the target protein, the value of the anisotropy increases.

5.4.2 Materials and Methods: Fluorescence anisotropy

Fluorescence anisotropy was used in this work to measure the binding affinity of peptide 9 for MDM2RING, MDM2RING△C or UbcH5a. To determine the dissociation constant of peptide 9 with MDM2RING, fluorescein-labeled peptide 9 (FITC-peptide 9) was used. As a negative control, a FITC-truncated peptide was synthesised. All peptides were dissolved in 100% DMSO.

Fluorescence anisotropy experiments were performed in 96-well black plastic plates using a Thermo-fluorescence reader. Fluorescence anisotropy was measured using the following conditions: the excitation wavelength was set to 490 nm, the emission fluorescence was

measured at 530 nm, with an accompanying cutoff at 515 nm. Serial dilutions were prepared prior to being titrated into the fluorescein-labelled peptides. MDM2RING and MDM2RING△C were prepared in Tris-buffered solution (20 mM Tris, pH7.2, 150 mM NaCl, 10 μM $ZnSO_4$), UbcH5a was also prepared in the same solution minus $ZnSO_4$. The final concentration ranges of those three proteins were from 0.02 to 20 μM. The final reaction volume was 200 μl, each containing target protein and 250 nM fluorescein-labelled peptide 9. To allow the reaction to reach equilibrium, the samples were incubated for 30 minutes at room temperature, the fluorescence anisotropy of each well was then measured. To minimise the decay of fluorescein, the plate was covered with foil during the incubation. Averaged fluoresce anisotropy was plotted as a function of the protein concentration. All averaged fluorescence anisotropy values were determined from at least three sets of samples. The dissociation constant (Kd) was calculated using the Hill coefficient using the equation below (Heyduk & Lee, 1990):

$$F = F_L + \left(\frac{F_{LP} - F_L}{2[L]_T}\right)\left([L]_T + [P]_T + Kd - \sqrt{([L]_T + [P]_T + Kd)^2 - 4[L]_T[P]_T}\right)$$

F measured average fluorescence polarization

F_L fluorescence polarization of free labelled peptide

F_{LP} maximum fluorescence polarization of the peptide-protein

Kd equilibrium dissociation constant of the peptide-protein complex

$[L]_T$ total concentration of labelled peptide

$[P]_T$ total concentration of protein

5.4.3 Results and Discussions: Fluorescence anisotropy

In our fluorescence anisotropy experiments, peptide 9 was labeled with a FITC probe, which is excited by light at a wavelength of 495 nm, and emits a fluorescence signal at 530 nm. The initial assumption is that when FITC-peptide 9 binds to the target protein, MDM2RING, the complex would immobilise the labeled peptide making the fluorescence signal readily detectable. Using this method, the binding affinities of peptide 9 to MDM2RING and MDM2RING△C can be calculated.

The C8-binding site of MDM2RING has been shown to be buried within the dimer (Figure 5-1B). Another construct, MDM2RING△C, lacking the C-tail, was used in this experiment as its C8-binding site is likely be solvent exposed and accessible for peptide 9-binding. Therefore, if the binding site of peptide 9 within MDM2 is as expected, the C8-binding site of the RING domain, binding affinity of peptide 9 to MDM2RING△C should be higher than that seen with MDM2RING. In addition, to exclude the possibility that peptide 9 binds nonspecifically, BSA protein was used as a negative control in this assay. No significant fluorescence anisotropy change of peptide 9 in the presence of BSA was seen (Figure 5-6A), suggesting peptide 9 binds specifically. Fluorescence anisotropy studies showed that peptide 9 interacted with MDM2RING and MDM2RING△C (Figure 5-6A). The Kd of FITC-peptide 9 with MDM2RING was approximately 355.6 ± 113.6 nM, that of MDM2RING△C, Kd = 314.3 ± 157.9 nM (Figure 5-6B).

Previous work in Kathryn Ball's lab had characterised a truncated peptide which did not inhibit FLMDM2 E3 ligase activity. We used the truncated peptide (missing residues of IA at the C-terminus) as negative control for fluorescence anisotropy, and showed that no binding was detectable between the truncated peptide and MDM2RING.

(A)

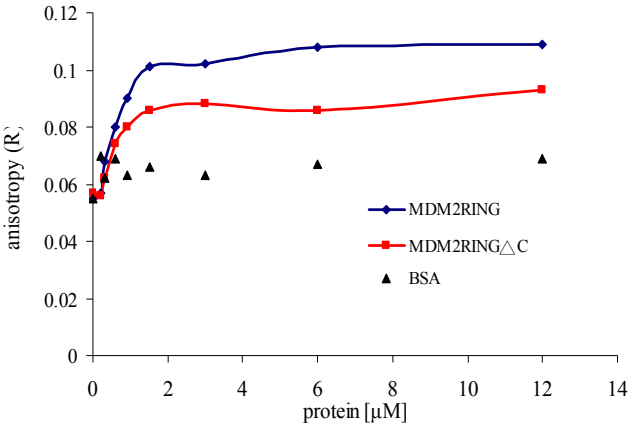

(B) **(C)**

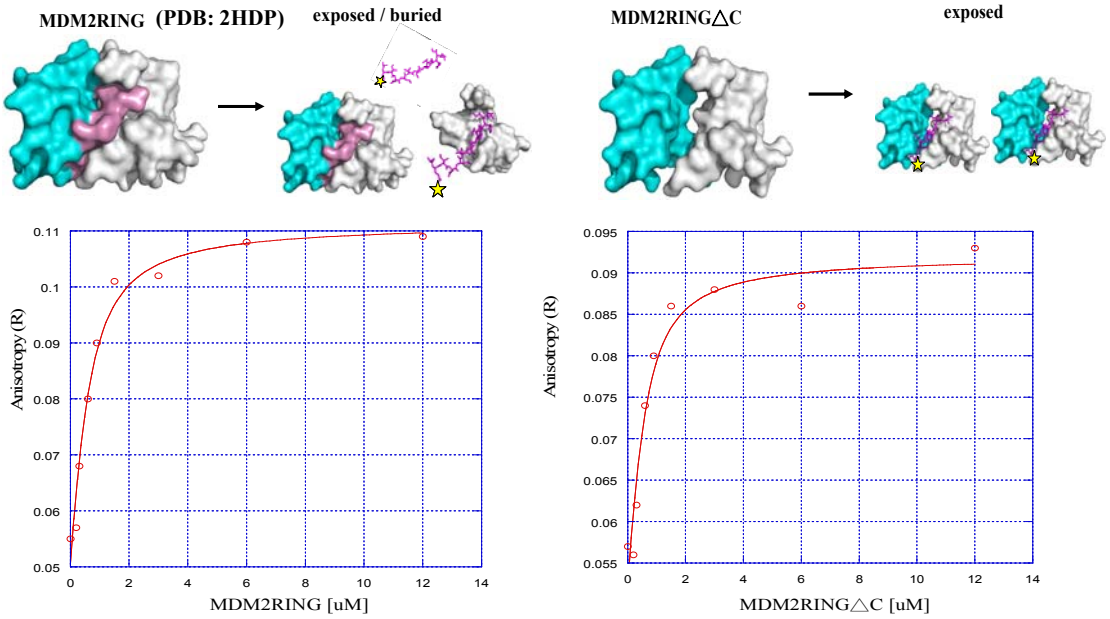

	Kd (nM)
MDM2RING	355.6 ± 113.6
MDM2RING△C	314.3 ± 157.9

Figure 5-6: Fluorescence anisotropy analysis of the interaction of peptide 9 with MDM2 RING domain. (A) Fluorescence anisotropy change of FITC-peptide 9 with three proteins: MDM2RING (red line), MDM2RING△C (blue line) and BSA (▲). (B)The Kd of FITC-peptide 9 to MDM2RING is calculated to be 355.6 ± 113.6 nM. (C) The Kd of FITC-peptide 9 to MDM2RING△C is 314.3 ± 157.9 nM. The Kd was calculated as described as in the Materials and Methods section.

5.5 ESI-MS: the interaction of peptide 9 and MDM2RING

5.5.1 The principle of ESI-MS

To further confirm that peptide 9 binds to MDM2RING, we carried out ESI-MS (electrospray ionization mass spectrometry) experiments. ESI-MS is commonly used to identify the mass of a molecule, and has recently also been used in the study of protein-ligand interactions (Burkitt, et al., 2003; Blackburn, et al., 2010; Keith-Roach, 2010). The output of ESI-MS is similar to that of MALDI-TOF-MS (introduced in Chapter 2). The mass of a molecule measured by these two mass spectrometry methods are both based on the ratio of the mass to charge (m/z) value (Feng & Konishi, 1992; Hillenkamp, et al., 1991; Richard, 1997). Since matrix and sample are ionised by a high voltage laser used in MALDI-TOF, oligomers or a protein-ligand complex are easily separated into discrete species. ESI-MS is a gentle method to ionise the molecules, producing less fragmentation of complexes, which is especially important for weakly bound complexes using noncovalent interactions (Bruce, et al., 1991; Katta & Chait, 1991). In ESI-MS experiments, by determining the charge of ions in the sample, the mass can be calculated and for protein-ligand interactions, the m/z shift of the complex compared to that expected from apo-protein provides the required information. .

5.5.2 Materials and Methods: ESI-MS

Positive-ion ESI mass spectra were generated by the instrument (LCQ Deca, ThermoFischer) to monitor the charge state distribution of proteins and of the protein-peptide complex. There were two proteins studied in the work: 14 μM MDM2RING△C and 10 μM UbcH5a. Moreover, proteins were titrated with peptide 9. For protonation of proteins, both were exchanged into experimental ESI-MS buffer (20 mM ammonium acetate, pH6.0). peptide 9 was dissolved in 50% MeOH with 50% ddH_2O (v/v) for interaction studies with MDM2RING△C. peptide 9 was dissolved in 2.5% acetic acid with 95% ddH_2O for interaction studies with UbcH5a. The protein-peptide 9 complex was incubated in an eppendorf at room temperature for 30 minutes prior to infusion. The parameters for the operation were set as below: analyte flow rate 15 μl min^{-1}; capillary voltage 3.3 kV; cone voltage 30 V; source block temperature 80℃ and desolvation gas temperature 100℃. The ESI mass spectrum plots relative abundance as a function of mass-to-charge (m/z). The mass of each charge state species was calculated using the deconvolution program.

5.5.3 Results and Discussions: ESI-MS data of MDM2 RING△C and peptide 9

- ***apo-MDM2 RING△C***

MDM2RING△C was chosen to the study the interaction with peptide 9 using ESI-MS as MDM2RING△C is single species (a dimer, as discussed in Chapter 2) and also has been shown to have high affinity to peptide 9 (Figure 5-6). As high concentrations of salts and detergents can interfere with ESI-MS analysis, after extensive trials, we finally found appropriate conditions for the ionisation of MDM2RING△C. MDM2RING△C protein was expressed and purified in media and buffers containing zinc acetate, rather than zinc sulfate, as acetate is volatile and can improve protonation during the electrospray process. Additionally, to eliminate salt effects and have high mass accuracy in the ESI-MS experiment, the protein was buffer exchange into the "experimental" buffer (20 mM ammonium acetate, pH6.0) prior to ESI-MS analysis.

The ESI-MS mass spectrum of apo-MDM2RING△C showed a discrete charge state distribution (Figure 5-7A) and the resulting ESI-spectrum illustrated that MDM2RING△C was likely to be folded as only a narrow range of charge-states are dominant in the spectrum. Protein calculator (http://www.scripps.edu /~cdputnam/protcalc.html), a program designed to predict molecular weight, the amounts of basic amino acids and pI from a protein sequence. A theoretical pI of MDM2RING△C is 6.3 (Table 5-2A). The pH value of the experimental buffer used in ESI-MS is 6.0; this means that MDM2RING△C should carry positive ions in the ESI-MS experiments (Table 5-2A). Considering MDM2RING△C has a number of basic amino acids (9 lysines, 3 arginines and 3 histidines), the measured charge distribution of the protein could have up to 15 protons attached. There were two dominant charge state species seen in the ESI-MS spectrum: "P7" ($[MDM2RING△C+7H]^{7+}$) at an m/z of 1567.6 and "P6" ($[MDM2RING△C +6H]^{6+}$) at an m/z of 1828.8 (Figure 5-7A). Here, "P" represents protein (MDM2RING△C) and "number" represents the charge state. It is evident that some basic amino acids are buried in the folded protein and therefore, these two peaks with fewer protons were observed (Patriksson et al., 2007; Lafitte et al., 1999). A more detailed analysis showed that there were secondary peaks at an m/z of 1558.7 and 1818.1 (lower intensities) immediately adjacent to the major peaks. A deconvolution software package was used to calculate masses. The mass of the two species of MDM2RING△C were 10,966 and 10,903 Daltons, respectively (Figure 5-7B, Table 5-2B). The difference in the mass (△mass = 63)

between the two species suggested that one form may be MDM2RING△C with two zinc ions (10,966 Daltons) and the other could be MDM2RING△C with one zinc ion (10,903 Daltons). The mass of one zinc molecule is 65.38 Daltons. This suggests that MDM2RING△C might lose one zinc molecule during the expression or purification process. Overall, the ESI-MS spectrum demonstrated that MDM2RING△C is a well-folded protein, suitable for ligand-binding experiments.

(A)

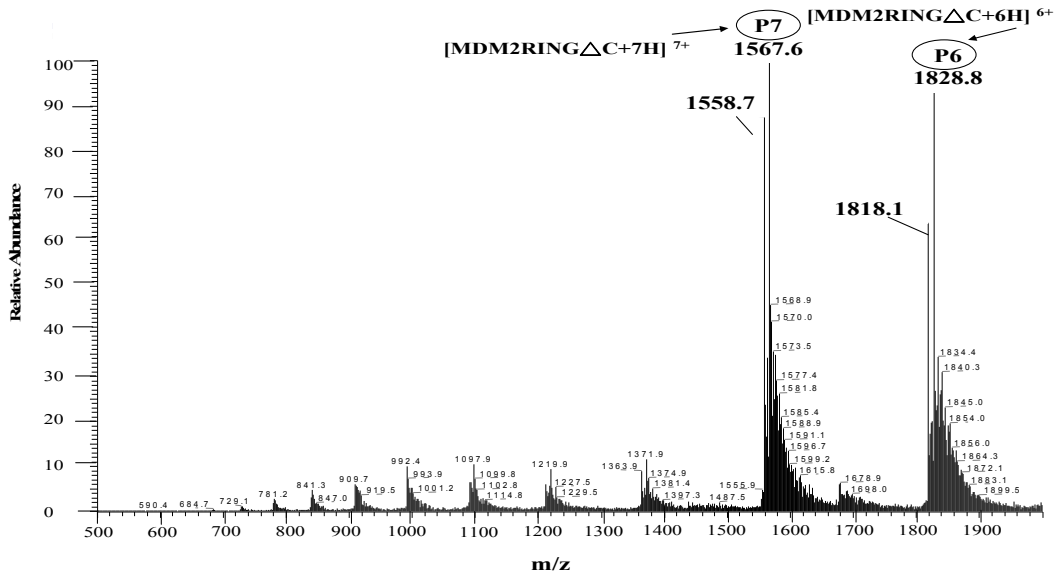

(B)

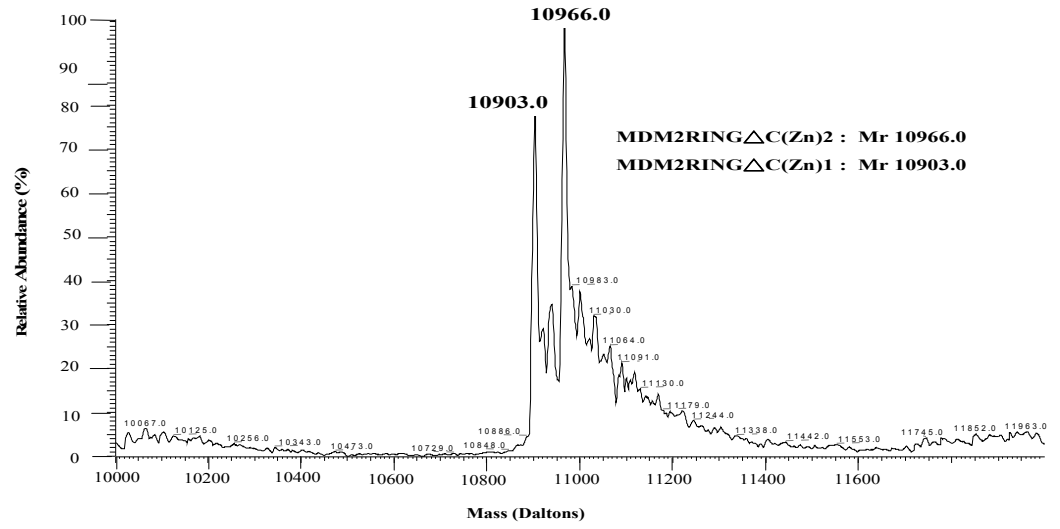

Figure 5-7: The ESI mass spectrum of MDM2RING△C (14 µM in 20 mM ammonium acetate). (A) The original ESI-MS spectrum shows there are two major charge state species: P7 and P6 with 7 and 6 protons attached, respectively. (B) The mass-converted deconvolution

spectrum of MDM2RING△C. Two major species are detected: MDM2RING△$C(Zn)_2$ and MDM2RING△$C(Zn)_1$. Data was obtained on an LCQDeca (ThermoFischer instrument). The source temperature was 80℃.

Table 5-2: The theoretical and experimental mass and charge state of MDM2RING△C. (A) The theoretical pI and the numbers of basic amino acids in MDM2RING△C. (B) After the deconvolution process, the average of the experimentally derived mass is less than 1% different from the theoretical mass. (C) The mass is calculated from the higher charge part of the ESI-mass spectrum of MDM2RING△C with two strong maxima of around seven and six attached protons.

(A)

MDM2RING△C
**estimated pI = 6.3*
**basic amino acids:*
lysine (9); arginine (3), histidine (3)

(B)

*after deconvolution	mass (experimental)
MDM2RING△C-(Zn)2	10966
MDM2RING△C-(Zn)1	10903
	mass (theoretical)
MDM2RING△C-(Zn)2	10979.8
accuracy (experimental mass/ theoretical mass)	99.9%

(C)

Peaks	charge ions	m/z	mass	estimated composition
P7	7+	1567.6	10966.2	MDM2RING△C-(Zn)2
	7+	1558.7	10903.9	MDM2RING△C-(Zn)1
P6	6+	1828.8	10966.8	MDM2RING△C-(Zn)2
	6+	1818.1	10902.6	MDM2RING△C-(Zn)1

- ***Expected m/z value of MDM2 RING△C-peptide 9***

To evaluate the binding affinity and the stoichiometry of peptide 9 with MDM2RING△C, we carried out titration experiments using ESI-MS. In this experiment, peptide 9 was dissolved in 10% MeOH, because DMSO has deleterious effects upon ESI-MS. In the experiments, 14 μM MDM2RING△C in solution (buffer with 10% MeOH) was used and peptide 9 was titrated into MDM2RING△C, using several protein: ligand (P:L) ratios, such as 1:2, 1:4, 1:8, and 1:10, followed by incubating at room temperature for 30 minutes prior to ESI-MS analysis. If peptide 9 bound to MDM2RING△C, an m/z shift should be observed. The calculated molecular weight of the complex (PL) was 12379.3 Daltons (10979.8+1399.5 = 12379.3). The mass of peptide 9 used in the work was 1399.5 Daltons. Therefore, peaks at m/z of 1768.5 and 2063.2 for $[PL+7H]^{7+}$ and $[PL+6H]^{6+}$ (Table 5-3) might be expected.

Table 5-3: The theoretical peaks expected in the m/z axis of the ESI-MS spectrum of MDM2RING△C-peptide 9.

	mass (Daltons)
peptide (L)	1399.5
MDM2RING△ (P)	10979.8
P+L	12379.3
charge state species (in theory)	**expected peak at m/z**
[PL+7H]7+	(12379.3+7) / 7 = 1769.5
[PL+6H]6+	(12379.3+6) / 6 = 2064.2

- ***peptide 9 was detected using ESI-MS***

Representative plots of the ion intensities of peptide 9 as a function of the m/z value with different ratios of protein to peptide (P:L) clearly revealed that peptide 9 was saturated at a ratio of 1:8 or 1: 10. As Figure 5-8 shows, the predominant peaks representing peptide 9 in this spectrum were seen in with a protein: peptide ratio of 1: 10. There were two dominant peaks at m/z values of 700.7 and 1399.5, that represented the species "L2" ([peptide 9 +2H]$^{2+}$) and "L1" ([peptide 9+1H]$^{1+}$), respectively. Here, "L" represents peptide 9 and "number" represents the charge state. After deconvolution, the mass of peptide 9 was 1399.4 and 1398.5 Daltons, respectively.

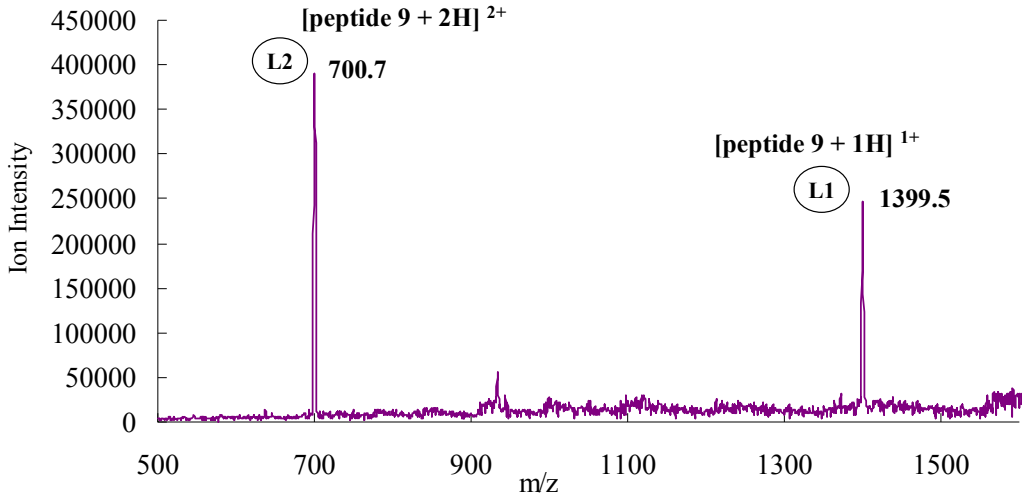

Peaks	m/z	charge state [H+]	thoretical mass (Daltons)	experimental mass (Daltons)	Accuracy (%)
L2	700.7	2	1399.5	1399.4	100.0%
L1	1399.5	1	1399.5	1398.5	99.9%

Figure 5-8: ESI-MS data of peptide 9 detected at different titration points. (A) There are two dominant species in a solution: "L2" ([peptide 9 + 2H]$^{2+}$) and "L1" ([peptide 9 + 1H]$^{1+}$) at the m/z value of 700.7 and 1399.5.

- ***apo-MDM2RING△C in ESI-MS buffer (20 mM ammonium acetate with (10% MeOH)***

In this work, peptide 9 was largely insoluble in ddH_2O, therefore, 10%MeOH was added to dissolve peptide 9. Following mixing of peptide 9 (dissolved in 90% water and 10% MeOH (v/v)) with MDM2RING △ C, the pH of the sample was monitored throughout the experiment, and was shown to be between pH5.5~ 6.0. ESI-MS titration experiments were carried out in a buffer in which MDM2RING△C is stable and monodisperse. Under these buffer conditions, MDM2RING△C and peptide 9 carry positive ions. The spectra of the titration experiments showed there were distinct charge state species in solution (Figure 5-9 & 5-10, Table 5-4). The data from the experiment (protein only) showed that there were two major peaks with m/z values of 1591.1 ("P7", $[MDM2RING△C +7H]^{7+}$) and 1854.1 ("P6", $[MDM2RING △ C+6H]^{6+}$), with calculated masses of 11,137.7 and 11,118.0 Daltons, respectively (Figure 5-9). The accuracy associated with the theoretical mass of the apo-protein was approximately 98.6% and 98.8 %, respectively. In ESI-MS experiments, it has been shown that identical samples in different sample buffers can generate different spectra, due to interactions with different adducts as a result of ionisation with different charge-states.

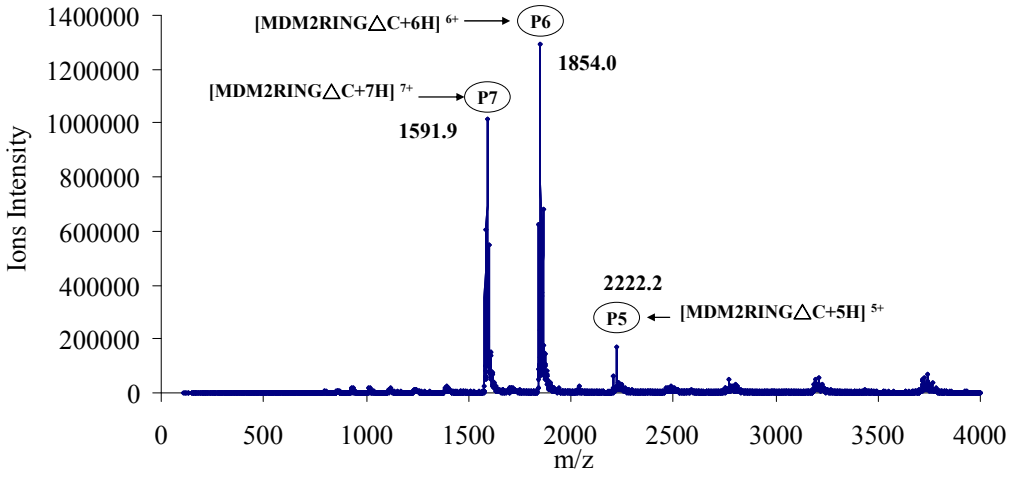

ratio (P:L)	peaks	m/z	charge state [H+]	theoretical mass (Daltons)	experimental mass (Daltons)	Accuracy (%)	Oligomeric state
apo-protein	P7	1591.1	7	10979.8	11130.7	98.6%	monomer
	P6	1854.0	6	10979.8	11118.0	98.8%	monomer
	P5	2222.2	5	10979.8	11106.0	98.9%	monomer

Figure 5-9: ESI-MS spectrum of apo-MDM2RING△C (in 20 mM ammonium acetate with 5% MeOH). There are two major charge state species with m/z value of 1591.1 (with 7 protons) and 1854.0 (with 6 protons). The experimental mass is shown in the table. Major charge state species are labelled as P7, P6, and P5.

- ***New peaks observed in the spectrum of MDM2RING△C in the presence of peptide 9***

In the presence of peptide 9, new peaks are observed in the spectra (PPL8, PPL7 and PPL6) and the relative abundance of original peaks representing apo-MDM2RING△C (P7, P6 and P5) reduced (Figure 5-10). With high concentrations of peptide 9 in solution (P:L =1:8), L1 and L2, representing peptide 9, became more dominant because peptide 9 is readily ionised with positive charge.

On the basis of the ESI-MS data, the experimental mass of P7, P6, and P5 (ratios of 1:2, 1:4, and 1:8) was approximately 11062 ~112459 Daltons, demonstrating that these species existed as an apo-monomer (Table 5-4B). In theory, if peptide 9 did not interact with MDM2RING△C, the P3 (at an m/z pf 3197.0) and P2 (at an m/z of 3741.2) species (Figure 5-11) detected in the sample (P:L =1:8) would correspond to the charge state with three protons ($[MDM2RING△C +3H]^{3+}$) and two protons ($[MDM2RING△C +2H]^{2+}$), with a calculated mass for P3 and P2 of 9588.0 and 7480.4 Daltons, respectively, with an accuracy of 87.7% and 68.1% compared to the theoretical mass of monomeric MDM2RING△C (Table 5-4B). Because the level of accuracy was very low, this suggests that the P3 and P2 species are not monomeric MDM2RING△C.

After a manual calculation, the data (Table 5-4C) showed the charged states of those new species are PPL8 (at an m/z of 2864.6), PPL7 (at an m/z of 3209.3) and PPL6 (at an m/z of 3741.2) being likely +8, +7 and +6, respectively, with an experimental mass range of about 22323 ~ 22919 Daltons (Table 5-4C). According to the mass of these species, the PPL8, PPL7 and PPL6 species were likely the 2MDM2RING△C-peptide 9 complex (2P + L) (theoretical mass: 23359.1 Daltons). The experimental mass of each species compared to the theoretical mass of each species was at least 96% accurate (Table 5-4C). For example, the data obtained from the (P:L=1:8) sample showed the experimental mass of the predominant PPL8 in the charge state of 8 protons was approximately 22908.8 Daltons, with an accuracy of 98.1% (Figure 5-10 & Table 5-4C).

Consistent with our fluorescence anisotropy experiments, these data provided evidence that peptide 9 interacts with MDM2RING△C. Our initial assumption is that peptide 9 binds to the C8-binding interface interface of MDM2RING△C at ratio of 1:1; however, the

MDM2RING△C-peptide 9 (P+L) complex was not detected. Instead, in the presence of peptide 9, MDM2RING△C is predominately dimeric, forming the 2MDM2RING△C – peptide 9 complex (PPL). Presumably, peptide 9 interacts with the C8-binding interface of each MDM2RING△C. The data suggest that, under the conditions of the mass spectrometry experiment, peptide 9 interacts with a ring dimer and appears not to disrupt the protein-protein interface.

Figure 5-10: ESI-MS spectra of MDM2RING△C with peptide 9. The ESI- MS spectra show that relative abundance against the m/z function, and four samples are tested: apo-protein, P:2L (1:2), P:4L (1:4), and P:8L (1:8). After peptide 9 is incubated with MDM2 RING△C, three charge species appear: PPL8, PPL7 and PPL6. In the spectrum generated with a ratio (1:8), the m/z value of each species is shown and the possible composition in each species is presented: protein (green sphere) and peptide 9 (yellow arrows).

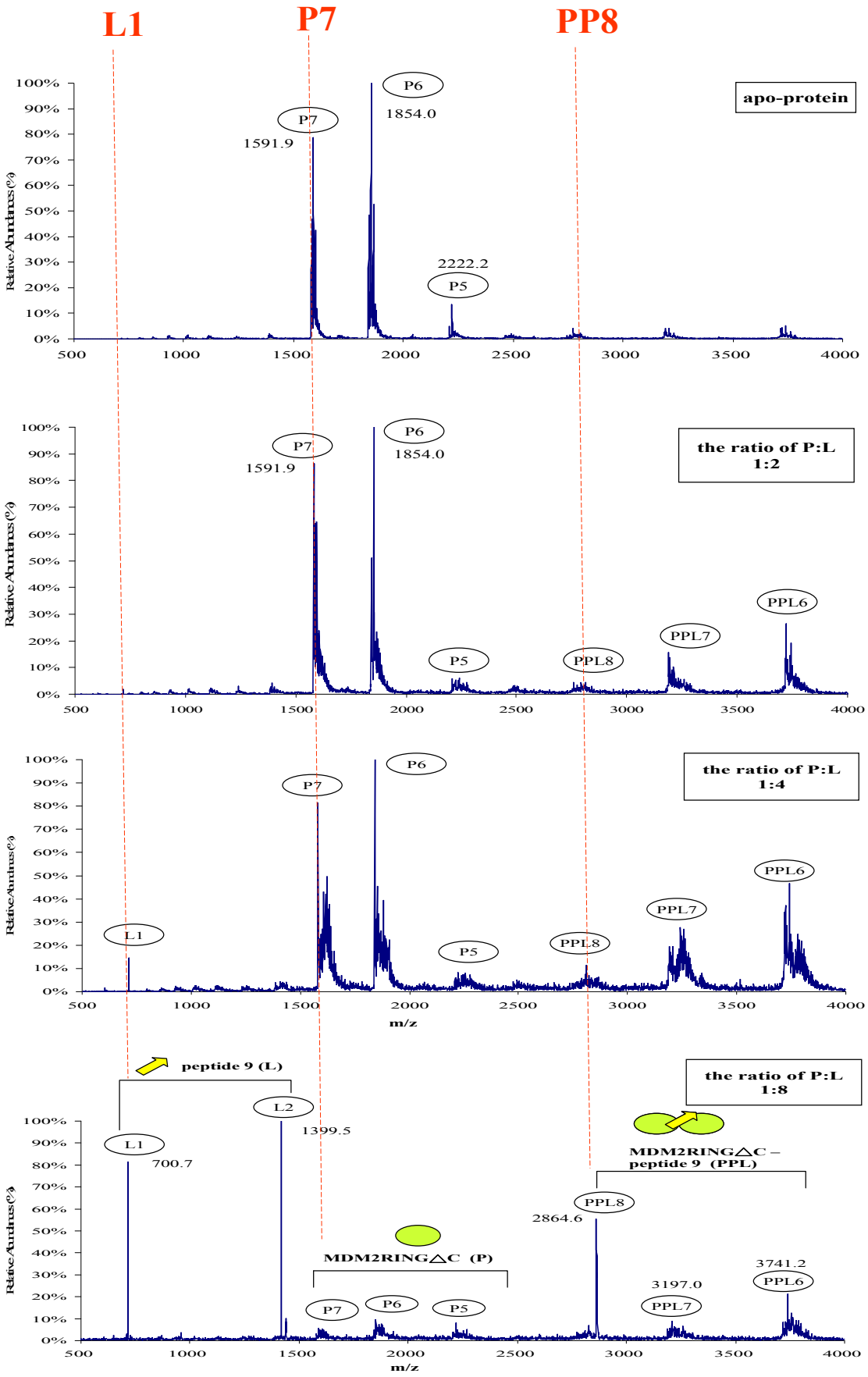
L1
P7
PP8
apo-protein
P6
1854.0
P7
1591.9
2222.2
P5
the ratio of P:L
1:2
PPL6
PPL7
PPL8
the ratio of P:L
1:4
L1
the ratio of P:L
1:8
peptide 9 (L)
L2
1399.5
700.7
MDM2RING△C –
peptide 9 (PPL)
2864.6
MDM2RING△C (P)
3741.2
3197.0
Relative Abundance(%)
m/z

Table 5-4: Estimated charge-states and molecular weights of MDM2RING△C monitored by the ESI-MS.

(A)

oligomeric state	mass (Da)
P: MDM2RING△C	10979.8
L: peptide 9	1399.5
P+L	12379.3
2(PL)	24758.6
2P+L	23359.1

(B)

ratio (P:L)	peaks	m/z	charge state [H+]	theoretical mass (Daltons)	experimental mass (Daltons)	Accuracy (%)
apo-protein	P7	1591.1	7	10979.8	11130.7	98.6%
	P6	1854.0	6	10979.8	11118.0	98.8%
	P5	2222.3	5	10979.8	11106.5	98.9%
1:2	P7	1581.5	7	10979.8	11063.5	99.2%
	P6	1853.7	6	10979.8	11116.2	98.8%
	P5	2239.4	5	10979.8	11192.0	98.1%
	P4	2861.1	4	10979.8	11440.4	96.0%
	P3	3190.0	3	10979.8	9567.0	87.1%
	P2	3743.2	2	10979.8	7484.4	68.2%
1:4	P7	1581.4	7	10979.8	11062.8	99.2%
	P6	1842.7	6	10979.8	11050.2	99.4%
	P5	2222.3	5	10979.8	11106.5	98.9%
	P4	2865.9	4	10979.8	11459.6	95.8%
	P3	3191.1	3	10979.8	9570.3	87.2%
	P2	3739.7	2	10979.8	7477.4	68.1%
1:8	P7	1581.4	7	10979.8	11062.8	99.2%
	P6	1853.1	6	10979.8	11112.6	98.8%
	P5	2222.3	5	10979.8	11106.5	98.9%
	P4	2864.6	4	10979.8	11454.4	95.9%
	P3	3197.0	3	10979.8	9588.0	87.3%
	P2	3741.2	2	10979.8	7480.4	68.1%

(C)

ratio (P:L)	peaks	m/z	charge state [H+]	theoretical mass (Daltons)	experimental mass (Daltons)	Accuracy (%)
1:2	PPL8	2861.1	8	23359.1	22880.8	98.0%
	PPL7	3190.0	7	23359.1	22323.0	95.6%
	PPL6	3743.2	6	23359.1	22453.2	96.1%
1:4	PPL8	2865.9	8	23359.1	22919.2	98.1%
	PPL7	3191.1	7	23359.1	22330.7	95.6%
	PPL6	3739.7	6	23359.1	22432.2	96.0%
1:8	PPL8	2864.6	8	23359.1	22908.8	98.1%
	PPL7	3197.0	7	23359.1	22372.0	95.8%
	PPL6	3741.2	6	23359.1	22441.2	96.1%

5.6 Does peptide 9 also bind to E2 protein, UbcH5a?

The importance of the MDM2-C terminus for MDM2 E3 ligase activity has been confirmed by mutagenesis, deletion, and biochemical studies (Kawai et al., 2007; Linke et al., 2008; Uldrijan 2007). They suggest that the MDM2 C-terminus is responsible for the dimerisation that is a determinant for MDM2 E3 ligase activity. Moreover, there is one report showing that MDM2-MDMX△C7 is E3 active and MDMX-MDM2△C7 does not have E3 activity (Uldrijan et al., 2007). This result suggests that MDMX C-terminus rescues the function of MDM2 C-terminus. Other reports mention that MDM2 C-terminus may be involved in the interaction with its cognate E2 protein (Poyurovsky et al., 2007). We assumed that MDMX C-terminus should have the same interactions as MDM2 C-terminus and presumably also interact with MDM2 cognate E2 proteins.

5.6.1 Thermal denaturation assay: the interaction of UbcHa5a and peptide 9

In this work, to verify the assumption that peptide 9 might interact with MDM2 cognate E2, peptide 9 (an MDMX C-terminal 12 residues) was used to study the interaction with one of MDM2 cognate E2 partners, UbcH5a. Firstly, to examine if peptide 9 binds to UbcH5a and affects the thermal stability of UbcH5a, we used the thermal denaturation assay to characterise the thermal unfolding transition peak of UbcH5a. The theoretical basis of thermal denaturation assay was described in detail in Chapter 3. The technique can be used to detect the midpoint temperature (Tm) of a thermal unfolding transition peak which is an indicator of the thermal stability. The fluorescence emission (RFU) of 2.5 μM apo-UbcH5a started to increase at 52℃, reaching a maximum at 62℃ (blue line, Figure 5-11), while the fluorescence emission of the solution containing 2.5 μM apo-UbcH5a with 25 μM peptide 9 increased from 41℃ to a maximum of 59℃ (red line, Figure 5-11). The fluorescence intensity of the complex was higher than that of apo-UbcH5a. To exclude the possibility that the higher fluorescence intensity might be generated by peptide 9, we also monitored the thermal unfolding transition peak of peptide 9 alone (25 μM) (orange line, Figure 5-11). The data showed that peptide 9 itself did not affect the background in the experiment. The increased fluorescence intensities detected in the presence of 2.5 μM apo-UbcH5a with 25 μM peptide 9 suggested that peptide 9 might induce conformational changes in UbcH5a, exposing interior hydrophobic residues, detectable by an increased signal from the SYPRO Orange dye. Plotting the gradient of fluorescence intensities as a function of temperature revealed that the Tm of the thermal unfolding transition of UbcH5a was 58℃, the Tm of the

UbcH5a-peptide 9 complex dropped to 54℃ (Figure 5-11). Taken together, this significant reduction in the Tm of the complex and the increased fluorescence intensities detected in the presence of 2.5 µM apo-UbcH5a with 25 µM peptide 9 suggested that peptide 9 might destabilise UbcH5a exposing more hydrophobic residues to the environment.

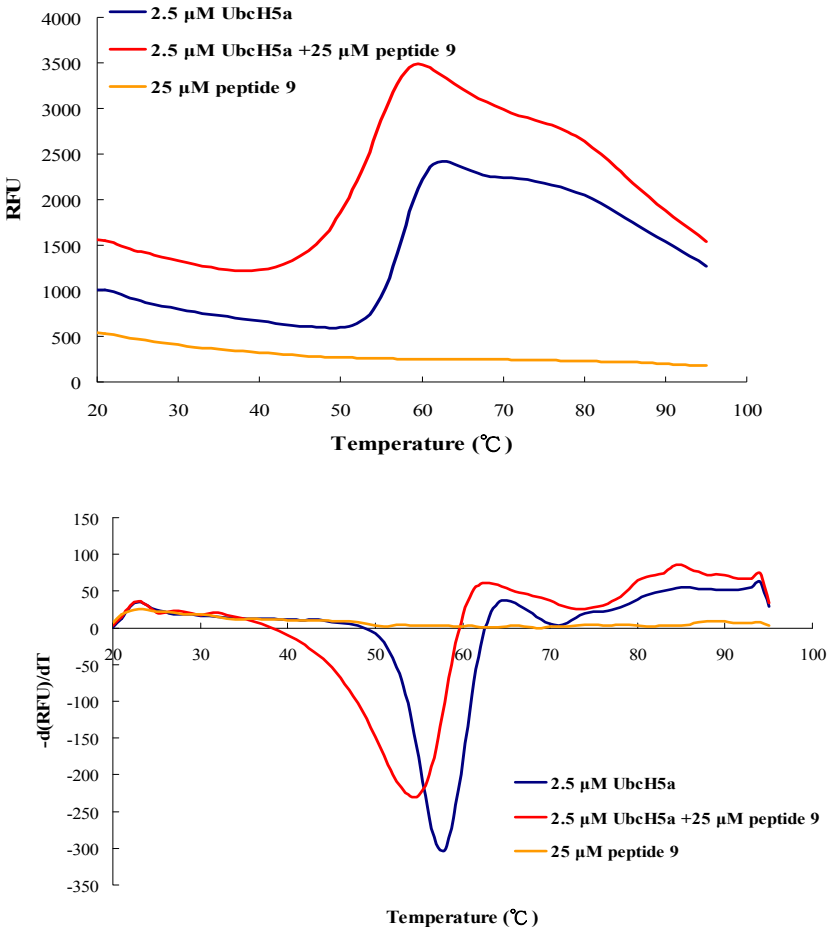

	Melting temperature
2.5 µM UbcH5a	58℃
2.5 µM UbcH5a +25 µM peptide 9	54℃
25 µM peptide 9	N.D.

Figure 5-11: Thermal stability of UbcH5a, the UbcH5a-peptide 9 complex and peptide 9. The melting point (Tm) of the thermal unfolding transition of each sample is monitored over the range of 20℃ to 95℃ by TDA, using SYPRO Orange fluorescence dye. The unfolding transition curve of apo-UbcH5a, UbcH5a-peptide 9, and peptide 9 are coloured in blue, red, and orange, respectively.

5.6.2 Fluorescence anisotropy studies: the interaction of UbcHa5a with peptide 9

To evaluate the binding affinities of peptide 9 to UbcH5a, we utilised the fluorescence anisotropy technique. In this work, UbcH5a was titrated into two derivates of fluorescein (FITC) labeled peptides, FITC- N'-peptide 9, and FITC-C'-peptide 9, the FITC moiety being attached onto the N-terminus and C-terminus of peptide 9, respectively. FITC-truncated peptide, lacking of the last two amino acids compared to peptide 9, was used a negative control. Different concentrations of UbcH5a were incubated with 250 nM peptides for 60 minutes; changes in fluorescence anisotropy were measured. The data showed that both FITC-labeled peptide 9 molecules interacted with UbcH5a because both fluorescence anisotropy curves ascended according to the plot of the gradient of anisotropy as a function of concentrations of UbcH5a (Figure 5-12). The calculated Kd of UbcH5a to FITC-N'peptide 9 and FITC-C' peptide 9 were 101.4 ±70.7 nM and 143.1 ± 60.0 nM, respectively. The result showed that UbcH5a has similar binding affinities with these two peptides. Changes in the fluorescence anisotropy curve were observed; demonstrating that peptide 9 interacted with UbcH5a. As expected, a negative control, FITC-truncated peptide 9 did not bind to UbcH5a.

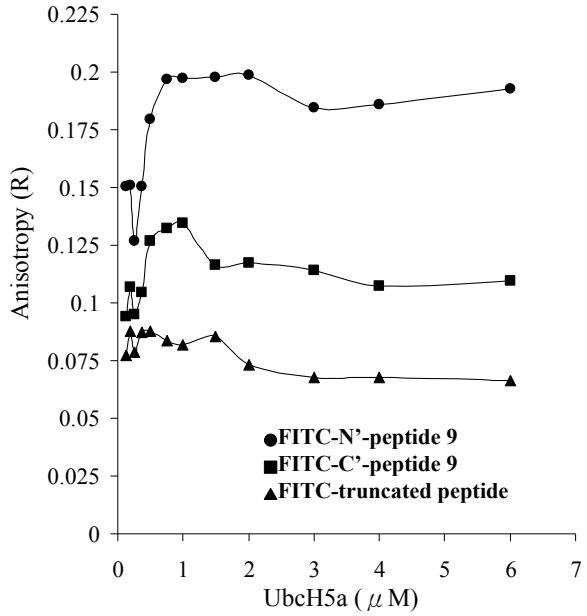

UbcH5a with	Kd (nM)
FITC-N'-peptide 9	101.4 ±70.7
FITC-C'-peptide 9	143.1 ± 60.0
FITC-truncated peptide	N.D.

Figure 5-12: Fluorescence anisotropy binding studies. UbcH5a titrated into different fluorescein (FITC)-labelled peptides (250 nM): FITC-N'-peptide 9 (●), FITC-C'- peptide 9 (■), and FITC-mutant peptide (▲). N.D.: not determined.

5.6.3 ESI-MS study: the interaction of UbcHa5a and peptide 9

- ***ESI-MS spectrum of apo-UbcH5a***

To confirm the interaction between UbcH5a and peptide 9, we used ESI-MS to monitor peak distributions in the spectra of both UbcH5a and the UbcH5a-peptide 9 complex. The mass spectrum of apo-UbcH5a showed a classical bell-shaped charge state distribution (Figure 5-13). The dominant peak was P9 ($[UbcH5a+9H]^{9+}$)at m/z of 2071.1. There were other peaks present representing, species with different charge states. Based on the amino acid sequence of UbcH5a, the Protein Calculator 3.3 program calculated a mass of 18896.5 Daltons, with an estimated pI value of 7.94, with 28 basic amino acids including 10 lysines, 6 arginines and 12 histidines (Table 5-5). Moreover, apo-UbcH5a was stored in a solution of 20 mM ammonium acetate, pH6.0, showing that apo-UbcH5a was positively charged under these conditions. The ESI-MS spectrum of apo-UbcH5a showed the dominant species in solution carried 9 protons (at m/z=2071.1) which has the experimental mass was 18630.9 Daltons with an accuracy of 98.1 %. (theoretical mass: 18896.5 Daltons) (Figure 5-13), in broad agreement with the calculated charge. Moreover, if UbcH5a was unfolded, more positive charges would be seen due to the presence of the 22 basic amino acids of UbcH5a. Therefore, the ESI-MS data demonstrated that under this buffer condition UbcH5a is folded.

Table 5-5: Theoretical and experimental mass and charge states of UbcH5a. (A) The theoretical pI and the numbers of basic amino acids in UbcH5a. (B) Experimental mass and charge state of apo-UbcH5a was obtained by ESI-MS.

UbcH5a
*theoretical mass = *18896.5 Daltons*
**estimated pI = 7.9*
**basic amino acids (28):*
lysine (10); arginine (6), histidine (12)

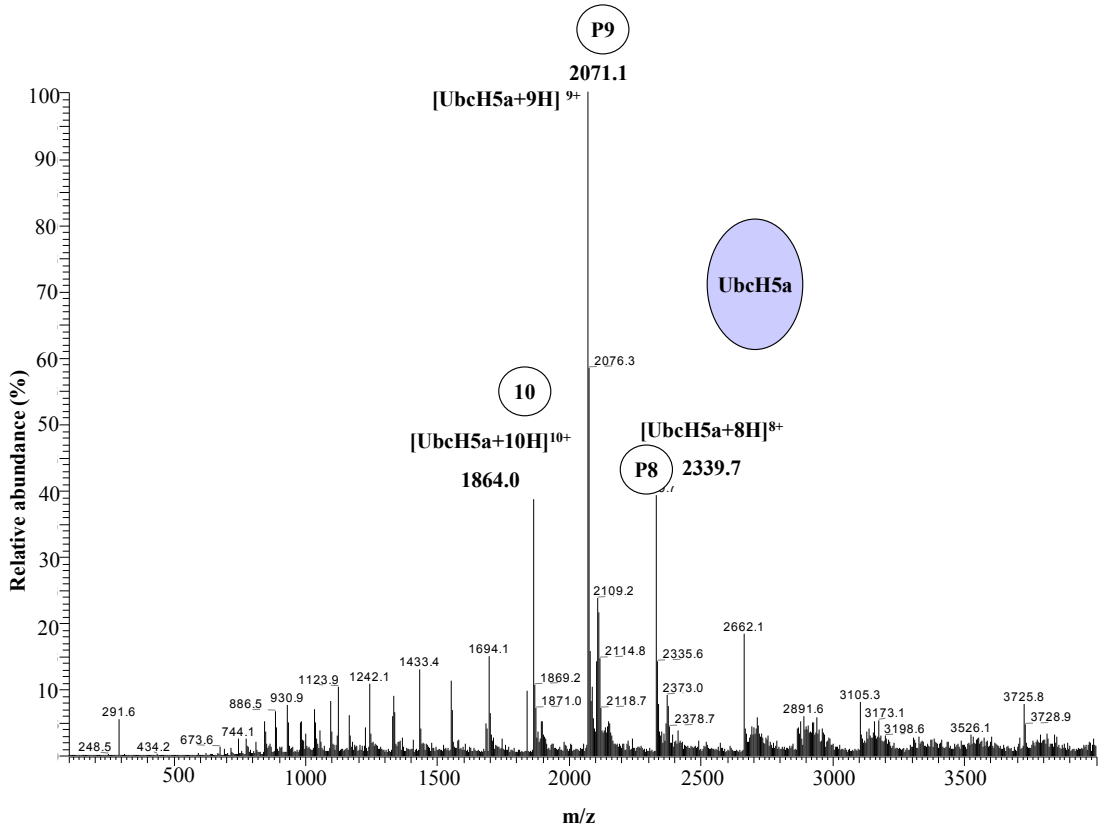

peak	m/z	charge state [H+]	theoretical mass (Daltons)	experimental mass (Daltons)	accuracy (%)	species
P10	1863.4	10	18996.5	18624.0	98.0%	monomer
P9	2071.1	9	18996.5	18630.9	98.1%	monomer
P8	2333.1	8	18996.5	18656.8	98.2%	monomer

Figure 5-13: ESI-MS spectrum of apo-UbcH5a. A characteristic bell-shaped charge state distribution is observed. The dominant peak (P9) at an m/z value of 2071.1 represents $[UbcH5a+9H]^{9+}$. Data are collected on LCQDeca (Thermo Fisher Instrument). Samples are tested at pH6.0 (20mM ammonium acetate) with a source temperature of 80℃. Experimental mass of three species, P8, P9 and P10, were showed in the table, all with an accuracy of at least 98% (compared to the theoretical mass).

- ***ESI-MS spectrum of the UbcH5a in the presence of -peptide 9***

Following addition of 200 μM peptide 9 into a solution of 20 μM UbcH5a, numerous new peaks were detected (Figure 5-14A). The significant differences seen in the data in the presence of peptide 9 might be due to the pH effect. As a consequence of reduced solubility of the UbcH5a-peptide 9 complex when compared to that of the peptide 9-MDM2RING2△C complex (solubilised in 90% 20 mM ammonium acetate + 10% MeOH, pH6.0), the UbcH5a-peptide 9 complex was soluble under more acidic condition (pH4.5). Acidic solutions certainly increase the protonisation of proteins, providing an explanation for the new charge state species which appeared at pH4.5. In agreement with the prediction, Figure 5-14A showed species with a charge state of 20 protons at an m/z of 931.8, with an experimental mass of 18616.0.

- ***pH effect on the oligomeric state of UbcH5a***

A pH effect on the oligomeric state of UbcH5a required consideration that the peaks seen were as a result of the effect of solution pH. Some proteins exist in different forms at different pH (Cheng et al., 1996), and it could be supposed that the peaks newly seen represented the dimeric UbcH5a, charge states. The experimental masses are shown in the Figure 5-14, suggesting that UbccH5a could dimerised under low pH concentration, irrespective of any interaction with peptide 9. If peptide 9 did not interact with UbcH5a, there should be peaks (at an m/z of 716 or 1399.5) representing peptide 9 as illustrated in Figure 5-8. However, there are no significant peaks at these points, demonstrating that peptide 9 interacted with UbcH5a and the new peaks were the UbcH5a-peptide 9 complex, rather than dimeric protein. Furthermore, apo-UIbcH5a in two pH buffers was analysed by DLS. The hydrodynamic diameter of UbcH5a measured under both conditions was 4.6 nm. The hydrodynamic diameter of UbcH5a calculated from a crystal structure of human UbcH5a (PDB: 2C4P) is 4.8 nm for a monomer (Figure 5-16B). These results confirmed that UbcH5a existed as a monomer in the initial ESI-MS buffer solution (pH6.0) and acidic solution (pH4.5). Those data suggest that new species are not dimeric UbcH5a; those represent the newly formation of UbcH5a-peptide 9 complex (detailed in the following text).

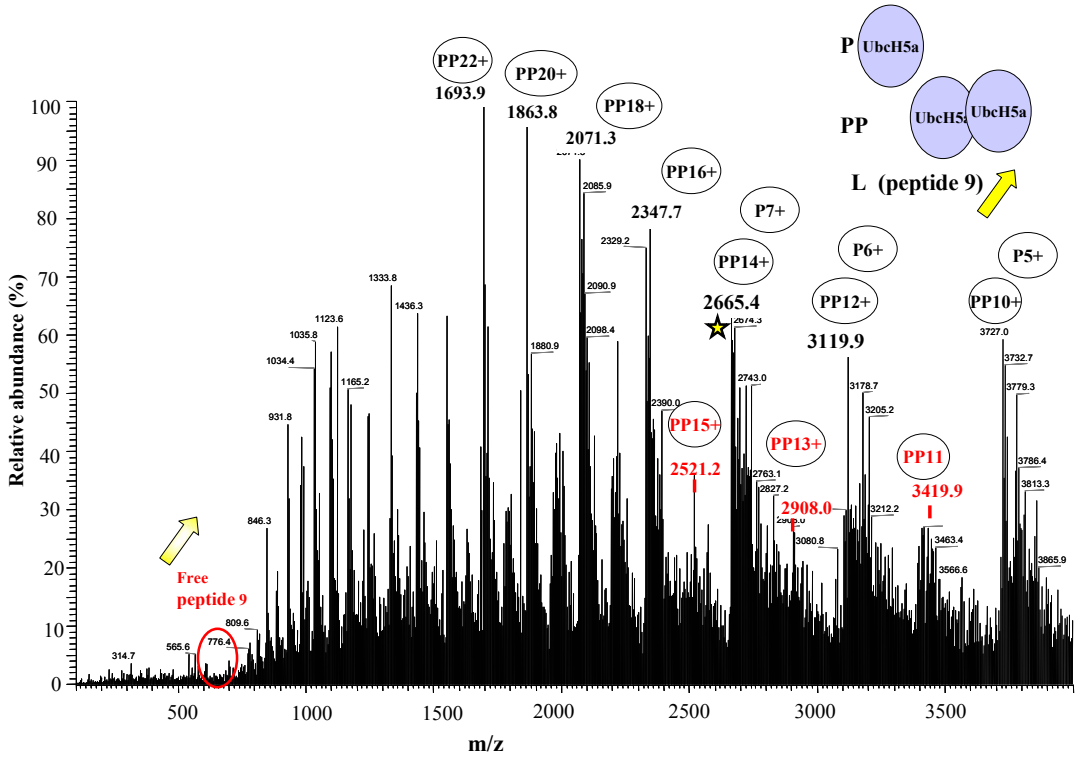

peaks	m/z	charge state [H+]	theoretical mass (Daltons)	experimental mass (Daltons)	accuracy (%)	species
P20	931.8	20	18896.0	18616.0	98.5%	monomer (P)
PP16	2347.7	16	37792	37547.2	99.4%	PP
P8	2347.7	8	18896	18773.6	99.4%	P
PP15	2521.2	15	37792	37803.0	100.0%	PP
PP14	2665.4	14	37792	37301.6	98.7%	PP
P7	2665.4	7	18896	18650.8	98.7%	P
PP13	2908.0	13	37792	37791.0	100.0%	PP
PP12	3119.9	12	37792	37426.8	99.0%	PP
P6	3119.9	6	18896	18713.4	99.0%	P
PP11	3419.9	11	37792	37607.9	99.5%	PP
PP10	3722.0	10	37792	37210.0	98.5%	PP
PP5	3722.0	5	18896	18605.0	98.5%	P

Figure 5-14: ESI-MS data of UbcH5a in the presence of peptide 9. Experimental mass showed that new peaks could be dimeric UbcH5a. However, no free peptide 9 was detected at m/z of 716 (red, circle). Therefore, those newly formation of peaks should represent other species in solution (seen Figure 5-15). "PP" represents dimeric species.

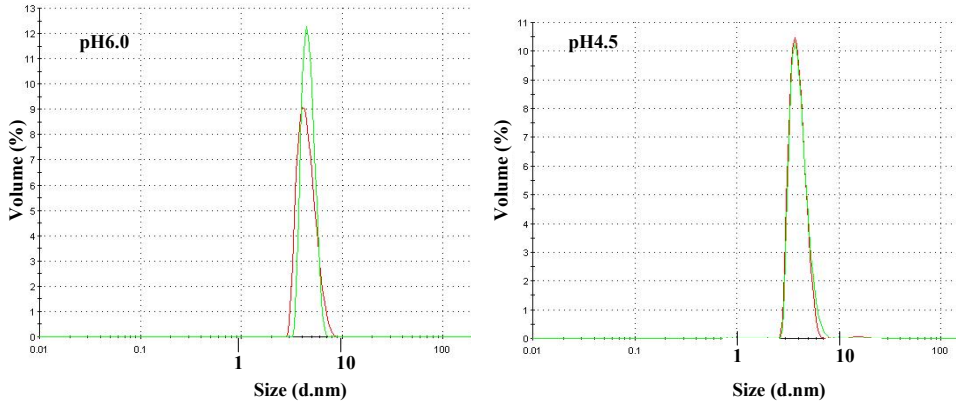

Methods		Hydrodynamic Diameter (nm)
DLS	pH6.0	4.6
	pH4.5	4.6
PDB (2C4P)	Monomer	4.8

Figure 5-15: The oligomeric states of UbcH5a in pH 6.0 and pH6 4.5 were measured by the dynamic light scattering (DLS). The hydrodynamic diameters of UbcH5a in both buffers were 4.6 nm, consistent with that observed in the crystal structure (PDB: 2C4P).

- ***ESI-MS spectrum of the UbcH5a-peptide 9 complex***

After superimposing these two spectra (Figure 5-16A), the relative abundance of the major peaks in the spectrum of apo-UbcH5a (green lines) diminished, and more new peaks (black lines) appeared. In particular, some new peaks were seen between two "original" peaks. For example, there was new peak at an m/z of 2521.2 between the original peaks at the m/z of 2347.4 and 2665.4. Following deconvolution, this peak (PL8) has an m/z of 2521.2 corresponding to a charge state of 8 protons, with a mass of 20161.6 Daltons, closer to the theoretical mass of the UbcH5a-peptide 9 complex, 20295.5 Daltons, with an accuracy of 99.3% (Table 5-6) The experimental mass of each of the other new peaks with different charge states were also closer to the theoretical mass, demonstrating that peptide 9 interacts with UbcH5a, forming a complex.

(A)

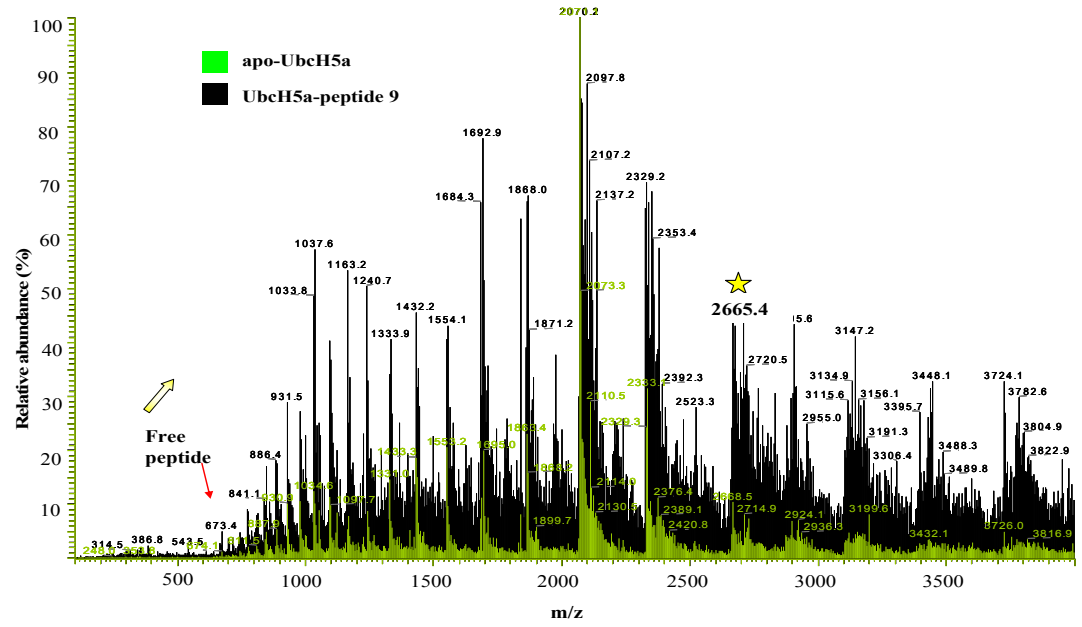

(B)

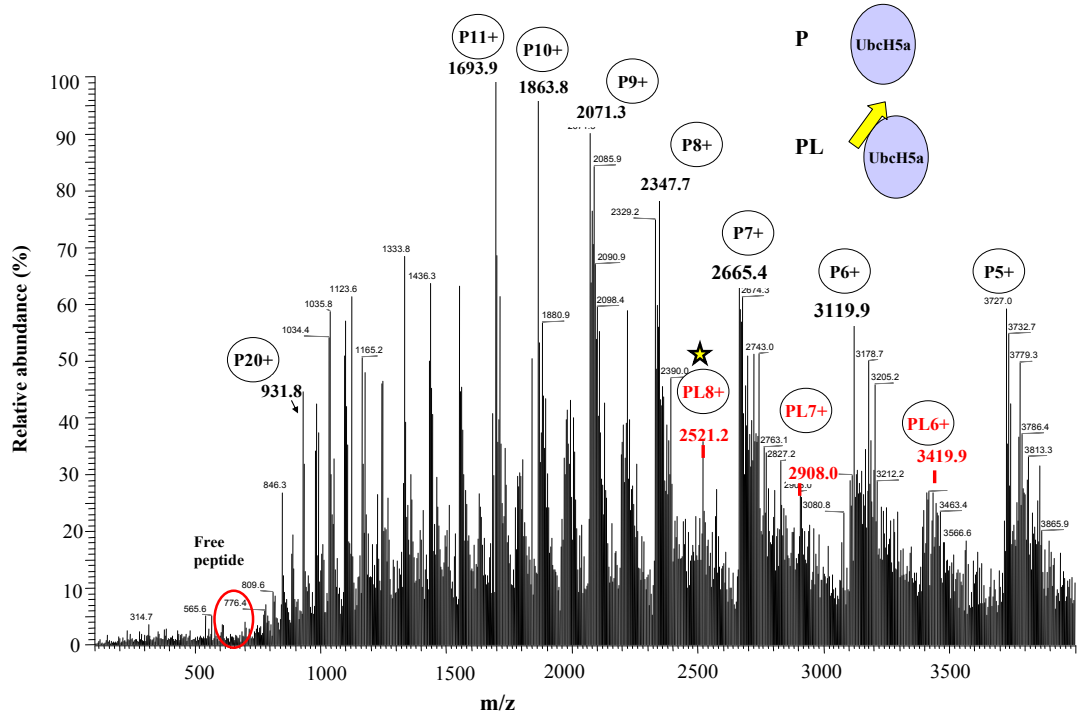

Figure 5-16: Positive ion ESI mass spectrum of apo-UbcH5a and the complex of UbcH5a-peptide 9. (A) Comparison of the spectra of apo-UbcH5a (green line) and the UbcH5a complexed with peptide 9 (black lines). (B) The UbcH5a-peptide 9 complex ESI mass spectrum reveals that there are monomers and the UbcH5a-peptide 9 complex in the sample. The graph shows the different charge state distributions between the two ESI mass spectra. Species (PL8) at 2521.2 m/z are discussed in the text (yellow star).

Table 5-6: Predictions the masses, the charge state species, and the oligomeric states of the samples: apo-UbcH5a, the UbcH5a-peptide 9 complex.

peaks	m/z	charge state [H+]	theoretical mass (Daltons)	experimental mass (Daltons)	accuracy (%)	species
P20	931.8	20	18896.5	18616.0	98.5%	monomer (P)
P8	2347.7	8	18896.5	18773.6	99.3%	monomer (P)
PL8	2521.2	8	20295.5	20161.6	99.3%	PL
P7	2665.4	7	18896.5	18650.8	98.7%	monomer (P)
PL7	2908.0	7	20295.5	20349.0	99.7%	PL
P6	3119.9	6	18896.5	18713.4	99.0%	monomer (P)
PL6	3419.9	6	20295.5	20513.4	98.9%	PL
P5	3722.0	5	18896.5	18605.0	98.5%	monomer (P)

5.6.4 HSQC NMR study: the interaction of UbcHa5a and peptide 9

- ***^{1}H, ^{15}N- HSQC NMR spectra of UbcH5a titrated with peptide 9***

To identify the residues in UbcH5a interacting with peptide 9, we carried out preliminary experiments using ^{1}H,^{15}N-HSQC NMR. However, the results revealed that no detectable chemical shifts in the ^{1}H,^{15}N-HSQC NMR spectra. Instead, overall signal intensities of cross-peaks decrease (Figure 5-17). Besides, the sample aggregated easily upon titration with high concentration of peptide 9. NMR experiments require higher concentration of proteins and in this case 25 μM was used. Aggregation may result from the equilibrium between high concentrations of proteins and peptides. Additionally, the TDA data also revealed that peptide 9 may destabilise UbcH5a, this might explain the aggregation phenomena observed during the NMR experiments. Therefore, under the given experimental conditions, ^{1}H, ^{15}N-HSQC NMR was not useful in attempts to identify residues in ^{15}N-UbcH5a responsible for peptide 9-binding.

- ***peptide 9 disrupts the UbcH5a-MDM2RING△C interaction***

^{1}H,^{15}N-HSQC NMR experiments can be used to monitor antagonist-mediated dissociation of a protein-protein interaction (D'Silva et al., 2005). In general, the protein-protein complex (>40 kDa) produces a poorly dispersed NMR spectrum as the large complex generates broad NMR resonances, resulting in the disappearance of cross-peaks (Pellecchia et al., 2002; Rehm et al., 2002; Riek et al., 2000). In the presence of the antagonist, the protein-protein interaction dissociates, resulting in the reappearance of the cross-peaks of the labelled protein.

According to our previous work, peptide 9 can interact with MDM2RING△C and also with UbcH5a. It will be interesting to further understand whether peptide 9 is able to dissociate the UbcH5a-MDM2RING△C complex. First, apo-^{15}N-UbcH5a provides a well dispersed NMR spectrum with clear cross-peaks (Figure 5-18A). In the HSQC spectrum of ^{15}N-UbcH5a complexed with MDM2RING△C, some cross-peaks disappear (Figure 5-18B) as the large complex broadens the resonance (reducing the signal intensity). As expected, following addition of peptide 9, cross-peaks re-appear, providing evidence that peptide 9 dissociated the UbcH5a-MDM2RING△C complex (Figure 5-18C).

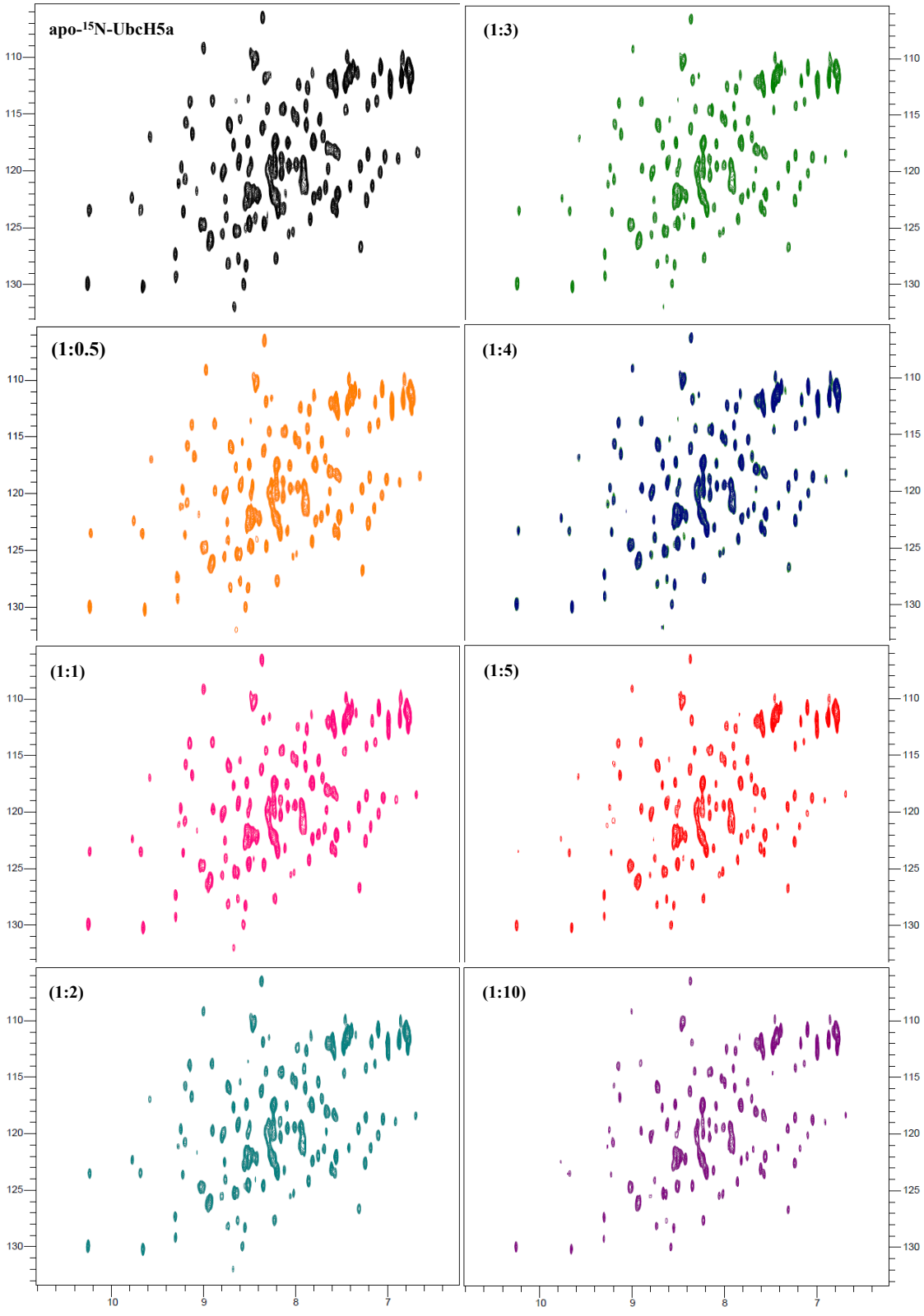

Figure 5-17: ^{1}H-^{15}N HSQC spectrum of folded UbcH5a with various concentrations of peptide 9. The protein concentration is 25 μM. The titration ratios of protein to peptide tested are 1:0.5, 1:1, 1:2, 1:3, 1:4, 1:5, and 1:10.

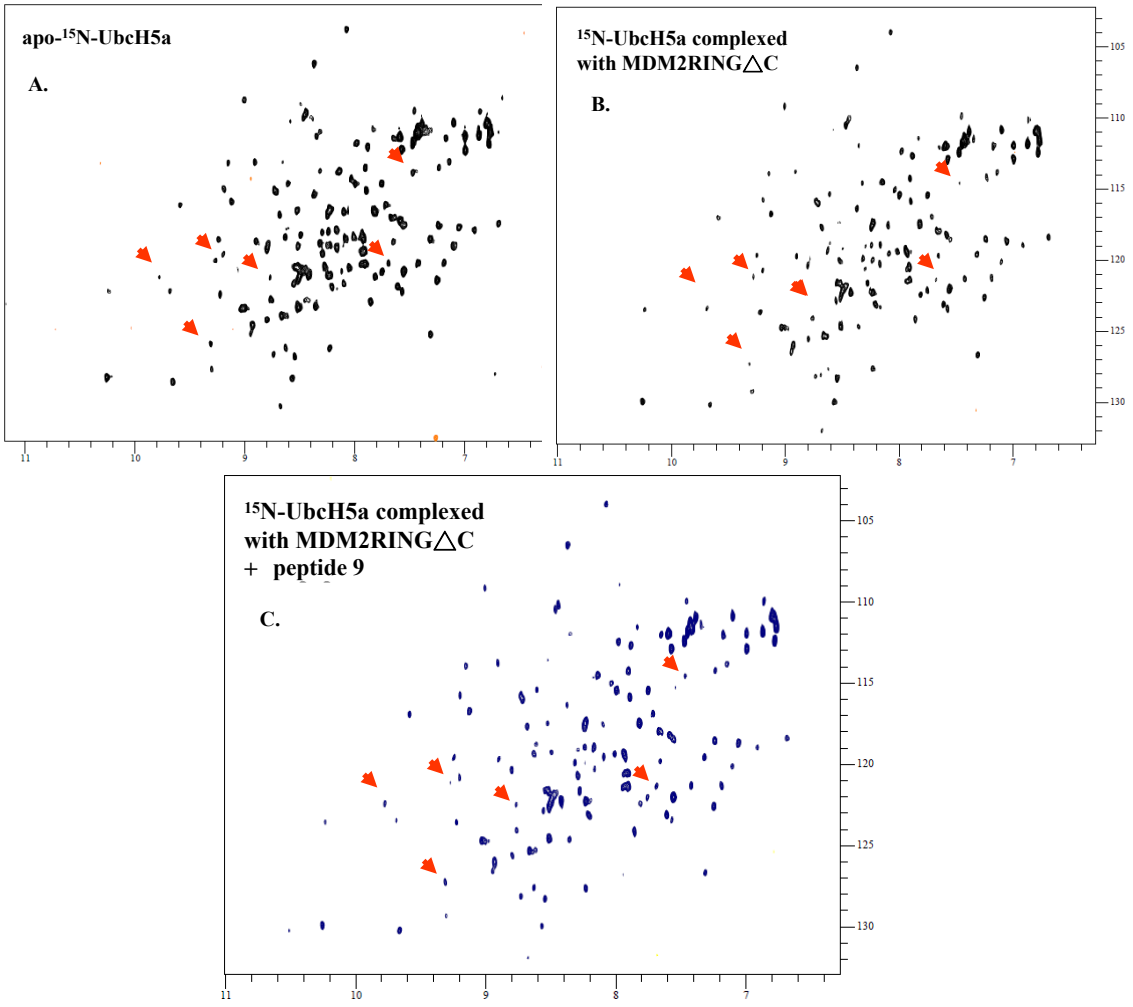

Figure 5-18: NMR analysis of the peptide 9 disrupting the interaction between UbcH5a and MDM2RING△C. (A) ^{1}H-^{15}N HSQC spectrum of ^{15}N-labelled UbcH5a (25 μM). (B) ^{1}H-^{15}N HSQC spectrum of ^{15}N-labelled UbcH5a (25 μM) complexed with MDM2RING△C (25 μM). Unlabelled MDM2RING△C is incubated with ^{15}N-UbcH5a for 1 hour at 4℃ prior to the NMR experiment. Some cross-peaks disappeared (red arrows compared to A). (C) ^{1}H-^{15}N HSQC spectrum of ^{15}N-labelled UbcH5a complexed with MDM2RING△C in the presence of peptide 9 (25 μM). Peptide 9 was added into the solution containing the complex and incubated for 1 hour at 4℃ prior to the experiments. The HSQC spectra showed that those cross-peaks re-appear (red arrows compared to B).

5.8 Summary

In conclusion, peptide 9, (the C-terminal 12 amino acids of MDMX C) has been proven to bind to FLMDM2 by *in vivo* and *in vitro* pulldown experiments (courtesy of Dr Susanne Patterson, unpublished data). Tryptophan intrinsic fluorescence was used to show that peptide 9 formed a complex with FLMDM2. Peptide 9 binding caused a blue-shift in the tryptophan fluorescence signal suggesting that either peptide 9 directly interacts with a tryptophan or induces an allosteric effect which buries tryptophan in a more hydrophobic environment (section 5.2). Modelling studies using the X-ray structure of the MDM2RING-MDMXRING complex suggested that a possible binding site for peptide 9 was at the dimer interface. Calculation of buried surfaces of peptide 9 docked onto MDM2RING showed the importance of the two terminal amino acids (I489-A490) (section 5.3). Fluorescence anisotropy studies of FITC-peptide9 binding to MDM2RING and MDM2RING△C show that Kd values are similar (with Kd values of 355nM and 314nM respectively). ESI-MS data from MDM2RING△C show that it behaves as a folded monomer. On addition of peptide 9 there are significant changes in peak intensities and some new peaks appear which are consistent with one molecule of peptide 9 binding to a dimer of MDM2RING△C. In addition, fluorescence anisotropy, ESI-MS and the thermal denaturation assay were used to show that peptide 9 also interacts with UbcH5a. Interestingly peptide 9 was found to decrease the thermal stability of UbcH5a.

Our *in vitro* ubiquitination assay data showed that peptide 9 had potent inhibitory effect upon MDM2-mediated ubiquitination of p53. Presumably, peptide 9 inhibits MDM2-mediated ubiquitination by interacting with MDM2 or UbcH5a. These results suggest that peptide 9 could be a good lead for further drug development studies. Although the binding mode of peptide 9 with MDM2 and/or UbcH5a is as yet unknown, in the following chapter, modelling and virtual screening is used to derive a possible binding interface based upon all available data. Some peptide 9 mimetics are found to be inhibitory to MDM2RING E3 ligase activity.

6 Virtual screening for new MDM2 E3 inhibitors

This chapter describes how we successfully used a virtual screening methodology for the development of MDM2 E3 inhibitors. There were three druggable target sites: (i) the C8-binding site of MDM2RING, (ii) the E2-binding site of MDM2RING and (iii) the E3-binding site of UbcH5a. Four inhibitors and one activator selected from millions of chemical compounds were shown to affect full-length MDM2 E3 activity. Additionally, four inhibitors and two activators were selected and shown to affect MDM2RING (residues 386-491) E3 activity.

6.1 Introduction

MDM2, a oncoprotein, is critical in regulating the level of p53 in cells; therefore, MDM2 has become an attractive drug target for anti-tumour therapy. As p53 plays a significant role in cell cycle arrest and apoptosis (Levine et al., 2006; Coutts & La Thangue., 2007; Brooks & Gu, 2004; Moll & Petrenko, 2003), reduction in the cellular concentration of p53 can result in tumour formation, such as sarcomas, brain tumour (Vogelstein et al., 2000; Vousden & Lane, 2007), MDM2 regulates p53 by interacting with p53 thorough its N-terminal hydrophobic and acidic domains. Ubiquitination of p53 is achieved by the E3 ligase activity of the C-terminal RING domain of MDM2 (Figure 6-1). To date, a number of drugs have been developed to inhibit the interaction between p53 and MDM2, such as Nutlin, Rita or MI-43 (Vassilev et al., 2004; Vassilev 2004; Issaeva et al., 2004; Shangary et al., 2008). These drugs were designed to mimic the structure of the p53 residues that bind to the surface of MDM2, Phe19-Trp23-Leu26. Few drug leads, such as HL198 (Yang et al., 2005), have been designed to inhibit MDM2 E3 ligase activity. Therefore, designing ligands to inhibit MDM2 E3 activity is a major goal of this project.

Ubiquitination is a well-characterised global posttranslational mechanism in cells used to determine the fate of proteins. The type of the linkage of ubiquitin attached to protein determined the protein fate, as introduced in Chapter 1. MDM2 is a RING-type E3 ligase and its cognate E2 partner is UbcH5a. The interaction of E2-E3 is essential for the transfer of ubiquitin to the substrate (Christensen & Klevit, 2009; Deshaies & Joazeiro, 2009). However, the RING-type E3-dependent ubiquitination mechanism is still unclear, providing exciting opportunities to search for MDM2 E3 ligands. The study of the effects of ligands on MDM2 is likely to provide insight into the mechanism of MDM2-dependent ubiquitination, in particular, the role of the C-terminus of MDM2 and the interactions between MDM2 with UbcH5a might be characterised.

A number of promising results will be discussed in this chapter: several small molecules found to affect MDM2 E3 activity were identified using a virtual screening strategy (VS). The aim was the development of small molecules that can inhibit MDM2 E3 ligase activity thus rescuing p53 activity. MDM2 E3 activity is associated with the RING domain; therefore one of our target sites is the MDM2 RING domain. The second target is UbcH5a, because the MDM2 RING domain interacts with its cognate E2 protein for successful ubiquitination.

There are three potential drug target sites (Figure 6-1): (1) the C8-binding site of MDM2RING, (2) the E2-binding site of MDM2RING, and (3) the E3-binding site of UbcH5a, the MDM2 cognate protein. In the following sections, the strategy behind selection of those MDM2 E3 ligase target sites will be presented followed by an outline of the virtual screening strategy used and will conclude with experiments to validate the efficacy of the small molecules selected on MDM2 E3 ligase activity.

(A)

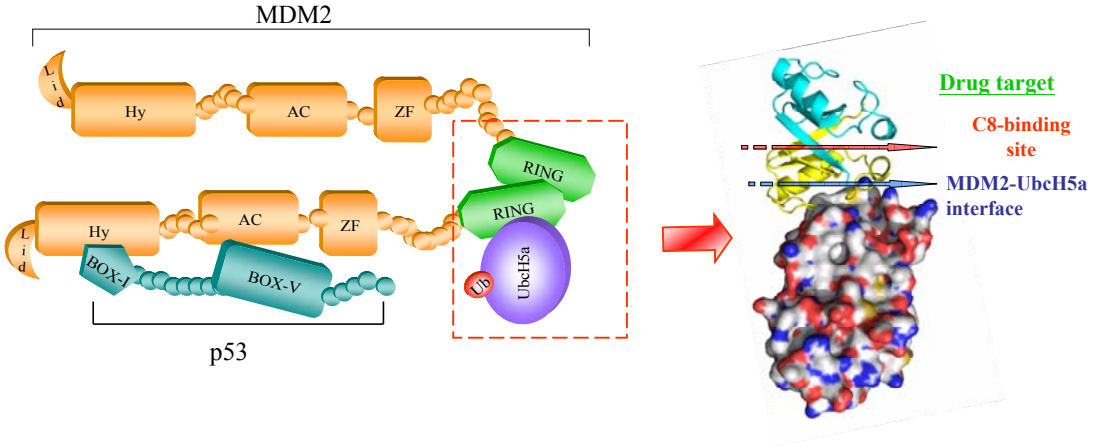

(B)

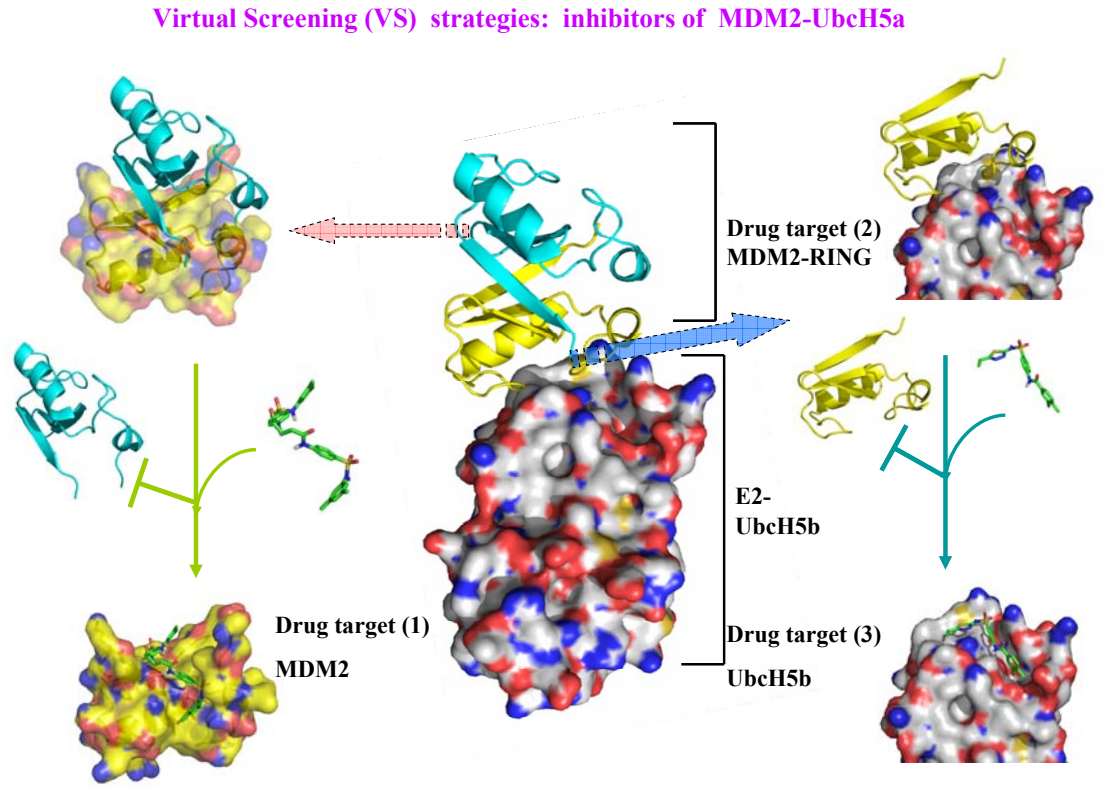

Figure 6-1: Protein-protein interactions: MDM2 and its binding partner. (1) A schematic diagram shows the interaction interface of MDM2 (orange) and p53 (cyan), through the two dominant binding motifs: the hydrophobic domain (Hy) of MDM2 with the BOX-I motif of p53, and the acidic domain (AC) of MDM2 with the BOX-V motif of p53. MDM2 binding partner, UbcH5a (purple), interacts with MDM2 through the RING domain (RING) (green). Dimerisation of MDM2 is achieved through its RING domain, especially the C-terminal region (or C-tail). ZF is a zinc finger motif. The red dashed line highlights the targets: MDM2-MDM2 C8-binding site and MDM2-UbcH5a interface. (B) Three potential target sites: (1) C8-binding site of MDM2, (2) the UbcH5a-binding site of MDM2; (3) the MDM2-binding site of UbcH5a2. MDM2 E3 ligands are shown in green stick representations. The MDM2-UbcH5a complex model was built based on the cIAP2-UbcH5b complex (PDB: 3EB6).

6.2 Virtual screening strategy

Virtual screening (VS) is a powerful technique saving time and resources during the drug discovering process. VS is a combination of several programs, the basis of which was described in Chapter 1. In this section, the programs used in this project will be briefly introduced. UFSRAT and LIDAEUS were used to design the template and also in the selection of small molecules from the database; EDULISS is a database of small molecules; AutoDock is used to simulate of the binding mode of small molecules onto the target site, and to predict binding energy (△G) and binding affinity (Kd).

In this work, the virtual screening strategy developed utilised several steps. Figure 6-2 outlines a virtual screening strategy and all other strategies used in this chapter were broadly similar: (1) The first step is to determine what the target site is and to define which residues in the target protein may be involved in the interaction with residues of its partner (Figure 6-2 A); (2) The second step is template design. The template is usually designed according to the structure of the target protein's partner. There are several programs available for template design including UFSRAT and LIDAEUS (Figure 6-2 B, C & D). (3) After information about the target site and appropriate small molecule libraries are generated from steps 1 and 2, AutoDock is used to simulate small molecules binding to the target site. A ranked list dependent upon the simulated binding energy between the target and the small molecules is produced by AutoDock (Figure 6-2E). (4) The simulated binding modes of the small molecules onto the target, together with an estimate of the binding energy are used to guide the purchase of a number of small molecules to be further characterised.

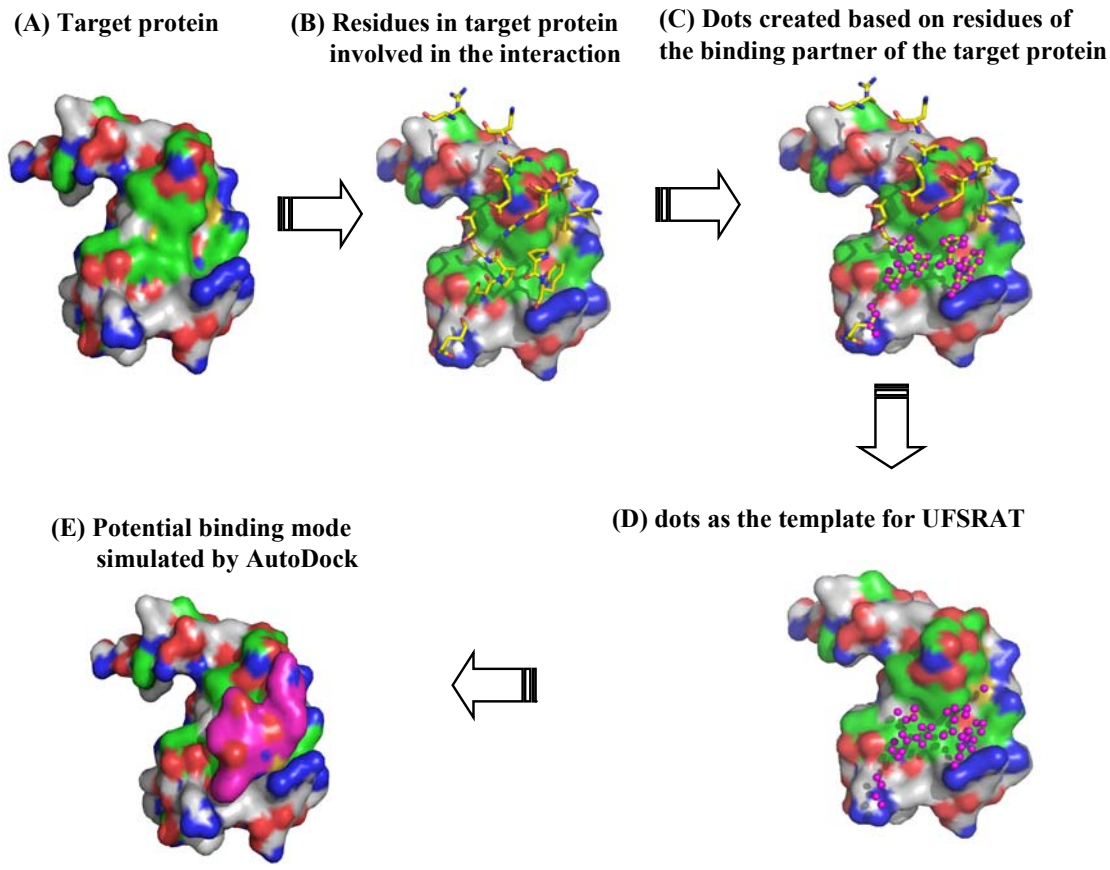

Figure 6-2: Outline of the virtual screening strategy used. (A) Determine the target protein. MDM2RING, and define the target site (green). (B) Define the potential interacting residues of the MDM2-binding partner, UbcH5a, (yellow stick representation) located in the E2 binding surface of MDM2 (green surface representation). (C) Create the dots (magenta), representing each atom in a residue, that may be involved in an interaction with the target. (D) These dots form the template for UFSRAT, to search the EDULISS database for small molecules with matching atoms. (E) Simulation of the binding mode of small molecules onto the target site by AutoDock. A molecule found by UFSRAT is shown in a magenta surface representation. The MDM2 structure shown was based on the published crystal structure (PDB: 2VJE).

6.3 Drug target site (1): the C8-binding site of MDM2

6.3.1 Biochemical studies identifying the MDM2 dimerisation site as a druggable target

The MDM2 RING domain has E3 ligase activity and exists in different oligomeric forms. It is well-known that the dimerisation of MDM2 is related to its E3 ligase activity and numerous reports illustrate the importance of the C-terminal amino acids for MDM2 E3 ligase activity and oligomerisation, showing that MDM2 homodimers and MDM2-MDMX heterodimers are essential for E3 ligase activity (Sharp et al., 1999; Tanimura et al., 1999; Stad et al., 2001). It has also been reported that monomeric MDM2 RING has reduced levels of E3 activity (Poyurovsky et al., 2007). A solution structure of MDM2-MDM2 homodimer (PDB: 2HDP) (Kostic et al., 2006) and a crystal structure of MDM2-MDMX heterodimer (PDB: 2VJE) (Linke et al., 2008) clearly showed that the C-terminus of each subunit is located in the C8-binding site, interacting with the other subunit (Figure 6-3A). cIAP/XIAP and BRCA1/BARD1 heterodimers have a similar interaction that involves the same residues in dimerisation and E3 ligase activity (Brzovic et al., 2001; Silke et al., 2005).

Several MDM2 C-terminal mutants have been studied and highlight the importance of the MDM2 C-terminus, and the MDMX C-terminus for MDM2 E3 ligase activity (Poyurovsky et al., 2007; Linke et al., 2008; Uldrijan et al., 2007). Previous reports show that MDM2 deletion mutant, MDM2△C7 is monomeric and has no E3 activity (Poyurovsky et al., 2007; Uldrijan et al., 2007). The MDM2 RING mutant, F490Q, exists as a monomer and has reduced E3 activity. Surprisingly, the C-terminus of MDMX can rescue the E3 activity of the MDM2 RING F490Q mutant, revealing that the compact C-terminus of MDM2 is a key determinant for its E3 activity (Uldrijan et al., 2007; Poyurovsky et al., 2007). The Y489A mutation in MDM2 was also found to completely abolish its E3 ligase activity (Linke et al., 2008). The equivalent residue in cIAP2, F602, mutated to alanine also resulted in reduced E3 activity and disruption in the dimerisation of cIAP2 (Mace et al., 2008). The six C-terminal residues of cIAP1, a homologue of cIAP2, were mutated and disrupted the heterodimerisation of cIAP1/XIAP E3 ligase activity (Silke et al., 2005). These reports indicate that the C-terminus of RING type E3 ligase is critical to its E3 activity, and that the integrity of the C-terminus of E3 RING domain is critical for the E2-E3 interaction (Petersen et al., 2007).

The STP program was used to identify druggable sites in MDM2RING, to test the hypothesis that the C8-binding site of MDM2 is a druggable target (Figure 6-3B). STP is a simulation program used to predict potential binding sites ("hot spots") in proteins (Mehio et al., 2010). A great deal of work has focused on and characterised hot spots within proteins. A number of common features found in hot spots include specific residue composition and conformations which can suggest protein-protein interaction sites in proteins (Huang et al., 2006; Morita et al., 2008; White et al., 2008). Potential binding sites (or hot spots) for MDM2 are shown in Figure 6-3B. The blue colour suggests the region is unlikely to be a site of protein-protein/ligand interactions, the red means the region is likely to be involved in protein-protein/ligand interactions. Analysis by STP suggests the C8-binding site of MDM2 is indeed a hot spot. Overall, those findings suggest that the C8-binding site of MDM2 is a good druggable target site and that the C-terminus of MDM2 (or MDMX) is a good starting template for virtual screening.

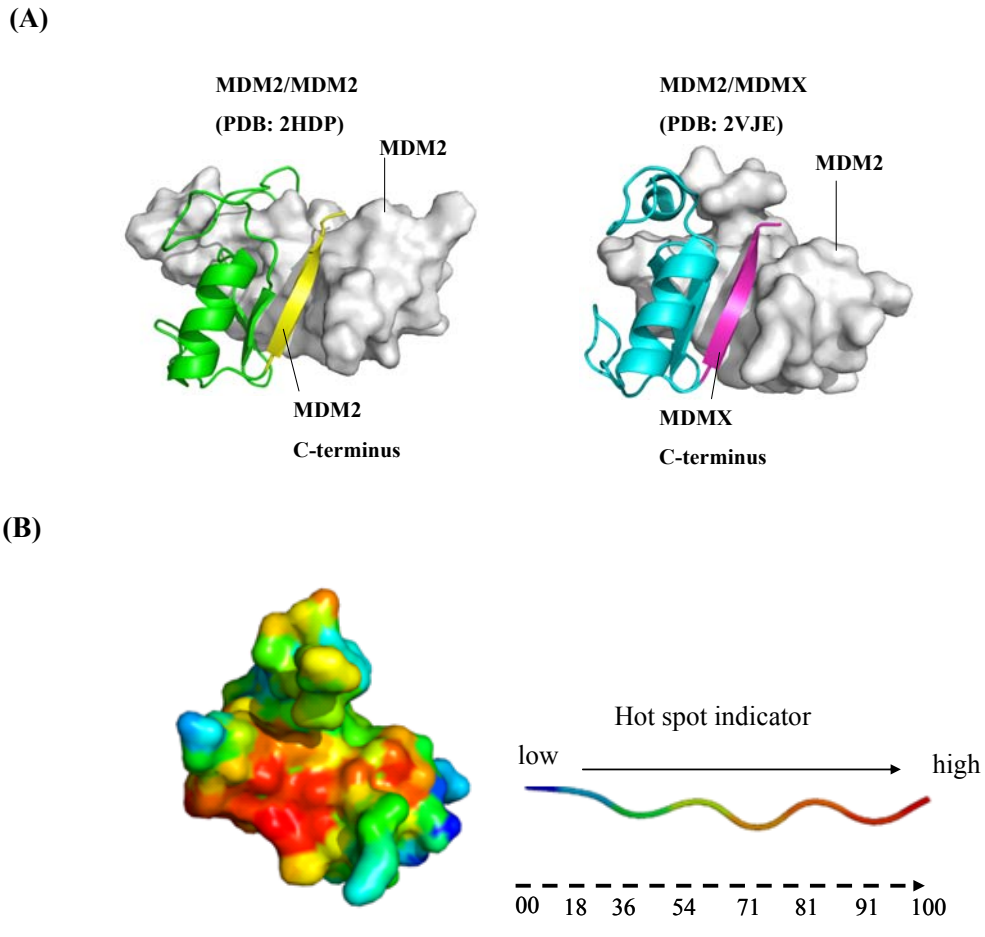

Figure 6-3: The C8-binding site of MDM2 is a druggable target site. (A) Left: MDM2/MDM2 homodimer (PDB code: 2HDP), right: MDM2/MDMX heterodimer (PDB code:

2VJE). The C-terminus of MDM2 (yellow β-strand) or MDMX (magenta β-strand) interacts with the C8-binding site of the other MDM2 subunit (in white surface representation). (B) The output from the STP programme. The hot spots predicted by STP are shown in red and orange, highlighting the C8-binding site as a potential interaction site for proteins or small molecules.

6.3.2 Virtual screening for inhibitors of MDM2 dimerisation

Following selection of the C8-binding site of MDM2RING as a druggable target site, the next step was to define a virtual screening template. There were two candidates available: the MDM2 C-terminus and the MDMX C-terminus. MDM2 can form both homodimers and heterodimers with MDMX through the C-terminal fragments. Enzyme activities and binding affinities have shown that MDM2/MDMX heterodimers have greater E3 ligase activity than MDM2/MDM2 homodimers (Badciong & Haas, 2002; Kawai et al., 2007; Singh et al., 2007). This implies that C-terminal MDMX may have stronger binding affinity to the C8-binding site of MDM2 than the C-terminus of MDM2. MDMX C-terminus is therefore likely to be a better candidate template for virtual screening. Furthermore, previous work also revealed that the peptide 9, the last twelve MDMX C-terminal residues, has high binding affinity with MDM2 and also inhibits MDM2 E3 ligase activity (Chapter 5). The decision to use peptide 9 as a virtual screening template is further supported by studies using PISA of the correlation of the buried surface areas of both MDM2 and MDMX C-terminal regions with the C8-binding site of MDM2 subunit (as described in Chapter 5). When the sequences of the C-terminal 12 residues in MDM2 and MDMX were aligned, the results showed that MDM2 C-terminus has three hydrophilic, two aromatic and no charged residues, whereas MDMX C-terminus contains one hydrophilic, one aromatic and three positively charged residues (Figure 6-4A). Comparisons of the structures of MDM2-MDM2 C-terminus and MDM2-MDMX C-terminus revealed they have similar binding modes at the C8-binding site (Figure 6-4C). According to a study of buried surface areas of MDM2-MDM2 C-terminus and MDM2-MDMX C-terminus, the data provide explanation why the MDM2/MDMX heterodimers are preferred over MDM2/MDM2 homodimers. The buried surface of MDM2-MDMX C-terminus is 503.1 Å whereas that of MDM2-MDM2 C-terminus is 387 Å. Larger buried surfaces between two proteins or protein-ligand usually suggests there is higher possibility that binding affinities should be higher, consistent with larger numbers of H-bonds and *van der Waal* contacts between the two molecules. For example, there are eight H-bonds within the MDM2-MDMX C-terminal complex and only three within the MDM2-MDM2 C-terminal complex (Figure 6-4B). MDM2 C-terminal residues, L487 and Y489,

form three H-bonds with MDM2 residues, G456 and L458. MDMX- C-terminal residues, K486, F488, I489, and A490, interact with the residues of MDM2RING, N433, K446, K454, T455, G456, and L458 forming eight H-bonds (Figure 6-4C). Overall, analysis of this binding site data suggests that MDMX C-terminus is a good template for virtual screening.

(A)

(B)

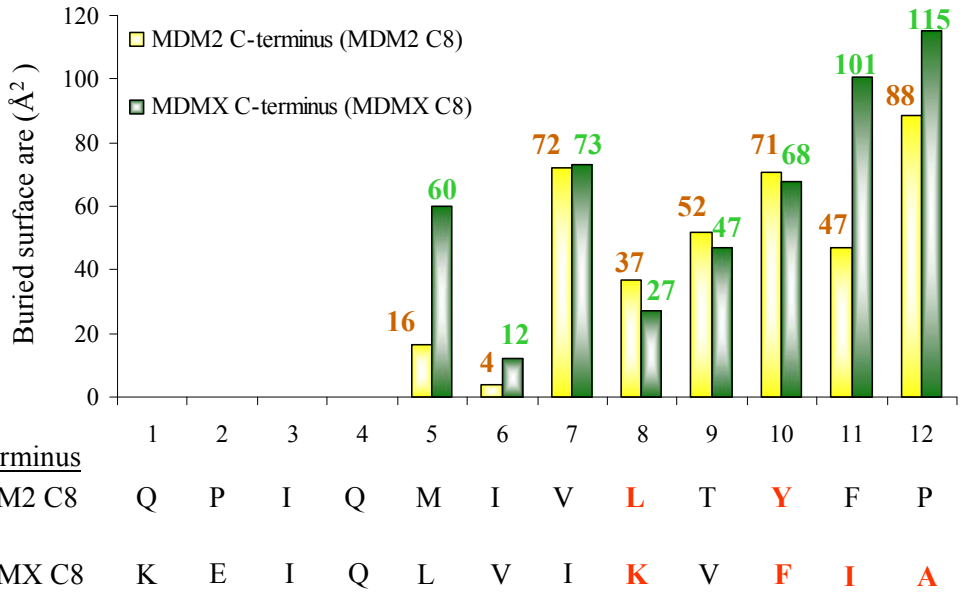

	Buried sureface area (Å²)	H-bonds
MDM2 C-terminus	387.0	3
MDMX C-terminus	503.1	8

(C)

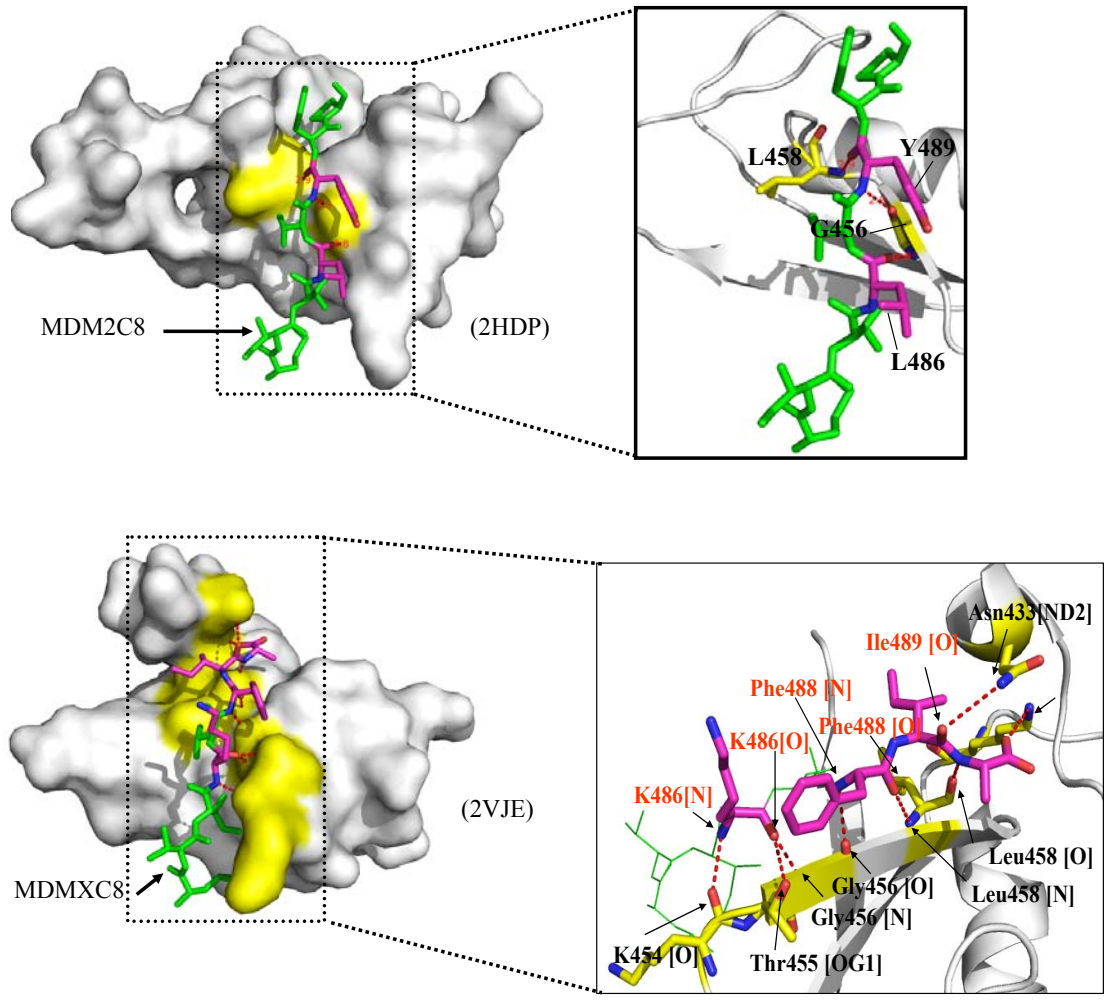

Figure 6-4: Comparison of the two template candidates for the C8-binding site of MDM2: MDM2 C-terminus and MDMX C-terminus. (A) Alignment of the final 12 C-terminal residues. Residues are coloured according to their characteristics. (B) Comparisons of buried surface areas with those two complexes. The graph represents the buried surface area of each residue in MDM2 C-terminus (green) or MDMX C-terminus (yellow) complexed with another MDM2RING. Residues forming H-bonds are highlighted in red. The table summarises overall buried surface areas and the number of H-bonds within each complex. (C) Comparisons of the modelled structure of two peptide candidates with MDM2 subunit. MDM2 C-terminus (MDM2C8) and MDMX C-terminus (MDMXC8) both are coloured in green stick representations, and MDM2RING is coloured in a white surface representation. Residues in MDM2RING that interact with MDM2 C-terminus or MDMX C-terminus are shown in yellow. Residues of MDM2C8 or MDMXC8 forming H-bonds with MDM2 are coloured in magenta sticks.

6.3.3 Virtual screening results: MDMX-C terminus mimetic

Following selection of both target and template, virtual screening experiments were initiated. In this work, the combination of virtual screening strategies was as follows: (1) 1000 small molecules from the EDULISS database were selected using UFSRAT; (2) binding modes, binding energies and binding affinities were simulated using AutoDock. Following manual evaluation of both the simulated binding mode and predicted substrates of the small molecules, the top 10 compounds were purchased.

The template for the UFSRAT search was the eight residues of the MDMX C-terminal octapeptide, LVIKVFIA (Figure 6-5A). The aim was to find small non-peptide molecules with drug-like characteristics (Bemis & Murcko, 1996; Bemis & Murcko, 1999; Lipinski et al., 1997). UFSRAT is a structural similarity simulation program, and a smaller template is a better starting point to select similar compounds from the EDULISS database. Importantly, a proportion of the druggable dimer surface is composed of the C-terminal octapeptide (Figure 6-5A). Out of a total of 1082.4 $Å^2$, the MDMX octapeptide contributed 503.1 $Å^2$ (Figure 6-4). The residues responsible for the formation of H-bonds with MDM2 were included in the template. Residues of MDM2 within 4Å of the template, LVIKVFIA, are N433, A434, K446, G453, K454, T455, G456, H457, L458, M459, and V477 (yellow and pink surface, Figure 6-5B). There are eight H-bonds within the complex: K454[O], G456[O], L458[O], T455[OG1], G456[N], L458[N], N433[ND2] and K446 [NZ] of MDM2, respectively, interacts with K486 [N], F488 [N], A490 [N], K486[O], K486[O], F488 [O], I489[O] and A490[O] of MDMX C-terminus (red dashed line, Figure 6-5B; details in Figure 6-4C & Figure 5-4B). Those residues provide essential information on the interaction mode for AutoDock simulations.

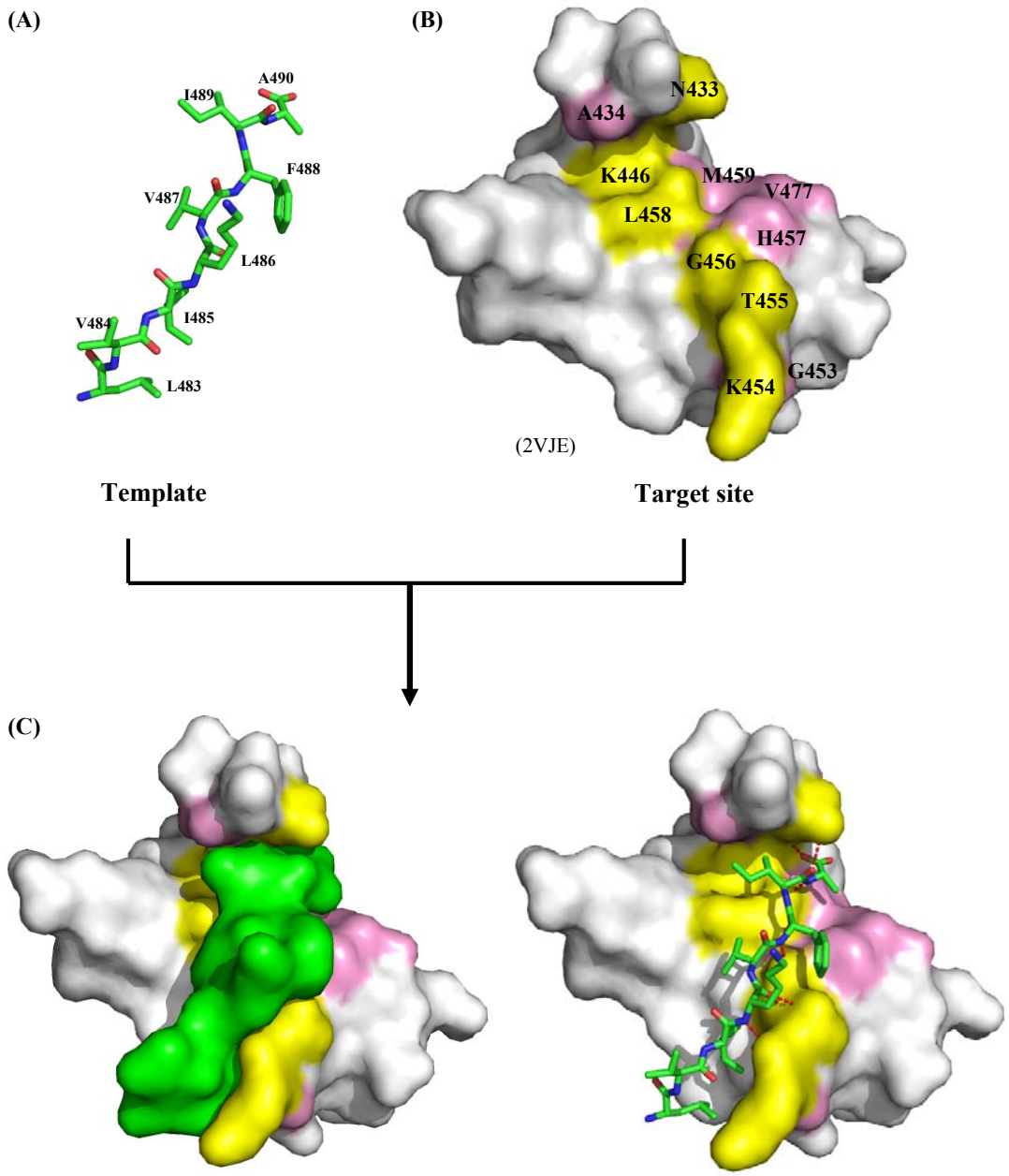

Figure 6-5: The modelled structure of MDM2-MDMX C-terminal octapeptide complex. (A) The structure of MDMX C-terminal octapeptide, 483LVIKVFIA490, is shown in green sticks. This structure is a template for a UFSRAT similarity search. (B) Residues in MDM2 are located within 4Å distance around the MDMX C-terminus are coloured in yellow and pink. Residues in MDM2 forming H-bonds with MDMX C-terminus are highlighted in yellow. (C) The binding mode of MDMX C-terminal octapeptide 9 (green surface/sticks) onto MDM2 C8-binding site (white surface). MDMX C-terminus are shown in green surface form (left panel) and green sticks (right panel). Red dashes represent H-bonds.

Because the template LVIKVFIA is a contiguous peptide, these eight residues provide a straightforward structural conformation for UFSRAT searches. 1000 compounds from the EDULISS program were firstly filtered by UFSRAT and those small molecules were a group of MDMX C-terminus mimetics, known as the D-series compounds (D-series). Similarities of those MDMX C-terminus mimetics to the template varied from 50.1 % to 35.7 % (Figure 6-6).

The top 1000 compounds were tested using AutoDock. Autodock requires the following information- a library of small molecules, the target site, and the putative binding residues of the target site. AutoDock data revealed that most of the selected compounds fitted well into the C8-binding site of MDM2 (Figure 6-7). Following manual analysis of the simulation data to evaluate the proposed binding mode of the small molecules to the target site, a ranked list was prepared. It was also important to consider the solubility, toxicity and suggested binding affinities of the hit compounds, to choose and purchase the "top ten" compounds from Spec. Co. Estimated binding energies ($\triangle$G) of these top 10 compounds to the C8-binding site of MDM2 varied from -9.3 kcal/mol to -7.7 kcal/mol with predicted binding affinities of 155.6 nM to 1.6 μM. More information on each compound, D01 ~ D10, is shown in Table 6-1.

Figure 6-6: Alignments of D-series onto MDMX-C octapeptide. S.I. (similarity) values are calculated by UFSRAT. D-series compounds are shown in green sticks and the template octapeptide in magenta lines. (C=green or magenta, N=blue, O=red, and S=yellow). * S.I. represents the value of "similarity" compared to the template, MDMX octapeptide.

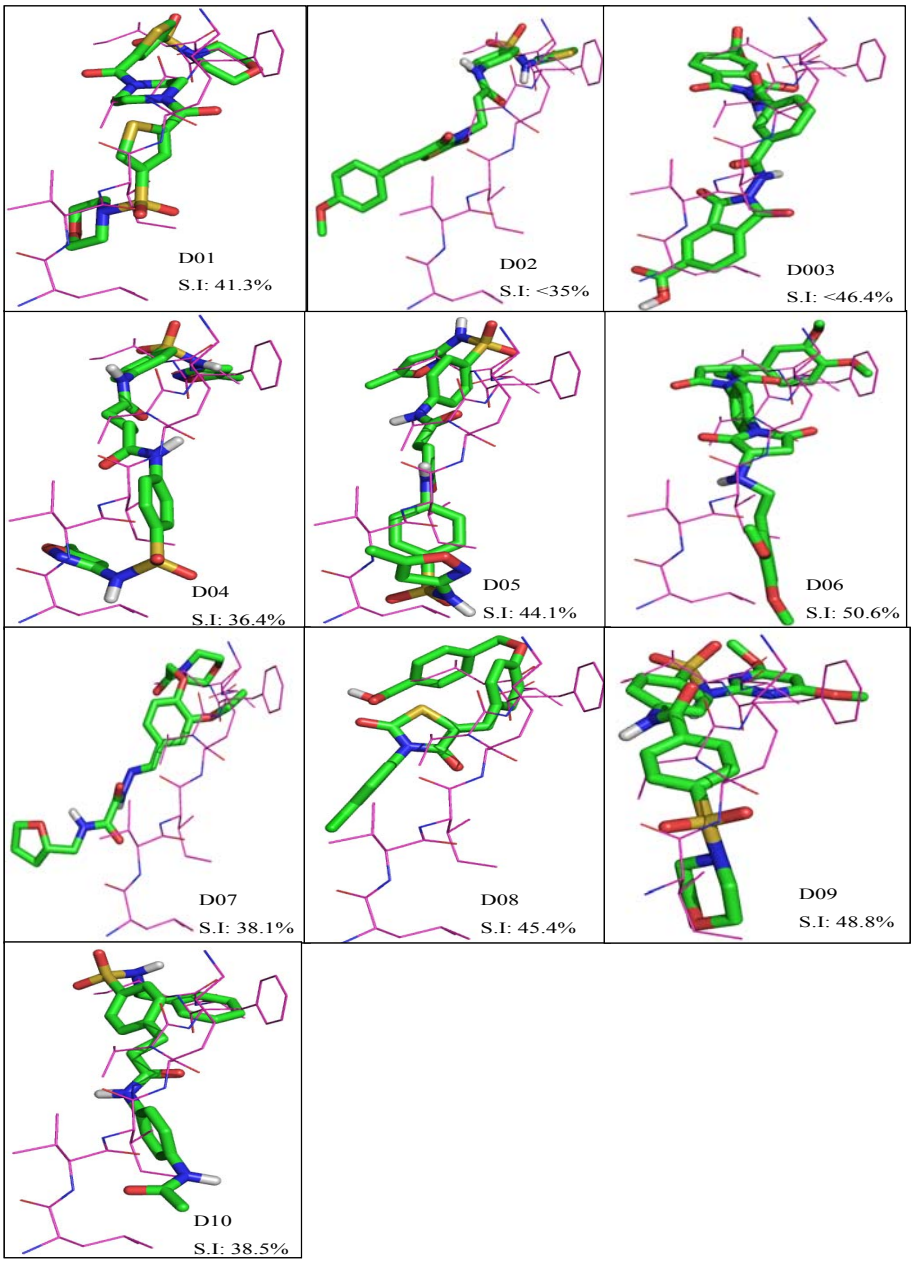

Table 6-1: Characteristics of the D-series compounds. Information includes the product code for the supplier. The estimated binding energies and affinities are estimated following the AutoDock simulation.

	Chemical structure	UFSRAT Similarity (%)	△G (kcal/mol)	estimated binding affinity	LogP	M.W.
D01	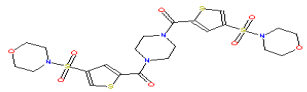 AK-918/ 13946031	0.4	-9.3	155.6 nM	-0.24	604.8
D02	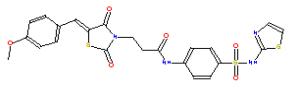 AG-690/ 11451258	N.D.	-9.2	190.3 nM	3.5	544.6
D03	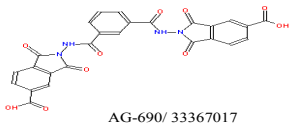 AG-690/ 33367017	0.5	-8.9	298.8 nM	3.1	542.4
D04	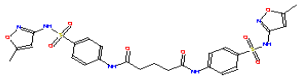 AN-329/ 40718894	0.4	-8.6	507.1 nM	3.9	602.7
D05	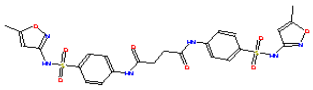 AN-329/ 40718906	0.4	-8.3	798.6 nM	3.5	588.6
D06	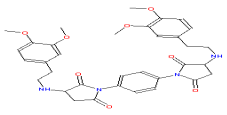 AN-919/ 14229174	0.5	-8.1	1.2 μM	1.9	630.7
D07	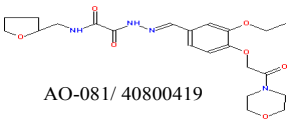 AO-081/ 40800419	0.4	-7.9	1.6 μM	0.2	462.5
D08	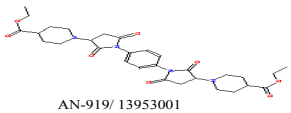 AN-919/ 13953001	0.5	-7.8	N.D.	0.2	582.7
D09	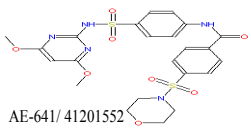 AE-641/ 41201552	0.5	N.D.	N.D.	1.7	536.6
D10	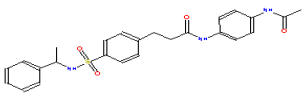 AH-487/ 42484048	0.4	-7.9	1.6 μM	3.4	465.6

Figure 6-7: The binding modes of the D-series compounds onto the C8-binding site of MDM2 as determined by AutoDock. Those compounds are shown in green sticks. The target site, the C8-binding site of MDM2, is coloured yellow and pink.

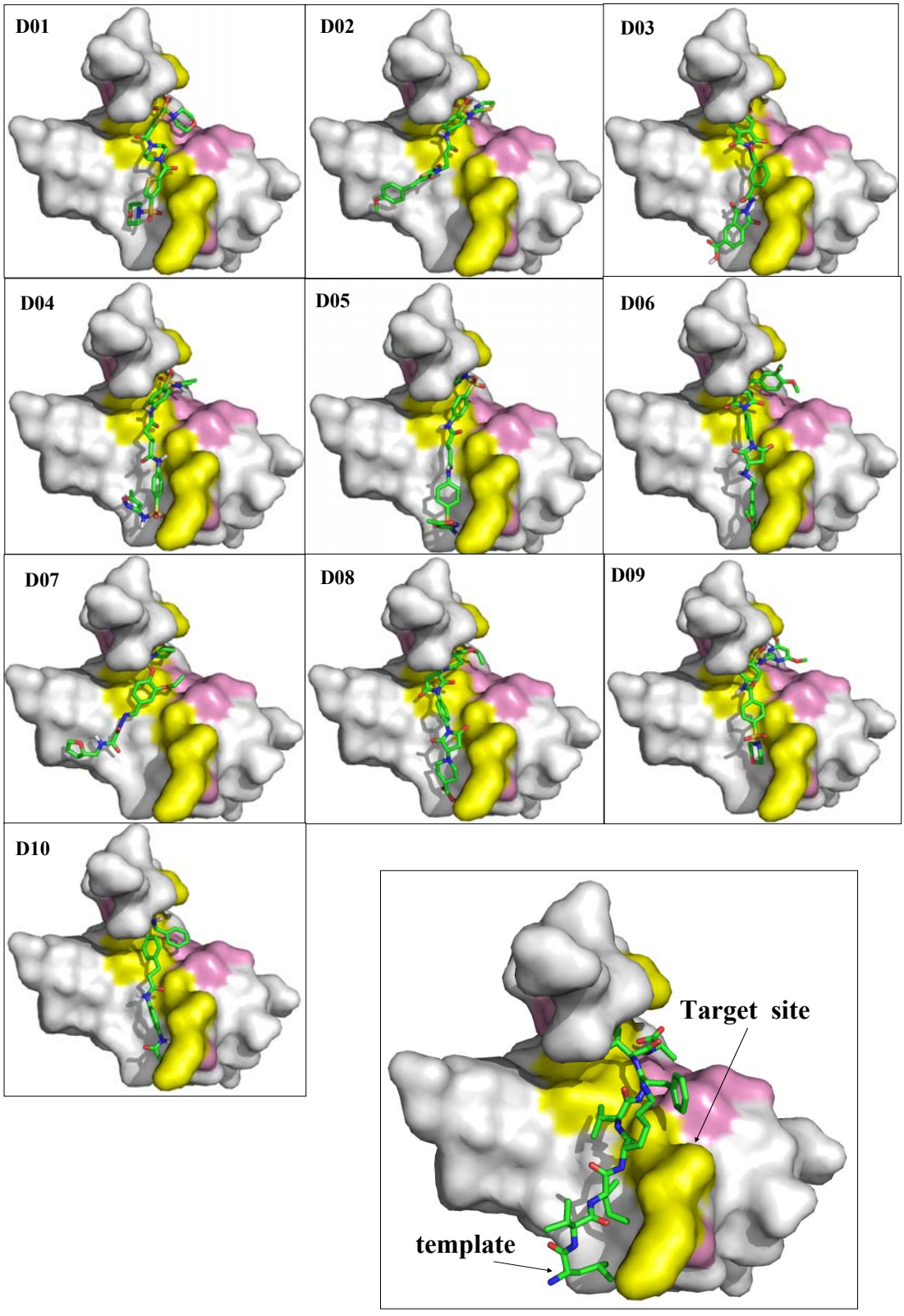

- ***Characterisation of the effects of the MDMX C-terminus mimetics on MDM2 E3 activity***

An *in vitro* ubiquitination assay was used to determine how the compounds selected by virtual screening affect MDM2 E3 activity. All compounds were dissolved in 100% DMSO. The assay was as follows: 500 μM of each compound was incubated with 100 ng FLMDM2 or with 100 ng MDM2RING and incubated at room temperature for 10 minutes. The other essential components for *in vitro* ubiquitination were added to start the reaction, followed by incubation at 30℃ for 10 minutes. To stop the ubiquitination, 2X loading dye solution was added into each sample. The samples were analysed on 4~12% gradient gels, ubiquitinated-p53 was detected by an anti-p53 antibody (D01). The *in vitro* ubiquitination assay was described in great detail in Chapter 3.

- ***Different D-series compounds inhibit FLMDM2 and MDM2RING E3 activity***

D-series compounds were designed to bind to the C8-binding site of MDM2, as reports have shown that dimerisation of MDM2 plays an important role in its E3 ligase activity. Inhibition of dimer formation by D-series compounds could therefore inhibit MDM2 E3 ligase activity. Exciting results showed that three compounds, D03, D04 and D05 (at a concentration of 500 μM) significantly inhibited FLMDM2 E3 ligase activity (Figure 6-8A). Interestingly, D04 and D05 are chemically closely related (Table 6-1). Correlation between the isoforms might imply that this type of compound tends to interact with FLMDM2. Although the exact binding mode of the compound-protein complex is as yet experimentally undetermined, such a small molecule might make a useful starting template for a second round of virtual screening.

Presumably, if those compounds bind to the C8-binding site of MDM2, there should be similar inhibition effects observed on MDM2RING E3 activity. However, D03 only slightly inhibited MDM2RING E3 activity, whilst D04 and D05 showed no inhibition of MDM2RING E3 activity (Figure 6-8B). It is still possible, however, that D04 and D05 compounds did bind to the C8-binding site of FLMDM2 and MDM2RING, but induced distinct effects. The D04/D05-binding may allosterically regulate the conformational structure of FLMDM2; hence they reduced the interaction of p53-FLMDM2 or FLMDM2-UbcH5a, but there was no effect on the interaction of p53-MDM2RING or MDM2RING-UbcH5a. It was reported that MDM2 RING domain allosterically controls FLMDM2

conformation and activity (Wawrzynow et al., 2009). Surprisingly, other compounds from the series, D07, D08, D09, and D10 (500 μM), significantly inhibit MDM2RING E3 ligase activity (Figure 6-8B), and reduce the possibility of the second ubiquitin being transferred to p53-Ub1. It has been noted that monomeric MDM2 mono-ubiquitinates p53, and dimeric or higher order MDM2 oligomers induce poly-ubiquitinated p53 (Cheng et al., 2009). Moreover, protein fate is determined by the type of ubiquitin linkage attached: mono-ubiquitinated protein is usually directed to non-proteolytic functions, such as endocytosis, transcriptional activation, or enzyme activation (Fang & Weissman, 2004; Marchenko, et al., 2007). D07, D08, D09, and D10 might provide a very useful model for the study of the MDM2-mediated mono/poly-ubiquitination mechanism.

(A)

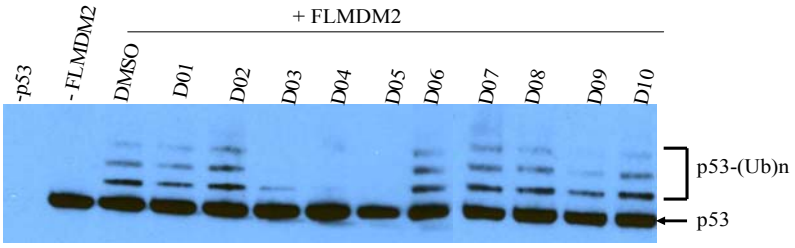

(B)

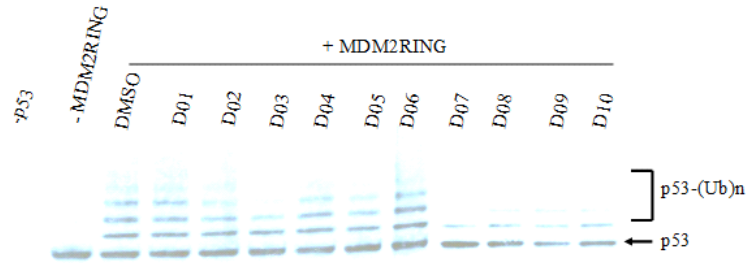

Figure 6-8: *in vitro* ubiquitination studies of the D-series compounds on FLMDM2 and MDM2RING E3 ligase activity. 500 μM compounds are incubated with 100 ng FLMDM2 or 100 ng MDM2RING for 10 minutes at R.T. Then other components required for *in vitro* ubiquitination (detail described in Section 3.1) are added and incubated at 30℃ for another 10 minutes. These samples are analysed using 4~12% gradient gels and ubiquitinated p53 are detected by anti-p53 antibody D01.

- ***Potential interactions between D-series compounds and MDM2RING domain***

To clarify whether there are similar binding patterns between those complexes of MDM2 and D-series compounds, we analysed the simulated docking model to determine which residues of MDM2 interact with docked D-series compound (Figure 6-9). We illustrate the MDM2 residues that are located within 4Å distance around each of the docked D-series compounds according to the docking models. Specifically, MDM2 residues that potentially interact with D03, D04, and D05 are shown in green and those that might interact with D07, D08, D09 and D10 are shown in yellow. Defining any specific binding pattern related to FLMDM2 or MDM2RING E3 ligase activities proved difficult. Previous work has indicated that MDM2 is a highly flexible protein, consisting of several functional motifs and flexible linkers (Nicholson & Hupp, 2010). The flexibility of MDM2 highlights that MDM2 functions are regulated allosterically by several distinct MDM2-binding partners, for example, p53, ATP, RNA repressor, or the MDMX C-terminus mimetics in this work, binding to distinct motifs within MDM2 and allosterically regulating its conformation and function. This might also explain why the MDMX C-terminal mimetics (D-series) have different effects on FLMDM2 and MDM2RING E3 ligase activities.

			FLMDM2 E3 ligase inhibitors				**MDM2RING E3 ligase inhibitors**			
	D01	D02	D03	D04	D05	D06	D07	D08	D09	D10
L430										
P431										
N433										
A434										
E436										
V439										
K446										
C449										
V451										
G453										
K454										
T455										
G456										
H457										
L458										
M459										
V477										
M484										
V486										
L487										
T488										
Y489										

Figure 6-9: Potential interactions between MDM2RING and selected compounds. This table lists of MDM2 residues located within 4 Å distance around each D-series compound. FLMDM2 E3 ligase inhibitors, D03, D04, and D05, are highlighted in green; MDM2RING E3 ligase inhibitors, D07, D08, D09, and D10 are highlighted in yellow; other compounds were coloured in cyan.

Although we have not yet clarified why D-series compounds have different effects on FLMDM2 and MDM2RING, with respect to development of potential anti-cancer therapies, it is encouraging that D-series compounds can indeed inhibit MDM2 E3 ligase activity. There is still a great deal of work required to optimise those selected compounds; however, results demonstrate that our virtual screening strategy can be used as a promising primary screening system to search for compounds that can inhibit FLMDM2 or MDM2RING E3 ligase activity.

6.4 A model for the structure of the UbcH5a-MDM2RING complex

In the ubiquitination pathway, numerous reports have shown that E3-E2 binding is essential for the transfer of ubiquitin to the E3 substrate or E3 itself (autoubiquitination), including the following targets UbcH7-E6AP, UbcH7-cCb1, UbcH5b-cIAP2, UbcH5-CHIP, Uve1a-UbcH13-CHIP (Huang et al., 1999; Mace et al., 2008; Xu et al., 2008; Zhange et al., 2005; Zheng et al., 2000). This raises an interesting question: what might the consequence be if a small molecule disrupts the E2-E3 interaction? It is presumed that ubiquitination does not proceed without the E2-E3 interaction. Because the MDM2 RING domain interacts with E2 proteins, such as UbcH5a, and facilitates transfer of the ubiquitin molecule from E2 to the substrate of MDM2, e.g. p53 or itself. In the next two sections, our aim is to find by virtual screening small molecules to interrupt the interaction of UbcH5a (E2) and MDM2 (E3). Two main target sites were studied: the E2-binding site of MDM2 and the E3-binding site of UbcH5a.

- ***Building a model of the UbcH5a-MDM2 complex***

The first step is to build a good model of the UbcH5a-MDM2 complex. To date, there is no known crystal structure of an UbcH5a-MDM2 complex. As an alternative approach, we decided to build a model of the UbcH5a-MDM2 complex based upon other known crystal structure of the cIAP2-UbcH5b complex (PDB: 3EB6) (Mace et al., 2008) to use as our reference. Although the structures of other E3s with their cognate E2s are also known, the overall structure and amino acid sequences of cIAP2 has higher degree of similarity to MDM2 than the other available structures. Firstly, cIAP2, Baculoviral IAP repeat-containing protein 3, is also a RING-type E3 protein. Secondly, other RING-type E3 proteins, such as BRCA1-BARD1 or Ring1b-Bmil, dimerise when they interact with sections of α-helix but not β-sheets as seen with MDM2 or cIAP2 (Figure 6-10A). MDM2 and cIAP2 RING domains are both located at the C-terminus of the proteins, whereas BRCA1-BARD1 and Ring1b-Bmil RING domains are found at the N-terminus. Moreover, based on the amino acid sequences (Figure 6-10B), cIAP2 shares 35% identity with MDM2. Sequence alignments of the RING domains of various E3 proteins were analysed using MyHints, a database which includes a tool for analyzing protein sequences (Pagni et al., 2007). Furthermore, the phylogram also suggested that cIAP2 has a closer evolutionary relationship to MDM2 than any other characterised proteins (Figure 6-10C). The phylogram was generated using the ClustalW program, and is a branching diagram that graphically indicate

the evolutionary relationship among the species based upon the similarities and differences seen in the amino acid sequences (Figure 6-10C). Another key reason for selecting the reference structure used is that the cIAP2 cognate E2 protein is UbcH5b, a homolog of UbcH5a. The similarity of UbcH5b to UbcH5a is 99% and the identity is 89% (Figure 6-11). The cIAP2-UbcH5b structure therefore is the most appropriate reference for our model of MDM2-UbcH5b.

(A)

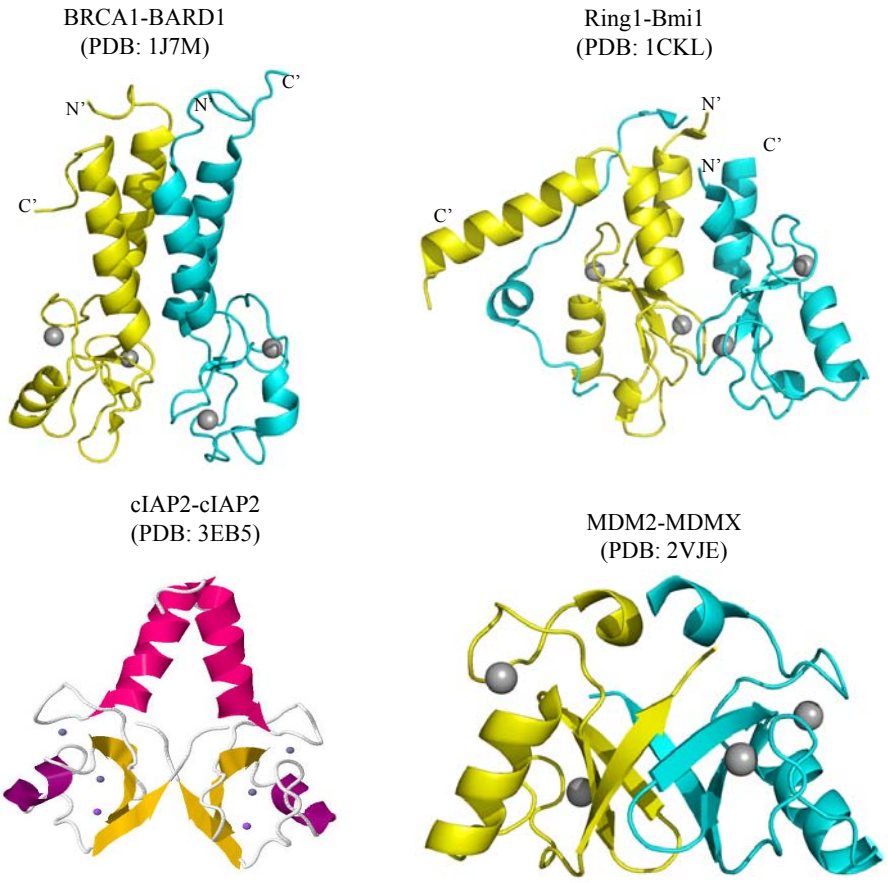

(B)

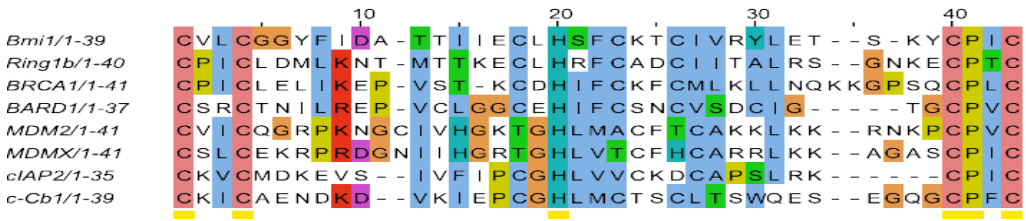

(C)

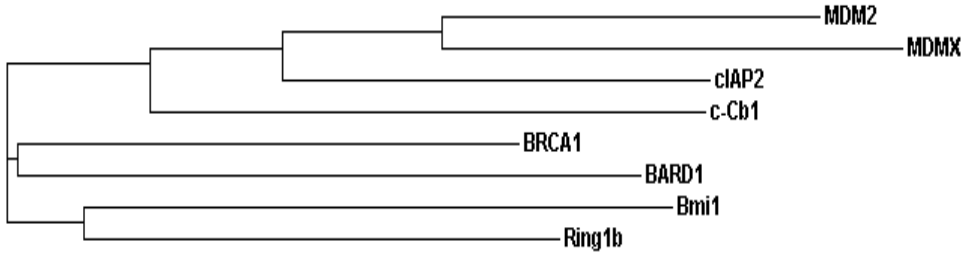

Figure 6-10: Comparison of E3 heterodimer/homodimer and the E2-E3 complex. (A) Overlay of the MDM2– MDMX heterodimer with Ring1b-Bmi1 heterodimer and BRCA1-BARD1 heterodimer. The structure of cIAP2 homodimer has higher similarity to MDM2-MDMX and both dimerise through their C-terminal β-sheet. Four zinc ions seen in these homodimers/heterodimers are shown in gray. BRAC1, Ring1, and MDM2 are coloured yellow, and BARD1, Bmi1 and MDMX are coloured cyan. (B) Sequence alignment of the RING domain of E3 proteins prepared using the MyHints. Yellow bars below the sequences represent highly conserved residues. (C) Phylogram of the RING domains of E3 proteins, the distance represents their evolutionary relationship.

(A)

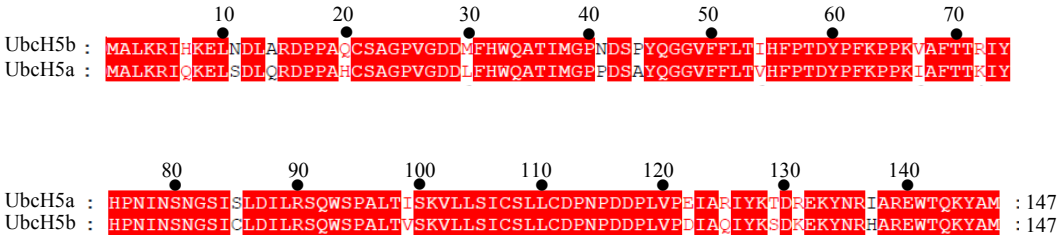

(B)

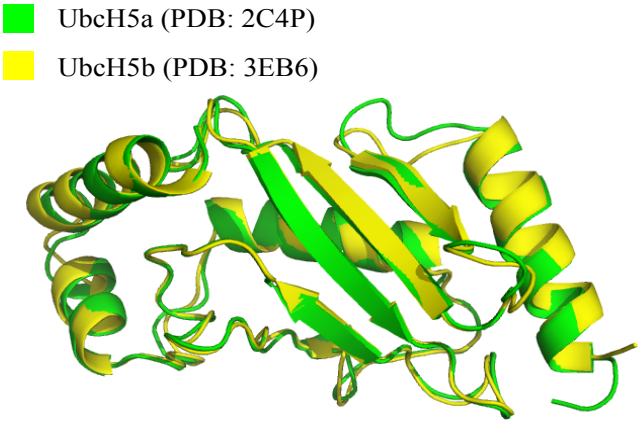

Figure 6-11: Comparison of UbcH5a and UbcH5b. (A) Sequence alignment and (B) superposition of the two structures.

To build a model structure of the UbcH5b-MDM2 complex, the MDM2 molecule from the MDM2/MDMX complex (PDB: 2VJE) was superimposed onto the cIPA2 molecule of the UbcH5b-cIAP2 complex (PDB: 3EB6) (Figure 6-12). In this work, we used the TopMatch program, which is a suite of computational tools for the alignment and superposition of protein structures (http://topmatch.services.came.sbg.ac.at/) (Sippl & Wiederstein, 2008; Sippl, 2008). We also superpositioned the MDM2/MDMX heterodimer onto other E2-E3 structures, such as CHIP-Ubc13 or cCbl-UbcH7. In addition, previous work has described that while the RING domains of E3 proteins are very different in their amino acid sequences, they have a conserved functional structure. These superposition results revealed that the RING domain of MDM2 overlaid well with all the RING domains of these E2-E3 proteins (Figure 6-12). The overlay with cIAP2-UbcH5a was particularly close (r.m.s.d. of 1.3 Å over the 121 Core Cα atoms). MDM2 also has this conserved functional structure for interaction with E2 proteins: the α helix in MDM2 or in other E3 proteins play a critical role in the interaction with the N-terminal fragments of E2 proteins (Figure 6-12).

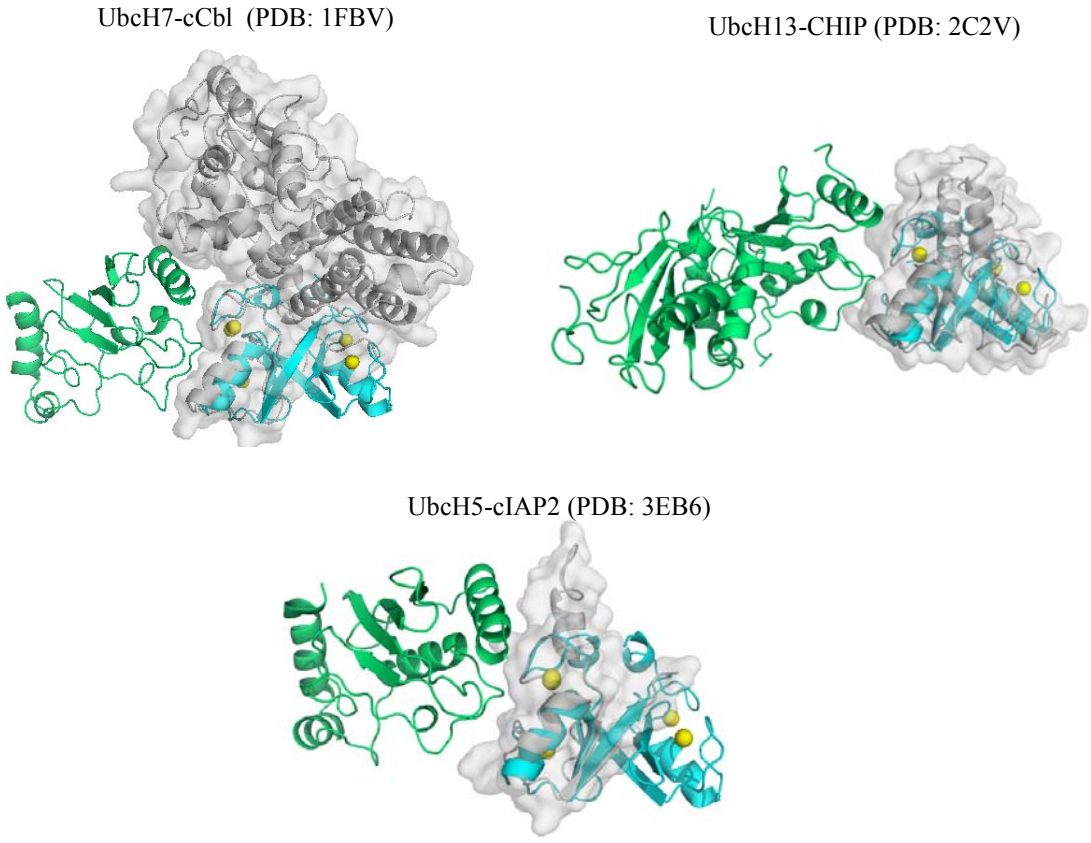

Figure 6-12: Schematic representation of the superposition of MDM2-MDMX heterodimers onto other E2-E3 complexes. (A) UbcH7-cCbl (PDB: 1FBV); (B) Ubc13-CHIP (PDB: 2C2V); (C) UbcH5b-cIAP2 (PDB: 3EB6). MDM2-MDMX heterodimer is shown in cyan, other E3 proteins are shown in grey, E2 proteins are shown in lime green and zinc ions are depicted as yellow spheres.

- ***A more detailed view of a new model of the UbcH5a-MDM2 complex***

After the model of the UbcH5b-MDM2 complex was generated, closer inspection of the complex showed that there were no clashes with UbcH5b. Crystal structures of the RING domain of MDM2, cIAP2, UbcH5b are shown in cyan, yellow and green, respectively (Figure 6-13A). Both E3s have similar ββαβ structures (Figure 6-13B). Analysis of the sequence alignment reveals that MDM2 has additional residues 448GC449 and 471RNKP474 when compared with the sequence of cIAP2 (Figure 6-13C &D). The model suggests residues 448GC449 extend the β1 of MDM2 and result in a different orientation of the following loop (452HGKT455), located between the β1 and β2 (red circle, Figure 6-13A & B). The loop of MDM2 is orientated away from the surface of UbcH5b. This region is also the ATP-binding site, suggesting that orientation of the loop could be correlated to ATP-binding. Furthermore, the MDM2-UbcH5b model showed that residues in UbcH5b, D59 and F62, were located within 4Å distance around the MDM2 471RNKP474 motif. This suggests that this motif could be critical to interactions with UbcH5b or UbcH5a. Overall, the model of the UbcH5b-MDM2 provides an excellent starting point for virtual screening.

Figure 6-13: A new model of UbcH5b-MDM2. (A) An MDM2 molecule (PDB: 2VJE) is superimposed onto the cIAP2 molecule of UbcH5a-cIPA2 (PDB: 3EB6). MDM2 is shown in cyan, cIPA2 is shown in yellow, and UbcH5b is presented in green surface. The interactive regions of the E2-E3 binding site are the N-loop and the α-β3 loop (shown as arrow). (B) Superimposition of the structure of MDM2RING onto the structure of cIAP2. Red circle highlights the different orientation of the loop 452HGKT456 of MDM2, when compared to that of cIAP2. (C) Sequence alignment of MDM2 and cIAP2. Starred residues illustrate additional interaction seen in MDM2. Magenta bars highlight the ATP binding site (GCIVHGKT) and the RNKP motif. (D) Close up view of the orientation of the loop (452HGKT454, yellow) and the motif (471RNKP474, magenta) of MDM2 to the UbcH5a surface. Residues in blue surface are D59 and F62 in UbcH5a, may interact with the RNKP motif of MDM2.

(A)

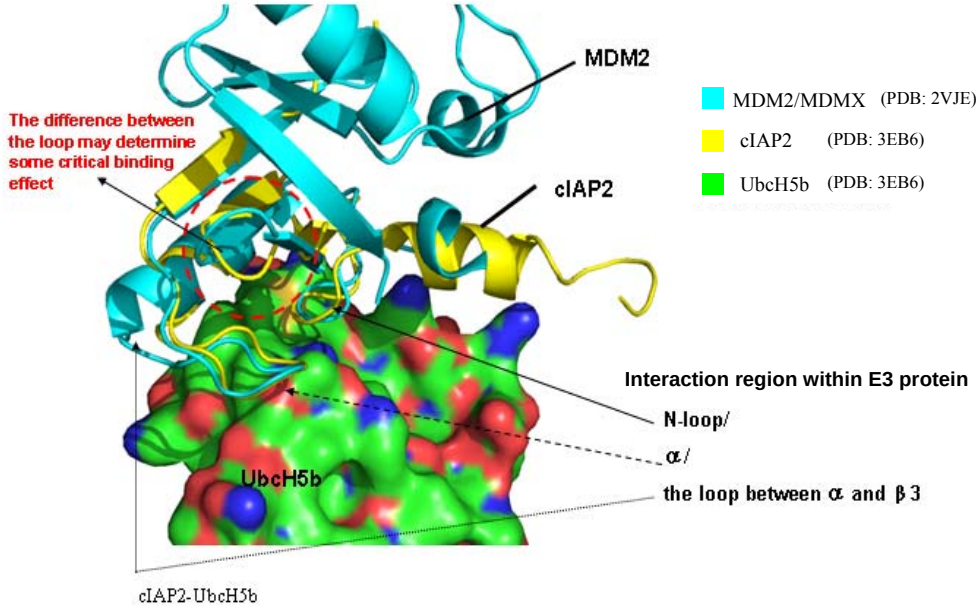
MDM2
The difference between the loop may determine some critical binding effect
cIAP2
MDM2/MDMX (PDB: 2VJE)
cIAP2 (PDB: 3EB6)
UbcH5b (PDB: 3EB6)
Interaction region within E3 protein
N-loop/
α/
the loop between α and β3
UbcH5b
cIAP2-UbcH5b

(B) **(C)**

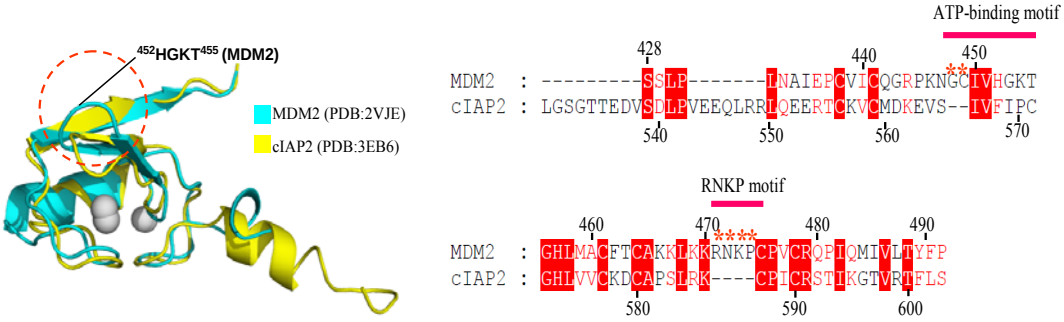
452HGKT455 (MDM2)
MDM2 (PDB:2VJE)
cIAP2 (PDB:3EB6)
ATP-binding motif
MDM2 : ---------SSLP-------LNAIEPCVICQGRPKNGCIVHGKT
cIAP2 : LGSGTTEDVSDLPVEEQLRRLQEERTCKVCMDKEVS--IVFIPC
RNKP motif
MDM2 : GHLMACFTCAKKLKKRNKPCPVCRQPIQMIVLTYFP
cIAP2 : GHLVVCKDCAPSLRK----CPICRSTIKGTVRTFLS

(D)

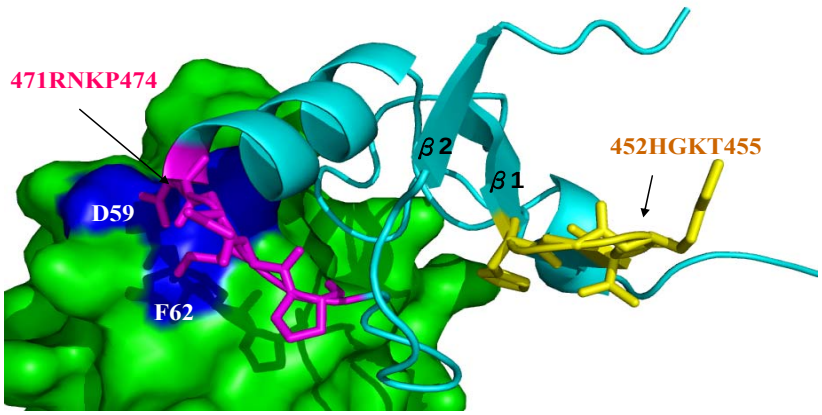
471RNKP474
D59
F62
β2
β1
452HGKT455

6.5 Drug target site (2): the UbcH5a-binding site of MDM2

In this section, the aim was to find small molecules that could bind to the UbcH5a binding site of MDM2 and disrupt the E2-E3 interaction. The virtual screening strategy adopted included the following steps: (1) define and characterise the target site, the UbcH5a-binding site of MDM2, (2) create a docking template using UFSRAT, (3) simulate the putative binding interaction using Autodock, and (4) evaluate the effect of small molecules on the E3 activity of MDM2 by an *in vitro* ubiquitination assay (Figure 6-14).

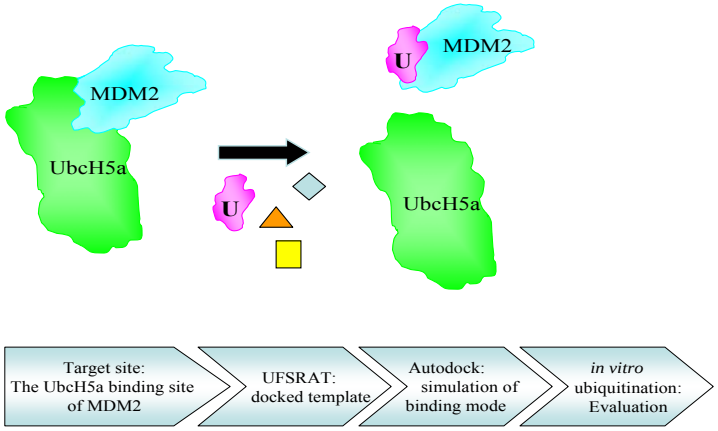

Figure 6-14: Graphical representation of the aims of the project and the virtual screening strategy employed. The UbcH5a-binding site in MDM2 is characterised and defined. Small molecules including the U series (shown in magenta) are hypothesised to bind to the UbcH5a-binding site of MDM2 (cyan) as above.

6.5.1 Define the target site in the UbcH5a-binding interface of MDM2

A model of the UbcH5b-MDM2 complex was built; residues in the interface between the two proteins are likely to be involved in the interaction and therefore it is necessary to carefully define these residues. Since there is no crystal structure available, the putative E2-binding residues in MDM2 were predicted based on the known structures of cIAP2-UbcH5b. On the basis of the cIAP2-UbcH5b crystal structure, several residues of cIAP2 involved in the interaction with UbcH5b are highlighted in Figure 6-15A: Glu553, Val559, Met561, Asn562, Leu585, Pro589, and Arg592. The interface residues in MDM2 are Ala434, Val439, Ile440, Gln442, Leu468, Pro476, Val477 and Arg479 (Figure 6-15A). Consistent with our putative E2-binding residues, previous mutagenesis data show that I440, L468, P476 and

R479 MDM2 mutants abolished MDM2 E3 activity, V439 reduced E3 activity (Linke et al., 2008). Previous work also indicates that there is a conserved shallow groove shared by these E2-E3 complexes, including cIPA2-UbcH5b, c-Cbl-UbcH7, and CHIP-Ubc13 (Mace et al., 2008). This E2-binding groove is surrounded by a small hydrophobic region at the centre of the E2-binding site, with an acidic region toward the N-terminal end and an arginine residue on the C-terminal side (Mace et al., 2008; Zhang et al., 2005; Zheng et al., 2000). To determine whether our putative UbcH5a-binding site has a similar groove in MDM2RING, residues that might interact with UbcH5b were highlighted on the surface of MDM2 RING (Figure 6-15B). The selected MDM2 residues have similar characteristics to those of the E2-binding residues in cIPA2, and are also very similar to those seen in c-Cbl and CHIP. The corresponding E2-binding site in MDM2 also includes a hydrophobic centre, a conserved arginine residue (R479), and an acidic group. The E2-binding site within those E3 proteins has distinct contacts around the major E2-binding site and those additional contacts may determine the specificity of the E2-E3 interaction. Overall, the target site of the UbcH5b-binding site in MDM2 was defined for our virtual screening system shown in Figure 6-15.

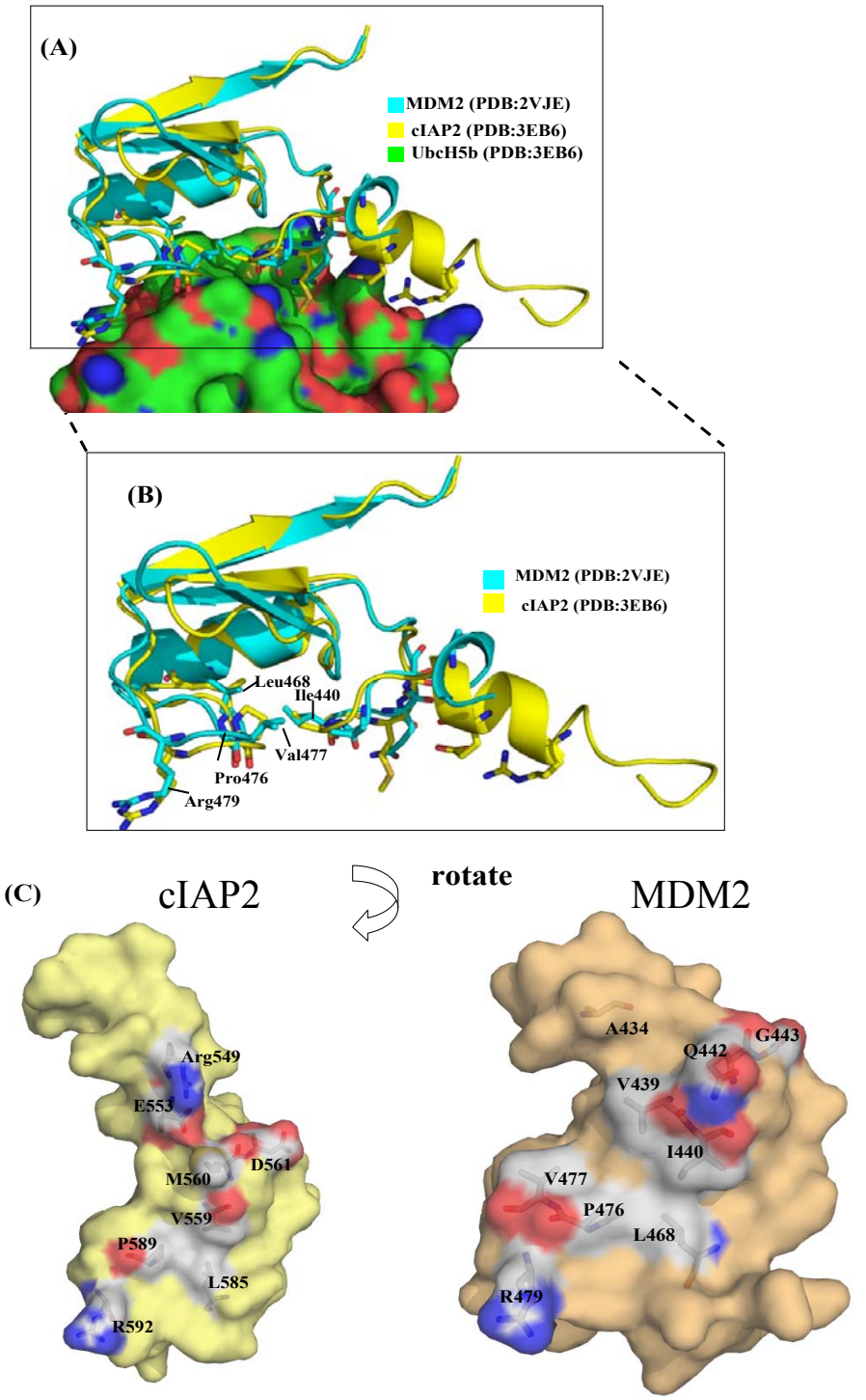

Figure 6-15: Conserved features of the E2-binding groove on E3 proteins. (A) Schematic representation showing the known UbcH5b-binding residues in cIAP2 (yellow sticks) and the equivalent residues in MDM2 (in cyan residues) orientate to the E2 surface (in green). (B) Close-up view of the corresponding E2-binding residues of MDM2 to cIAP2. (C) There is a shallow groove on each E3 protein: a hydrophobic centre (white), acidic region (red), and a conserved Arg residue (blue). cIPA2 and MDM2 are shown coloured in light yellow and light orange surface representation, respectively. Residues of E3 ligases involved in the E2-binding interaction are shown as sticks.

6.5.2 Virtual screening results of the UbcH5a-binding site of MDM2

Because our aim is to find small molecules to bind to the E2-binding site of MDM2, an appropriate template for our virtual screening system will be residues of the MDM2-binding partner, UbcH5a. Although our model was the MDM2/UbcH5b complex, UbcH5a has high sequence identity with UbcH5b and both are MDM2 cognate E2 proteins. Therefore, residues of UbcH5b involved in the E2-E3 interaction are suitable candidates to define a template for drug design. To define which residues in UbcH5b are most appropriate to act as our template, the cIAP2-UbcH5b structure and data from previous work carried out in the group were used as references. Until now, there is only one structure of the UbcH5b-RING type E3 complex, the UbcH5b-cIAP2 (Mace et al., 2008). Residues of UbcH5b, Met1, Lys4, Arg5, Lys8, Glu9, Asp12, Arg15, Pro61, Phe62, Gln92, Ser94, Pro95, Ala96 and Thr98 confer cIAP2-binding (Mace et al., 2008). The UbcH5c-BRCA1 interaction studied by NMR and chemical shift analysis indicated that Arg5, Lys8 and Ala96 in UbcH5c are required for binding of BRCA1 (Christensen et al., 2007). Based on previous studies, we decided to utilise the same residues of UbcH5b, which interact with cIAP2, as our template candidates. Presumably, those equivalent residues are likely to be involved in interaction with MDM2. In Figure 6-16, we presented the interface of MDM2-UbcH5b, and also showed the putative MDM2-binding residues in UbcH5b. Most candidate residues were in the groove (hydrophobic patch) and some were outside of the hydrophobic groove and those residues may provide specificity for the E2-E3 interaction (Figure 6-16).

Figure 6-16: Residues potentially involved in the interaction between MDM2 and UbcH5b. (A) Schematic representation shows the residues responsible for the UbcH5b-MDM2 interactions. UbcH5b and MDM2 are shown as green and cyan surface, respectively. Residues of MDM2 and UbcH5b in the interaction surface are shown in sticks and coloured white and yellow. (B) A flow chart of the virtual screening strategy used to find UbcH5b-mimetic small molecules, U-series compounds (in magenta), in the UbcH5b-binding site of MDM2. Atom types are also depicted (C=white or yellow or magenta, O=red, and N=blue).

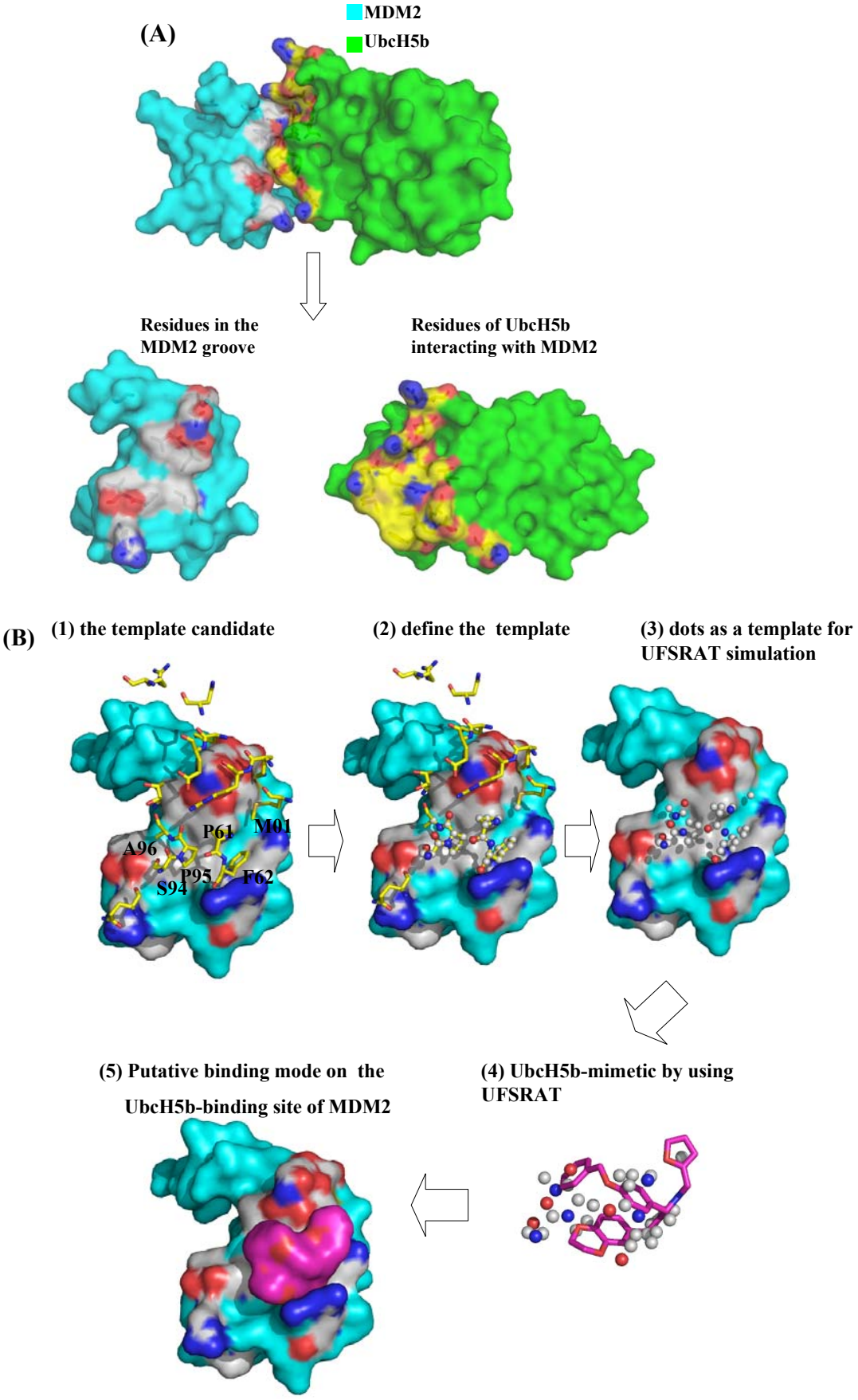
(A)
MDM2
UbcH5b
Residues in the MDM2 groove
Residues of UbcH5b interacting with MDM2
(B)
(1) the template candidate
(2) define the template
(3) dots as a template for UFSRAT simulation
A96
P61
M01
P95
F62
S94
(4) UbcH5b-mimetic by using UFSRAT
(5) Putative binding mode on the UbcH5b-binding site of MDM2

Residues in E2 proteins mostly interact with residues in the groove of E3 proteins. For example, in the complex of cCbl-UbcH7, Phe62, Phe62, Pro97 and Ala98 of UbcH7 interact with most residues in the cCbl groove regions, Ile383, Cys404, Ser407, Trp408, Pro417, Phe 418 and Arg420 (Zheng et al., 2000). In the Ubc13-CHIP U box, there is a similar binding pattern, Arg7, Lys10, Met64, Ser96, Pro97, and Ala99 of Ubc13 interact with a hydrophobic groove in CHIP, such as Phe238, Ile236 and Pro270 (Zhang et al., 2005). This data suggested that residues in UbcH5b which are around the E2-binding area of MDM2 may provide the major binding interactions with MDM2. The MDM2-binding residues of interest in UbcH5b were non-continuous; therefore an alternative approach was used to determine the template. The template for UFSRAT shown in dots in Figure 6-16B was generated based on the distributions of the atoms of Met1, Pro61, Phe62, Ser94, Pro95 and Ala96 of UbcH5b. The final template was located in the centre of the hydrophobic groove. There are some charged MDM2 residues around that might provide some additional binding. Since the target site, the UbcH5a-binding site of MDM2, and the template for UFSRAT simulation have been determined, virtual screening could be used to search for UbcH5b-mimetic antagonists of MDM2.

1000 small molecules from the EDULISS database were chosen following a UFSRAT run based on their UbcH5b-mimetic conformations (step 4, Figure 6-16B). Next, Autodock simulations were used to predict the putative binding mode, energy, and affinities. Following this second round of screening, 200 compounds were selected and ranked by their putative binding affinities to MDM2 (step 5, Figure 6-16B). Estimated binding affinities of those compounds ranged from 117.8 nM to 94.5 μM, with binding energies of from -9.5 kcal/mol to -5.5 kcal/mol. The mimetic compounds with the optimum binding mode to the target (Figure 6-17), good solubility and low toxicity were selected. The top hit molecules were manually inspected based on the putative binding model, binding affinity and the solubility, nine were selected and purchased from Spec. Co. (Table 6-2) Effects of those UbcH5b-mimetic antagonists, or U-series compounds were evaluated by *in vitro* ubiquitination experiments.

Figure 6-17: The estimated binding modes of small molecules bound to the UbcH5a-binding site of MDM2 were shown. Small molecules (U-series, U01 ~ U09) are shown in magenta sticks and the template candidate for virtual screening (yellow sticks). MDM2 is coloured in cyan. The residues located around the UbcH5a-binding site of MDM2 are coloured based on the atomic properties of the residues.

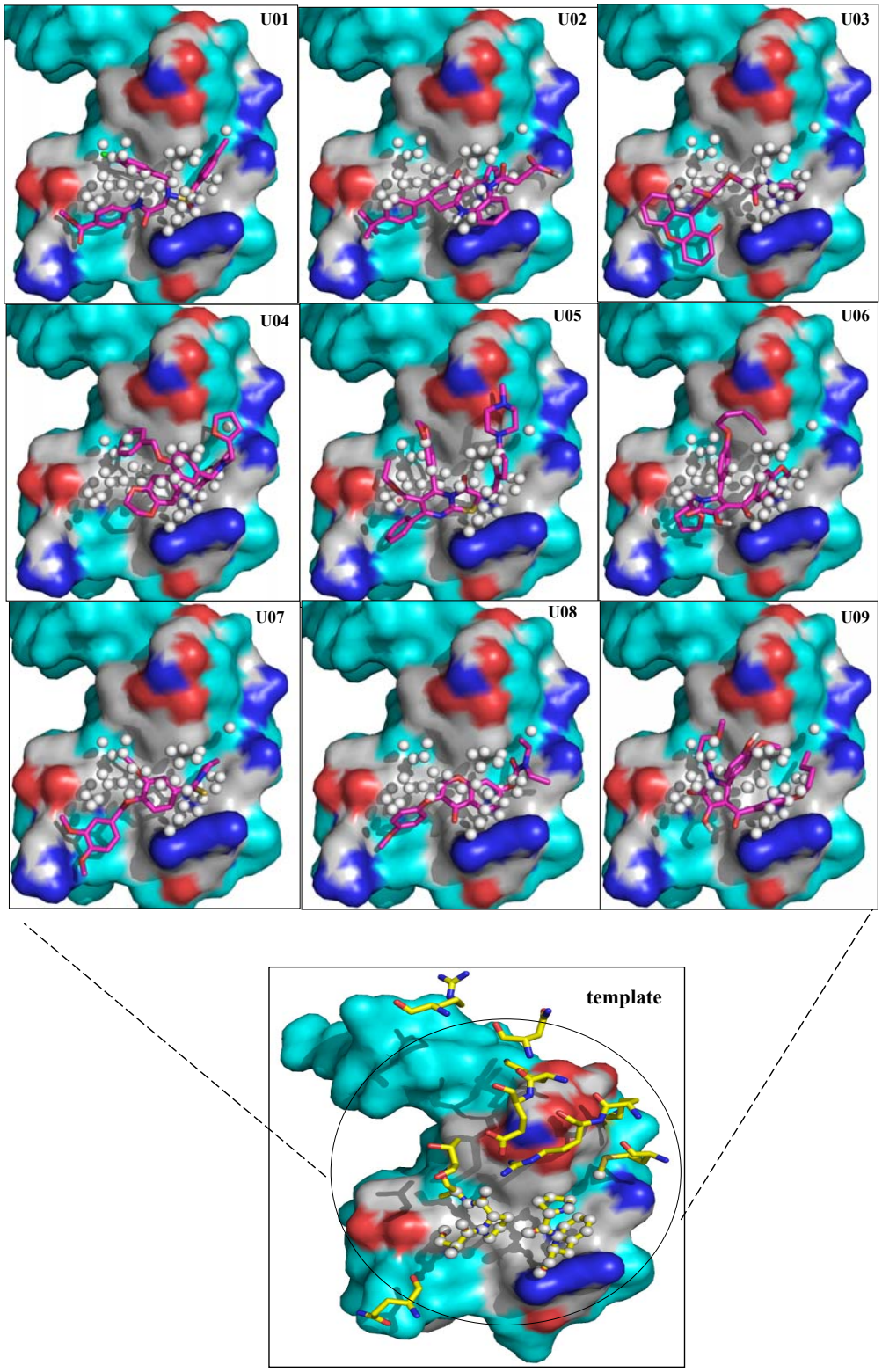

Table 6-2: Characteristics of the U-series compounds. The chemical structures of these U-series compounds are shown in the table. All of those compounds are purchased from Spec Co. Molecular weight (M.W.), LogP are also shown. Estimated △G and estimated binding affinity of each compound with the target are calculated by AutoDock.

	Chemical structure	△G (kcal/mol)	estimated binding affinity	LogP	M.W.
U01	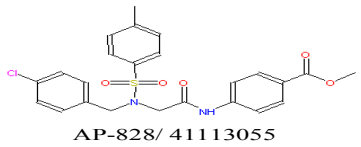 AP-828/ 41113055	-9.5	111.8 nM	4.9	487.0
U02	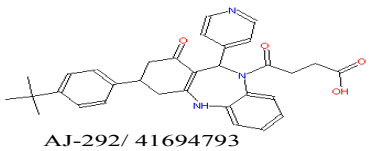 AJ-292/ 41694793	-8.4	674.1 nM	4.3	523.6
U03	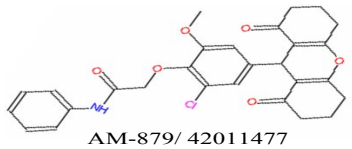 AM-879/ 42011477	-7.0	7.1 μM	2.9	508.0
U04	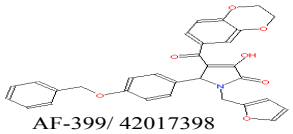 AF-399/ 42017398	-7.0	7.0 μM	4.2	523.5
U05	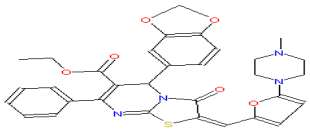 AN-698/ 40716539	-6.7	13.2 μM	3.9	598.7
U06	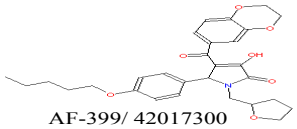 AF-399/ 42017300	-6.5	18.3 μM	4.1	507.6
U07	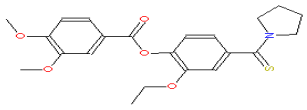 AN-698/ 41081135	-6.0	39.6 μM	4.4	415.5
U08*	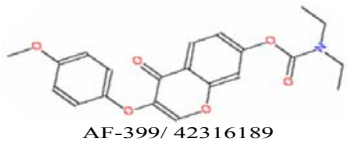 AF-399/ 42316189	-5.9	52.3 μM	3.7	383.4
U09*	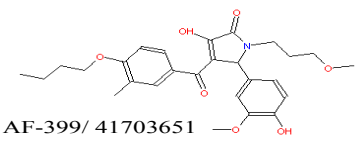 AF-399/ 41703651	N.D.	N.D.	3.3	483.6

6.5.3 Evaluation of UbcH5a-mimetics on MDM2 E3 activity

Effects of the UbcH5b mimetic antagonists (U-series compounds) on MDM2 E3 ligase activity were evaluated by an *in vitro* ubiquitination assay. In this work, two MDM2 proteins were used: FLMDM2 and MDM2RING. Different effects were seen with these compounds on FLMDM2 and MDM2RING (Figure 6-18). In these experiments, 500 μM compound was incubated with FLMDM2 or MDM2RING for 10 minutes, and the other components required for *in vitro* ubiquitination were added (ubiquitin, E1, UbcH5a, p53). The reaction time for *in vitro* ubiquitination was 10 minutes and then 2X loading dye was added to stop the reaction. The ubiquitination levels of p53 were detected by an anti-p53 antibody, D01, as discussed earlier in Chapter 3. Initially, our results showed that 500 μM U05 activated FLMDM2 E3 ligase activity significantly, for example, more ubiquitin was attached to p53, (Figure 6-18A, work carried out by Dr. Susanne Patterson). U02, U4, and U06 slightly inhibited FLMDM2 E3 activity. However, subsequent experiments could not replicate this result. In subsequent experiments, U05 had lost its activity, and no strong ladders of ubiquitinated-p53 were observed on the gel (Figure 6-17B). It is likely that U05 is unstable or the activity was caused by an impurity in the initial batch of compound.

(A)

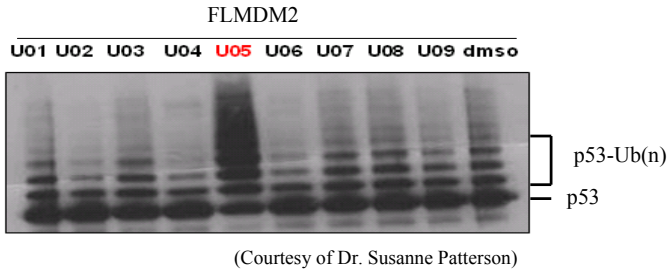

(Courtesy of Dr. Susanne Patterson)

(B)

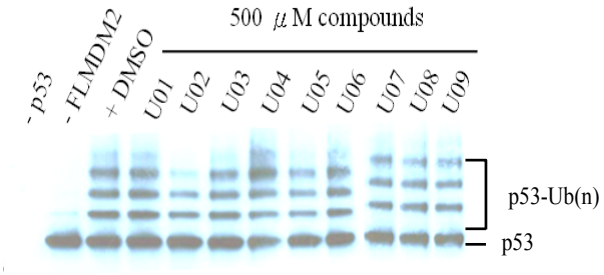

Figure 6-18: Evaluation of U-series compounds to FLMDM2 E3 activity. (A) 500 μM U-series compounds are tested in this work. U05 is found to activate FLMDM2 E3 activity. This experiment was carried out by Dr. Susanne Patterson. (B) U05 lost its activation effect MDM2 E3 activity after several weeks.

- ***The potential interaction between U05 and MDM2RING***

On the basis of the model of the U05-MDM2 complex, the distances of those MDM2 residues Val439, Ile440, Gln442, Leu468, Arg471, Lys473, Pro474, Cys475, Pro476 and Arg479 were within 4Å of the U05 molecule. Those MDM2 residues were consistent with our proposed E2-binding residues. Especially, the atoms of U05 may form H-bonds with the Ile440 carboxyl-amide or carboxyl-oxygen (Figure 6-19A). It is consistent with the report that the equivalent residue in cIAP2 is Val558 which forms an H-bond with Arg5 of UbcH5b (Mace et al., 2008), suggesting that the interaction of U05 and MDM2 is likely to form an H-bond. To test this assumption, more U05-mimetics (Figure 6-19B) were tested.

The chemical name of U05 is ethyl 5-(1, 3-benzodioxol-5-yl)-2-{[5-(4-methyl-1-piperazinyl)-2-furyl] ethylene}-3-oxo-7-phenyl-2, 3-dihydro-5H-[1, 3] diazole [3, 2-a] pyramid- dine-6-carboxylate. Experiments in the Ball group tested the effects of U05 mimetic compounds on MDM2 (Figure 6-19), and the U05 mimetic compounds (HP-series compounds) were solubilised in DMSO, and immediately tested by *in vitro* ubiquitination experiments to determine any effects on FLMDM2. These U05-like compounds activated FLMDM2 E3 ligase activity (Figure 6-18B), behaving in a similar fashion to U05. However, the activating ability diminished in subsequent repeats of the experiments. New U05 compound was purchased, and tested. The result is similar to previous experiments, revealing that U05 or U05-mimetics lose their activation ability possibly due to the instability of U05 and U05-mimetic compounds. Reasons behind the activation of MDM2 E3 activity by U05 or U05-mimetic compounds are still unclear. The MDM2 E3 activity may be activated by one specific chemical that might be essential for the synthesis of these group compounds. Another possible explanation is that these compounds might activate MDM2 E3 activity by an allosteric mechanism. For example, U05 attaches to FLMDM2 inducing a conformational change in FLMDM2, accelerating the rate of transfer of ubiquitin from UbcH5a to the substrate using an as yet unknown mechanism.

Figure 6-19: Evaluation of U05 and U05 mimetic compounds (HP series) on FLMDM2 E3 activity. (A) Schematic representation shows a putative interaction between U05 and MDM2 Ile440. Distances between these putative H-bonds are highlighted in red dashed lines. The MDM2 is shown as a surface in cyan, U05 was magenta stick. (B) The effects of U05 and U05 mimetic compounds are tested on FLMDM2 E3 activity. (C) Chemical structures of U05 and U05 mimetic compounds. The core structure within all compounds was highlighted (in red dashed circle) on U05.

(A)

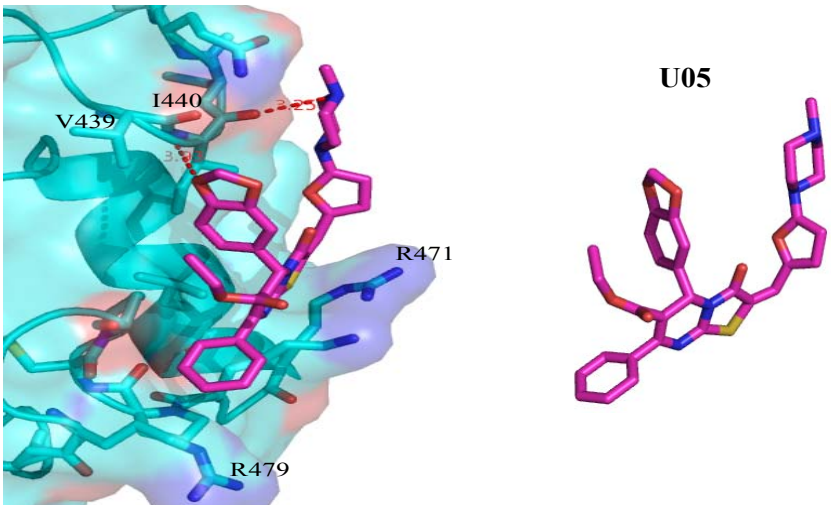

(B)

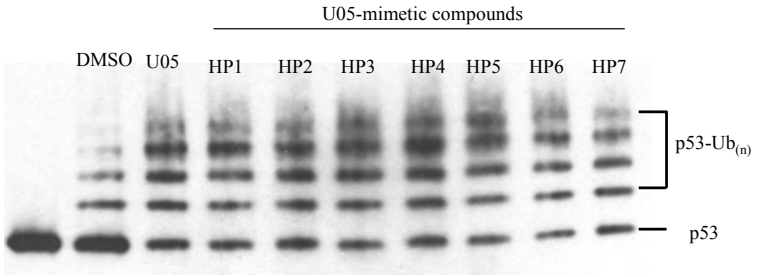

(Courtesy by Vivien Landre)

(C)

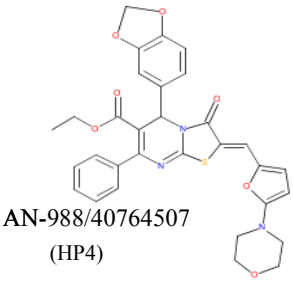

AN-988/40764507
(HP4)

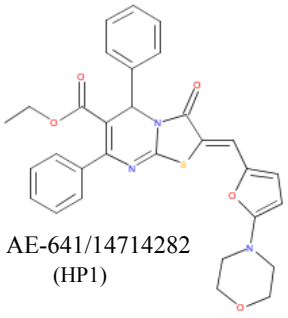

AE-641/14714282
(HP1)

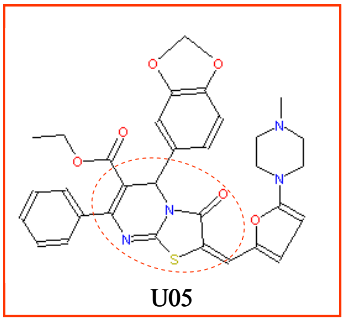

U05

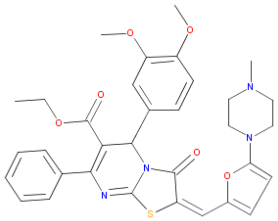

AN-698/40716451
(HP3)

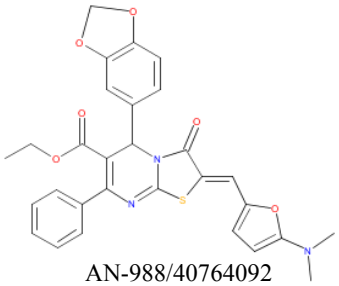

AN-988/40764092
(HP6)

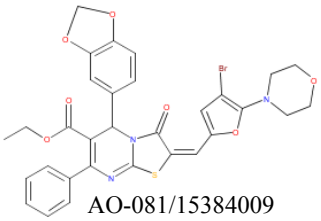

AO-081/15384009
(HP5)

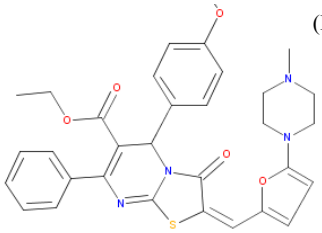

AN-698/40716535
(HP2)

- ***U04 and U06 activate MDM2RING E3 ligase activity***

Different effects of UbcH5b-mimietics on MDM2RING E3 ligase activities were observed. 500 μM U04 and U06 activated MDM2RING E3 activity significantly and several ubiquitinated p53 ladders were observed (Figure 6-20A). U04 and U06 produce different effects on FLMDM2 (inhibition) and MDM2RING (activation). Other compounds, such as U01, U02, U03, U05, U07 and U08 slightly inhibited MDM2RING E3 activity. The chemical formula of U04 is 5-[4-(benzyloxy)-phenyl]-4-(2,3-dihydro-1,4-benzodioxin-6-ylcarbonyl) -1- (2-furylmethyl)-3-hydroxy-1,5-dihydro-2H-pyrrol-2-one, and the chemical formula of U06 is 4-(2,3-dihydro-1,4- benzodioxin- 6- ylcarbonyl)-3-hydroxy-5-[4-(pentyloxy)phenyl]-1- (tetra-hydro-2- furanyl-methyl)-1,5-dihydro-2H-pyrrol-2. Surprisingly, both of them have similar structures but their estimated binding modes were dissimilar (Figure 6-20B). MDM2 residues within 4Å of U04 were Val439, I440, Cys441, Cys464, Lys467, Arg471 and Lys473, whereas within U06 they were Val439, Ile440, Gln442, Cys464, Lys467, Leu468, Arg471, Lys473, Pro474 and P476. A close examination showed that of those two putative complexes there were two possible H-bonds in the U04 and MDM2 Lys467 and Lys473 complex; one H-bond in U06 and MDM2 Lys473 complex (Figure 6-20B). There is one conserved MDM2 residue, Lys473, which might form an H-bond in both complexes.

Figure 6-20: Effects of the U-series compounds on MDM2RING. (A) 500 mM compounds are tested by *in vitro* ubiquitination to evaluate their effects on MDM2RING-mediated ubiquitination of p53. U04 and U06 significantly activate MDM2RING E3 ligase activity. (B) Putative interactions in the U04-MDM2 complex and the U06-MDM2 complex. The H-bonds are highlighted in red dash and the distances are shown. Chemical structures of U04 and U06 are also shown.

(A)

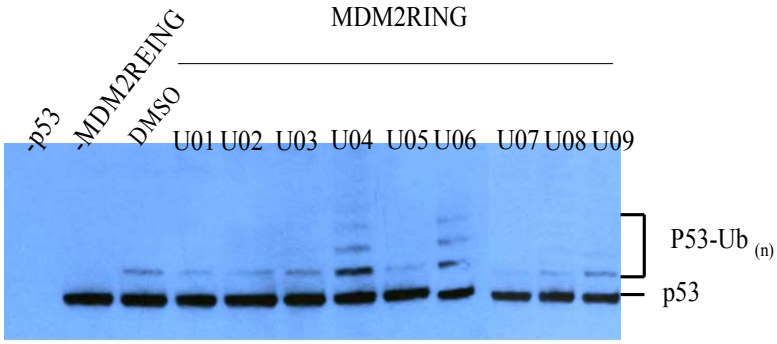
MDM2RING
-p53
-MDM2REING
DMSO
U01 U02 U03 U04 U05 U06 U07 U08 U09
P53-Ub (n)
p53

(B)

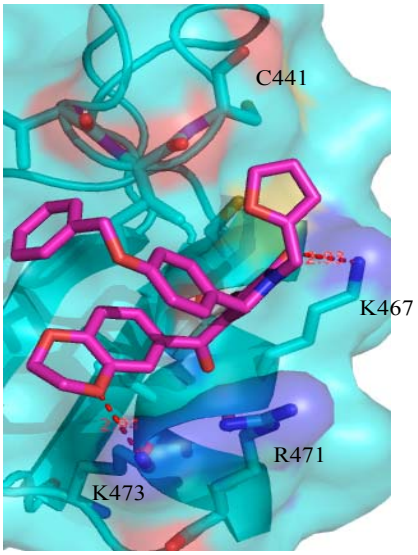
C441
K467
R471
K473

U04

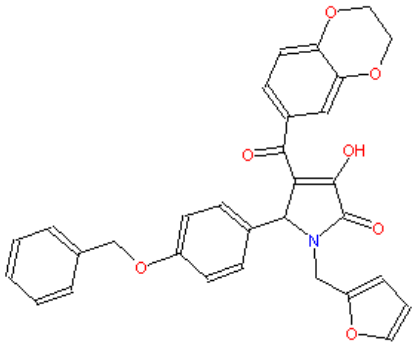
O
O
O
OH
O
N
O
O

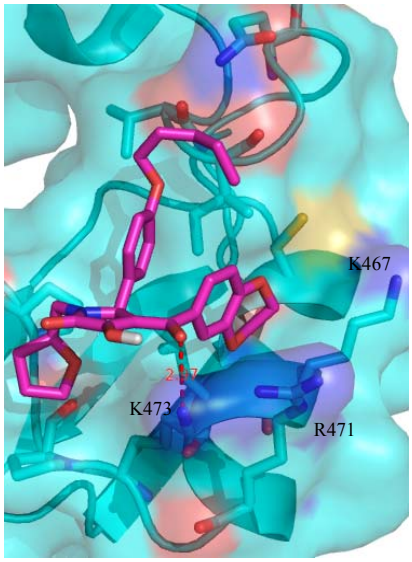
K467
K473
R471

U06

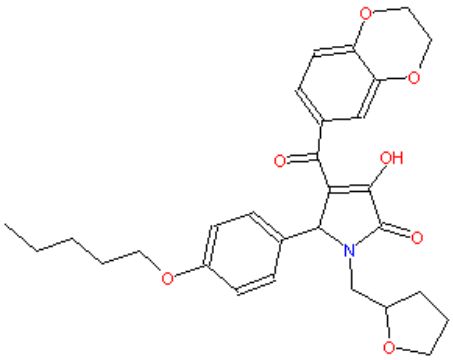
O
O
O
OH
O
N
O
O

- ***A potential mechanism for U04 and U06-mediated activation of MDM2RING E3 activity***

Because Lys473 is located in the α-β3 loop, U04/U06 might interact with Lys473 and the formation of the new H-bond might contribute to the conformational change seen in the C-terminus, β3, moving it from the buried C8-binding site to the surface of UbcH5a. Moreover, previous thermal denaturation experiments (section 5.6.1) had shown that peptide 9 (MDMX-analog peptide), destabilizes binding of UbcH5a. A number of reports suggest that MDM2RING C-terminal domains are responsible for MDM2-mediated ubiquitination. Taken together, we propose a model (Figure 6-21) that UbcH5a or UbcH5a-mimetic compounds (U04 and U06) interact with MDM2RING, affecting the conformation of MDM2RING to expose the C-terminal residues (C-tail) removing it from the C8-binding site and allowing it to interact with UbcH5a. This new conformation allows an increase in the rate of transfer of ubiquitins from UbcH5a to the MDM2 substrate, p53. To determine the binding mode of U04 and U06 with MDM2 RING, we also carried out crystallisation trials. However, no crystals diffracting to high resolution have been obtained.

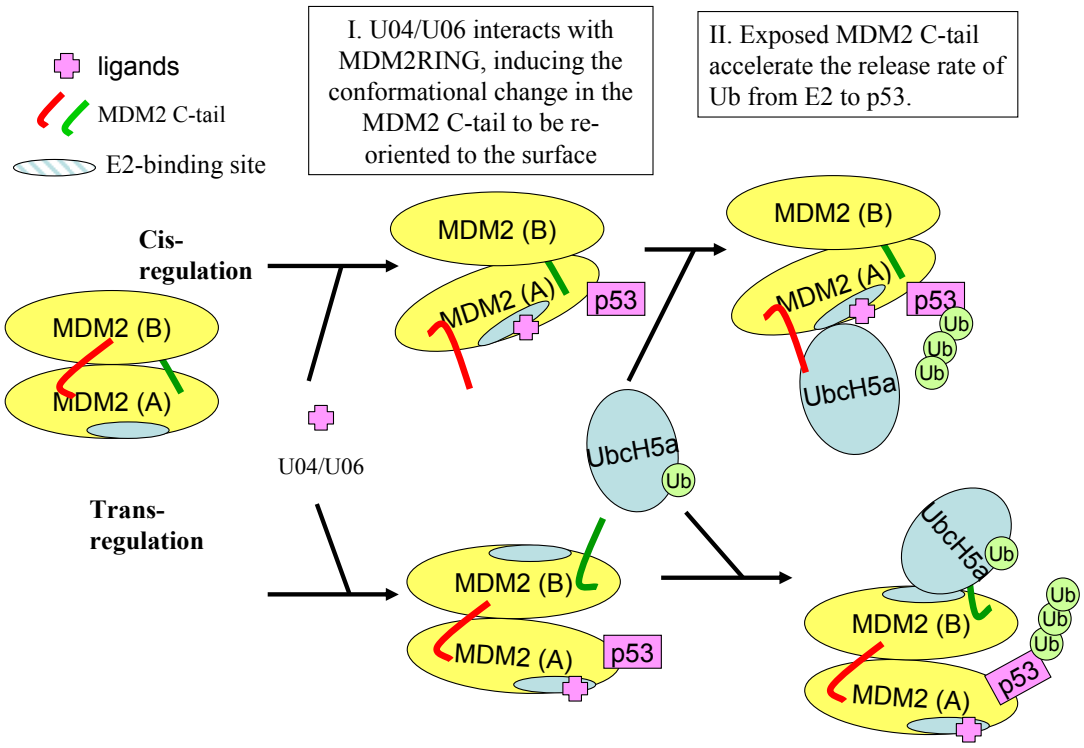

Figure 6-21: Model for UbcH5a-mimetic, U04/U06, mediated activation of MDM2 E3 activity. Our data suggest that UbcH5a or UbcH5a mimetic binds to the E2-binding site of MDM2RING domain may induce the conformational change in the MDM2 C-tail from the C8-binding site to the surface, interacting with UbcH5a (cis-regulation, upper panel; trans-regulation, lower panel) and accelerating the poly-ubiquitination of p53.

- ***Different effects of U04 and U06 on FLMDM2 and MDM2RING E3 activity***

Results show that U04 and U06 contributed differently to the E3 activity of FLMDM2 (Figure 6-19) and MDM2RING (Figure 6-20). We assumed that a remote domain in FLMDM2 is also involved in controlling MDM2 E3 ligase activity. Several reports have mentioned a possible mechanism suggesting remote domains in a protein can regulate the E3 ligase activity (such as IAP protein or CHIP proteins) (Mace et al., 2008; Zhang et al., 2005). IAP antagonist has different levels of autoubiquitination when compared to BIR3-CARD-RING protein and RING alone, showing that those differences may be due to IAP antagonist binding to BIR domains resulting in conformational change affecting its E3 activity (Mace et al., 2008). Moreover, CHIP U-box forms a symmetrical complex with Ubc13, but in the absence of Ubc13, the TPR domain of CHIP occludes the E2-binding site and becomes an asymmetrical dimer (Zhang et al., 2005).

Therefore, it is likely that our FLMDM2 may also occlude the UbcH5a-binding site. UbcH5a is a larger protein and it is possible that UbcH5a binds to another domain within FLMDM2 to induce the conformational change, exposing the E2-binding site. However, small molecules, such as U04/U06, might not provide enough interactions to induce the conformational change of FLMDM2. This idea is supported by the data showing that U04/U06 did not activate FLMDM2 E3 activity (Figure 6-19). In contrast, for the MDM2RING protein, U04/U06 might be able directly to interact with the MDM2RING E2-binding site (Figure 6-21); the evidence comes from the data that U04/U06 activates MDM2 E3 activity (Figure 6-20). Nevertheless, more work is required to investigate and fully understand the mechanism of the E2-E3 interaction, and clarify how remote domains in a protein regulate the E3 ligase activity.

In summary, MDM2 E3 activators were found using our virtual screening system. For future studied, U04 and U06 can be used as the starting templates for a second round of screening.

6.6 Drug target site (3): the MDM2-binding site of UbcH5a

In this section, the aim is to search for small molecules that can bind to the MDM2-binding site on UbcH5a (Figure 6-22). The virtual screening strategy includes defining the target site in UbcH5a, generation of a candidate template using LIDAEUS, and estimation of the docking mode using AutoDock simulation, and finally assaying the effects of those small molecules on MDM2 E3 activities by i*n vitro* ubiquitination.

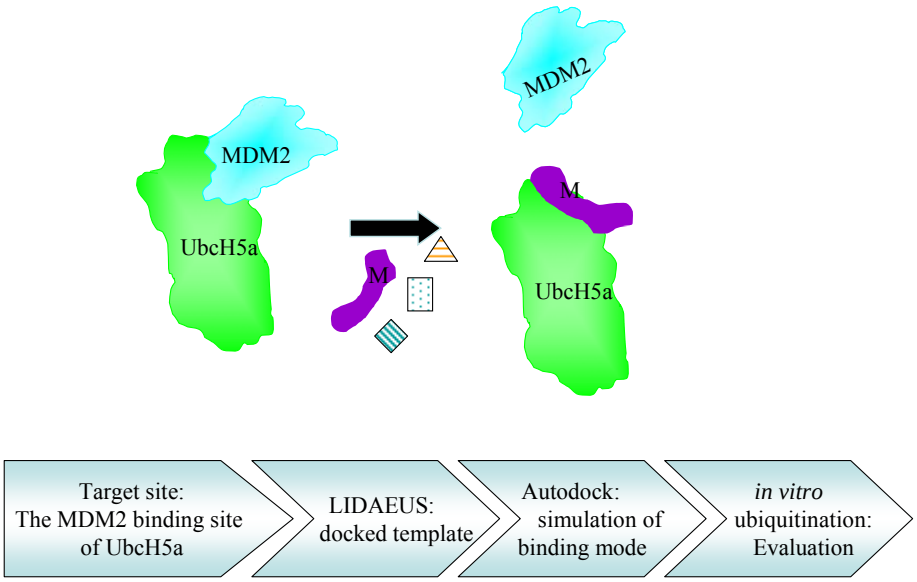

Figure 6-22: Project aim and the virtual screening strategy: small molecules binding to the MDM2-binding site in UbcH5a. Small molecules (purple), M-series, presumably bound to the MDM2-binding site in UbcH5a (green), disrupting the interaction with MDM2 (cyan). The flow chart illustrates the virtual screening process.

6.6.1 Define the MDM2-binding site in UbcH5b

As in previous work, a new model of UbcH5b-MDM2 was used for virtual screening. UbcH5a has 99% similarity and shares almost 89 % identity with UbcH5b (Figure 6-11), showing that UbcH5b is an appropriate drug target model in our UbcH5a-MDM2 study. To design ligands that disrupt the UbcH5a-MDM2 interaction, the structure of UbcH5b-cIAP2 and other relevant data were used as references to define residues important in the interaction (Mace et al., 2008; Zhange et al., 2005). Structures of the UbcH5b-cIAP2 complex and our new model of the UbcH5b-MDM2 complex showed that the N-terminal region of UbcH5b from each complex is involved in E3-binding (Figure 6-23). Previous structural studies showed that the cIAP2-binding residues in UbcH5a were located in α1 helix (Lys4, Arg5, Lys8, Glu9), in the loop of β3-β4 (residues Pro61, and Phe62), and the loop between the 3_{10}

helix and α2 helix (Gln92, Ser94, Pro95, Ala96, and Thr98) (Figure 6-23A) (Mace et al., 2008). Our initial concept was to define the MDM2-binding site in UbcH5b to enable our virtual screening to search for potential ligands. However, on the basis of the crystal structure of UbcH5b-cIAP2 or UbcH5b-MDM2, the residues responsible for interaction with cIAP2 in the UbcH5b surface are extensive and shallow (Figure 6-23B), revealing that this initial target site was not ideal for designing inhibitors of protein-ligand interactions. Therefore, we decided to search for another potential target site in UbcH5b. Detailed analysis of the crystal structure of UbcH5b-MDM2 showed there was cavity near the MDM2-binding surface (Figure 6-23B), which was surrounded by residues Arg5, Glu9, Asp12, Leu13, Thr98, Pro95, Ala96, Ile99 and Ser100 (Figure 6-23C). Numerous reports in literature have discussed the significance of cavities in proteins, providing a critical binding site for protein-protein interactions or protein-ligand interactions (Vassilev et al., 2004). One promising example is the cavity in the MDM2 N-terminal hydrophobic domain that interacts with p53 or p53-peptidomimetics, such as Nutlin.

Figure 6-23: Schematic representations of residues involved in the UbcH5b-cIAP2 or UbcH5b-MDM2 interactions. (A) Residues of UbcH5b (white), cIAP2 (yellow) or MDM2 (cyan) in the E2-E3 interactions are shown in sticks. Cys85 in UbcH5b, an active site for the attachment of ubiquitin is depicted in orange spheres. (B) Upper panel shows the UbcH5b-MDM2 interactions and the interface in UbcH5a were highlighted in white surface representation. Red dashed lines highlight our new target site, which contains a cavity. Residues around the cavity are labelled and the site points for the template candidate used for screening generated using LIDAEUS, based on the chemical features of key residues in the new target site. Different colours represent distinct properties: red dots - hydrogen acceptor, blue dots - hydrogen donor and white dots - hydrophobic atoms.

(A)

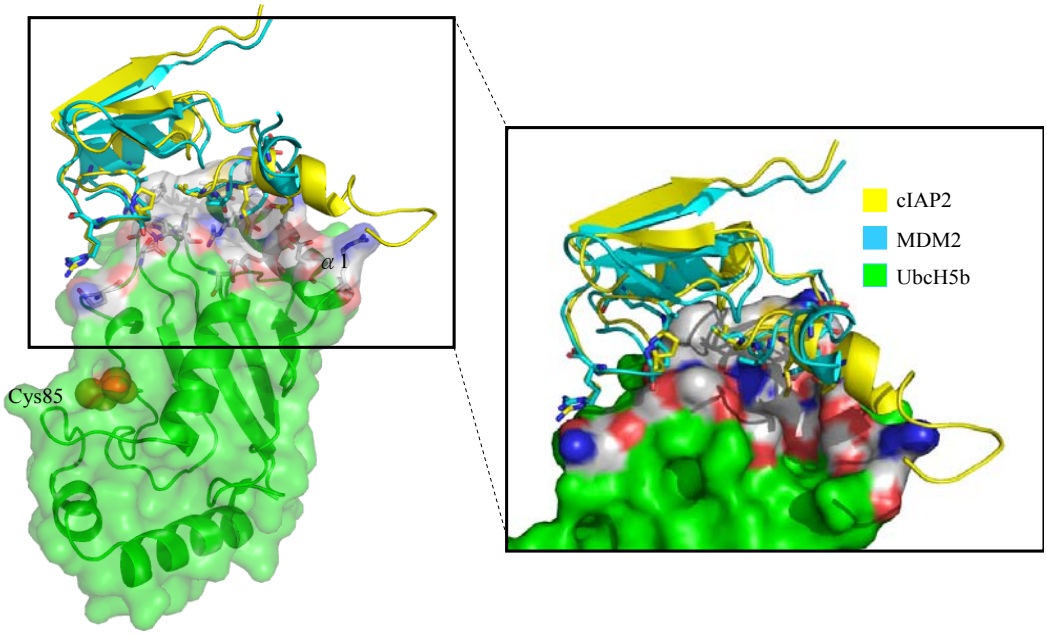
α 1
Cys85
cIAP2
MDM2
UbcH5b

(B)

(C)

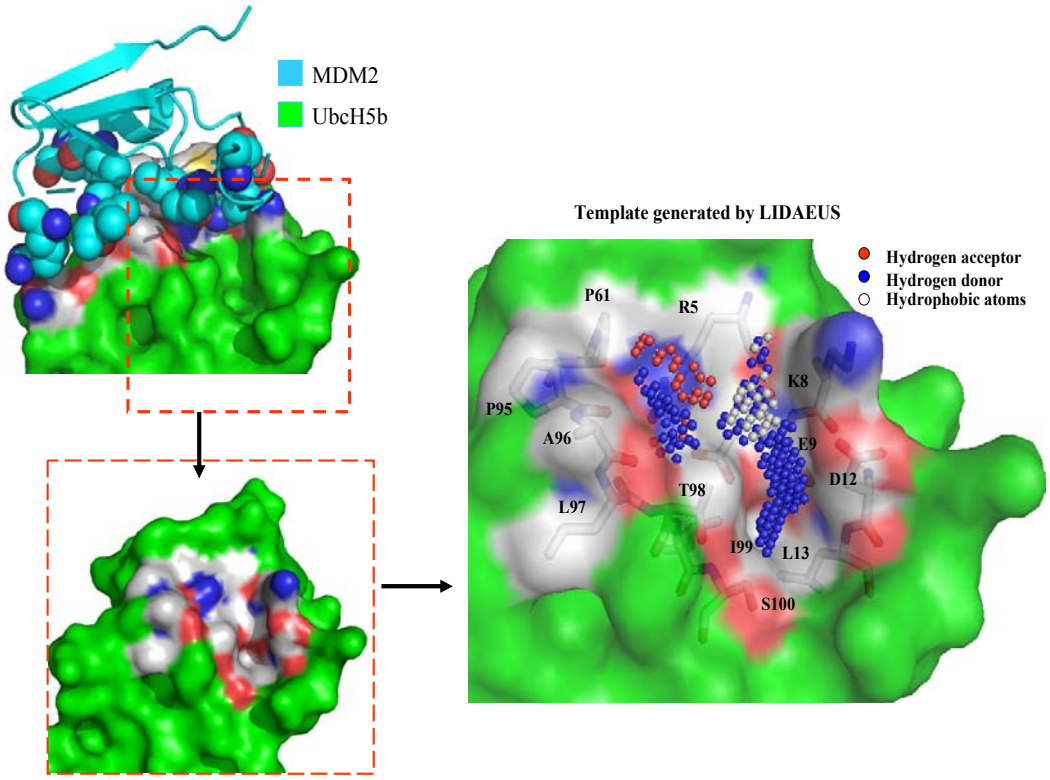
MDM2
UbcH5b
Template generated by LIDAEUS
Hydrogen acceptor
Hydrogen donor
Hydrophobic atoms
P61
R5
K8
P95
A96
E9
D12
T98
L97
I99
L13
S100

6.6.2 Virtual screening data: the E2-binding site of UbcH5a

After the new target site in UbcH5b was selected and characterised, the next step was to set up an initial screening run. The program, LIDAEUS was used to create putative site points as the template. As shown in Figure 6-23C, characteristics of those site points were assigned as hydrogen acceptors (red dots) or donors (blue dots), respectively, based on the surrounding residues of the target cavity. In our model, hydrogen donor (blue) site points were created to interact with the oxygen atoms of Glu9, Asp12, on the right-hand site in new target site and Ala96, Leu97, Thr98 and Ile99 resides in left-hand site. Hydrogen acceptor (red) site points were created for the interaction with UbcH5b residue Arg5. Some hydrophobic molecules (shown in white dots) were assigned to provide additional interaction abilities. Presumably, those site points might make electrostatic or hydrophobic interactions with residues in UbcH5b.

Using a combination of EDULISS and LIDAEUS, 1000 small molecules, possessing similar electrostatic chemical properties as the template (dots, Figure 6-23C) were selected from the 5 million compounds in the database. These, 1,000 compounds were subjected to a second round of screening by Autodock (Figure 6-24). Following AutoDock, 200 potential small molecules were ranked by binding affinity. Using a combination of the results of the estimated binding affinity, binding mode, toxicity and solubility to rank molecules, 10 compounds, the M-series, were purchased to test effects on the target, UbcH5a. Chemical structures of these 10 small molecules (all from Spec. Co.) and their binding energy with the target were shown in Table 6-3. Estimated $\triangle G$ values of those compounds were -8.3 ~ -7.2 kcal/mol and estimated affinities were between 900 nM ~ 5,000 nM.

Figure 6-24: Modelled structures of 10 selected ligands with the target site of UbcH5b. The models are built on the basis of AutoDock simulation and structures are rendered by PyMol. UbcH5b is presented in green surface form. 10 selected ligands (M01 ~ M10) are shown in green sticks. The dots generated using LIDAEUS (As template reference) shown here represent hydrogen acceptor (red), hydrogen donor (blue) and hydrophobic atoms (white**).**

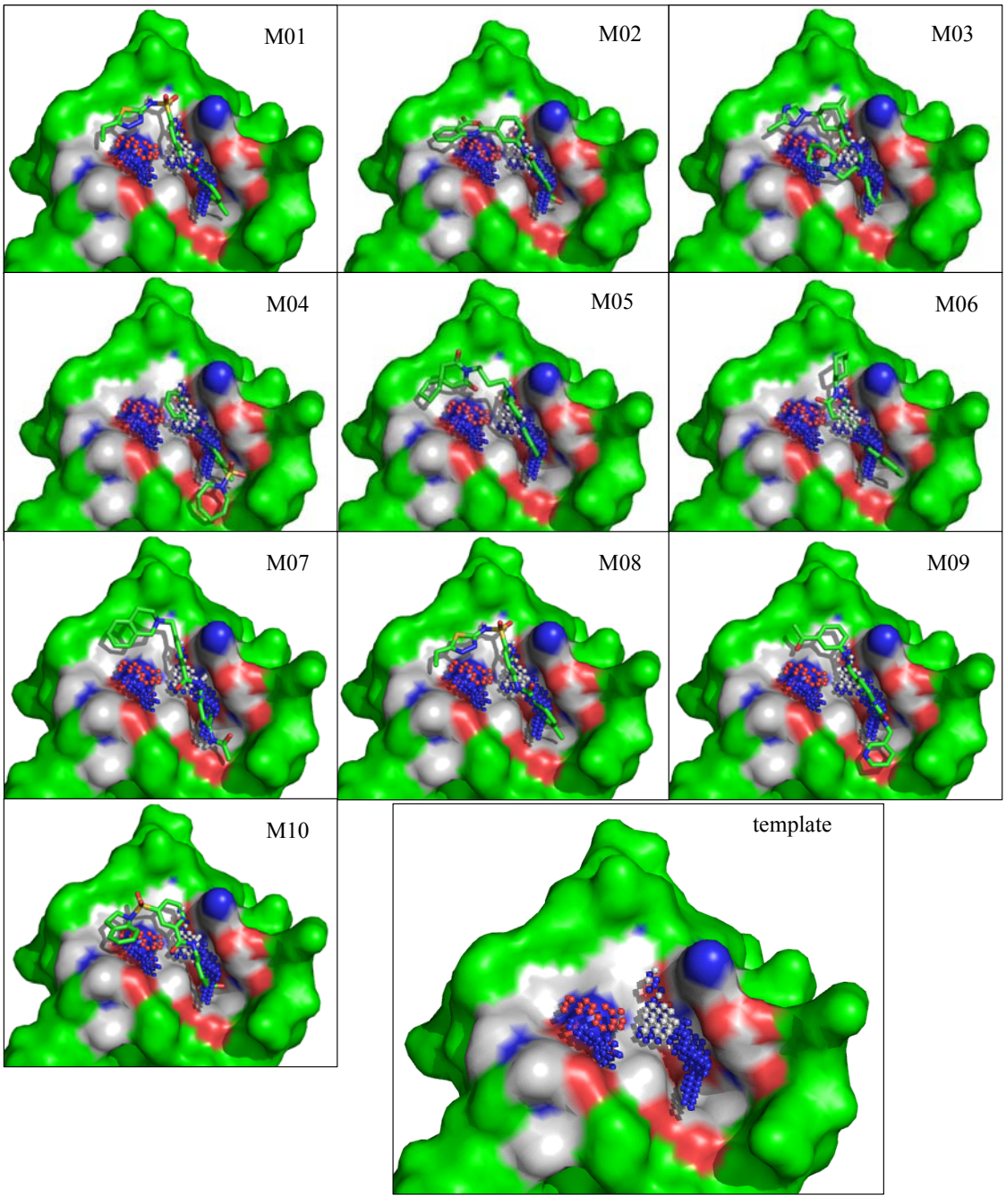

Table 6-3: Characteristics of the M-series compounds. Chemical structures of those M-series compounds are shown in the table. All of those compounds are purchased from Spec Co. Molecular weight (M.W.), and LogP are also shown. Estimated △G and estimated binding affinity of each compound with the target was calculated using AutoDock.

	Chemical structures	△G (kcal/mol)	estimated binding affinity	LogP	M.W.	Hydrogen acceptor	Hydrogen donor
M01*	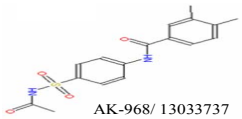 AK-968/ 13033737	-8.3	900 nM	2.5	346.4	5	2
M02	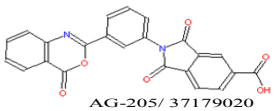 AG-205/ 37179020	-7.6	2.9 μM	2.7	412.4	7	1
M03	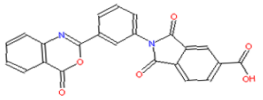 AK-968/ 15602020	-7.5	4.0 μM	3.2	508.1	5	1
M04	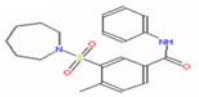 AK-968/ 12440623	-7.4	3.5 μM	3.2	372.5	3	1
M05	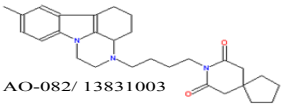 AO-082/ 13831003	-7.4	4.1 μM	3.6	447.6	3	0
M06	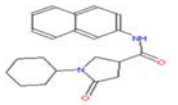 AH-487/ 34800028	-7.3	4.8 μM	2.6	336.4	2	1
M07	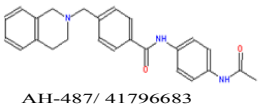 AH-487/ 41796683	-7.2	5.0 μM	3.5	399.5	3	2
M08*	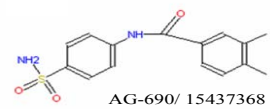 AG-690/ 15437368	-8.3	900 nM	2.3	304.4	5	2
M09*	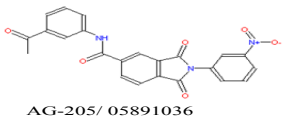 AG-205/ 05891036	-7.3	4.7 μM	3.3	429.4	5	1
M10*	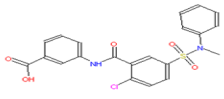 AP-866/ 42031623	-7.3	4.2 μM	3.8	444.9	5	2

6.6.3 *in vitro* ubiquitination studies: effects of the M-series compounds on the UbcH5a-cognate E3 interaction

UbcH5b or UbcH5a interact with E3 ligases, such as MDM2, CHIP or cIAP2, and interfere with E3-mediated ubiquitination. These M-series compounds (M01~M10) could potentially bind to the E3-binding interface of UbcH5b and interrupt the interaction between UbcH5a and E3 ligase, abolishing E3-mediated ubiquitination. Previous reports have shown that each E2 protein can interact with many E3 ligases. The E3-binding sites in E2 proteins are quite similar, but there should be other determinants for specific E3 recognition. Therefore, in these experiments, two E3 ligases, CHIP (U-type E3) and MDM2 (RING-type) were used to verify the specificities of those M-series compounds to distinct E3 proteins. CHIP is a U-type E3 ligase and MDM2 is a RING-type E3 ligase. Compounds were tested at a concentration of 500 mM using MDM2-mediated ubiquitination or CHIP-mediated ubiquitination. Results showed that a number of compounds inhibited MDM2-mediated ubiquitination, including M01, M02, M08, and especially M09 and M10 (Figure 6-25A). Another experiment with CHIP-mediated ubiquitination showed that M01 produced some inhibition whilst M09 showed significant inhibition (Figure 6-25B).

(A)

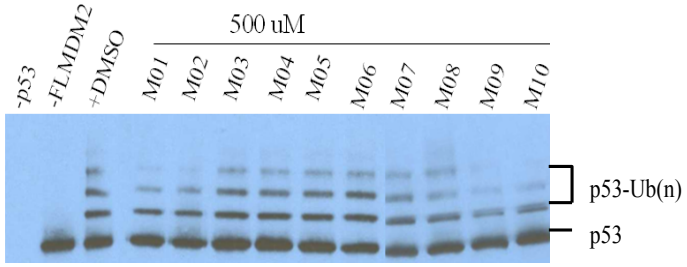

(B)

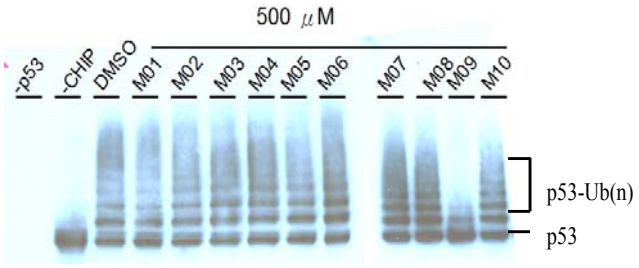

Figure 6-25: The inhibitory abilities of 10 compounds (M-series) are tested using *in vitro* ubiquitination with two types of E3 ligases. (A) RING type E3 ligase, MDM2-mediated ubiquitination and (B) U type E3 ligase, CHIP- mediated ubiquitination.

- ***TDA studies: M09 interacts with UbcH5a***

[The thermal denaturation assay (TDA) was described in greater detail in Chapter 3]

The TDA results showed that M09 induced a significant positive shift in the Tm of UbcH5a, from 58℃ to 79℃ (red line, Figure 6-26). After addition of 25 μM M09 to 2.5 μM UbcH5a, there were two peaks in the Tm panel: one Tm peak was similar to that of apo-UbcH5a at 58℃, with a second peak at 79℃ (Figure 6-26A). The 2.5 μM UbcH5a-250 μM M09 complex produced one peak at 58℃, following with the second peak at 82℃ (Figure 6-26B). This large effect on Tm provides evidence that M09 binds UbcH5a.

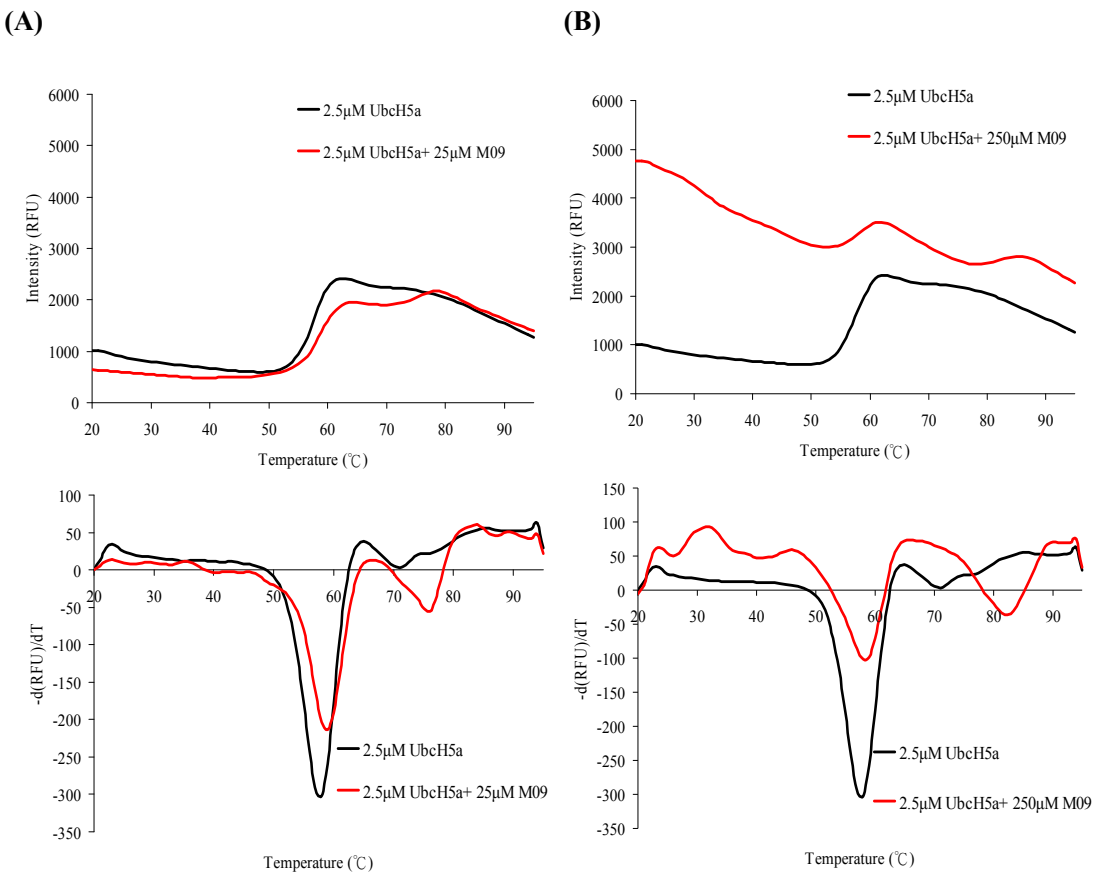

Figure 6-26: The unfolding transition curves of UbcH5a with M09. Apo-UbcH5a, M08-UbcH5a and M09-UbcH5a are, respectively, in red, blue and green lines. (A) with 25 μM compound, and (B) with 250 μM compound.

- ***Potential interactions between M09 and UbcH5a***

Gels showed that M09 could inhibit both CHIP- and MDM2-mediated ubiquitination (Figure 6-25). Moreover, based on previous thermal denaturation assay data (Figure 6-26), M09 seemed to affect the stability of UbcH5a. The putative binding mode of the M09-UbcH5b complex showed that UbcH5b residues, Met01, Lys04, Arg05, Lys8, Glu09, Asn12, Leu13, Pro61, Thr98, Ser100 and Lys101 were located within 4Å distance around the M09 molecule (Figure 6-27), and six putative H-bonds were formed to UbcH5b residues Arg5, Leu13, Thr98 and Ser100. Greater understanding of the interaction between M09 and UbcH5a is required to improve specificity against different E2-E3 interactions. Crystallisation and HSQC NMR experiments were carried out. However, M09 was insoluble at higher concentrations and precluded structural studies of the interaction between UbcH5a and M09.

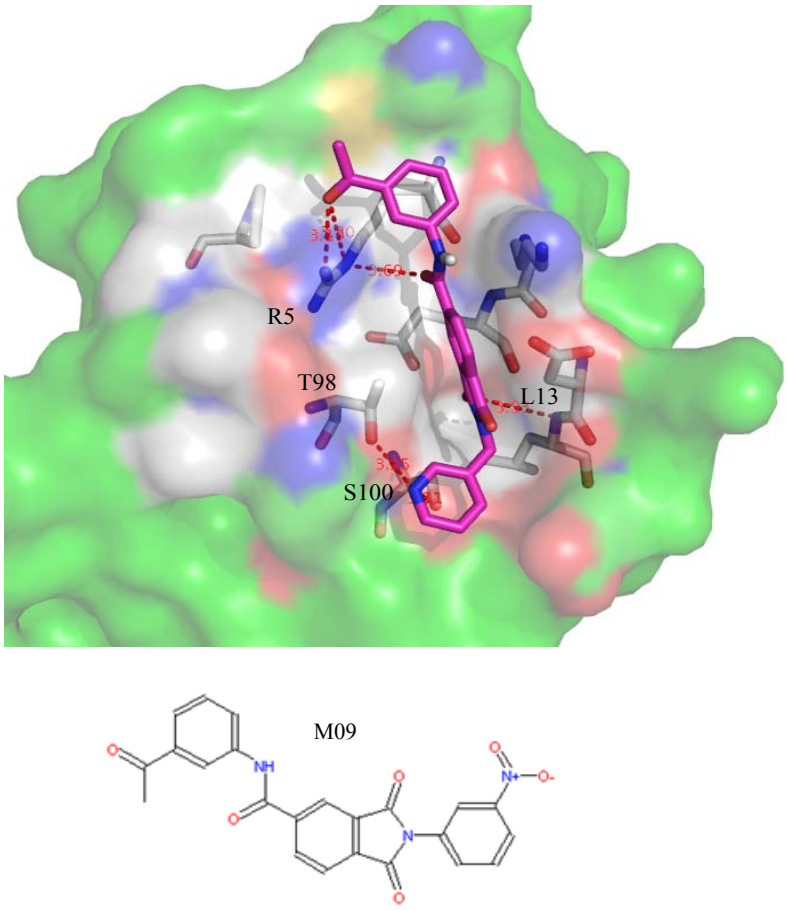

Figure 6-27: Potential interaction between M09 and UbcH5a. Six possible H-bonds in the M09-UbcH5b complex are highlighted in red dashed lines. The chemical structure of M09 is shown. UbcH5b is shown in green surface form. UbcH5b residues interacting with M09 are highlighted in white surface, M09 as magenta sticks. Atom types characterisation were coloured (C=white & magenta, O=red, N=blue).

6.7 Summary

To summarise, using VS, several small molecules have been found to affect MDM2-mediated ubiquitination (Figure 6-28). Several simulation programs were used for VS, including EDULISS (chemical database), UFSRAT (structural similarity simulation), LIDAEUS (rigid body docking), STP (potential binding site detection) and AutoDock (to predict putative binding modes). Those MDM2 E3 inhibitors/activators were chosen from millions of available chemicals. D03, D04, D05 inhibited FLMDM2 E3 activity and D06, D08, D09 and D10 inhibited MDM2RING E3 activity. U05 and U05-like seemed to activate FLMDM2 E3 activity, but the U05 series compound is unstable with time. Furthermore, U04 and its analog U06 both activated MDM2RING E3 activity. M09 inhibited MDM2 and CHIP-mediated ubiquitination of p53.

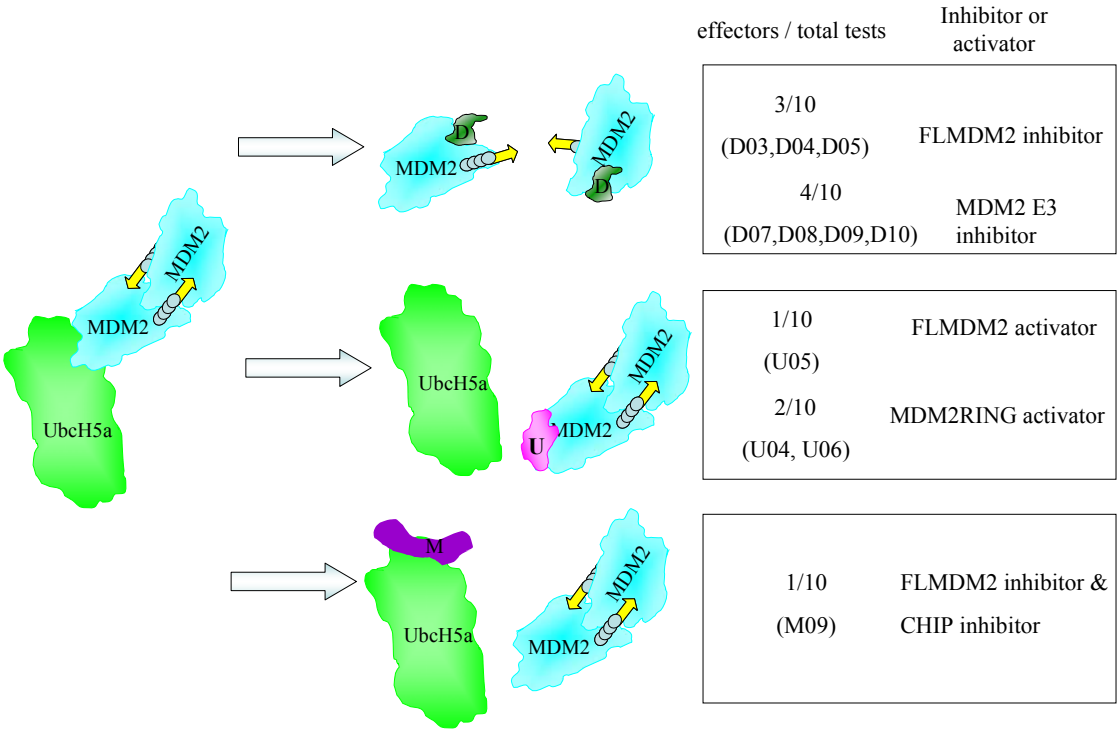

Figure 6-28: Overall MDM2 E3 antagonists/ agonists.

7 Summary and future work

This thesis has described biochemical and biophysical studies of MDM2-ligand interactions, aiming to inhibit ubiquitination of p53 as a potential cancer therapy. Several approaches were taken, including structural studies, *in silico* screening for drug development, and enzymatic assays to provide insight into the following areas:

1. Biochemical and biophysical characterisations of MDM2RING (residues 386-491), MDM2RING△C (residues 386-478) and UbcH5a (Chapter 2, 3 and 4)
2. Studies of peptide 9, a potent MDM2 inhibitor (Chapter 5)
3. Small molecules inhibitors/activators of MDM2 E3 activity were selected using virtual screening (Chapter 6).

7.1 Biochemical and biophysical characterisations of MDM2RING, MDM2RING△C and UbcH5a

MDM2 is a major regulator of the level of p53 in the cell during transrepression and ubiquitination. A huge number of studies have investigated the interaction between the hydrophobic domain of MDM2 and p53, several molecules have been designed to interrupt the interaction and rescue p53 function. However, studies of MDM2-mediated ubiquitination of p53 are limited. Additionally, UbcH5a, one of MDM2 cognate E2s, is essential for MDM2-mediated ubiquitination. Therefore, the structure of MDM2-UbcH5a could provide insight into the E2-E3 mechanism and also act as a drug target for the development of small molecule inhibitors.

7.1.1 Major findings and conclusions

- Recombinant proteins: MDM2RING (residues 386-491), MDM2RING△C (residues 386-478) and UbcH5a (residue 1-148) were successfully cloned, expressed and purified (section 2.4 & 2.5) and molecular weights were confirmed by MALDI-TOF MS (section 2.6).
- *in vitro* ubiquitination data presented showed that MDM2RING and MDM2RING△C are E3 active ubiquitinating p53, suggesting a potential p53-binding motif in the N-terminal

fragment preceding the RING domain. A model was proposed to explain the mechanism of FLMDM2- and MDM2RING-mediated ubiquitination of p53 (section 3.1).

- MDM2RING tends to become higher order structured oligomers at high concentration (section 3.2). Negative staining TEM provides evidence that MDM2RING forms large (>660 kDa) regular donut-like structure (section 4.2)
- The thermal denaturation assay (TDA) was used to detect the folding state of our constructs.
  - ○ The thermal denaturation assay demonstrated that our purified MDM2RING is a metal-binding protein. Experiments carried out in the presence of EDTA showed that EDTA chelates metals out of MDM2RING, inducing protein unfolding (section 3.3.1).
  - ○ The thermal denaturation assay provides evidence that ATP binds to and stabilises MDM2RING, improving the Tm value from 47.6 ℃ to 62 ℃ (section 3.3).
  - ○ UbcH5a is a folded protein and its Tm is 55.4℃. Moreover, in the presence of MDM2RING, the Tm shifts to 53.4℃, revealing MDM2RING binds to and destabilizes UbcH5a (section 3.3).
- Circular Dichroism analysis of UbcH5a revealed that the protein is composed of 31.4% α-helix and 19.3% β-sheets, consistent with the published crystal structure (PDB: 2C4P) (section 3.4).
- Structural studies of the MDM2-UbcH5a complex.
  - ○ After extensive crystallisation trials, only microcrystals were found (section 4.1).
  - ○ 1D-NMR demonstrated that both MDM2RING and UbcH5a are folded following expression and purification (section 4.3.3).
  - ○ ^{15}N-UbcH5a provides a properly dispersed HSQC-NMR spectrum. Also 65% assignment was achieved using available NMR data (NMR code: 6584) (section 4.3).
  - ○ In the presence of MDM2RING△C, residues involved in the UbcH5a-binding were observed (section 4.3.3). Some are located in the known E2-E3 binding interfaces, and others are allosterically regulated in the ubiquitin-binding backside of UbcH5a.

7.1.2 Future work

- Further studies to optimise crystallisation are required to obtain useful crystals of the MDM2-UbcH5a complex. Such crystals could provide detailed information about the

complex for further drug development. Additional constructs are required to increase the likelihood of obtaining a stable E2-E3 complex providing a good target for crystallisation.

- It will be of interest to investigate our hypothesis that there is a new p53-binding site (residues 386-400) essential for FLMDM2- and MDM2RING- mediated ubiquitination. Further work is necessary to fully characterise the interaction of short MDM2RING peptides with p53. For example, *in vitro* ubiquitination assays can be used to test whether several MDM2RING deletion mutants ubiquitinate p53. MDM2RING peptides are synthesised and test their binding ability with p53 using the ELISA or pull-down methods.

7.2 Studies of peptide 9, a potent MDM2 inhibitor

Peptide 9, the twelve C-terminal amino acids of MDMX, was selected by K. Ball's group, showing that it binds to FLMDM2. Similar results were obtained using pull-down methods. Peptide 9 was presumed to bind to the C8-binding site of MDM2RING domain. To further study how peptide 9 interacts with FLMDM2, and MDM2RING, a number of biophysical methods were used, for example, intrinsic tryptophan fluorescence, thermal denaturation assay, fluorescence anisotropy, and electrospray ionisation mass spectrometry. In addition, some reports have been described that the MDMX or MDM2 C-terminal fragments might be involved in E2-binding; therefore, peptide 9 was also tested with respect to its binding to UbcH5a.

7.2.1 Major findings and conclusions

- *in vitro* ubiquitination data revealed that peptide 9 can inhibit FLMDM2 and MDM2RINIG (residues 386-491), suggesting that peptide 9 binds to MDM2RING (section 5.1).
- Intrinsic tryptophan data shows that peptide 9 binds to FLMDM2, resulting in an increase in the fluorescence intensity. Furthermore, peptide 9-binding inducing the blue shift demonstrates that the peptide 9-binding reoriented tryptophan into a non-polar environment (section 5.2).
- The study of buried surface area (BSA) of the complex can predict the potential binding ability and the numbers of H-bonds, providing additional evidence in support of successful protein-ligand.

- ○ BSA data suggest that the MDMX C-terminus makes additional H-bonds to MDM2RING compared to MDM2-terminal fragments (section 5.3 & section 6.3). The two C-terminal amino acids (I490 and A491) are critical for the formation of the three additional H-bonds. This result suggests why a peptide missing these residues lost its inhibitory effect on MDM2 E3 activity (section 5.3).

- Fluorescence anisotropy data showed that peptide 9 binds to MDM2RING and MDM2RING△C. The Kd values of peptide 9 to MDM2RING and MDM2RING△C were 355.6 ±113.6 nM and 314.3 ± 157.9 nM, respectively (section 5.4).

- Thermal denaturation assay showed a significantly negative Tm shift for UbcH5a in the presence of peptide 9, from 58 ℃to 54℃ (section 5.6.1) . Furthermore, the fluorescence anisotropy assay showed the Kd value of the FITC-N' labeled peptide 9 to UbcH5a is 101.4 ±70.7 nM (section 5.6.2). The data provide evidence that peptide 9 binds to UbcH5a and destabilises the protein.

- ^{1}H-^{15}N HSQC NMR data demonstrate that peptide 9 dissociate the UbcH5a-MDM2RING△C complex (section 5.6.4).

- Electrospray ionisation mass spectrometry is used to monitor the folding state of a protein, and also provide information of a potential protein-ligand complex. For example, whether peptide 9 is complexed with MDM2RING△C or UbcH5a.

  - ○ ESI-MS data showed that monomeric-MDM2RING△C was predominant, which also reflects that the interaction of dimeric MDM2RING△C (observed in the SEC method) is likely hydrophobic and not electrostatic (section 5.5).

  - ○ In the presence of peptide 9, there were new peaks generated, PPL6, PPL7 and PPL8. The calculated molecular weight following deconvolution of the data suggested that the complex consists of peptide 9 interacting with two MDM2RING△C molecules (section 5.5).

  - ○ A characteristic bell shaped charge state curve was observed in the ESI-MS profile of UbcH5a, providing evidence that UbcH5a is a folded protein (section 5.6).

  - ○ In the presence of peptide 9, many peaks were generated in the ESI-MS profile of UbcH5a. According to the calculated molecular weight, the new species was the UbcH5a-peptide 9 complex, providing evidence that there was interaction between UbcH5a and peptide 9 (section 5.6.3).

7.2.3 Future work

- On the basis of the ESI-MS profile, we proposed a hypothesis that peptide 9 promotes the dimerisation of MDM2RING△C. To further confirm the hypothesis, ITC or SPR experiments could provide information on the binding ratio of peptide 9 to MDM2RING△C. However, ITC requires large amounts of both peptides and proteins, and as peptide 9 tends to be insoluble at a high concentration, SPR (Surface Plasma Resonance) would be a more appropriate technique.
- Thermal denaturation, fluorescence anisotropy and ESI-MS data demonstrated that peptide 9 interacts with UbcH5a. To further detect how peptide 9 effects the conformational change of UbcH5a, intrinsic tryptophan fluorescence will provide insight into the mechanism of peptide 9 induced conformational change of UbcH5a.
- Several biophysical experiments provide evidence that peptide 9 binds to MDM2RING, MDM2RING△C and UbcH5a. However, NMR data did not show significant changes on chemical shifts of the cross-peaks. Instead, dramatic reductions in signal intensity, and some visible aggregates were observed. Therefore, to study the peptide 9-binding site within MDM2RING or UbcH5a, mutagenesis experiments combined with other biophysical experiments could provide additional information to identify residues key to the interaction.

7.3 Small molecules against MDM2 E3 activity were selected using virtual screening

Transrepression and ubiquitination are two major MDM2-mediated regulation mechanisms of the p53 level in cells. Several small molecules have been found to inhibit transrepression, for example, Nutlin, through inhibition of the interaction between p53 and the MDM2 hydrophobic domain. However, only a few small molecules have been found that are inhibitory to MDM2 E3 ligase activity. Since MDM2 RING domain possesses an E3 ligase for ubiquitination and it has been widely noted that dimerisation of MDM2 and the E2-E3 interaction are essential for ubiquitination. Therefore, in the present work, small molecules inhibitors were selected using virtual screening approaches (consisting of EDULISS, UFSRAT, LIDAEUS and AutoDock programs) with the aim of disrupting these interactions.

7.3.1 Project aims

- To find small molecules that bind to the C8-binding site of MDM2RING-MDM2RING
- To find small molecules that bind to the E2-binding site of MDM2RING
- To find small molecules that bind to the E3-binding site of UbcH5a

7.3.2 Major findings and conclusions

- To screen for small molecules-binding to the C8-binding site, the eight C-terminal amino acids from MDMX were used as a drug template. After virtual screening, using rounds of EDULISS, LIDAEUS and AutoDock, 10 compounds (D-series) were purchased and tested their effectiveness on FLMDM2- and MDM2RING-mediated ubiquitination.
    - D03, D04 and D05 completely inhibit FLMDM2 but not MDM2RING, whilst D07, D08, D09 and D10 inhibit MDM2RING but not FLMDM2. The data suggested that those D-series compounds contributed to conformational changes in FLMDM2 and MDM2RING; therefore resulting in distinct inhibitory effects (section 6.3).
    - D07, D08, D09 and D10 block the MDM2RING-mediated poly-ubiquitination on p53. Only monoubiquitinated-p53 was observed (section 6.3), suggesting that those compounds might induce MDM2RING to become monomeric.
- On the basis of the known crystal structure of the cIAP2-UbcH5a complex, a new model of the MDM2RING-UbcH5a complex was built, showing that no clash between these two proteins and that the modelled complex was a reliable drug target (section 6.4).
- U-series compounds were designed using the EDULISS, LIDAEUS and AutoDock methods to bind to the E2-binding site of MDM2RING.
    - U05 was found to activate FLMDM2-mediated ubiquitination of p53; however, it lost activity over time. Similar results were found with U05-mimetics also being activatory to FLMDM2-mediated ubiquitination. This activity was also lost over time. This suggested that U05 and U05-mimetics did have effects on FLMDM2 E3 activity, but over time the molecules became unstable (section 6.5).
    - U04 and U06 activated MDM2RING-mediated ubiquitination of p53, but had no effects on FLMDM E3 activity. Those differences could be due to the distinct conformational changes on FLMDM2 and MDM2RING (section 6.5).

- Taken together with findings that UbcH5a interacts with peptide 9, we propose a model that U04/U06 binds to the E2-binding site of MDM2 and induces the exposure of the C-terminus of MDM2 (peptide 9 analog) onto the surface of MDM2RING, facilitating the UbcH5a-MDM2 C-terminus interaction. Moreover, the thermal denaturation data showed that peptide 9 destabilise UbcH5a, suggesting that the C-terminus of MDM2 could induce conformational flexibility of UbcH5a releasing the Ub from UbcH5a to the substrate, p53 (section 6.5).

- Virtual screening was used to design compounds (M-series) to bind to the E3-binding site of UbcH5a. M09 was found to inhibit CHIP- and MDM2-mediated ubiquitination, suggesting the M09 binds to UbcH5a and inhibits the E2-E3 interaction. The thermal denaturation data showed that M09-binding increases the stability of UbcH5a (Section 6.6).

7.3.3 Future work

- D03, D04 and D05 can inhibit FLMDM2-mediated ubiquitination, but the binding affinity is as yet unknown. Therefore, for any future work, measurement of the binding affinity is essential to provide information on the efficiency of those compounds. Moreover, those compounds are able to be used as a starting point for the second round of virtual screening to provide better inhibitors.

- We proposed a hypothesis that MDM2RING C-terminus is important to the release of ubiquitin from UbcH5a to the substrate, p53. It was assumed that U04/U06 induces conformational changes in the MDM2 C-terminus, resulting in greater surface exposure to facilitate the MDM2 C-terminus to interact with UbcH5a, enhancing ubiquitin loading onto the substrate. To further confirm the hypothesis, MDM2RING△C should be tested. Presumably, there is no difference in MDM2RING△C-mediated ubiquitination of p53 in the presence or absence of U04/U06.

- M09 can inhibit CHIP- and MDM2-mediated ubiquitination with low-specificity and low levels of inhibition to both E3 activities. Using M09 as a starting point for second round of virtual screening should enable an increase in specificity.

- All those small molecules have been tested in crystallisation trials with MDM2RING or UbcH5a. However, no crystals suitable for X-ray diffraction studies were grown. The crystal structure of the protein-ligand complex would provide detailed information about

the binding pattern and would increase the success rate of small molecule selection using virtual screening. Therefore, new constructs could be made to repeat these trials.

- Lead optimisation of selected small molecules (inhibitors/activators) is required using similarity or quantitative structure-activity relationship (QSAR) to increase their effectiveness against MDM2 E3 ligase activity. The further aim of the project is to solve the 3-dimensional structure of the newly discovered MDM2-UbcH5a complex, complexes of MDM2 with small molecules, and complexes of UbcH5a with small molecules, in order to provide detail information on the interaction between the druggable target and the small molecule (inhibitors/activators).

8 References

Ajay, A., Walters, W.P. & Murcko, M.A. (1998). Can we learn to distinguish between 'drug-like' and 'nondrug-like' molecules? *J. Med. Chem.* **41,** 3314-3324.

Ardley, H. C. & Robinson, P. A. (2005). E3 ubiquitin ligases. *Essays Biochem.* **41,** 15-30

Argentini, M., Barboule, N. & Wasylyk, B. (2001). The contribution of the acidic domain of MDM2 to p53 and MDM2 stability. *Oncogene.* **20,** 1267 – 1275.

Arkin, M. R. & Wells, J. A. (2004). Small-molecule inhibitors of protein-protein interactions: progressing towards the dream. *Nat Rev Drug Discov.* **3,** 301-317.

Arva, N. C., Gopen, T. R., Talbott, K. E., Campbell, L. E., Chicas, A., White, D. E., Bond, G. L., Levine, A. J. & Bargonetti, J. (2005). A chromatin-associated and transcriptionally inactive p53-Mdm2 complex occurs in mdm2 SNP309 homozygous cells. *J Biol Chem.* **280,** 26776-26787.

Ashcroft, M., Ludwig, R. L., Woods, D. B., Copeland, T. D., Weber, H. O., MacRae, E. J. & Vousden, K. H. (2002). Phosphorylation of HDM2 by Akt. *Oncogen.* **21,** 1955 – 1962.

Badciong, J. C. & Haas, A. L. (2002). MdmX is a RING finger ubiquitin ligase capable of synergistically enhancing Mdm2 ubiquitination. *J Biol Chem.* **277,** 49668-49675.

Banin, S., Moyal, L., Shieh, S., Taya, Y., Anderson, C. W., Chessa, L., Smorodinsky, N. I., Prives, C., Reiss, Y., Shiloh, Y. & Ziv, Y. (1998). Enhanced phosphorylation of p53 by ATM in response to DNA damage. *Science.* **281,** 1674-1677.

Bartel, F., Meye, A., Wu¨rl, P., Kappler, M., Bache, M., Lautenschla¨ger, C., Gru¨nbaum, U., Schmidt, H. & Taubert, H. (2001). Amplification of the MDM2 gene, but not expression of splice variants of MDM2 MRNA, is associated with prognosis in soft tissue sarcoma. *Int. J. Cancer.* **95,** 168–175.

Bartke, T., Pohl, C., Pyrowolakis, G. & Jentsch, S. (2004). Dual role of BRUCE as an antiapoptotic IAP and a chimeric E2/E3 ubiquitin ligase. *Mol. Cell.* **14,** 801–811

Barlev, N. A., Liu, L., Chehab, N. H., Mansfield, K., Harris, K. G., Halazonetis, T. D. & Berger, S. L. (2001). Acetylation of p53 activates transcription through recruitment of coactivators/histone acetyltransferases. *Mol Cell.* **8,** 1243-1254.

Bayer, P., Arndt, A., Metzger, S., Mahajan, R., Melchior, F., Jaenicke, R. & Becker, J. (1998). Structure determination of the small ubiquitin-related modifier SUMO-1. *J Mol Biol.* **280,** 275-286.

Beaudenon, S.L., Huacani, M. R., Wang, G., McDonnell, D. P. & Huibregtse, J. M. (1999). Rsp5 ubiquitin-protein ligase mediates DNA damage-induced degradation of the large subunit of RNA polymerase II in Saccharomyces cerevisiae. *Mol Cell Biol.* **19,** 6972-6979.

Beavis R. C. & Chait, B. T. (1989a). Matrix-assisted laser-desorption mass spectrometry using 355 nm radiation Rapid Commun. *Mass Spectrom.* **3,** 436–439.

Beavis, R. C. & Chait, B. T. (1989b). Cinnamic acid derivatives as matrices for ultraviolet laser desorption mass spectrometry of proteins. Rapid Commun. *Mass Spectrom.* **3,** 432–435.

Beck, J. L., Colgrave, M. L., Ralph, S. F. & Sheil, M. M.. (2001). Electrospray ionization mass spectrometry of oligonucleotide complexes with drugs, metals, and proteins. *Mass Spectrom Rev.* **20,** 61-87.

Bemis, G.W. & Murcko, M.A. (1996). The properties of known drugs. 1. Molecular frameworks. *J. Med. Chem.* **39,** 2887-2893.

Bemis, G.W. & Murcko, M.A. (1999). Properties of known drugs. 2. Side chains. *J. Med. Chem.* **42,** 5095-5099.

Bender, A. & Glen, R. C. (2004). Molecular similarity: a key technique in molecular informatics. *Org Biomol Chem.* **2,** 3204-3218.

Blackburn, E. A., Maclean, J. K., Sherborne, B. S. & Walkinshaw, M. D. (2010). Estimating the affinity of protein-ligand complex from changes to the charge-state distribution of a protein in electrospray ionization mass spectrometry. *Biochem Biophys Res Commun.* **403,** 190-193.

Bodenhausen, G. & Ruben, D. J. (1980). Natural abundance nitrogen-15 NMR by enhanced heteronuclear spectroscopy. *Chemical Physics Letters.* **69,** 185-189

Boddy, M. N., Freemont, P. S. & Borden, K. L. B. (1994). The p53-associated protein MDM2 contains a newly characterized zinc binding domain called the RING finger. *Trends Biochem. Sci.* **19,** 198–199.

Bogan, A. A. & Thorn, K. S. (1998). Anatomy of hot spots in protein interfaces. *J. Mol. Biol.* **280,** 1–9.

Bond, G. L., Hu, W., Bond, E. E., Robins, H., Lutzker, S. G., Arva, N. C., Bargonetti, J., Bartel, F., Taubert, H., Wuerl, P., Onel, K., Yip, L., Hwang, S. J., Strong, L. C., Lozano, G. & Levine, A. J. (2004). A single nucleotide polymorphism in the MDM2 promoter attenuates the p53 tumor suppressor pathway and accelerates tumor formation in humans. *Cell.* **119,** 591-602.

Borden, K. L. (2000). RING domains: master builders of molecular scaffolds? *J. Mol. Biol.* **295,** 1103-1112.

Böttger, A., Böttger, V., Sparks, A., Liu, W. L., Howard, S. F. & Lane, D. P. (1997). Design of a synthetic Mdm2-binding mini protein that activates the p53 response in vivo. *Curr Biol.* **7,** 860-869.

Bo¨ttger, V., Bo¨ttger, A., Garcia-Echeverria, C., Ramos, Y. FM., van der Eb, A. J., Jochemsen, A. G. & Lane, D. P. (1999). Comparative study of the p53-mdm2 and p53-MDMX interfaces. *Oncogene.* **18,** 189–199.

Bowman, A. L., Nikolovska-Coleska, Z., Zhong, H., Wang, S. & Carlson, H. A. (2007). Small molecule inhibitors of the MDM2-p53 interaction discovered by ensemble-based receptor models. *J Am Chem Soc.* **129,** 12809-12814.

Breitschopf, K., Bengal, E., Ziv, T., Admon, A. & Ciechanover, A. (1998) A novel site for ubiquitination: the N-terminal residue, and not internal lysines of MyoD, is essential for conjugation and degradation of the protein. *EMBO J.* **17,** 5964–5973

Bresson, C., Colin, C., Chartier, F. & Moulin, C. (2005). Cobalt speciation study in the cobalt-cysteine system by electrospray ionization mass spectrometry and anion-exchange chromatography inductively coupled plasma atomic emission spectrometry. *Appl Spectrosc.* **59,** 696-705.

Brooks, C. L. & Gu, W. (2003). Ubiquitination, phosphorylation and acetylation: the molecular basis for p53 regulation. *Curr. Opin. Cell Biol.* **15,** 164–171.

Brooks, C. L. & Gu, W. (2004). Dynamics in the p53-Mdm2 ubiquitination pathway. *Cell Cycle.* **3,** 895-899.

Brooks, C. L. & Gu, W. (2006). p53 ubiquitination: Mdm2 and beyond. *Mol Cell.* **21,** 307-315.

Brown, C. J., Srinivasan, D., Jun, L. H., Coomber, D., Verma, C. S. & Lane, D. P. (2008). The electrostatic surface of MDM2 modulates the specificity of its interaction with phosphorylated and unphosphorylated p53 peptides. *Cell Cycle.* **7,** 608-610.

Brown, D.R., Thomas, C.A., & Deb, S.P. (1998). The human Oncoprotein MDM2 arrests the cell cycle: Elimination of its cell-cycle-inhibitory function induces tumorigenesis. *EMBO J.* **17:** 2513–2525

Brzovic, P. S., Lissounov, A., Christensen, D. E., Hoyt, D. W. & Klevit, R. E. (2006). A UbcH5/ubiquitin noncovalent complex is required for processive BRCA1-directed ubiquitination. *Mol Cell.* **21,** 873-880.

Brzovic, P. S., Rajagopal, P., Hoyt, D. W., King, M. C., Klevit, R. E. (2001). Structure of a BRCA1-BARD1 heterodimeric RING-RING complex. *Nat Struct Biol.* **8,** 833-837.

Buchwald, G., van der Stoop, P., Weichenrieder, O., Perrakis, A., van Lohuizen, M. & Sixma, T. K. (2006). Structure and E3-ligase activity of the Ring-Ring complex of polycomb proteins Bmi1 and Ring1b. *EMBO J.* **25,** 2465-2474.

Burch, L., Shimizu, H., Smith, A., Patterson, C. & Hupp, T. R. (2004). Expansion of protein interaction maps by phage peptide display using MDM2 as a prototypical conformationally flexible target protein. *J Mol Biol.* **337,** 129-145.

Burkitt, W. I., Derrick, P. J., Lafitte, D. & Bronstein, I. (2003). Protein-ligand and protein-protein interactions studied by electrospray ionization and mass spectrometry. *Biochem Soc Trans.* **31,** 985-989.

Canon, F, Paté F, Meudec E, Marlin T, Cheynier V, Giuliani A, Sarni-Manchado P. (2009). Characterization, stoichiometry, and stability of salivary protein-tannin complexes by ESI-MS and ESI-MS/MS. *Anal Bioanal Chem.* **395,** 2535-2545.

Carroll, P. E., Okuda, M., Horn, H. F., Biddinger, P., Stambrook, P. J., Gleich, L. L., Li, Y-Q., Tarapore, P. & Fukasawa, K. (1999). Centrosome hyperamplification in human cancer: chromosome instability induced by p53 mutation and/or Mdm2 overexpression. *Oncogene.* **18,** 1935–1944.

Ceccarelli, D. F., Tang, X., Pelletier, B., Orlicky, S., Xie, W., Plantevin, V., Neculai, D., Chou, Y. C., Ogunjimi, A., Al-Hakim, A., Varelas, X., Koszela, J., Wasney, G. A., Vedadi, M., Dhe-Paganon, S., Cox, S., Xu, S., Lopez-Girona, A., Mercurio, F., Wrana, J., Durocher, D., Meloche, S., Webb, D. R., Tyers, M., Sicheri, F. (2011). An allosteric inhibitor of the human cdc34 ubiquitin-conjugating enzyme. *Cell.* **145,** 1075-1087.

Chang, J. Y., Alkan, S. S., Hilschmann, N. & Braun, D. G. (1985). Thrombin specificity. Selective cleavage of antibody light chains at the joints of variable with joining regions and joining with constant regions. *Eur J Biochem.* **151,** 225-230.

Chayen, N. E. (2004). Turning protein crystallisation from an art into a science. *Curr Opin Struct Biol.* **14,** 577-583.

Chayen, N. E. (2005). Methods for separating nucleation and growth in protein crystallisation. *Prog Biophys Mol Biol.* **88,** 329-337.

Chen, D., Kon, N., Li, M., Zhang, W., Qin, J. & Gu, W. (2005). ARFBP1/Mule is a critical mediator of the ARF tumor suppressor. *Cell.* **121,** 1071–1083.

Cheng, Q, Chen L, Li Z, Lane WS, Chen J. (2009). ATM activates p53 by regulating MDM2 oligomerization and E3 processivity. *EMBO J.* **28,** 3857-3867.

Chi, S.W., Lee, S. H., Kim, D. H., Ahn, M. J., Kim, J. S., Woo, J. Y. et al. (2005). Structural details on mdm2-p53 interaction. *J. Biol. Chem.* **280,** 38795–38802.

Chipuk, J.E., Kuwana, T., Bouchier-Hayes, L., Droin, N.M., Newmeyer, D.D., Schuler, M. & Green, D.R. (2004). Direct activation of Bax by p53 mediates mitochondrial membrane permeabilization and apoptosis. *Science.* **303,** 1010–1014.

Christensen, D. E., Brzovic, P. S. & and Klevit, R. E. (2007). E2–BRCA1 RING interactions dictate synthesis of mono- or specific polyubiquitin chain linkages. *Nat. Struct. Mol. Biol.* **14,** 941–948.

Chuikov, S., Kurash, J.K., Wilson, J.R., Xiao, B., Justin, N., Ivanov, G.S., McKinney, K., Tempst, P., Prives, C., Gamblin, S.J., Barlev, N. A. & Reinberg, D. (2004). Regulation of p53 activity through lysine methylation. *Nature.* **432,** 353–360.

Chung, C. W. (2007) The use of biophysical methods increases success in obtaining liganded crystal structures. Acta Crystallogr. *Sect. D: Biol. Crystallogr.* **63,** 62–71.

Ciechanover, A., Breitschopf, K., Hatoum, O. A. & Bengal, E. (1999) Degradation of MyoD by the ubiquitin pathway: regulation by specific DNA-binding and identification of a novel site for ubiquitination. *Mol. Biol. Rep.* **26,** 59–64.

Clackson, T. & Wells, J.A. (1995). A hot spot of binding energy in a hormone–receptor interface. *Science.* **267,** 383-386.

Coccetti, P., Tripodi, F., Tedeschi, G., Nonnis, S., Marin, O., Fantinato, S., Cirulli, C., Vanoni, M. & Alberghina, L. (2008). The CK2 phosphorylation of catalytic domain of Cdc34 modulates its activity at the G(1) to S transition in Saccharomyces cerevisiae. *Cell Cycle*. **7,** 1391–1401

Cochran, A. G. (2000). Antagonists of protein-protein interactions. *Chem Biol.* **7,** 85-94.

Coles, M., Heller, M. & Kessler, H. (2003). NMR-based screening technologies. *Drug Discov Today.* **8,** 803-810.

Cook, W. J., Jeffrey, L. C., Xu, Y. & Chau, V. (1993). Tertiary structures of class I ubiquitin-conjugating enzymes are highly conserved: crystal structure of yeast Ubc4. *Biochemistry.* **32,** 13809-13817.

Dai, M.S., Zeng, S.X., Jin, Y., Sun, X.X., David, L. & Lu, H. (2004). Ribosomal protein L23 activates p53 by inhibiting MDM2 function in response to ribosomal perturbation but not to translation inhibition. *Mol. Cell. Biol.* **24,** 7654–7668.

Dang, J., Kuo, M. L., Eischen, C. M., Stepanova, L., Sherr, C. J. &oussel, M. F. (2002). domain of Mdm2 can inhibit cell proliferation. *Cancer Res.* **62,** 1222 – 1230.

Danovi, D., Meulmeester, E., Pasini, D., Migliorini, D., Capra, M., Frenk, R., de Graaf, P., Francoz, S., Gasparini, P., Gobbi, A., Helin, K., Pelicci, P. G., Jochemsen, A. G. & Marine, J. C. (2004). Amplification of Mdmx (or Mdm4) directly contributes to tumor formation by inhibiting p53 tumor suppressor activity. *Mol. Cell. Biol.* **24,** 5835–5843.

Daphne Kan's thesis (2007) "Studies of protein-ligand interactions and the discovery of new cyclophilin inhibitors." (University of Edinburgh)

Dastidar, S. G., Lane, D. P. & Verma, C. S. (2008). Multiple peptide conformations give rise to similar binding affinities: molecular simulations of p53-MDM2. *J Am Chem Soc.* **130,** 13514-13515.

Daujat, S., Neel, H. &Piette, J. (2001). MDM2: life without p53. *Trends Genet.* **17,** 459–464.

DeLano, W. L. (2002). Unraveling hot spots in binding interfaces: progress and challenges. *Curr. Opin. Struct. Biol.* **12,** 14–20.

Deng, L., Wang, C., Spencer, E., Yang, L., Braun, A., You, J., Slaughter, C., Pickart, C., & Chen, Z. J. (2000). Activation of the IkappaB kinase complex by TRAF6 requires a dimeric ubiquitin-conjugating enzyme complex and a unique polyubiquitin chain. *Cell.* **103,** 351-61.

Deshaies, R. J. (1999). SCF and Cullin/Ring H2-based ubiquitin ligases. *Annu Rev Cell Dev Biol.* **15,** 435-467.

Deshaies, R. J. & Joazeiro, C. A. (2009). RING domain E3 ubiquitin ligases. *Annu Rev Biochem.* **78,** 399-434.

Dimasi, J. A. (2001). Risks in new drug development: approval success rates for investigational drugs. *Clin Pharmacol Ther.* **69,** 297-307.

Dömling, A. (2008). Small molecular weight protein-protein interaction antagonists: an insurmountable challenge? *Curr Opin Chem Biol.* **12,** 281-291.

Dornan, D., Wertz, I., Shimizu, H., Arnott, D., Frantz, G.D., Dowd, P., O'Rourke, K., Koeppen, H. & Dixit, V.M. (2004). The ubiquitin ligase COP1 is a critical negative regulator of p53. *Nature.* **429,** 86–92.

Dornan, D., Shimizu, H., Perkins, N. D. & Hupp, T. R. (2003). DNA-dependent acetylation of p53 by the transcription coactivator p300. *J Biol Chem.* **278,** 13431-12441.

Dornan, D. & Hupp TR. (2001). Inhibition of p53-dependent transcription by BOX-I phospho-peptide mimetics that bind to p300. *EMBO Rep.* **2,** 139-144.

Duncan, K., Umen, J. G. & Guthrie, C. (2000). A putative ubiquitin ligase required for efficient mRNA export differentially affects hnRNP transport. *Curr Biol.* **10,** 687-696.

Durbin, S. D. & Feher, G. (1996). Protein crystallization. *Annu Rev Phys Chem.* **47,** 171-204.

Elenbaas, B., Dobbelstein, M., Roth, J., Shenk, T. & Levine, A. J. (1996). The MDM2 oncoprotein binds specifically to RNA through its RING finger domain. *Mol. Med.* **2,** 439 – 451.

Englander, S.W. (2006) Hydrogen exchange and mass spectrometry: a historical perspective. *J Am Soc Mass Spectrom.* **17,** 1481–1489

Ericsson, U. B., Hallberg, B. M., Detitta, G. T., Dekker, N. & Nordlund, P. (2006) Thermofluor-based high-throughput stability optimization of proteins for structural studies. *Anal. Biochem.* **357,** 289–298.

Fang, S., Jensen, J. P., Ludwig, R. L., Vousden, K. H. & Weissman, A. M. (2000). Mdm2 is a RING finger-dependent ubiquitin protein ligase for itself and p53. *J. Biol. Chem.* **275,** 8945–8951.

Fang, S. & Weissman, A. M. (2004). A field guide to ubiquitylation. *Cell Mol Life Sci.* **61,** 1546-1561.

Fejzo, J, Lepre CA, Peng JW, Bemis GW, Ajay, Murcko MA, Moore JM. (1999). The SHAPES strategy: an NMR-based approach for lead generation in drug discovery. *Chem. Biol.* **6,** 755-769.

Feldman, R. M., Correll, C. C., Kaplan, K. B. & Deshaies, R. J. (1997). A complex of Cdc4p, Skp1p, and Cdc53p/cullin catalyzes ubiquitination of the phosphorylated CDK inhibitor Sic1p. *Cell.* **91,** 221-30.

Feng, R. & Konishi, Y. (1992). Analysis of antibodies and other large glycoproteins in the mass range of 150,000-200,000 Da by electrospray ionization mass spectrometry. *Anal Chem.* **64,** 2090-2095.

Finch, R.A., Donoviel, D.B., Potter, D., Shi, M., Fan, A., Freed, D.D., Wang, C.Y., Zambrowicz, B.P., Ramirez-Solis, R., Sands, A.T. & Zhang, N. (2002). mdmx is a negative regulator of p53 activity in vivo. *Cancer Res.* **62,** 3221–3225.

Fraser, J. A., Vojtesek, B. & Hupp, T. R. (2010). A novel p53 phosphorylation site within the MDM2 ubiquitination signal: I. phosphorylation at SER269 in vivo is linked to inactivation of p53 function. *J Biol Chem.* **285,** 37762-37772.

Freedman, D. A. & Levine, A. J. (1998). Nuclear export is required for degradation of endogenous p53 by MDM2 and human papillomavirus E6. Mol. Cell. Biol. **18,** 7288 – 7293.

Freedman, D. A., Wu, L. & Levine, A.J. (1999). Functions of the MDM2 oncoprotein. *Cell. Mol. Life Sci.* **55,** 96–107.

Freire, E. (1995). Differential scanning calorimetry. *Methods Mol. Biol.* **40,** 191–218.

Ganem, B., Li, Y. –T. & Henion, J. D. (1991). Observation of Noncovalent enzymesubstrate and Enzyme-Product Complexes by Ion-Spray Mass Spectrometry. *J. Am. Chem. Sco.* **113,** 7818-7819

Ganguli, G. & Wasylyk, B. (2003). p53-Independent Functions of MDM2. *Mol. Cancer Res.* **1,** 1027 – 1035.

Geyer, R.K., Yu, Z.K. & Maki, C.G. (2000). The MDM2 RING-finger domain is required to promote p53 nuclear export. *Nat. Cell Biol.* **2,** 569–573.

Ghosh, M., Huang, K. & Berberich, S. J. (2003). Overexpression of Mdm2 and MdmX fusion proteins alters p53 mediated transactivation, ubiquitination, and degradation. *Biochemistry.* **42,** 2291-2299.

Giraud MF, Desterro JM, Naismith JH. (1998). Structure of ubiquitin-conjugating enzyme 9 displays significant differences with other ubiquitin-conjugating enzymes which may reflect its specificity for sumo rather than ubiquitin. *Acta Crystallogr D Biol Crystallogr.* **54(Pt 5**), 891-898.

Glickman, M. H. & Ciechanover, A. (2002). The ubiquitinproteasome proteolytic pathway: destruction for the sake of construction. *Physiol. Rev.* **82,** 373–428

Goldberg, Z., Vogt, Sionov, R., Berger, M., Zwang, Y., Perets, R., Van Etten, R. A., Oren, M., Taya, Y. & Haupt, Y. (2002). Tyrosine phosphorylation of Mdm2 by c-Abl: implications for p53 regulation. *EMBO J.* **21,** 3715-3727.

Goodsell, D. S., Morris, G. M. & Olson, A. J. (1996). Automated docking of flexible ligands: applications of AutoDock. *J Mol Recognit.* **9,** 1-5.

Grier, J. D., Xiong, S., Elizondo-Fraire, A. C., Parant, J. M. & Lozano, G. (2006). Tissue-specific differences of p53 inhibition by Mdm2 and Mdm4. *Mol. Cell Biol.* **26,** 192–198.

Gu, J., Kawai, H., Nie, L., Kitao, H., Wiederschain, D., Jochemsen, A.G., Parant, J., Lozano, G. & Yuan, Z.M. (2002). Mutual dependence of MDM2 and MDMX in their functional inactivation of p53. *J. Biol. Chem.* **277,** 19251–19254.

Gu, W. & Roeder, R. G. (1997). Activation of p53 sequence-specific DNA binding by acetylation of the p53 C-terminal domain. *Cell.* **90,** 595 – 606.

Haas, A. L., Bright, P. M. & Jackson, V. E. (1988). Functional diversity among putative E2 isozymes in the mechanism of ubiquitin-histone ligation. *J Biol Chem.* **263,** 13268-13275

Haas, A. L. & Rose, I. A. (1982). The mechanism of ubiquitin activating enzyme. A kinetic and equilibrium analysis. *J Biol Chem.* **257,** 10329-10337.

Harris, S. L. & Levine, A. J. (2005). The p53 pathway: positive and negative feedback loops. *Oncogene.* **24,** 2899-2908.

Haupt, Y., Maya, R., Kazaz, A. & Oren, M. (1997). Mdm2 promotes the rapid degradation of p53. *Nature.* **387,** 296-299.

Hauser, H. P., Bardroff, M., Pyrowolakis, G. & Jentsch, S. (1998). A giant ubiquitin-conjugating enzyme related to IAP apoptosis inhibitors. *J Cell Biol.* **141,** 1415-1422

Herrmann, J., Lerman, L. O. & Lerman, A.(2007). Ubiquitin and ubiquitin-like proteins in protein regulation. *Circ Res.* **100,** 1276-1291.

Hernandez-Valladares, M., Kim, T., Kannan, B., Tung, A., Aguda, A. H., Larsson, M., Cooper, J. A. & Robinson, R. C. (2010). Structural characterization of a capping protein interaction motif defines a family of actin filament regulators. *Nat Struct Mol Biol.* **17,** 497-503.

Hershko, A. & Ciechanover, A. (1998). The ubiquitin system. *Annu. Rev. Biochem.* **67,** 425-479.

Hershko, A., Heller, H., Elias, S. & Ciechanover, A. (1983). Components of ubiquitin-protein ligase system. Resolution, affinity purification, and role in protein breakdown. *J Biol Chem.* **258,** 8206-8214.

Hicke, L. (1999). Gettin' down with ubiquitin: turning off cell-surface receptors, transporters and channels. *Trends Cell Biol.* **9,** 107-112.

Hill, R. B. & DeGrado, W. F. (2000). A polar, solvent-exposed residue can be essential for native protein structure. *Structure.* **8,** 471-879.

Hillenkamp, F., Karas, M., Beavis, R. C., Chait, B. T. (1991). Matrix-assisted laser desorption/ionization mass spectrometry of biopolymers. *Anal Chem.* **63,** 1193-1203.

Hochstrasser, M. (2000). Evolution and function of ubiquitinlike protein-conjugation systems. *Nat. Cell Biol.* **2,** 153-157

Hochstrasser, M. (1996). Ubiquitin-dependent protein degradation. *Annu Rev Genet.* **30,** 405-39.

Hofmann, R. M. & Pickart, C. M. (1999). Noncanonical MMS2-encoded ubiquitin- conjugating enzyme functions in assembly of novel polyubiquitin chains for DNA repair. *Cell.* **96,** 645-653.

Hoeflich, K. P. & Ikura, M. (2002). Calmodulin in action: diversity in target recognition and activation mechanisms. *Cell.* **108,** 739-742.

Hoege, C., Pfander, B., Moldovan, G. L., Pyrowolakis, G. & Jentsch S. (2002). RAD6-dependent DNA repair is linked to modification of PCNA by ubiquitin and SUMO. *Nature.* **419,** 135-141.

Hollstein, M., Rice, K., Greenblatt, M. S., Soussi, T., Fuchs, R., Sørlie, T., Hovig, E., Smith-Sørensen B, Montesano, R. & Harris, C. C. (1994). Database of p53 gene somatic mutations in human tumors and cell lines. *Nucleic Acids Res.* **22,** 3551-3555.

Honda, R., Tanaka, H. & Yasuda, H. (1997). Oncoprotein MDM2 is a ubiquitin ligase E3 for tumor suppressor p53. *FEBS Lett.* **420,** 25-27.

Honda, R. & Yasuda, H. (1999). Association of p19(ARF) with Mdm2 inhibits ubiquitin ligase activity of Mdm2 for tumor suppressor p53. *EMBO J.* **18,** 22 – 27.

Honda, R. & Yasuda, H. (2000). Activity of MDM2, a ubiquitin ligase, toward p53 or itself is dependent on the RING finger domain of the ligase. *Oncogene.* **19,** 1473-1476.

Hori, M., Shimazaki, J., Inagawa, S., Itabashi, M., and Hori, M. (2000). Alternatively spliced MDM2 transcripts in human breast cancer in relation to tumor necrosis and lymph node involvement. *Path. Int.* **50,** 786-792.

Houben, K., Dominguez, C., van Schaik, F. M., Timmers, H. T., Bonvin, A. M. & Boelens, R. (2004). Solution structure of the ubiquitin-conjugating enzyme UbcH5B. *J Mol Biol.* **344,** 513-526.

Hsin, K. Y., Morgan, H. P., Shave, S. R., Hinton, A. C., Taylor, P. & Walkinshaw, M. D. (2011). EDULISS: a small-molecule database with data-mining and pharmacophore searching capabilities. *Nucleic Acids Res.* **39,** 1042-1048.

Hu, C. Q. & Hu, Y. Z. (2008). Small molecule inhibitors of the p53-MDM2. *Curr Med Chem.* **15,** 1720-1730.

Hu, M., Li, P., Li, M., Li, W., Yao, T., Wu, J.W., Gu, W., Cohen, R.E. & Shi, Y. (2002). Crystal structure of a UBP-family deubiquitinating enzyme in isolation and in complex with ubiquitin aldehyde. *Cell.* **111,** 1041-1054.

Huang, D. T., Paydar, A., Zhuang, M., Waddell, M. B., Holton, J. M. & Schulman, B. A. (2005). Structural basis for recruitment of Ubc12 by an E2 binding domain in NEDD8's E1. *Mol Cell.* **17,** 341-350.

Huang, L., Kinnucan, E., Wang, G., Beaudenon, S., Howley, P. M., Huibregtse, J. M., Pavletich, N. P. (1999). Structure of an E6AP-UbcH7 complex: insights into ubiquitination by the E2-E3 enzyme cascade. *Science.* **286,** 1321-1326.

Huibregtse, J. M., Scheffner, M., Beaudenon, S. & Howley, P. M. (1995). A family of proteins structurally and functionally related to the E6-AP ubiquitin-protein ligase. *Proc Natl Acad Sci USA.* **92,** 2563-2567.

Huibregtse, J. M., Scheffner, M. & Howley, P. M. (1993). Localization of the E6-AP regions that direct human papillomavirus E6 binding, association with p53, and ubiquitination of associated proteins. *Mol Cell Biol.* **13,** 4918-4927.

Huibregtse, J. M., Yang, J. C. & Beaudenon, S. L. (1997). The large subunit of RNA polymerase II is a substrate of the Rsp5 ubiquitin-protein ligase. *Proc Natl Acad Sci U S A.* **94,** 3656-3661.

Issaeva, N., Bozko, P., Enge, M., Protopopova, M., Verhoef, L. G., Masucci, M., Pramanik, A. & Selivanova, G. (2004). Small molecule RITA binds to p53, blocks p53-HDM-2 interaction and activates p53 function in tumors. *Nat Med.* **10,** 1321-1328.

Ito, A., Lai, C-H., Zhao, X., Saito, S., Hamilton, M. H., Appella, E. & Yao, T-P. (2001). p300/CBP-mediated p53 acetylation is commonly induced by p53-activating agents and inhibited by MDM2. *EMBO J.* **20,** 1331–1340.

Iwakuma, T. & Lozano, G. (2003). MDM2, an introduction. *Mol Cancer Res.* **1,** 993-1000.

Jackson, M. W. & Berberich, S.J. (2000). MdmX protects p53 from Mdm2-mediated degradation. *Mol. Cell. Biol.* **20,** 1001-1007.

Jensen, J. P., Bates, P. W., Yang, M., Vierstra, R. D. & Weissman, A. M. (1995). Identification of a family of closely related human ubiquitin conjugating enzymes. *J Biol Chem.* **270,** 30408-30414.

Jiang, F. & Basavappa, R. (1999). Crystal structure of the cyclin-specific ubiquitin-conjugating enzyme from clam, E2-C, at 2.0 A resolution. *Biochemistry.* **38,** 6471-6478.

Joazeiro, C. A. & Weissman, A. M. (2000). RING finger proteins: mediators of ubiquitin ligase activity. *Cell.* **102,** 549-552.

Johnson, W.C., Jr. (1990). Protein secondary structure and circular dichroism: a practical guide. *Proteins.* **7,** 205-14.

Johnston, S. C., Riddle, S. M., Cohen, R. E. & Hill, C. P. (1999). Structural basis for the specificity of ubiquitin C-terminal hydrolases. *EMBO J.* **18,** 3877-3887.

Jones, S. & Thornton, J.M. (1996). Principles of protein–protein interactions. *Proc. Natl Acad. Sci. USA.* **93,** 13-20.

Jordan, M. A. (2002). Mechanism of action of antitumor drugs that interact with microtubules and tubulin. *Curr. Med. Chem. Anti-Canc. Agents*. **2,** 1-17.

Juven-Gershon, T. & Oren, M. (1999). Mdm2: the ups and downs. *Mol. Med.* **5,** 71-83.

Juven-Gershon, T., Shifman, O., Unger, T., Elkeles, A., Haupt, Y. & Oren, M. (1998). The Mdm2 oncoprotein interacts with the cell fate regulator Numb. *Mol. Cell. Biol.* **18,** 3974 -3982.

Kalus, W., Baumgartner, R., Renner, C., Noegel, A., Chan, F. K., Winoto, A. & Holak, T. A. (1997). NMR structural characterization of the CDK inhibitor p19INK4d. *FEBS Lett.* **401,** 127-132.

Kamadurai, H. B., Souphron, J., Scott, D. C., Duda, D. M., Miller, D. J., Stringer, D., Piper, R. C. & Schulman, B. A. (2009). Insights into ubiquitin transfer cascades from a structure of a UbcH5B approximately ubiquitin-HECT(NEDD4L) complex. *Mol Cell.* **36,** 1095-1102.

Kamijo, T., Weber, J.D., Zambetti, G., Zindy, F., Roussel, M.F. & Sherr, C.J. (1998). Functional and physical interactions of the ARF tumor suppressor with p53 and Mdm2. *Proc. Natl. Acad. Sci. USA.* **95,** 8292-8297.

Kamura, T., Koepp, D. M., Conrad, M. N., Skowyra, D., Moreland, R. J., Iliopoulos, O., Lane, W. S., Kaelin, W. G. Jr, Elledge, S. J., Conaway, R. C., Harper, J. W. & Conaway, J. W. (1999). Rbx1, a component of the VHL tumor suppressor complex and SCF ubiquitin ligase. *Science.* **284,** 657-661.

Katta, V. & Chait, B. T. (1991). Observation of the heme-globin complex in native myoglobin by electrospray-ionization mass spectrometry. *J. Am. Chem. Sco.* **113,** 8534-8535

Kawai, H., Lopez-Pajares, V., Kim, M. M., Wiederschain, D., Yuan, Z. M. (2007). RING domain-mediated interaction is a requirement for MDM2's E3 ligase activity. *Cancer Res.* **67,** 6026-6030.

Keith-Roach, M. J. (2010). A review of recent trends in electrospray ionisation-mass spectrometry for the analysis of metal-organic ligand complexes. *Anal Chim Acta.* **678,** 140-148.

Kelly, S. M. & Price, N. C. (1997). The application of circular dichroism to studies of protein folding and unfolding. *Biochim. Biophys. Acta.* **1338,** 161-185.

Kelly, S. M. & Price, N. C. (2000). The use of circular dichroism in the investigation of protein structure and function. *Curr Protein Pept Sci.* **1,** 349-384.

Kerscher, O., Felberbaum, R. & Hochstrasser, M. (2006). Modification of proteins by ubiquitin and ubiquitin-like proteins. *Annu Rev Cell Dev Biol.* **22,** 159-180.

Khosravi, R., Maya, R., Gottlieb, T., Oren, M., Shiloh, Y. & Shkedy, D. (1999). Rapid ATM-dependent phosphorylation of MDM2 precedes p53 accumulation in response to DNA damage. *Proc Natl Acad Sci U S A.* **96,** 14973-14977.

Kim, H. T., Kim, K. P., Lledias, F., Kisselev, A. F., Scaglione, K. M., Skowyra, D., Gygi, S. P. & Goldberg, A. L (2007). Certain Pairs of Ubiquitin-conjugating Enzymes (E2s) and Ubiquitin-Protein Ligases (E3s) Synthesize Nondegradable Forked Ubiquitin Chains Containing All Possible Isopeptide Linkages. *J Biol Chem.* **282,** 17375-17386.

Klemperer, N. S., Berleth, E. S. & Pickart, C. M. (1989) A novel, arsenite-sensitive E2 of the ubiquitin pathway: purification and properties. *Biochemistry.* **28,** 6035–6041

Ko, L. J. & Prives, C. (1996). p53: puzzle and paradigm. *Genes Dev.* **10,** 1054–1072.

Kobet, E., Zeng, X., Zhu, Y., Keller, D. & Lu, H. (2000). MDM2 inhibits p300-mediated p53 acetylation and activation by forming a ternary complex with the two proteins. *Proc Natl Acad Sci U S A.* **97,** 12547-12552.

Koepp, D. M, Harper, J. W. & Elledge, S. J. (1999). How the cyclin became a cyclin: regulated proteolysis in the cell cycle. *Cell.* **97,** 431-434.

Kostic, M., Matt, T., Martinez-Yamout, M. A., Dyson, H. J. & Wright, P. E. (2006). Solution structure of the Hdm2 C2H2C4 RING, a domain critical for ubiquitination of p53. *J Mol Biol*. **363,** 433-450

Krummel, K.A., Lee, C.J., Toledo, F. & Wahl, G.M. (2005). The C-terminal lysines fine-tune P53 stress responses in a mouse model but are not required for stability control or transactivation. *Proc. Natl. Acad. Sci. USA.* **102,** 10188-10193.

Kubbutat, M. H., Jones, S. N. & Vousden, K. H. (1997). Regulation of p53 stability by Mdm2. *Nature.* **387,** 299-303.

Kumar, S., Kao, W.H. & Howley, P. M. (1997). Physical interaction between specific E2 and Hect E3 enzymes determines functional cooperativity. *J Biol Chem.* **272,** 13548-13554.

Kumar, S., Talis, A. L. & Howley, P. M. (1999). Identification of HHR23A as a substrate for E6-associated protein-mediated ubiquitination. J Biol Chem. **274,** 18785-18792.

Kussie, P. H., Gorina, S., Marechal, V., Elenbaas, B., Moreau, J., Levine, A. J. & Pavletich, N. P. (1996). Structure of the MDM2 oncoprotein bound to the p53 tumor suppressor transactivation domain. *Science.* **274,** 948-953.

Lafitte, D., Heck, A. J., Hill, T. J., Jumel, K., Harding, S. E. & Derrick, P. J. (1999). Evidence of noncovalent dimerization of calmodulin. *Eur J Biochem.* **261,** 337-344.

Lahav-Baratz, S., Sudakin, V., Ruderman, J. V. & Hershko, A. (1995). Reversible phosphorylation controls the activity of cyclosome-associated cyclin-ubiquitin ligase. *Proc Natl Acad Sci U S A.* **92,** 9303-9307.

Lai, Z., Freedman, D. A., Levine, A. J. & McLendon, G. L. (1998). Metal and RNA binding properties of the hdm2 RING finger domain. *Biochemistry*. **37,** 7005-7015.

Lai, Z., Yang, T., Kim, Y. B., Sielecki, T. M., Diamond, M. A., Strack, P., Rolfe, M., Caligiuri, M., Benfield, P. A., Auger, K. R. & Copeland, R. A. (2002). Differentiation of Hdm2-mediated p53 ubiquitination and Hdm2 autoubiquitination activity by small molecular weight inhibitors. *Proc. Natl Acad. Sci. USA.* **99,** 14734-14739.

Lam, Y. A., Pickart, C. M., Alban, A., Landon, M., Jamieson, C., Ramage, R., Mayer, R. J., Layfield, R. (2000). Inhibition of the ubiquitin-proteasome system in Alzheimer's disease. *Proc Natl Acad Sci U S A.* **97,** 9902-9906.

Lane, D. P. (1992). Cancer. p53, guardian of the genome. *Nature.* **358,** 15-16.

Lane, D. P. (2004). Transcription– Guarding the genome by sensing DNA damage. Nat Rev *Cancer.* **4,** 4727-4237.

Laney, J. D. & Hochstrasser, M. (1999). Substrate Targeting in the Ubiquitin System. *Cell.* **97,** 427-430.

Lauria, A., Tutone, M., Ippolito, M., Pantano, L. & Almerico, A. M. (2010). Molecular modeling approaches in the discovery of new drugs for anti-cancer therapy: the investigation of p53-MDM2 interaction and its inhibition by small molecules. *Curr Med Chem.* **17,** 3142-3154.

Lavin, M. F. & Gueven, N. (2006). The complexity of p53 stabilization and activation. *Cell Death Differ*. **13,** 941‐950.

Law, M. J., Martenson, R. E. & Deibler, G. E. (1984). Cleavage of rabbit myelin basic protein by thrombin. *J Neurochem*. **42,** 559-568.

Lee, I. & Schindelin, H. (2008). Structural insights into E1-catalyzed ubiquitin activation and transfer to conjugating enzymes. *Cell.* **134,** 268-278.

Lees, J. G., Smith, B. R., Wien, F., Miles, A. J. & Wallace, B. A. (2004). CDtool-an integrated software package for circular dichroism spectroscopic data processing, analysis, and archiving. *Anal Biochem.* **332,** 285-289.

Leng, R.P., Lin, Y., Ma, W., Wu, H., Lemmers, B., Chung, S., Parant, J.M., Lozano, G., Hakem, R., & Benchimol, S. (2003). Pirh2, a p53-induced ubiquitin-protein ligase, promotes p53 degradation. *Cell.* **112,** 779-791.

Lepre, C. A., Moore, J. M. & Peng, J. W. (2004). Theory and applications of NMR-based screening in pharmaceutical research. *Chem Rev.* **104,** 3641-3676.

Levine AJ. (1997). p53, the cellular gatekeeper for growth and division. *Cell.* **88,** 323-331.

Li, M., Brooks, C. L., Kon, N. & Gu, W. (2004). A dynamic role of HAUSP in the p53-Mdm2 pathway. *Mol. Cell.* **13,** 879-886.

Li, M., Brooks, C. L., Wu-Baer, F., Chen, D., Baer, R. & Gu, W. (2003). Mono- versus polyubiquitination: differential control of p53 fate by Mdm2. *Science.* **302,** 1972-1975.

Li, M., Chen, D., Shiloh, A., Luo, J., Nikolaev, A.Y., Qin, J., and Gu, W. (2002). Deubiquitination of p53 by HAUSP is an important pathway for p53 stabilization. *Nature.* **416,** 648-653.

Liang, J., Edelsbrunner, H. & Woodward, C. (1998). Anatomy of protein pockets and cavities: measurement of binding site geometry and implications for ligand design. *Protein Sci.* **7,** 1884-1897.

Lin, Y., Hwang, W. C. & Basavappa, R. (2002). Structural and functional analysis of the human mitotic-specific ubiquitin-conjugating enzyme, UbcH10. *J Biol Chem.* **277,** 21913-21921.

Lin, H. K., Wang, L., Hu, Y. C., Altuwaijri, S. & Chang, C. (2002). Phosphorylation-dependent ubiquitylation and degradation of androgen receptor by Akt require Mdm2 E3 ligase. *EMBO J.* **21,** 4037 - 4048.

Linke, K., Mace, P. D., Smith, C. A., Vaux, D. L., Silke, J. & Day, C. L. (2008). Structure of the MDM2/MDMX RING domain heterodimer reveals dimerization is required for their ubiquitylation in trans. *Cell Death Differ.* **15,** 841-848.

Lipinski, C. A., Lombardo, F., Dominy, B.W. & Feeney, P. J. (1997). Experimental and computational approaches to estimate solubility and permeability in drug discovery and development settings. *Adv. Drug Deliv. Rev.* **23,** 3–25.

Liu, Z., Haas, A. L., Diaz, L. A., Conrad, C. A. & Gíudice, G. J. (1996). Characterization of a novel keratinocyte ubiquitin carrier protein. *J Biol Chem.* **271,** 2817-2822.
Llanos, S., Clark, P. A., Rowe, J. & Peters, G. (2001). Stabilization of p53 by p14ARF without relocation of MDM2 to the nucleolus. *Nat. Cell Biol.* **3,** 445-452.

Lo, Conte, L., Chothia, C. & Janin, J. (1999). The atomic structure of protein-protein recognition sites. *J. Mol. Biol.* **285,** 2177-2198.

Lo, M. C., Aulabaugh, A., Jin, G., Cowling, R., Bard, J., Malamas, M., Ellestad, G. (2004). Evaluation of fluorescence-based thermal shift assays for hit identification in drug discovery. *Anal Biochem.* **332,** 153-159.

Lohrum, M. A., Ashcroft, M., Kubbutat, M. H. & Vousden, K. H. (2000). Identification of a cryptic nucleolar-localization signal in MDM2. *Nat. Cell Biol.* **2,** 179-181

Lohrum, M. A., Ludwig, R. L., Kubbutat, M. H., Hanlon, M. & Vousden, K. H. (2003). Regulation of HDM2 activity by the ribosomal protein L11. *Cancer Cell,* **3,** 577 – 587.

Lois, L. M. & Lima, C. D. (2005). Structures of the SUMO E1 provide mechanistic insights into SUMO activation and E2 recruitment to E1. *EMBO J.* **24,** 439-451.

Loo, J. A. (1997). Studying noncovalent protein complexes by electrospray ionization mass spectrometry. *Mass Spectrom Rev.* **16,** 1-23.

Lorick, K. L., Jensen, J. P., Fang, S., Ong, A. M., Hatakeyama, S. & Weissman, A. M. (1999). RING fingers mediate ubiquitin-conjugating enzyme (E2)-dependent ubiquitination. *Proc Natl Acad Sci U S A.* **96,** 11364-11369.

Loughran, O. & La Thangue, N. B. (2000). Apoptotic and growth-promoting activity of E2F modulated by MDM2. *Mol. Cell. Biol.* **20,** 2186 – 2197.

Lu, X. (2005). p53: A heavily dictated dictator of life and death. *Curr Opin Genet Dev* **15,** 27-33.

Luque, I. & Freire, E. (2000). Structural stability of binding sites: consequences for binding affinity and allosteric effects. *Proteins.* **4,** 63-71.

Ma, B., Elkayam, T., Wolfson, H. & Nussinov, R. (2003). Protein–protein interactions: structurally conserved residues distinguish between binding sites and exposed protein surfaces. *Proc. Natl Acad. Sci. USA.* **100,** 5772-5777.

Mace, P. D., Linke, K., Feltham, R., Schumacher, F. R., Smith, C. A., Vaux, D. L., Silke, J., Day, C. L. (2008). Structures of the cIAP2 RING domain reveal conformational changes associated with ubiquitin-conjugating enzyme (E2) recruitment. *J Biol Chem.* **283,** 31633-31640.

Mancini, F., Gentiletti, F., D'Angelo, M., Giglio, S., Nanni, S., D'Angelo, C., Farsetti, A., Citro, G., Sacchi, A., Pontecorvi, A. & Moretti, F. (2004). MDM4 (MDMX) overexpression enhances stabilization of stress-induced p53 and promotes apoptosis. *J Biol Chem.* **279,** 8169-8180.

Marechal, V., Elenbaas, B., Piette, J., Nicolas, J. C. & Levine, A. J. (1994). The ribosomal L5 protein is associated with mdm-2 and mdm-2-p53 complexes. *Mol. Cell. Biol.* **14,** 7414 – 7420

Marine, J. C. & Jochemsen, A.G. (2005). Mdmx as an essential regulator of p53 activity. *Biochem. Biophys. Res. Commun.* **331,** 750-760.

Marine, J. C., Dyer, M. A. & Jochemsen, A. G. (2007).MDMX: from bench to bedside. *J Cell Sci.* **120(Pt 3)**, 371-8.

Marine, J. C. & Lozano, G. (2010). Mdm2-mediated ubiquitylation: p53 and beyond. *Cell Death Differ*. **17,** 93-102

Matsumoto, R., Tada, M., Nozaki, M., Zhang, C-L., Sawamura, Y. & Abe, H. (1998). Short alternative splice transcripts of the mdm2 oncogene correlate to malignancy in human astrocytic neoplasms. *Cancer Res.* **58,** 609-613.

Matsuura, T., Sutcliffe, J. S., Fang, P., Galjaard, R. J., Jiang, Y. H., Benton, C. S., Rommens, J. M. & Beaudet, A. L. (1997). *De novo* truncating mutations in E6-AP ubiquitin-protein ligase gene (UBE3A) in Angelman syndrome. *Nat Genet.* **15,** 74-77.

Mattos, C. & Ringe, D. (1996). Locating and characterizing binding sites on proteins. Nat. *Biotechnol.* **14,** 595-599.

Maya, R., Balass, M., Kim, S-T., Shkedy, D., Leal, J-F. M., Shifman, O., Moas, M., Buschmann, T., Ronai, Z., Shiloh, Y., Kastan, M. B., Katzir, E. & Oren, M. (2001). ATM-dependent phosphorylation of Mdm2 on serine 395: role in p53 activation by DNA damage. *Genes Dev.* **15,** 1067-1077.

Mayo, L. D., Turchi, J. J. & Berberich, S. J. (1997). Mdm-2 phosphorylation by DNA-dependent protein kinase prevents interaction with p53. *Cancer Res.* **57,** 5013-5016.

McCoy MA, Gesell JJ, Senior MM, Wyss DF. (2003). Flexible lid to the p53-binding domain of human Mdm2: implications for p53 regulation. *Proc Natl Acad Sci U S A.* 1**00,** 1645-1648.

McGrath, J. P., Jentsch, S. & Varshavsky, A. (1991). UBA 1: an essential yeast gene encoding ubiquitin-activating enzyme. *EMBO J.* **10,** 227-236.

McPherson, A. (1999). Crystallization of biological macromolecules (New York, Cold Spring Harbor Laboratory Press).

McPherson, A. (2004). Introduction to protein crystallization. *Methods.* **34,** 254-265.

Meek, D. W. (2004). The p53 response to DNA damage. *DNA Repair. (Amst).* **3,** 1049-1056

Meulmeester, E., Frenk, R., Stad, R., de Graaf, P., Marine, J. C., Vousden, K. H. & Jochemsen, A. G. (2003). Critical role for a central part of Mdm2 in the ubiquitylation of p53. *Mol Cell Biol.* **23,** 4929-4938.

Michael, D. & Oren, M. (2003). The p53-Mdm2 module and the ubiquitin system. *Semin Cancer Biol.* **13,** 49-58.

Midgley, C. A., Desterro, J. M., Saville, M. K., Howard, S., Sparks, A., Hay, R. T. & Lane, D. P. (2000). An N-terminal p14ARF peptide blocks Mdm2-dependent ubiquitination in vitro and can activate p53 in vivo . *Oncogene.* **19,** 2312 -2323.

Mihara, M., Erster, S., Zaika, A., Petrenko, O., Chittenden, T., Pancoska, P. & Moll, U.M. (2003). p53 has a direct apoptogenic role at the mitochondria. *Mol. Cell.* **11,** 577–590.

Miura, T., Klaus, W., Gsell, B., Miyamoto, C. & Senn, H. (1999). Characterization of the binding interface between ubiquitin and class I human ubiquitin-conjugating enzyme 2b by multidimensional heteronuclear NMR spectroscopy in solution. *J Mol Biol.* **290,** 213-228.

Moll, U. M. & Petrenko, O. (2003). The MDM2-p53 interaction. *Mol Cancer Res.* **1,** 1001-1008.

Momand, J., Jung, D., Wilczynski, S. & Niland, J. (1998). The MDM2 gene amplification database. *Nucleic Acids Res.* **26,** 3453–3459

Momand, J., Zambetti, G. P., Olson, D. C., George, D. & Levine, A. J. (1992). The mdm-2 oncogene product forms a complex with the p53 protein and inhibits p53-mediated transactivation. *Cell.* **69,** 1237–1245.

Momand, J., Wu, H-H. & Dasgupta, G. (2000). MDM2-master regulator of the p53 tumor suppressor protein. *Gene (Amst.).* **242,** 15-29.

Moore, J. M. (1999). NMR techniques for characterization of ligand binding: utility for lead generation and optimization in drug discovery. *Biopolymers.* **51,** 221-243.

Morris, G. M., Huey, R. & Olson, A. J. (2008).Using AutoDock for ligand-receptor docking. Curr Protoc Bioinformatics. Chapter 8:Unit 8.14.

Morris, G. M., Huey, R., Lindstrom, W., Sanner, M. F., Belew, R. K., Goodsell, D. S. & Olson, A. J. (2009). AutoDock4 and AutoDockTools4: Automated docking with selective receptor flexibility. *J Comput Chem.* **30,** 2785-2791.

Mossessova, E. & Lima, C. D. (2000). Ulp1-SUMO crystal structure and genetic analysis reveal conserved interactions and a regulatory element essential for cell growth in yeast. *Mol Cell.* **5,** 865-876.

Nakamura, S., Roth, J. A. & Mukhopadhyay, T. (2000). Multiple lysine mutations in the C-terminal domain of p53 interfere with MDM2-dependent protein degradation and ubiquitination. *Mol Cell Biol.* **20,** 9391-9398.

Nicholson, J. & Hupp, T. R. (2010). The molecular dynamics of MDM2. *Cell Cycle.* **9,** 1878-1881

Nooren, I. M. & Thornton, J. M. (2003). Diversity of protein-protein interactions. *EMBO J.* **22,** 3486-3492.

Norgan, A. P., Coffman, P. K., Kocher, J. P., Katzmann, D. J. & Sosa, C. P. (2011). Multilevel Parallelization of AutoDock 4.2. *J Cheminform.* **3,** 12.

Nuber, U., Schwarz, S., Kaiser, P., Schneider, R. & Scheffner, M. (1996). Cloning of human ubiquitin-conjugating enzymes UbcH6 and UbcH7 (E2-F1) and characterization of their interaction with E6-AP and RSP5. *J Biol Chem.* **271,** 2795-2800.

Ogawara, Y., Kishishita, S., Obata, T., Isazawa, Y., Suzuki, T., Tanaka, K., Masuyama, N. & Gotoh, Y. (2002). Akt enhances Mdm2-mediated ubiquitination and degradation of p53. *J. Biol. Chem.* **277,** 21843-21850.

Oliner, J. D., Pietenpol, J. A., Thiagalingam, S., Gyuris, J., Kinzler, K. W. Vogelstein, B. (1993). Oncoprotein MDM2 conceals the activation domain of tumour suppressor p53. *Nature (Lond.).* **362,** 857-860.

Ozkan, E., Yu, H., & Deisenhofer, J. (2005). Mechanistic insight into the allosteric activation of a ubiquitin-conjugating enzyme by RING-type ubiquitin ligases. *Proc Natl Acad Sci U S A.* **102,** 18890-18895.

Page, A. M. & Hieter, P. (1999). The anaphase-promoting complex: new subunits and regulators. *Annu Rev Biochem.* **68,** 583-609.

Pantoliano, M. W., Petrella, E. C., Kwasnoski, J. D., Lobanov, V. S., Myslik, J., Graf, E., Carver, T., Asel, E., Springer, B. A., Lane, P. & Salemme, F. R. (2001) High-density miniaturized thermal shift assays as a general strategy for drug discovery. *J. Biomol. Screening.* **6,** 429-440.

Parant, J., Chavez-Reyes, A., Little, N.A., Yan, W., Reinke, V., Jochemsen, A.G. & Lozano, G. (2001). Rescue of embryonic lethality in Mdm4-null mice by loss of Trp53 suggests a nonoverlapping pathway with MDM2 to regulate p53. *Nat. Genet.* **29,** 92-95.

Passmore, L. A. & Barford, D. (2004). Getting into position: the catalytic mechanisms of protein ubiquitylation. *Biochem J.* **379,** 513-525.

Patriksson, A., Marklund, E. & van der Spoel, D. (2007). Protein structures under electrospray conditions. *Biochemistry.* **46,** 933-945.

Patel, S. & Player, M. R. (2008). Small-molecule inhibitors of the p53-HDM2 interaction for the treatment of cancer. *Expert Opin Investig Drugs.* **17,** 1865-1882.

Pellecchia, M., Sem, D. S. & Wüthrich, K. (2002). NMR in drug discovery. Nat Rev Drug Discov. 1, 211-219.

Petroski, M. D. (2008). The ubiquitin system, disease, and drug discovery. *BMC Biochem.* **9,** Suppl 1:S7.

Pickart, C. M. (2000). Ubiquitin in chains. *Trends Biochem Sci.* **25,** 544-548.

Pickart CM. (2001a). Ubiquitin enters the new millennium. *Mol Cell.* **8,** 499-504.

Pickart, C. M. (2001b). Mechanisms underlying ubiquitination. *Annu. Rev. Biochem.* **70,** 503-533

Pickart, C. M. & Eddins, M. J. (2004). Ubiquitin: structures, functions, mechanisms. *Biochim Biophys Acta.* **1695,** 55-72.

Pomerantz, J., Schreiber-Agus, N., Liegeois, N.J., Silverman, A., Alland, L., Chin, L., Potes, J., Chen, K.,Orlow, I., Lee, H.W., Cordon-Cardo C. & DePinho, R. A. (1998). The Ink4a tumor suppressor gene product, p19Arf, interacts with MDM2 and neutralizes MDM20s inhibition of p53. *Cell.* **92,** 713–723.

Poyurovsky, M. V., Jacq, X., Ma, C., Karni-Schmidt, O., Parker, P. J., Chalfie, M., Manley, J. L. & Prives,C. (2003) Nucleotide binding by the Mdm2 RING domain facilitates Arf-independent Mdm2 nucleolar localization. *Mol. Cell.* **12,** 875–887.

Poyurovsky, M. V., Priest, C., Kentsis, A., Borden, K. L., Pan, Z. Q., Pavletich, N. & Prives, C. (2007). The Mdm2 RING domain C-terminus is required for supramolecular assembly and ubiquitin ligase activity. *EMBO J.* **26,** 90-101.

Priest, C., Prives, C. & Poyurovsky, M. V. (2010). Deconstructing nucleotide binding activity of the Mdm2 RING domain. *Nucleic Acids Res.* **38,** 7587-7598.

Qiu, L., Joazeiro, C., Fang, N., Wang, H. Y., Elly, C., Altman, Y., Fang, D., Hunter, T. & Liu, Y. C. (2000). Recognition and ubiquitination of Notch by Itch, a hect-type E3 ubiquitin ligase. *J Biol Chem.* **275,** 35734-35737.

Rajapurohitam, V., Morales, C. R., El-Alfy, M., Lefrançois, S., Bedard, N., Wing, S. S. (1999). Activation of a UBC4-dependent pathway of ubiquitin conjugation during postnatal development of the rat testis. *Dev Biol.* **212,** 217-28.

Rehm, T., Huber, R. & Holak T. A. (2002). Application of NMR in structural proteomics: screening for proteins amenable to structural analysis. *Structure.* **10,** 1613-1618.

Reverter, D. & Lima, C. D. (2005). Insights into E3 ligase activity revealed by a SUMO-RanGAP1-Ubc9-Nup358 complex. *Nature.* **435,** 687-92

Richard, B. C. (1997). Electrospray inoization mass spectrometry: Fundamentals instrumentation & applications.

Riek, R., Pervushin, K. & Wüthrich, K. (2000). TROSY and CRINEPT: NMR with large molecular and supramolecular structures in solution. *Trends Biochem Sci.* **25,** 462-468.

Ries, S., Biederer, C., Woods, D., Shifman, O., Shirasawa, S., Sasazuki, T., McMahon, M., Oren, M. & McCormick, F. (2000). Opposing effects of Ras on p53: transcriptional activation of mdm2 and induction of p19ARF. *Cell.* **103,** 321-330.

Rock, K. L. & Goldberg, A. L. (1999). Degradation of cell proteins and the generation of MHC class I-presented peptides. *Annu Rev Immunol.* **17,** 739-779.

Roderigo-Brenni, M. C. & Morgan, D. O. (2007). Sequential E2s drive polyubiquitin chain assembly on APC targets. *Cell.* **130,** 127–139

Rodriguez, M. S., Desterro, J. M., Lain, S., Midgley, C.A., Lane, D. P. & Hay, R.T. (1999). SUMO-1 modification activates the transcriptional response of p53. *EMBO J.* **18,** 6455–6461.

Rodriguez, M. S., Desterro, J. M., Lain, S., Lane, D. P. & Hay, R. T. (2000). Multiple C-terminal lysine residues target p53 for ubiquitin-proteasome-mediated degradation. *Mol Cell Biol.* **20,** 8458-8467.

Rossi, P., Swapna, G. V., Huang, Y. J., Aramini, J. M., Anklin, C., Conover, K., Hamilton, K., Xiao, R., Acton, T. B., Ertekin, A., Everett, J. K. & Montelione, G. T. (2010). A microscale protein NMR sample screening pipeline. *J Biomol NMR.* **46,** 11-22.

Roth, J., Dobbelstein, M., Freedman, D. A., Shenk, T. & Levine, A. J. (1998). Nucleo-cytoplasmic shuttling of the hdm2 oncoprotein regulates the levels of the p53 protein via a pathway used by the human immunodeficiency virus revprotein. *EMBO J.* **17,** 554 – 564,

Sadowski, M., Mawson, A., Baker, R. & Sarcevic, B. (2007). Cdc34 C-terminal tail phosphorylation regulates Skp1/cullin/F-box (SCF)-mediated ubiquitination and cell cycle progression. *Biochem. J.* **405,** 569–581

Sakata, E., Satoh, T., Yamamoto, S., Yamaguchi, Y., Yagi-Utsumi, M., Kurimoto, E., Tanaka, K., Wakatsuki, S. & Kato, K. (2010). Crystal structure of UbcH5b~ubiquitin intermediate: insight into the formation of the self-assembled E2~Ub conjugates. *Structure.* **18,** 138-47

Saleh, A., Collart, M., Martens, J. A., Genereaux, J., Allard, S., Cote, J. & Brandl, C.J. (1998). TOM1p, a yeast hect-domain protein which mediates transcriptional regulation through the ADA/SAGA coactivator complexes. *J Mol Biol.* **282**, 933-946.

Samalikova, M. & Grandori, R. (2003). Role of opposite charges in protein electrospray ionization mass spectrometry. *J Mass Spectrom.* **38,** 941-947.

Schaffer, M. L., Deshayes, K., Nakamura, G., Sidhu, S. & Skelton, N. J. (2003). Complex with a phage display-derived peptide provides insight into the function of insulin-like growth factor I. *Biochemistry.* **42,** 9324-9334.

Scheffner, M., Werness, B. A., Huibregtse, J. M., Levine, A. J., Howley, P. M. (1990). The E6 oncoprotein encoded by human papillomavirus types 16 and 18 promotes the degradation of p53. *Cell.* **63,** 1129-1136.

Scheffner, M., Huibregtse, J. M., Vierstra, R. D., & Howley, P. M. (1993). The HPV-16 E6 and E6-AP complex functions as a ubiquitin-protein ligase in the ubiquitination of p53. *Cell.* **75,** 495-505.

Schlott, T., Reimer, S., Jahns, A., Ohlenbusch, A., Ruschenburg, I., Nagel, H. & Droese M. (1997). Point mutations and nucleotide insertions in the MDM2 zinc finger structure of human tumours. *J Pathol.* **182,** 54-61.

Schon, O., Friedler, A., Bycroft, M., Freund, S. M. & Fersht, A. R. (2002). Molecular mechanism of the interaction between MDM2 and p53. *J. Mol. Biol.* **323,** 491-501.

Schon, O., Friedler, A., Freund, S. & Fersht, A. R. (2004). Binding of p53-derived ligands to MDM2 induces a variety of long range conformational changes. *J Mol Biol.* **336,** 197-202.

Schreiber, S. L. & Crabtree, G. R. (1992). The mechanism of action of cyclosporin A and FK506. *Immunol Today.* **13,** 136-142.

Schulman, B. A. & Harper, J. W. (2009). Ubiquitin-like protein activation by E1 enzymes: the apex for downstream signalling pathways. *Nat Rev Mol Cell Biol.* **10,** 319-331.

Shangary, S & Wang, S. (2008). Targeting theMDM2-p53 Interaction for Cancer Therapy. *Clin Cancer Res.* **14,** 5318-5324.

Shangary, S. & Wang, S. (2009). Small-molecule inhibitors of the MDM2-p53 protein-protein interaction to reactivate p53 function: a novel approach for cancer therapy. *Annu Rev Pharmacol Toxicol.* **49,** 223-241

Sharma, S., Zheng, H., Huang, Y. J., Ertekin, A., Hamuro, Y., Rossi, P., Tejero, R., Acton, T. B., Xiao, R., Jiang, M., Zhao, L., Ma, L. C., Swapna, G. V., Aramini, J. M. & Montelione, G. T. (2009). Construct optimization for protein NMR structure analysis using amide hydrogen/deuterium exchange mass spectrometry. *Proteins.* **76,** 882-894

Shave, S. R., Taylor, P., Walkinshaw, M., Smith, L., Hardy, J. & Trew, A. (2008). Ligand discovery on massively parallel systems. *IBM Journal of Research and Development.* **52,** 57 - 67.

Sherr, C.J. (2001). The INK4a/ARF network in tumour suppression. *Nat. Rev. Mol. Cell Biol.* **2,** 731-737.

Sherr, C. J. & Weber, J. D. (2000). The ARF/p53 pathway. *Curr. Opin. Genet. Dev.* **10,** 94–99.

Shieh, S. Y., Ahn, J., Tamai, K., Taya, Y. & Prives, C. (2000). The human homologs of checkpoint kinases Chk1 and Cds1 (Chk2) phosphorylate p53 at multiple DNA damage-inducible sites. *Genes Dev.* **14,** 289-300.

Shimizu, H., Burch, L. R., Smith, A. J., Dornan, D., Wallace, M., Ball, K. L. & Hupp, T. R. (2002). The conformationally flexible S9-S10 linker region in the core domain of p53 contains a novel MDM2 binding site whose mutation increases ubiquitination of p53 in vivo. *J Biol Chem.* **277,** 28446-28458.

Shimizu, H. & Hupp, T. R. (2003). Intrasteric regulation of MDM2. *Trends Biochem Sci.* **28,** 346-349.

Shinozaki, T., Nota, A., Taya, Y. & Okamoto, K. (2003). Functional role of Mdm2 phosphorylation by ATR in attenuation of p53 nuclear export. *Oncogene.* **22,** 8870-8880.

Shirangi, T. R., Zaika, A., & Moll, U.M. (2002). Nuclear degradation of p53 occurs during down-regulation of the p53 response after DNA damage. FASEB J. 16, 420–422. Shmueli, A. & Oren, M. (2004). Regulation of p53 by MDM2: fate is in the numbers. *Mol Cell.* **13,** 4–5

Shmueli, A. & Oren, M. (2004). Regulation of p53 by Mdm2: fate is in the numbers. *Mol Cell.* **3,** 4-5.

Shuker, S. B., Hajduk, P. J., Meadows, R. P. & Fesik, S. W. (1996). Discovering high-affinity ligands for proteins: SAR by NMR. *Science.* **274,** 1531-1534.

Shvarts, A., Steegenga, W. T., Riteco, N., van Laar, T., Dekker, P., Bazuine, M., van Ham, R. C., van der Houven van Oordt, W., Hateboer, G., van der Eb, A. J. & Jochemsen, A. G. (1996). MDMX: a novel p53-binding protein with some functional properties of MDM2. *EMBO J.* **15,** 5349-5357.

Sidhu, S. S., Fairbrother, W. J. & Deshayes, K. (2003). Exploring protein–protein interactions with phage display. *Chembiochem.* **4,** 14-25.

Sigalas, I., Calvert, A. H., Anderson, J. J., Neal, D. E. & Lunec, J. (1996). Alternatively spliced mdm2 transcripts with loss of p53 binding domain sequences: transforming ability and frequent detection in human cancer. *Nat. Med.* **2,** 912-917.

Singh, R. K., Iyappan, S. & Scheffner, M. (2007). Hetero-oligomerization with MdmX rescues the ubiquitin/Nedd8 ligase activity of RING finger mutants of Mdm2. *J Biol Chem.* **282,** 10901-10907.

Sinz, A. (2007). Investigation of protein-ligand interactions by mass spectrometry. *Chem Med Chem.* **2,** 425-31.

Skowyra, D., Craig, K. L., Tyers, M., Elledge, S. J. & Harper, J. W. (1997). F-box proteins are receptors that recruit phosphorylated substrates to the SCF ubiquitin-ligase complex. *Cell.* **91,** 209-219.

Sotriffer, C. A., Flader, W., Winger, R. H., Rode, B. M., Liedl, K. R. & Varga JM. (2000). Automated docking of ligands to antibodies: methods and applications. *Methods.* **20,** 280-291.

Spence, J., Gali, R. R., Dittmar, G., Sherman, F., Karin, M., & Finley D. (2000). Cell cycle-regulated modification of the ribosome by a variant multiubiquitin chain. *Cell.* **102,** 67-76.

Spence, J., Sadis, S., Haas, A. L. & Finley, D. (1995). A ubiquitin mutant with specific defects in DNA repair and multiubiquitination. *Mol Cell Biol.* **15,** 1265-1273.

Staub, O., Gautschi, I., Ishikawa, T., Breitschopf, K., Ciechanover, A., Schild, L. & Rotin, D. (1997). Regulation of stability and function of the epithelial Na+ channel (ENaC) by ubiquitination. *EMBO J.* **16,** 6325-6336.

Stad, R., Ramos, Y. F., Little, N., Grivell, S., Attema, J., van Der, Eb, A. J. & Jochemsen, A. G. (2000). Hdmx stabilizes Mdm2 and p53. *J Biol Chem.* **275,** 28039-28044.

Stad, R., Little, N.A., Xirodimas, D.P., Frenk, R., van der Eb, A.J., Lane, D.P., Saville, M.K., & Jochemsen, A.G. (2001). Mdmx stabilizes p53 and Mdm2 via two distinct mechanisms. *EMBO Rep.* **2,** 1029-1034.

Stevens, C., Pettersson, S., Wawrzynow, B., Wallace, M., Ball, K., Zylicz, A. & Hupp, T. R. (2008) ATP stimulates MDM2-mediated inhibition of the DNA-binding function of E2F1. *FEBS J.* **275,** 4875-4886.

Steven R. Shave's thesis (2009) "The development of high performance structure and ligand based virtual screening techniques. (University of Edinburgh)

Stites, W.E. (1997). Protein–protein interactions: interface structure, binding thermodynamics and mutational analysis. *Chem. Rev.* **97,** 1233-1250.

Stoll, R., Renner, C., Hansen, S., Palme, S., Klein, C., Belling, A. et al. (2001). Chalcone derivatives antagonize interactions between the human oncoprotein MDM2 and p53. *Biochemistry.* **40,** 336-344.

Stommel, J. M. & Wahl, G. M. (2005). A new twist in the feedback loop: stress-activated MDM2 destabilization is required for p53 activation. *Cell Cycle.* **4,** 411-417.

Stommel, J. M. & Wahl, G. M. (2004). Accelerated MDM2 auto-degradation induced by DNA-damage kinases is required for p53 activation. *EMBO J.* **23,** 1547-1556.

Summers, M. K., Pan, B., Mukhyala, K. & Jackson, P. K. (2008) The unique N terminus of the UbcH10 E2 enzyme controls the threshold for APC activation and enhances checkpoint regulation of the APC. *Mol. Cell.* **31,** 544-556

Takagi, M., Absalon, M.J., McLure, K.G. & Kastan, M.B. (2005). Regulation of p53 translation and induction after DNA damage by ribosomal protein L26 and nucleolin. *Cell.* **123,** 49-63.

Tamborini, E., Della, Torre, G., Lavarino, C., Azzarelli, A., Carpinelli, P., Pierotti, M. A. & Pilotti, S. (2001). Analysis of the molecular species generated by MDM2 gene amplification in liposarcomas. *Int J Cancer.* **92,** 790-796.

Tao, W. & Levine, A. J. (1999). P19(ARF) stabilizes p53 by blocking nucleocytoplasmic shuttling of Mdm2. *Proc. Natl. Acad. Sci. USA.* **96,** 6937-6941.

Taylor, P., Blackburn, E., Sheng, Y. G., Harding, S., Hsin, K. Y., Kan, D., Shave, S. & Walkinshaw, M. D. (2008). Ligand discovery and virtual screening using the program LIDAEUS. *British Journal of Pharmacology.* **153,** 555-567

Teague, S. J. (2003). Implications of protein flexibility for drug discovery. (2003). *Nature Rev. Drug Discov.* 2, 527-541.

Thut, C. J., Goodrich, J. A. & Tjian, R. (1997). Repression of p53-mediated transcription by MDM2: a dual mechanism. *Genes Dev.* **11,** 1974-1986.

Toledo, F. & Wahl, G. M. (2006). Regulating the p53 pathway: In vitro hypotheses, in vivo veritas. *Nat Rev Cancer.* **6,** 909-923.

Tong, H., Hateboer, G., Perrakis, A., Bernards, R. & Sixma, T. K. (1997). Crystal structure of murine/human Ubc9 provides insight into the variability of the ubiquitin-conjugating system. *J Biol Chem.* **272,** 21381-21387.

Tovar, C., Rosinski, J., Filipovic, Z., Higgins, B., Kolinsky, K., Hilton, H. et al. (2006). Small-molecule MDM2 antagonists reveal aberrant p53 signaling in cancer: implications for therapy. *Proc. Natl Acad. Sci. USA.* **103,** 1888-1893.

Thrower, J. S., Hoffman, L., Rechsteiner, M. & Pickart, C. M. (2000). Recognition of the polyubiquitin proteolytic signal. *EMBO J.* **19,** 94-102.
Turner, G. C., Du, F. & Varshavsky, A. (2000). Peptides accelerate their uptake by activating a ubiquitin-dependent proteolytic pathway. *Nature.* **405,** 579-583.

Tyers, M. & Jorgensen, P. (2000). Proteolysis and the cell cycle: with this RING I do thee destroy. *Curr Opin Genet Dev.* **10,** 54-64.

Uldrijan, S., Pannekoek, W. J. & Vousden, K. H. (2007). An essential function of the extreme C-terminus of MDM2 can be provided by MDMX. *EMBO J.* **26,** 102-112.

Uhrinova, S., Uhrin, D., Powers, H., Watt, K., Zheleva, D., Fischer, P., McInnes, C. & Barlow, P. N. (2005). Structure of free MDM2 N-terminal domain reveals conformational adjustments that accompany p53-binding. *J Mol Biol.* **350,** 587-598.

van Demark, A. P., Hofmann, R. M., Tsui, C., Pickart, C. M. & Wolberger, C. (2001). Molecular insights into polyubiquitin chain assembly: crystal structure of the Mms2/Ubc13 heterodimer. *Cell.***105,** 711-720.

van Wijk, S. J. L. & Timmers, H. T. M. (2010). The family of ubiquitin-conjugating enzymes (E2s): deciding between life and death of proteins. *FASEB J.* **24,** 981-993

Vassilev, L. T. (2007). MDM2 inhibitors for cancer therapy. *Trends Mol Med.* **13,** 23-31.

Vassilev, L. T., Vu, B. T., Graves, B., Carvajal, D., Podlaski, F., Filipovic, Z., Kong, N., Kammlott, U., Lukacs, C., Klein, C., Fotouhi, N. & Liu, E. A. (2004). In vivo activation of the p53 pathway by small-molecule antagonists of MDM2. *Science.* **303,** 844-848.

Viegas, A., Macedo, A. L. & Cabrita, E. J. (2009). Ligand-based nuclear magnetic resonance screening techniques. *Methods Mol Biol.* **572,** 81-100.

Vijay-Kumar S, Bugg CE, Cook WJ. (1987). Structure of ubiquitin refined at 1.8 A resolution. *J Mol Biol.* **194,** 531-544.

Vogelstein, B., Lane, D. & Levine, A. J. (2000). Surfing the p53 network. (2000). *Nature.* **408,** 307-310.

Vousden, K. H. & Lane, D. P. (2007). p53 in health and disease. *Nat Rev Mol Cell Biol.* **8,** 275-283.

Vousden, K. H. & Lu, X. (2002). Live or let die: the cell's response to p53. *Nat Rev Cancer.* **2,** 594-604.

Vousden, K. H & Prives C. (2009). Blinded by the Light: The Growing Complexity of p53. *Cell.* **137,** 413-431.

Wallace, M., Worrall, E., Pettersson, S., Hupp, T. R. & Ball, K. L. (2006). Dual-site regulation of MDM2 E3-ubiquitin ligase activity. *Mol Cell.* **23,** 251-263.

Walden, H., Podgorski, M. S. & Schulman, B. A. (2003). Insights into the ubiquitin transfer cascade from the structure of the activating enzyme for NEDD8. *Nature.* **422,** 330-334.

Waterman, H., Levkowitz, G., Alroy, I. & Yarden, Y. (1999). The RING finger of c-Cbl mediates desensitization of the epidermal growth factor receptor. *J Biol Chem.* **274,** 22151-22154.

Wawrzynow, B., Pettersson, S., Zylicz, A., Bramham, J., Worrall, E., Hupp, T. R., & Ball, K. L. (2009). A function for the RING finger domain in the allosteric control of MDM2 conformation and activity. *J Biol Chem.* **284,** 11517-11530.

Wawrzynow, B., Zylicz, A., Wallace, M., Hupp, T. & Zylicz, M. (2007) MDM2 chaperones the p53 tumor suppressor. *J. Biol. Chem.* **282,** 32603-32612.

Weber, L. (2010). Patented inhibitors of p53-Mdm2 interaction (2006 - 2008). *Proc Natl Acad Sci U S A. Expert Opin Ther Pat.* **20,** 179-91.

Wefes, I., Mastrandrea, L. D., Haldeman, M., Koury, S. T., Tamburlin, J., Pickart, C. M. & Finley, D. (1995). Induction of ubiquitin-conjugating enzymes during terminal erythroid differentiation. *Proc Natl Acad Sci U S A.* **92,** 4982-4986.

Wei, D. & Sun, Y. (2010). Small RING finger proteins RBX1 and RBX2 of SCF E3 ubiquitin ligases: the role in cancer and as cancer targets. *Genes Cancer.* **1,** 700-707.

Weissman A. M. (2001). Themes and variations on ubiquitylation. *Nat. Rev. Mol. Cell Biol.* **2,** 169-178

Wenzel, D. M., Stoll, K. E. & Klevit, R. E. (2011). E2s: structurally economical and functionally replete. *Biochem J.* **433,** 31-42.

Whitby, F.G., Xia, G., Pickart, C. M. & Hill, C. P. (1998). Crystal structure of the human ubiquitin-like protein NEDD8 and interactions with ubiquitin pathway enzymes. *J Biol Chem.* **273,** 34983-34991.

Whitmore, L. & Wallace, B. A. (2004). DICHROWEB, an online server for protein secondary structure analyses from circular dichroism spectroscopic data. *Nucleic acids Res.* **32,** 668-673.

Windheim, M., Peggie, M. & Cohen, P. (2008). Two different classes of E2 ubiquitin-conjugating enzymes are required for the mono-ubiquitination of proteins and elongation by polyubiquitin chains with a specific topology. *Biochem. J.* **409,** 723-729

Winn, P. J., Religa, T. L., Battey, J. N., Banerjee, A., and Wade, R. C. (2004) Determinants of functionality in the ubiquitin conjugating enzyme family. *Structure.* **12,** 1563–1574

Worrall, E. G., Wawrzynow, B., Worrall, L., Walkinshaw, M., Ball, K. L. & Hupp, T. R. (2009). Regulation of the E3 ubiquitin ligase activity of MDM2 by an N-terminal pseudo-substrate motif. *J Chem Biol.* **3,** 113-129.

Worrall, E. G., Worrall, L., Blackburn, E., Walkinshaw, M. & Hupp, T. R. (2010). The effects of phosphomimetic lid mutation on the thermostability of the N-terminal domain of MDM2. *J Mol Biol.* **398,** 414-428.

Worthylake, D. K., Prakash, S., Prakash, L. & Hill, C. P. (1998). Crystal structure of the Saccharomyces cerevisiae ubiquitin-conjugating enzyme Rad6 at 2.6 A resolution. *J Biol Chem.* **273,** 6271-6276.

Wu, G., Chen, Y. G., Ozdamar, B., Gyuricza, C. A., Chong, P. A., Wrana, J. L., Massagué, J. and Shi, Y. (2000) Structural basis of Smad2 recognition by the Smad anchor for receptor activation. *Science.* **287,** 92-97.

Wu, P. Y., Hanlon, M., Eddins, M., Tsui, C., Rogers, R. S., Jensen, J. P., Matunis, M. J., Weissman, A. M., Wolberger, C. & Pickart, C. M. (2003) A conserved catalytic residue in the ubiquitin-conjugating enzyme family. *EMBO J.* **22,** 5241-5250.

Wu, S. Y., McNae, I., Kontopidis, G., McClue, S. J., McInnes, C., Stewart, K. J., Wang, S., Zheleva, D. I., Marriage, H., Lane, D. P., Taylor, P., Fischer, P. M. & Walkinshaw, M. D. (2003). Discovery of a novel family of CDK inhibitors with the program LIDAEUS: structural basis for ligand-induced disordering of the activation loop. *Structure.* **11,** 399-410.

Wunderlich, M., Ghosh, M., Weghorst, K. & Berberich, S.J. (2004). MdmX represses E2F1 transactivation. Cell Cycle. **3,** 472-478.

Xirodimas, D.P., Stephen, C.W. & Lane, D.P. (2001). Cocompartmentalization of p53 and Mdm2 is a major determinant for Mdm2-mediated degradation of p53. *Exp. Cell Res.* **270,** 66-77.

Xirodimas, D.P., Saville, M.K., Bourdon, J.C., Hay, R.T., and Lane, D.P. (2004). Mdm2-mediated NEDD8 conjugation of p53 inhibits its transcriptional activity. *Cell.* **118,** 83-97

Xu, Y. (2003). Regulation of p53 responses by post-translational modifications. *Cell Death Differ.* **10,** 400-403.

Xuan, Y., Scheuermann, E. B., Meda, A. R., Hayen, H., von Wirén, N. & Weber, G. (2006). Separation and identification of phytosiderophores and their metal complexes in plants by zwitterionic hydrophilic interaction liquid chromatography coupled to electrospray ionization mass spectrometry. *J Chromatogr A.* **1136,** 73-81.

Yang, Y., Li, C. C. & Weissman, A. M. (2004). Regulating the p53 system through ubiquitination. *Oncogene.* **23,** 2096-2106.

Yang, Y., Ludwig, R. L., Jensen, J. P., Pierre, S. A., Medaglia, M. V., Davydov, I. V., Safiran, Y. J., Oberoi, P., Kenten, J. H., Phillips, A. C., Weissman, A. M. & Vousden, K. H. (2005). Small molecule inhibitors of HDM2 ubiquitin ligase activity stabilize and activate p53 in cells. *Cancer Cell.* **7,** 547–559.

Yang, Y., Moir, E., Kontopidis, G., Taylor, P., Wear, M. A., Malone, K., Dunsmore, C. J., Page, A. P, Turner, N. J. & Walkinshaw, M. D. (2007). Structure-based discovery of a family of synthetic cyclophilin inhibitors showing a cyclosporin-A phenotype in Caenorhabditis elegans. *Biochem Biophys Res Commun.* **363,** 1013-1009.

Yaron, A., Hatzubai, A., Davis, M., Lavon, I., Amit, S., Manning, A. M., Andersen, J. S., Mann, M., Mercurio, F. & Ben-Neriah, Y. (1998). Identification of the receptor component of the IkappaBalpha-ubiquitin ligase. *Nature.* **396,** 590-594.

Ye, Y. & Rape, M. (2009). Building ubiquitin chains: E2 enzymes at work. *Nature.* **10,** 755-764

Yee, A., Chang, X., Pineda-Lucena, A., Wu, B., Semesi, A., Le, B., Ramelot, T., Lee, G. M., Bhattacharyya, S., Gutierrez, P., Denisov, A., Lee, C. H., Cort, J. R., Kozlov, G., Liao, J., Finak, G., Chen, L., Wishart, D., Lee, W., McIntosh, L. P., Gehring, K., Kennedy, M. A., Edwards, A. M. & Arrowsmith, C. H. (2002). An NMR approach to structural proteomics. *Proc Natl Acad Sci U S A.* **99,** 1825-1830.

Yee, A., Gutmanas, A. & Arrowsmith, C. H. (2006). Solution NMR in structural genomics. *Curr Opin Struct Biol.* **16,** 611-617.

Yip. T. T., Nakagawa. Y. & Porath. J. (1989). Evaluation of the interaction of peptides with Cu(II), Ni(II), and Zn(II) by high-performance immobilized metal ion affinity chromatography. *Anal. Biochem.* **183,** 159-171.

Yin, Q., Lin, S. C., Lamothe, B., Lu, M., Lo, Y. C., Hura, G., Zheng, L., Rich, R. L., Campos, A. D., Myszka, D. G. et al. (2009) E2 interaction and dimerization in the crystal structure of TRAF6. *Nat. Struct. Mol. Biol.* **16,** 658-666

Yogosawa, S., Miyauchi, Y., Honda, R., Tanaka, H. & Yasuda, H. (2003). Mammalian Numb is a target protein of Mdm2, ubiquitin ligase. *Biochem. Biophys. Res. Commun.* **302,** 869 -872.

Yu, G. W., Allen, M. D., Andreeva, A., Fersht, A. R. & Bycroft, M. (2006). Solution structure of the C4 zinc finger domain of HDM2. *Protein Sci.* **15,** 384-389.

Yu, Z. K., Geyer, R. K., & Maki, C. G. (2000). MDM2-dependent ubiquitination of nuclear and cytoplasmic P53. *Oncogene.* **19,** 5892-5897.

Zacksenhaus, E. & Sheinin, R. (1990). Molecular cloning, primary structure and expression of the human X linked A1S9 gene cDNA which complements the ts A1S9 mouse L cell defect in DNA replication. *EMBO J.* **9,** 2923-2929.

Zhang, Y., Xiong, Y. & Yarbrough, W. G. (1998). ARF promotes MDM2 degradation and stabilizes p53: ARF-INK4a locus deletion impairs both the Rb and p53 tumor suppression pathways. *Cell.* **92,** 725-734.

Zhang, Y., Wolf, G.W., Bhat, K., Jin, A., Allio, T., Burkhart, W. A. & Xiong, Y. (2003). Ribosomal protein L11 negatively regulates oncoprotein MDM2 and mediates a p53-dependent ribosomal-stress checkpoint pathway. *Mol. Cell. Biol.* **23,** 8902-8912.

Zhang, Y. & Xiong, Y. (2001). Control of p53 ubiquitination and nuclear export by MDM2 and ARF. *Cell Growth Differ.* **12,** 175-186.

Zhang, Y., Xiong, Y. & Yarbrough, W.G. (1998). ARF promotes MDM2 degradation and stabilizes p53: ARF-INK4a locus deletion impairs both the Rb and p53 tumor suppression pathways. *Cell.* **92,** 725-734.

Zheng, N., Wang, P., Jeffrey, P. D. & Pavletich, N. P. (2000). Structure of a c-Cbl-UbcH7 complex: RING domain function in ubiquitin-protein ligases. *Cell.* **102,** 533-539.

Zhang, M., Windheim, M., Roe, S. M., Peggie, M., Cohen, P., Prodromou, C. & Pearl, L. H. (2005). Chaperoned ubiquitylation--crystal structures of the CHIP U box E3 ubiquitin ligase and a CHIP-Ubc13-Uev1a complex. *Mol Cell.* **20,** 525-538.

Zhou, B. P., Liao, Y., Xia, W., Zou, Y., Spohn, B. & Hung, M. C. (2001). HER-2/neu induces p53 ubiquitination via Akt-mediated MDM2 phosphorylation. *Nat. Cell Biol.* **3,** 973-982.

Zhu, Q., Yao, J., Wani, G., Wani, M. A. & Wani, A. A. (2001). Mdm2 mutant defective in binding p300 promotes ubiquitination but not degradation of p53: evidence for the role of p300 in integrating ubiquitination and proteolysis. *J Biol Chem.* **276,** 29695-29701.